

Axel H.E. Müller
Oleg Borisov *Editors*

Self Organized Nanostructures of Amphiphilic Block Copolymers II

Editorial Board:

**A. Abe · A.-C. Albertsson · K. Dušek · J. Genzer
W.H. de Jeu · S. Kobayashi · K.-S. Lee · L. Leibler
T.E. Long · I. Manners · M. Möller · E.M. Terentjev
M. Vicent · B. Voit · G. Wegner · U. Wiesner**

Advances in Polymer Science

Recently Published and Forthcoming Volumes

Self Organized Nanostructures of Amphiphilic Block Copolymers II

Volume Editors: Müller, A.H.E., Borisov, O.
Vol. 242, 2011

Self Organized Nanostructures of Amphiphilic Block Copolymers I

Volume Editors: Müller, A.H.E., Borisov, O.
Vol. 241, 2011

Bioactive Surfaces

Volume Editors: Börner, H.G., Lutz, J.-F.
Vol. 240, 2011

Advanced Rubber Composites

Volume Editor: Heinrich, G.
Vol. 239, 2011

Polymer Thermodynamics

Volume Editors: Enders, S., Wolf, B.A.
Vol. 238, 2011

Enzymatic Polymerisation

Volume Editors: Palmans, A.R.A., Heise, A.
Vol. 237, 2010

High Solid Dispersion

Volume Editor: Cloitre, M.
Vol. 236, 2010

Silicon Polymers

Volume Editor: Muzafarov, A.
Vol. 235, 2011

Chemical Design of Responsive Microgels

Volume Editors: Pich, A., Richtering, W.
Vol. 234, 2010

Hybrid Latex Particles – Preparation with Emulsion

Volume Editors: van Herk, A.M., Landfester, K.
Vol. 233, 2010

Biopolymers

Volume Editors: Abe, A., Dušek, K., Kobayashi, S.
Vol. 232, 2010

Polymer Materials

Volume Editors: Lee, K.-S., Kobayashi, S.
Vol. 231, 2010

Polymer Characterization

Volume Editors: Dušek, K., Joanny, J.-F.
Vol. 230, 2010

Modern Techniques for Nano- and Microreactors/-reactions

Volume Editor: Caruso, F.
Vol. 229, 2010

Complex Macromolecular Systems II

Volume Editors: Müller, A.H.E., Schmidt, H.-W.
Vol. 228, 2010

Complex Macromolecular Systems I

Volume Editors: Müller, A.H.E., Schmidt, H.-W.
Vol. 227, 2010

Shape-Memory Polymers

Volume Editor: Lendlein, A.
Vol. 226, 2010

Polymer Libraries

Volume Editors: Meier, M.A.R., Webster, D.C.
Vol. 225, 2010

Polymer Membranes/Biomembranes

Volume Editors: Meier, W.P., Knoll, W.
Vol. 224, 2010

Organic Electronics

Volume Editors: Meller, G., Grasser, T.
Vol. 223, 2010

Inclusion Polymers

Volume Editor: Wenz, G.
Vol. 222, 2009

Advanced Computer Simulation Approaches for Soft Matter Sciences III

Volume Editors: Holm, C., Kremer, K.
Vol. 221, 2009

Self-Assembled Nanomaterials II

Nanotubes
Volume Editor: Shimizu, T.
Vol. 220, 2008

Self-Assembled Nanomaterials I

Nanofibers
Volume Editor: Shimizu, T.
Vol. 219, 2008

Self Organized Nanostructures of Amphiphilic Block Copolymers II

Volume Editors: Axel H.E. Müller
Oleg Borisov

With contributions by

V. Aseyev · S. Beleguinou · N.A.M. Besseling
I. Botiz · M.A. Cohen Stuart · T. Hellweg
M. Junginger · A. de Keizer · K. Kita-Tokarczyk
G. Reiter · H. Schlaad · A. Taubert · H. Tenhu
F.M. Winnik · Y. Yan



Springer

Editors

Prof. Axel H.E. Müller
Makromolekulare Chemie II
and Bayreuther Zentrum für Kolloide
und Grenzflächen
Universität Bayreuth
95440 Bayreuth
Germany
axel.mueller@uni-bayreuth.de

Dr. Oleg Borisov
Institut Pluridisciplinaire de Recherche sur
l'Environnement et les Matériaux
UMR 5254 CNRS/UPPA
64053 Pau
France
oleg.borisov@univ-pau.fr

ISSN 0065-3195 e-ISSN 1436-5030
ISBN 978-3-642-22296-2 e-ISSN 978-3-642-22297-9
DOI 10.1007/978-3-642-22297-9
Springer Heidelberg Dordrecht London New York

Library of Congress Control Number: 2011934436

© Springer-Verlag Berlin Heidelberg 2011

This work is subject to copyright. All rights are reserved, whether the whole or part of the material is concerned, specifically the rights of translation, reprinting, reuse of illustrations, recitation, broadcasting, reproduction on microfilm or in any other way, and storage in data banks. Duplication of this publication or parts thereof is permitted only under the provisions of the German Copyright Law of September 9, 1965, in its current version, and permission for use must always be obtained from Springer. Violations are liable to prosecution under the German Copyright Law.

The use of general descriptive names, registered names, trademarks, etc. in this publication does not imply, even in the absence of a specific statement, that such names are exempt from the relevant protective laws and regulations and therefore free for general use.

Cover design: WMXDesign GmbH, Heidelberg

Printed on acid-free paper

Springer is part of Springer Science+Business Media (www.springer.com)

Volume Editors

Prof. Axel H.E. Müller
Makromolekulare Chemie II
and Bayreuther Zentrum für Kolloide
und Grenzflächen
Universität Bayreuth
95440 Bayreuth
Germany
axel.mueller@uni-bayreuth.de

Dr. Oleg Borisov
Institut Pluridisciplinaire de Recherche sur
l'Environnement et les Matériaux
UMR 5254 CNRS/UPPA
64053 Pau
France
oleg.borisov@univ-pau.fr

Editorial Board

Prof. Akihiro Abe
Professor Emeritus
Tokyo Institute of Technology
6-27-12 Hiyoshi-Honcho, Kohoku-ku
Yokohama 223-0062, Japan
aabe34@xc4.so-net.ne.jp

Prof. A.-C. Albertsson
Department of Polymer Technology
The Royal Institute of Technology
10044 Stockholm, Sweden
aila@polymer.kth.se

Prof. Karel Dušek
Institute of Macromolecular Chemistry
Czech Academy of Sciences
of the Czech Republic
Heyrovský Sq. 2
16206 Prague 6, Czech Republic
dusek@imc.cas.cz

Prof. Jan Genzer
Department of Chemical &
Biomolecular Engineering
North Carolina State University
911 Partners Way
27695-7905 Raleigh, North Carolina
USA

Prof. Dr. Wim H. de Jeu
DWI an der RWTH Aachen eV
Pauwelsstraße 8
D-52056 Aachen, Germany
dejeu@dwirwth-aachen.de

Prof. Shiro Kobayashi
R & D Center for Bio-based Materials
Kyoto Institute of Technology
Matsugasaki, Sakyo-ku
Kyoto 606-8585, Japan
kobayash@kit.ac.jp

Prof. Kwang-Sup Lee
Department of Advanced Materials
Hannam University
561-6 Jeonmin-Dong
Yuseong-Gu 305-811
Daejeon, South Korea
kslee@hnu.kr

Prof. L. Leibler
Matière Molle et Chimie
Ecole Supérieure de Physique
et Chimie Industrielles (ESPCI)
10 rue Vauquelin
75231 Paris Cedex 05, France
ludwik.leibler@espci.fr

Prof. Timothy E. Long

Department of Chemistry
and Research Institute
Virginia Tech
2110 Hahn Hall (0344)
Blacksburg, VA 24061, USA
telong@vt.edu

Prof. Ian Manners

School of Chemistry
University of Bristol
Cantock's Close
BS8 1TS Bristol, UK
ian.manners@bristol.ac.uk

Prof. Martin Möller

Deutsches Wollforschungsinstitut
an der RWTH Aachen e.V.
Pauwelsstraße 8
52056 Aachen, Germany
moeller@dwf.rwth-aachen.de

Prof. E.M. Terentjev

Cavendish Laboratory
Madingley Road
Cambridge CB 3 0HE, UK
emt1000@cam.ac.uk

Prof. Dr. Maria Jesus Vicent

Centro de Investigacion Principe Felipe
Medicinal Chemistry Unit
Polymer Therapeutics Laboratory
Av. Autopista del Saler, 16
46012 Valencia, Spain
mjvicent@cipf.es

Prof. Brigitte Voit

Leibniz-Institut für Polymerforschung
Dresden
Hohe Straße 6
01069 Dresden, Germany
voit@ipfdd.de

Prof. Gerhard Wegner

Max-Planck-Institut
für Polymerforschung
Ackermannweg 10
55128 Mainz, Germany
wegner@mpip-mainz.mpg.de

Prof. Ulrich Wiesner

Materials Science & Engineering
Cornell University
329 Bard Hall
Ithaca, NY 14853, USA
ubw1@cornell.edu

Advances in Polymer Sciences

Also Available Electronically

Advances in Polymer Sciences is included in Springer's eBook package *Chemistry and Materials Science*. If a library does not opt for the whole package, the book series may be bought on a subscription basis. Also, all back volumes are available electronically.

For all customers who have a standing order to the print version of *Advances in Polymer Sciences*, we offer free access to the electronic volumes of the Series published in the current year via SpringerLink.

If you do not have access, you can still view the table of contents of each volume and the abstract of each article by going to the SpringerLink homepage, clicking on "Browse by Online Libraries", then "Chemical Sciences", and finally choose *Advances in Polymer Science*.

You will find information about the

- Editorial Board
- Aims and Scope
- Instructions for Authors
- Sample Contribution

at springer.com using the search function by typing in *Advances in Polymer Sciences*.

Color figures are published in full color in the electronic version on SpringerLink.

Aims and Scope

The series *Advances in Polymer Science* presents critical reviews of the present and future trends in polymer and biopolymer science including chemistry, physical chemistry, physics and material science. It is addressed to all scientists at universities and in industry who wish to keep abreast of advances in the topics covered.

Review articles for the topical volumes are invited by the volume editors. As a rule, single contributions are also specially commissioned. The editors and publishers will, however, always be pleased to receive suggestions and supplementary information. Papers are accepted for *Advances in Polymer Science* in English.

In references *Advances in Polymer Sciences* is abbreviated as *Adv Polym Sci* and is cited as a journal.

Special volumes are edited by well known guest editors who invite reputed authors for the review articles in their volumes.

Impact Factor in 2010: 6.723; Section "Polymer Science": Rank 3 of 79

Preface

The spontaneous assembly of amphiphilic molecules in an aqueous environment represents a generic mechanism of self-organization on the supramolecular level exemplified by nature. In the living cell, the process of hierarchical assembly of bio(macro)molecules propagates from the nano- to the mesoscopic level and beyond, giving rise to highly organized structures, each perfectly adjusted for performing specific functions. This self-organization across multiple length scales occurs as an outcome of a delicate balance between a number of attractive and repulsive interactions: electrostatic, hydrophobic, hydrogen bonding, metal coordination, etc., each with its characteristic strength and range.

Recent advances in polymer chemistry, in particular, in controlled radical polymerization, have enabled the synthesis of complex macromolecular architectures with controlled topology, which comprise chemically different (functional) blocks of controlled length in well-defined positions. Block co- and terpolymers, molecular and colloidal polymer brushes, and star-like polymers present just a few typical examples. Furthermore, miktoarm stars, core-shell stars and molecular brushes, etc. exemplify structures where chemical and topological complexity are combined in one macromolecule.

Significant progress has been made in terms of understanding the self-assembly of amphiphilic diblock copolymers in selective solvents. In aqueous solutions, the assembly is typically driven by hydrophobic attraction between associating blocks and gives rise to diverse nanostructures (micelles, vesicles) and mesophases. Theory has established relationships between the macromolecular architectures of ionic/hydrophobic diblock copolymers and the equilibrium morphologies of the self-assembled aggregates. Unusual responsive properties of micelles with pH-sensitive coronas were predicted on the basis of the concept of coupling between ionization of the polyelectrolyte block and the aggregation state of the copolymer molecule and they have been recently observed in experiments. A multitude of experimental techniques, including radiation scattering, fluorescence spectroscopy, electron and atomic force microscopy, etc., have been used for structural and dynamic characterization of the block-copolymer self-assembly in solution and at liquid–solid and liquid–air interfaces.

Self-assembled structures of amphiphilic copolymers have been extensively explored in biomedicine as vectors for targeted delivery of drugs and biological molecules (enzymes, nucleic acids), in biomaterials engineering (antifouling surfaces), biosensors, etc. Further applications include food industry and agro-chemistry, uptake and pre-concentration of toxic organic compounds and heavy metal ions in water treatment, molecular templates for nano-electronic devices. Many water-based industrial formulations include polymeric amphiphiles that aggregate and co-assemble with other macromolecules, nanoparticles and surfactants to form nano-aggregates, and different types of mesophases and structures at interfaces. An important requirement for the biomedical applications are pronounced stimuli-responsive properties of the polymeric nano-structures, that is ability of a triggered response to smoothly varied external conditions (e.g., tiny variations in temperature or pH) or recognition of weak specific stimuli (e.g., trace concentrations of biologically active or toxic compounds).

The electrostatic attraction between oppositely charged ionic macromolecules and (bio)nanocolloids is an appealing alternative mechanism for building up functional nano-assemblies in aqueous media. The association of linear polyelectrolytes in solutions or at charged interfaces leads to interpolyelectrolyte complexes or polyelectrolyte multilayers. The strength of attractive electrostatic interactions can be easily tuned by the pH or ionic strength of the solution. Hence, electrostatically assembled structures exhibit pronounced stimuli-responsive features. The enormous diversity of possible combinations of co-assembling components, including oppositely charged ionic polymers, nucleic acids and proteins, metal/ligand complexes, and inorganic nano-particles, opens a fascinating perspective of the possibility to use this mechanism to design novel functional materials based on supramolecular and supracolloidal assemblies.

Furthermore, such advanced applications as (bio)nanoreactors or molecular templates require progressing beyond the most elementary forms of self-organization and generic types of copolymer nanostructures. We need to explore routes of self- and co-assembly of macromolecules into non-centrosymmetric multi-compartment supramolecular nano-assemblies. For example, construction of nanoreactors for enzymatic (cascade) reactions requires immobilization of multiple proteins in close proximity to each other in well-segregated (protective) environments. Such enzyme cascades are very promising in biotechnological applications. The development of pathways for fabrication of well-defined multi-domain nano-structures via the spontaneous assembly of elementary macromolecular building blocks represents one of the future challenges in supra-macromolecular chemistry.

Co-assembly of amphiphilic and bis-hydrophilic block copolymers with oppositely charged polyelectrolyte blocks gives rise to sophisticated nanostructures with compartmentalized core or corona domains. The combination of nano-sized compartments that differ in polarity and composition within one colloidally stable polymeric nanostructure is promising in the development of novel, highly effective, multifunctional polymeric reagents for wastewater treatment (e.g., an one-stage removal of organic impurities and heavy metal ions from aqueous environment) as well as smart nano-containers capable of incorporation of various physiologically active

compounds, e.g., proteins and nucleic acids. Co-assembly of two ionic-neutral block copolymers can lead to surface-compartmentalized polymer-based Janus nanoparticles (“Janus micelles”) with two chemically different “faces” exposed to the surrounding environment. Janus micelles with coronas solvated in a common good solvent (e.g., water), but laterally segregated, are promising as they can selectively incorporate different enzymes or metal nano-particles possessing catalytic activity in segregated compartments, thus offering opportunities for (bio)catalytic cascades. Janus micelles are intrinsically highly surface active; their use may cut down the use of conventional surfactants with concomitant environmental impact.

Biomedical applications strongly require nanostructures based on the assembly of amphiphilic macromolecules comprising functional blocks of biological origin (peptides, oligo- or polynucleotides, polysaccharides) or their synthetic analogs. A novel class of biohybrid copolymers comprising a synthetic block conjugated to a polypeptide or polynucleotide block has attracted considerable attention. Their self-assembly gives rise to diverse ordered structures in aqueous media and at solid–liquid interfaces. The ability of biopolymer blocks to take part in specific interactions (e.g., ligand–receptor, DNA hybridization, etc.) with target molecules opens up a fascinating perspective for the design of novel generations of label-free diagnostic systems, or of smart vector systems that can deliver drugs or biologically active molecules on the basis of self-assembled bio-hybrid structures.

Based on these considerations, the European Union funded a Marie Curie Research Training Network “Self-Organized Nanostructures of Amphiphilic Copolymers (POLYAMPHI).” This network, consisting of 14 research teams from 7 European countries, worked successfully from 2004 to 2008. Some of the results obtained in these collaborations are presented in these two volumes, supplemented by chapters dealing with additional aspects of the topic. Thus, we present a comprehensive overview of the state of the art in experimental research and theory of self-organization via self- and co-assembly of amphiphilic or hydrophilic ionic (macro)molecules in aqueous solutions and at interfaces.

Pau and Bayreuth
Summer 2011

Oleg Borisov
Axel Müller

Contents

Block Copolymer Surfactant Mixtures in Aqueous Solution: Can we Achieve Size and Shape Control by Co-Micellization?	1
Thomas Hellweg	
Non-ionic Thermoresponsive Polymers in Water	29
Vladimir Aseyev, Heikki Tenhu, and Françoise M. Winnik	
From Coordination Polymers to Hierarchical Self-Assembled Structures	91
Yun Yan, Arie de Keizer, Martien A. Cohen Stuart, and Nicolaas A.M. Besseling	
Processes of Ordered Structure Formation in Polypeptide Thin Film Solutions	117
Ioan Botiz, Helmut Schlaad, and Günter Reiter	
Amphiphilic Polymers at Interfaces	151
Katarzyna Kita-Tokarczyk, Mathias Junginger, Serena Belegriou, and Andreas Taubert	
Index	203

Block Copolymer Surfactant Mixtures in Aqueous Solution: Can we Achieve Size and Shape Control by Co-Micellization?

Thomas Hellweg

Abstract Amphiphilic block copolymers (BCPs) are used in a steadily growing number of applications and formulations such as cosmetics, detergents, coatings, and enhanced oil recovery. In most of these applications, BCPs are used in complex mixtures with normal surfactants to control the solution properties of the mentioned systems. In addition, these systems are used as templates for nanoparticle and mesoporous silica synthesis. Hence, a deeper understanding of the self-assembly processes and the formed structures is desirable to achieve a better control of the properties of the obtained inorganic materials. This article reviews the recent literature describing physicochemical aspects of the BCP/surfactant mixtures and attempts to identify some general features of the behavior of these systems.

Keywords Amphiphile · Block copolymer · Packing parameter · Scattering methods · Surfactant

Contents

1	Introduction	2
2	Triblock Copolymers	3
2.1	Ionic Surfactants	5
2.2	Nonionic Surfactants	10
3	Diblock Copolymers	11
3.1	Ionic Surfactants	12
3.2	Nonionic Surfactants	17
4	Other Systems	21
4.1	Amphiphilic Poly(<i>p</i> -phenylenes)	22
5	Summary and Outlook	22
	References	24

T. Hellweg (✉)

Physical Chemistry I and Bayreuth Centre for Colloids and Interfaces (BZKG),
Bayreuth University, Universitätsstraße 30, 95447 Bayreuth, Germany
e-mail: thomas.hellweg@uni-bayreuth.de

1 Introduction

Amphiphilic block copolymers (BCPs) have been subject of numerous studies during the last few decades. This is due to the unique properties that arise from the incompatibility of the blocks, leading to a large number of different self-assembled structures and mesophases in the bulk or in selective solvents [1–4]. Studies on the interaction of BCPs with different types of surfactant are also of great relevance because these mixtures can be found in an important number of technical products ranging from paints to cosmetic products to pharmaceutical formulations.

For technical purposes, triblock copolymers of poly(ethylene oxide) (PEO) and poly(propylene oxide) (PPO) are frequently used (often called poloxamers) [5]. Since approximately 1950, these polymers have been produced on large scale as Pluronics (BASF), Synperonics (ICI), or Genapol, and the self-assembly of these systems is already the subject of a large number of investigations (see e.g., [6–10]). More recently, BCPs have been used as templates for the preparation of ordered nanostructured inorganic materials such as SBA-15 [11–13], or in the synthesis of inorganic nanoparticles [14–23].

With respect to templating applications, it is desirable to develop techniques that allow control of the self-assembly process and tuning of the shape of the BCP aggregates. One possible way to achieve this goal is the co-micellization of BCPs with surfactants [20, 21, 24–32]. This approach might allow control of the packing, and hence the curvature, of the formed interface of the mixed micelles (see scheme in Fig. 1).

In surfactant solutions, the shape of the formed self-assembled structures can be predicted, introducing the packing parameter p [33]:

$$p = \frac{V}{al} \quad (1)$$

Here, a is the headgroup area, l the chain length, and V the chain volume of the surfactant. For $p < \frac{1}{3}$, spherical structures are formed. p values between $\frac{1}{3}$ and $\frac{1}{2}$ lead to preferentially cylindrical structures. Finally, $p > \frac{1}{2}$ favors flat layered structures (e.g. lamellar phases L_α). Similar considerations also seem to be valid for BCPs.

The most important parameters for the control of micellar shape in diblock copolymer solutions appear to be the cross-sectional area of the hydrophilic chain

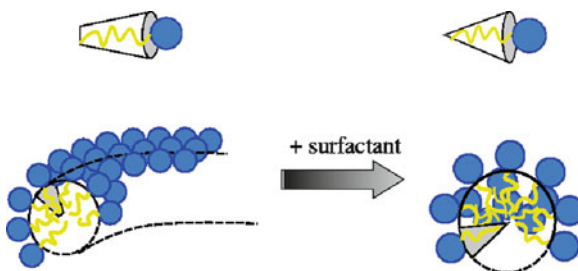


Fig. 1 The basic idea of structural control through co-micellization

(“headgroup”) and the ratio of the lengths of the two building blocks. This is similar to the situation in solutions of low molecular weight surfactants. For several nonionic surfactants (e.g., the group of alkyl oligo ethyleneoxide C_iE_j), the size per headgroup changes with temperature (due to a change in hydration) and thus the micelles transform from a spherical to a worm-like shape, even within a single phase region of the phase diagram [34, 35], as the temperature increases.

In the case of diblock copolymers containing a charged block, the structure of the micellar aggregates can be controlled by addition of salt, and transitions from spherical micelles to rod- and worm-like structures have been observed at high salt concentrations [36].

As already mentioned, co-micellization of BCPs with surfactants might also allow shape control of the formed structures. Similar concepts using surfactants and co-surfactants are already well known from microemulsion research [37–40]. In addition to templating applications, BCPs are also added to microemulsions and lead to a huge increase in solubilization power (efficiency boosting) [41–44]. In this case also, knowledge of the polymer–surfactant interaction is necessary to understand the fundamentals of this effect. However, the behavior of PEO–PPO–PEO triblock copolymers upon addition of surfactant seems to be different [24, 25, 31] to the behavior of poly(butadiene)-*b*-PEO diblock copolymers [29, 30]. Moreover, in membranes of living cells, low molecular weight amphiphiles interact with polar polymers. In this context, the interaction of Pluronics with lipids has also been studied [45–47]. However, these investigations are beyond the scope of this review.

This article aims to review the recent developments in the area of BCP–surfactant mixed systems in aqueous solution and is organized as follows: For historic reasons and due to the high number of publications devoted to Pluronics, triblock copolymers will be discussed first, and their behavior in aqueous mixtures with different surfactants will be reviewed (Section 2).

Section 3 then reviews the behavior of diblock copolymers in mixed micelles with surfactants. Section 4 discusses other polymer surfactant mixtures, such as mixtures of amphiphilic poly(*para*-phenylenes) (PPP) with nonionic surfactants [48]. The packing parameter and the curvature of an amphiphilic BCP are not only influenced by means of co-micellization with a surfactant. Both parameters can also be influenced by changing the solvent quality for one of the blocks, e.g., by adding alcohol or salt. Denkova et al. have shown that this also leads to structural changes [49]. However, despite the similarity of both approaches, the present review will only focus on aqueous BCP surfactant mixtures. Surfactants can also be used to assist structure formation in BCP thin films [50]. This is an area of growing importance, but is beyond the scope of the present contribution.

2 Triblock Copolymers

The self-assembly of triblock copolymers of the PEO–PPO–PEO type in aqueous solution was subject to a lot of studies investigating different aspects of these poloxamer polymers. This is due to the technical importance of these systems, which are

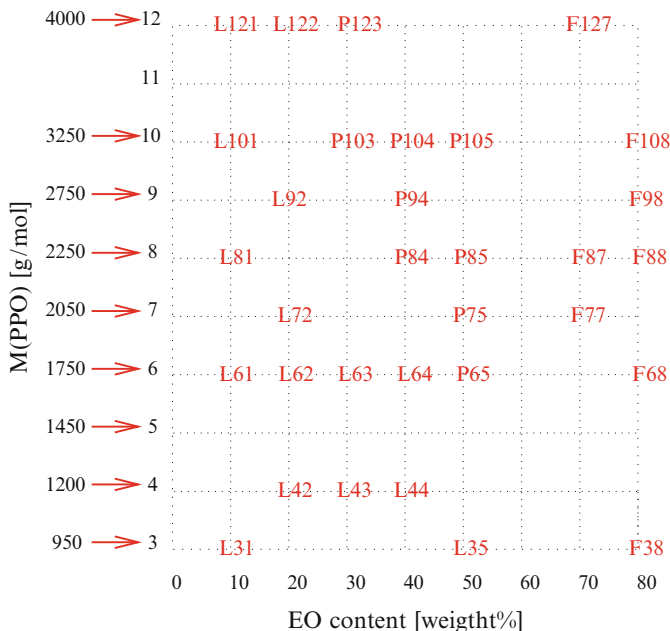


Fig. 2 Nomenclature of Pluronics [51]

produced under the trademarks Pluronic (BASF), Synperonic (ICI), and Genapol. In this review, we will use the Pluronics nomenclature. For Pluronics, all names start with P (paste), F (flakes), or L (liquid). In addition, the name contains information about the block length ratio in the respective polymer (e.g. the 3 in P123 indicates a PEO content of 30 wt%). The first one or two numbers are a code for the molecular weight of the PPO block. The 12 in P123 indicates for example a molar mass of the PPO block of 4000 g/mol.

Figure 2 gives a scheme that allows interpretation of the names of the different Pluronics commercially available.

Due to the hydrophobicity of the PPO block, these polymers are found to form micelles at intermediate concentrations and temperatures [52, 53] (approximately 1–4 wt% at room temperature). Alexandridis and coworkers reported that the hydrophobic cores of the formed micelles are nearly water-free and contain about 25% PEO. The structure of the obtained aggregates was investigated using light-scattering techniques [54], NMR self-diffusion measurements, and small-angle scattering experiments [7]. The number of studies dealing with co-micellization of PEO–PPO–PEO triblock copolymers with surfactants is still growing and the following discussion certainly will be far from complete. The section is divided into two subsections, starting with a discussion of the interaction with ionic surfactants. The second subsection treats triblock copolymers mixed with nonionic surfactants.

2.1 Ionic Surfactants

The investigations into the interaction of PEO–PPO–PEO triblock copolymers with ionic surfactants mainly focus on the surfactants sodium dodecyl sulfate (SDS) [25, 31, 55], dodecyl trimethyl ammonium bromide (DTAB) and hexadecyltrimethylammonium chloride (CTAC) [31].

To our knowledge, one of the first works systematically treating the interaction of PEO–PPO–PEO triblock copolymers with ionic surfactants was published by Almgren et al. [56]. This work presents data for the interaction of the polymers L64 (PEO₁₃PPO₃₀PEO₁₃; $M_w = 2900$ g/mol) and F68 (PEO₇₈PPO₃₀PEO₇₈; $M_w = 8600$ g/mol) with SDS. These two triblock copolymers do not form large multimolecular micelles at low temperatures (≈ 293 K) in aqueous solution. Under these conditions, only unimers are found. Upon addition of SDS to the solutions of L64 and F68, micellization is induced. At low SDS concentrations, the obtained micelles were found to be small (ca. 4–5 polymer molecules and 15 SDS molecules). Increasing the SDS concentration leads to a complete decomposition of these mixed micelles.

The polymer L64 is found to form micelles itself at higher temperatures (≈ 313 K) [56]. These micelles were studied in more detail by Holzwarth et al. using small angle neutron scattering [57]. The found aggregation numbers ranged from 37 at 310.65 K up to 54 at 328.15 K for the pure polymer. Also, these pure polymer micelles were found to decompose after addition of higher amounts of SDS [56].

One of the rare works on the kinetics of the formation of mixed micelles of Pluronics and surfactants also treats the system L64/SDS [58]. In temperature-jump experiments, the authors identified three different relaxation times for the L64/SDS mixture. The fastest ($\infty \mu\text{s}$) is associated with the binding of additional L64 unimers to the micelles. The two slower relaxation processes are interpreted as structural rearrangement of the mixed micelles and micelle clustering. These findings are qualitatively in agreement with the first kinetic investigation of these mixtures by Hecht and Hoffmann [59].

Thermodynamic aspects of the interaction of L64 and F68 with anionic surfactants were recently studied by De Lisi et al. [60–63]. The surfactants used were a series of sodium alkanoates with different alkyl chain lengths, allowing the study of the influence of the growing hydrophobicity of the chain. However, these works did not look at the micellar structure.

Xu and coworkers have used the MesoDyn approach to simulate structure formation in a mixture of L64 and P85 with SDS [64]. Unfortunately, this work starts at rather high L64 and P85 concentrations (15% and higher). Most of the experimental studies were done at lower volume fractions. Hence, no conclusions for a better understanding of the experimental findings published, e.g., by Hoffmann et al. [25, 65, 66] can be drawn. Also, high concentrations are probably of interest especially with respect to their applications. However, for high volume fractions no structural studies with small-angle neutron scattering (SANS) or small-angle

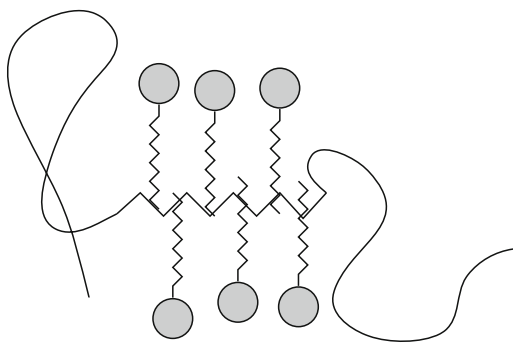
X-ray scattering (SAXS) have yet been done. The interaction of L64 with three different cationic surfactants was investigated by Mahajan et al. using SANS [67]. These authors employed the surfactants hexadecyltrimethylammonium bromide (HDTAB), tetradecyltrimethylammonium bromide (TTAB), and dodecyltrimethylammonium bromide (DTAB). For all studied cationic surfactants and all ratios of L64 to surfactant, the authors report ellipsoidal micelles. Since this is the preferred shape of the micelles of the pure cationic surfactants, they conclude that in this case the shape is dominated by the surfactant [67].

A recent study by Hamley et al. also treats the interaction of different poly(oxyalkylene) BCPs with SDS. One of the studied systems is P84 (PEO₁₉-PPO₄₃-PEO₁₉) and the found behavior was consistent with the previous works. The surfactant interacts with the hydrophobic parts of the Pluronic and subsequent formation of polymer–surfactant complexes is observed. Again, with increasing SDS content these complexes break down progressively.

Like Almgren et al., Hoffmann and coworkers have also looked in detail at the problem of decomposition of Pluronic micelles upon addition of surfactant [68]. In this work, the authors use different methods (e.g., surface tension measurements, calorimetry, and dynamic light scattering, DLS) to investigate the polymer F127 (PEO₉₇PPO₆₉PEO₉₇, M_w 12,500 g/mol). In aqueous solution, the pure polymer is found to form micelles with a hydrodynamic radius R_h of approximately 11 nm. Addition and subsequent increase of SDS leads to a decrease of the observed micellar size down to 1 nm. In these mixed micelles, one polymer molecule is surrounded by ca. 6 SDS molecules. Measurements of the birefringence of these solutions led the authors to predict an anisometric structure for the obtained aggregates (see Fig. 3). Mixed systems of F127 with the cationic surfactant TTAB were characterized by Wyn-Jones et al. [69]. The observations are very similar to the previous studies. TTAB binds to F127, leading to the formation of mixed micelles. These are then found to completely break down upon further increase of the TTAB concentration. Interesting is the finding that low TTAB concentrations induce a decrease in the critical micellization temperature (cmt) of the polymer.

Jansson and coworkers presented DLS and calorimetric investigations of the tri-block copolymers P123 and F127 [31]. First they characterized aqueous solutions

Fig. 3 Aggregates obtained in F127/SDS mixtures (redrawn after [68]). The hydrophobic PPO part interacts with the surfactant alkyl chains



of the two polymers at ca. 40°C and sufficiently high concentrations. Under these conditions, both polymers are found to form predominantly micelles. For P123, they estimate the critical micelle concentration (cmc) to be 0.2×10^{-3} wt%. This value is in good agreement with the results of Hoffmann and coworkers [65]. The size of the pure polymer micelles was characterized in terms of the hydrodynamic radius and found to be approximately 10 nm for P123 and 12.5 nm in the case of F127.

Then, these polymers were mixed with SDS or CTAC and the obtained structures investigated as a function of added surfactant concentration. Also in this case, disintegration of the polymer micelles starts upon addition of ionic surfactant. The authors identify three concentration regimes. At low surfactant concentrations, large mixed polymer/surfactant micelles are formed. This regime is followed by a region of intermediate surfactant concentrations where large mixed micelles coexist with smaller aggregates containing just one polymer molecule. Finally, at high surfactant content only small micellar species “survive”. These findings are in good overall agreement with the works of Hoffmann et al. [65, 68], Almgren and coworkers [56], and Wyn-Jones et al. [69]. The P123/hexadecylammonium chloride (C₁₆TAC) complexes were further characterized in a subsequent work by Jansson et al. [70]. In this study, one of the key tools was SAXS, which allows determination of the interaction between the mixed micelles. The authors use the structure factor $S(q)$ for this purpose and applied the recently developed generalized indirect Fourier transformation method to compute $S(q)$ from scattering functions [71].

Jansson et al. investigated the interaction of P123/C₁₆TAC micelles over a wide range of molar ratios (0–19.3). For low molar ratios, the structure factor is treated in terms of the Perkus–Yevick approximation (PY). High molar ratios (namely 19.3) were analyzed by applying the hyper-netted chain model (HNC). Figure 14 in [70] shows the computed structure factors of different samples. Based on the calculation of $S(q)$, the authors conclude that the pure P123 micelles exhibit only weak interparticle repulsive interactions that mainly arise from excluded volume effects. Upon addition of the hexadecylammonium chloride, the surfactant molecules associate with the P123 micelles, which leads to a steadily enhanced repulsion.

Finally, at the highest molar ratio all P123 micelles were decomposed and only small surfactant/P123 complexes remain. These exhibit strong electrostatic repulsion and the structure factor can be well described using a Yukawa-type potential and the HNC approximation. These findings are in line with the results of the earlier works.

To our knowledge, currently only one article on the subject of the interaction between Pluronics and gemini surfactants is available [72]. This work treats the interaction of the Pluronics F108 and P103 with gemini surfactants of the type (oligooxa)-alkanediyl- α, ω -bis(dimethyldodecylammonium bromide)/(12-EO_x-12) with x ranging from 0 to 3. The experimental method used in this work was isothermal titration calorimetry. The interaction between P103 and the cationic gemini surfactants leads to very strong enthalpy change compared to that using classical surfactants. Moreover, the interaction between these surfactants and P103 is stronger than that for F108. This fact is explained by the higher hydrophobicity of P103 due to the shorter PEO chains.

2.1.1 Systems with More Components

In systems designed for applications, more components are usually present. Oils are of high relevance in this context, but pharmacologically relevant compounds may also be added to Pluronics, since these BCPs are also discussed in the framework of drug delivery.

In this context, a work by Egger and coworkers should be mentioned in which they used the addition of C₈TAB to control the phase behavior of P105 in the ternary system (P105)/*o*-xylene/water. The studied system was polymer-rich and a copious phase behavior develops upon addition of the surfactant. This indicates that the surfactant has a strong influence on the curvature and elasticity of the P105 film separating the two immiscible components, water and *o*-xylene [73]. All structuring processes in equilibrium phases are determined by the free energy, and in systems exhibiting low interfacial tensions the most important contribution to the free energy arises from the curvature energy of the interfacial film. Its contribution is governed by the film elasticity, which can be described by two elastic constants κ and $\bar{\kappa}$. This relationship is quantitatively described by the Helfrich equation [74]:

$$F = \int_S \left(\frac{1}{2} \kappa (C_1 + C_2 - 2C_0)^2 + C_1 C_2 \bar{\kappa} \right) dS \quad (2)$$

Here, C_0 is the spontaneous (or “natural”) curvature and C_1 and C_2 are the principal curvatures of the film. S is the interfacial area in the sample. An interfacial film exhibits a stable equilibrium curvature if $-2\kappa < \bar{\kappa} < 0$ holds. This corresponds to a minimum in the curvature free energy. For flat interfaces (e.g., lamellar phases) C_0 is zero. Besides κ , an additional parameter is necessary for description of the behavior of phases consisting of stacked bilayers. This parameter is the compressibility modulus \bar{B} , which describes the interaction between the layers [75–77].

Information about the elasticity can be obtained using a variety of scattering methods. Small-angle scattering is mainly used for systems with small interlamellar spacing [75, 77–82], whereas light scattering can be applied for the study of swollen systems [76, 83, 84]. Neutron spin-echo spectroscopy has also been used to directly measure the bilayer dynamics in lamellar liquid crystalline phases [85–87].

In their publication Egger et al. mainly study the properties of a lamellar phase obtained in the quaternary system PEO₃₇-PPO₅₈-PEO₃₇ (P105)/C₈TAB/*o*-xylene/water [73].

The structure of a lamellar phase L_α is characterized by two important parameters, the interlamellar distance d and the already-mentioned elasticity of the amphiphilic film. The interlamellar distance is directly computed from the position of the Bragg singularities of the structure factor $S(q)$ by:

$$d = \frac{2n\pi}{q_{0,n}} \quad (3)$$

Here, $q_{0,n}$ is the q value associated with the corresponding peak-maximum of the n th-order peak. The scattering vector q is given by:

$$q = \frac{4\pi}{\lambda} \sin\left(\frac{\Theta}{2}\right) \quad (4)$$

with λ being the wavelength of the radiation and Θ the scattering angle.

The relative elasticity of the amphiphilic films determines the shape of the Bragg peaks, which can be analyzed using the model of Caillé [78, 88]. In this model, the peak is described by:

$$I(q) \propto |q - q_0|^{-2+\eta} \quad (5)$$

In the approach by Nallet and coworkers, smearing effects and form factor contributions are also included [75]. The description of the scattering pattern of a lamellar phase derived by Nallet et al. combines the form factor of the bilayer with a structure factor relating the broadness of the peak (quantified in terms of the Caillé-constant η) to the elasticity of the bilayer by:

$$\eta = \frac{q_0^2 k_B T}{8\pi \sqrt{\kappa \bar{B}}/d} \quad (6)$$

Here, k_B is the Boltzmann constant, κ is the splay modulus, and \bar{B} is the modulus associated with the barocline mode of the bilayer [75].

The findings of the work by Egger and colleagues can be summarized as follows [73]. The interlamellar spacing d is found to be of the order of 11–13 nm, dependent on the composition of the bilayer. d strongly depends on the polymer concentration, but is nearly independent of variations in surfactant concentration. A calculation of the space of the polymer at the interface gives values between 1 and 3 nm², which change as a function of the composition. The thickness of the whole layer is around 4–5 nm, but only an inner layer of about 1 nm (consisting mainly of the bromine counterions of the C₈TAB and water) dominates the form factor contribution in the X-ray measurements.

Moreover, a variation in the molar ratio of surfactant to polymer between 7 and 13 does not have any effect on the width of the first-order Bragg peak. In terms of the Caillé constant, this would usually be interpreted as a constant elasticity of the bilayer. However, neutron spin-echo experiments on the same system reveal that the addition of surfactant significantly changes the bending elasticity of the polymer-based lamellar phase (Egger et al., unpublished results). The width of the first-order Bragg peak remains constant because of the influence of the increasing electrostatic repulsion, which is due to the increased number of charges associated with the C₈TAB. This changes the compressibility of the bilayer stack (\bar{B}). Hence, decreasing κ is compensated by increasing \bar{B} in this system, leading to a nearly constant value of the Caillé constant η .

Several interesting works dealing with the incorporation and localization of hydrophobic compounds into Pluronic/surfactant mixed micelles were recently

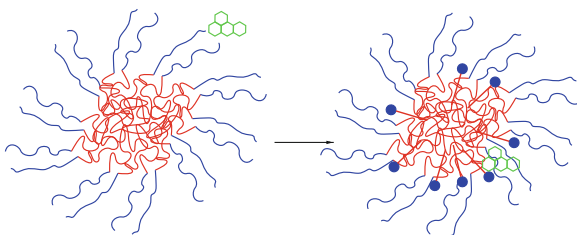


Fig. 4 F88 micelles in the absence (*left*) and presence (*right*) of the surfactant CTAC (*filled circles*). The *green symbols* represent the fluorescence dye. In pure F88 micelles the dye is located in the outer hydrophilic and water-swollen corona. When the surfactant is added, the electrostatic attraction between the dye C343 and the positively charged CTAC headgroups drags the dye inside the mixed micelles

published by Singh and coworkers and by Bhattacharyya et al. [89–92]. In these works, P123 and F88 are studied in the presence of CTAC. These aqueous ternary systems were mixed with small amounts of a fluorescent probe (C343) (see scheme in Fig. 4). The shift of the fluorescence gives information about the local environment of the fluorescence probe. The authors report the interesting finding that the CTAC addition drives the negatively charged fluorescence dye inside the micelles. This can be understood by assuming that the CTAC headgroups (positively charged) are located at the boundary between the hydrophobic and the hydrophilic part of the Pluronic micelle and that the electrostatic interaction “sucks” the fluorescence probe inside the mixed micelle. However, the length of the ethylene oxide block seems to be crucial for the penetration depth of the dye.

2.2 Nonionic Surfactants

Polar compounds like alcohols or sugars can be seen as the simplest case of a non-ionic “surfactant”. Therefore, we will start the discussion with mixtures of such OH-containing compounds with BCPs. Their influence on the structure formation in solutions of amphiphilic triblock copolymers was studied by Alexandridis et al. [93, 94].

In these works the influence of different alcohols (ethanol, glycerol, propylene glycol, and glucose) on the phase behavior of P105 was studied mainly by small-angle X-ray scattering. This is a simple process that involves looking at the liquid crystalline phases of the polymer and analyzing the respective peak positions as a function of alcohol concentration. Changes in the peak positions were attributed to changes in the “natural” curvature of the BCP film due to swelling of the different blocks by the added alcohols.

One of the best-investigated groups of nonionic surfactants are the oligo ethylene glycol mono-*n*-alkyl ethers (see e.g., [38, 95]). Calorimetry-based examinations of the interaction of one of these surfactants (hexaethylene glycol mono-*n*-dodecyl ether; C₁₂E₆) with the Pluronic F127 (PEO₉₇PPO₆₉PEO₉₇) and L64

(PEO₁₃PPO₃₀PEO₁₃) were published by Couderc and coworkers [96, 97]. The most important result of these studies is that there is a strong interaction between F127 and C₁₂E₆. In addition, the authors also investigated the influence of the homopolymers PEO and PPO on the cmc of C₁₂E₆. The homopolymers have no significant effect on the micelle formation. Hence, interaction (co-micellization) is related to the amphiphilic nature of the Pluronic. The cmc for the F127/C₁₂E₆ mixture was determined for several different ratios, and the authors were able to describe the observed behavior using a regular solution theory [96]. The same holds for the L64/C₁₂E₆ system [97]. In conclusion, these studies reveal that there is a synergy between F127 and C₁₂E₆ that makes this type of mixture interesting for technical solubilization problems.

The micellar shape of L64 micelles in the presence of the nonionic surfactant Triton X-100 was investigated by Mahajan and coworkers using SANS. They found that, in contrast to ionic surfactants, the shape is dominated by the L64 and that the formed mixed micelles are always spherical [67]. Without L64, Triton X-100 forms micelles of ellipsoidal shape. Unfortunately, the authors did not study other non-ionic surfactants with different headgroup areas and tail volumes. A study very similar to the one by Egger and coworkers [73] (see previous section) was published by Kunieda and coworkers. However, instead of a cationic surfactant these authors used penta(oxyethylene) dodecyl ether (C₁₂E₅) and penta(oxyethylene) oleyl ether (C_{18:1}E₅). The investigated Pluronics were P85 and P105 [98]. In this case, the surfactants can also be used to tune the phase behavior of the system and the properties of, e.g., the lamellar phase (interlamellar spacing, etc.). With C₁₂E₅, an extended lamellar phase region is formed in P86 solutions. With P105, the phase behavior was slightly different. Only upon addition of high amounts of C₁₂E₅ a lamellar polymer-rich phase was generated. This phase was found to coexist with a lamellar phase of pure C₁₂E₅.

In recent works, mixed systems of P123 and C₁₂E₆ were investigated by scattering techniques [99, 100], calorimetry [101], and rheology [102]. The most important findings in these works were a decrease in the critical aggregation concentration (cac) of the polymer, which was induced by the presence of the nonionic surfactant C₁₂E₆ and the sphere-to-rod transition that was induced by the surfactant.

3 Diblock Copolymers

A common point in several of the publications treating diblock copolymers is the fact that the used copolymers often comprise a PEO block as a hydrophilic part. A system very similar to the previously discussed Pluronics is a diblock copolymer of ethylene oxide and propylene oxide. This type of copolymers was studied by, e.g., Taboada et al. [103, 104]. Unfortunately, to our knowledge no data are available concerning the interaction of these PPO–PEO diblocks with surfactants. It would certainly be of interest to compare the behavior of these systems to the findings for Pluronic surfactant mixtures. However, as already mentioned, most of the diblock

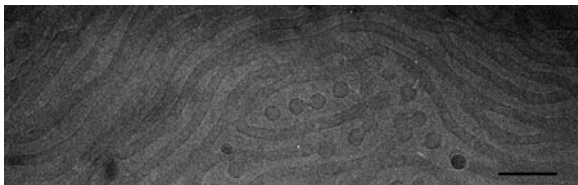


Fig. 5 Cryo-TEM image of solution of PEO₆₂-PB₄₀ in water. *Scale bar*: 100 nm

copolymers employed in studies on copolymer–surfactant interaction contain a PEO block. It is known that the presence of PEO in surfactant solutions leads to a significant decrease of the cmc of the respective surfactant. Often, a kind of pearl-necklace structure of micelles interconnected by the PEO was observed [105–107].

As hydrophobic block, several groups have used different chains. Polystyrene (PS) was studied by Bronstein and coworkers [27]. Nordskog and coworkers have investigated different PEO-*b*-polybutadiene copolymers (PEO₅₃-PB₃₇ [28], and PEO₆₂-PB₄₀ [29, 30], PEO₁₂₅-PB₁₅₅ [108]). Figure 5 shows an example of the structures found in aqueous solutions of PEO₆₂-PB₄₀. The polymer mainly forms rod-like aggregates. The other two investigated PB–PEO diblock copolymers also form rod-like structures in water when no surfactant is added. A homologous system with a slightly different block length was recently studied by Shimoni and Danino [109].

Works on the co-micellization of PEO-*b*-poly(methacrylate) (PEO-*b*-PMA) with charged surfactants were also published [110]. The PEO-*b*-PMA copolymers belong to the group of so-called double hydrophilic BCPs. A special case in this group are double hydrophilic BCPs, which have one block that can become hydrophobic upon heating or due to changes in other external parameters. An example of this kind of systems is PEO-*b*-poly(*N*-isopropylacrylamide) (PEO-*b*-PNIPAM), which was studied recently [111]. PNIPAM has a θ temperature of ca. 33°C in water and wants to phase-separate beyond this so-called lower critical solution temperature (LCST). In the following subsections all the mentioned works will be summarized.

3.1 Ionic Surfactants

Bronstein and coworkers have investigated PS-*b*-PEO (PS_{*n*}-*b*-PEO_{*m*}, with $n \approx 10$ and $m \approx 68$) in aqueous solution and in mixtures of this polymer with cetyl pyridinium chloride (CPC) and SDS [20, 21, 27]. DLS experiments on the pure PS-*b*-PEO solutions reveal two relaxation modes. The faster one is attributed to micelles and the slower one to micellar clusters. Addition of surfactant to these solutions significantly alters the structures found.

In contrast to the behavior of the triblock copolymers described in the previous section, the PS_{*n*}-*b*-PEO_{*m*} block copolymers were found to behave differently. Using DLS and ultracentrifugation, Bronstein et al. were able to show that the mixtures

are rather complex and contain micelles, micellar clusters, and supermicellar aggregates. At approximately $14\times$ cmc, excess micelles of the added surfactant are formed.

The same type of diblock copolymer with slightly different block length was also characterized by Castro et al. with respect to its interaction with SDS [112]. The polymer is poly(styrene oxide)-PEO with 17 and 65 monomer units, respectively. In aqueous solution, this polymer forms micelles with a hydrodynamic radius of approximately 12.7 nm and an aggregation number of ca. 150 [113]. On the basis of measurements of the dissymmetry of the static light scattering intensity [114], the structure of the formed polymer micelles was found to be spherical [113]. The cmc of this type of diblock copolymer was found to be very low.

Upon addition of SDS, the hydrodynamic radius of the formed structures decreases to approximately 1 nm, indicating a complete decomposition of the polymer micelles similar to that observed in the case of Pluronics. This would mean that this type of polymer behaves differently compared to the similar polymers studied by Bronstein et al. and also differently to the PB-*b*-PEO copolymers discussed next. The same authors additionally investigated a similar poly(styrene oxide)-PEO polymer with 15 and 63 monomer units) [115]. In this study, the authors used sodium decyl and sodium octyl sulfate as well as SDS as surfactants. Sodium dodecyl and sodium decyl sulfate were found to have a similar influence on the BCP micelles. The interaction between PS₁₅-*b*-PEO₆₃ and sodium octyl sulfate was found to be weaker than for the other two anionic surfactants, and higher amounts of this slightly more hydrophilic compound have to be added to obtain a decomposition of the BCP micelles. However, a problem in studies of BCPs with PS blocks is certainly the high glass transition temperature of the PS ($T_g \approx 378$ K) making equilibration rather slow. In solutions of only the polymers, the obtained micelles are usually completely frozen.

Nordskog et al. observed a behavior similar to that found by Bronstein et al. for mixed systems of PEO₆₂-*b*-PB₄₀ with DTAB [29]. In this work, worm-like BCP micelles were characterized by SANS, DLS, and Cryo-TEM. Upon addition of the cationic surfactant, the apparent hydrodynamic radius (R_h) calculated for these block copolymer solutions started to decrease until a plateau value of approximately 15 nm was reached. Further addition of surfactant did not lead to any further change in size of the mixed polymer/surfactant micelles. Using SANS it was possible to show that above a certain threshold concentration, excess micelles of the surfactant were formed. Below this threshold, all added surfactant is incorporated into mixed BCP/DTAB micelles and, hence, the change in size is due to structure reorganization induced by the DTAB.

The same polymer was also studied in mixtures with SDS [30]. With this anionic surfactant, the observed change in the apparent hydrodynamic radius was similar. In Fig. 6 the change is plotted schematically.

For all used surfactants, the found change occurs in a rather narrow interval of surfactant concentrations.

A series of PEO-PB copolymers mixed with SDS was also studied by Pispas and Hadjichristidis [116]. For the polymers PB₁₈₃-*b*-PEO₂₀₀ and PB₁₇₆-*b*-PEO₄₃₆,

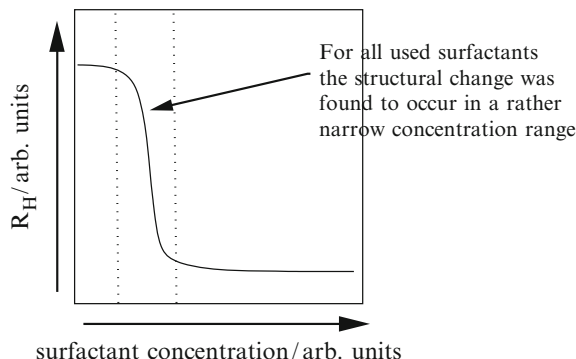


Fig. 6 Apparent hydrodynamic radius (R_h) of the mixed BCP/DTAB micelles as obtained from a second-order cumulant analysis of the intermediate scattering functions of the PEO₆₂-*b*-PB₄₀ surfactant mixtures in water. The above behavior was observed for SDS, CTAB, and also for C₁₂E₅

the behavior upon addition of SDS is very similar to the findings by Nordskog et al. However, for two slightly different polymers with shorter PB block (PB₂₂-*b*-PEO₃₇₇ and PB₂₆-*b*-PEO₈₆) the authors did not observe a monodisperse sample at high SDS concentrations. Laplace inversion of the correlation functions obtained using DLS always indicated the presence of a slow mode. This behavior corresponds to the findings reported for PEO₆₂-*b*-PB₄₀/SDS [30] and also to recent results by Shimoni and Danino [109]. At intermediate concentrations, these systems also exhibited a bimodal decay of the intensity correlation functions. At concentrations much higher than the cmc of SDS, the correlation function of the solutions of the PEO₆₂-*b*-PB₄₀/SDS mixtures became finally monomodal. This suggests that such a regime might also be reached for PB₂₂-*b*-PEO₃₇₇ and PB₂₆-*b*-PEO₈₆ upon further increase of the SDS concentration.

A diblock copolymer that is very close to PEO-*b*-PPO is the PEO-*b*-poly(butylene oxide) (PEO-*b*-PBO) system. This kind of BCP was mixed with SDS by Hamley and coworkers and they found a drastic increase of the observed hydrodynamic radius from about 9 nm to approximately 100 nm, even at the lowest studied SDS concentration. Such a big increase of R_h can only be interpreted by the formation of vesicles. Figure 7 is taken from the original paper [55] and the size distributions shown (obtained by DLS) clearly reveal the size increase. Only for the highest SDS concentration peaks, probably corresponding to excess SDS micelles can be observed. All measurements were done at 1 wt% of PEO₁₈-*b*-PBO₁₀. Looking at these results again shows that studies of PEO-*b*-PPO might also lead to unexpected interesting results.

The system MPEG₅₃-*b*-PNIPAM₁₁₃ (MPEG is PEO with a methyl endgroup) was studied by Pamies et al. [111]. SDS was used as surfactant component in this work too. Related to the thermo-responsive character of the PNIPAM block, this type of BCP exhibits an interesting self-assembly behavior. SDS has a strong influence on this behavior, and the finally obtained structure depends on the temperature and the SDS concentration. The results are summarized by the authors

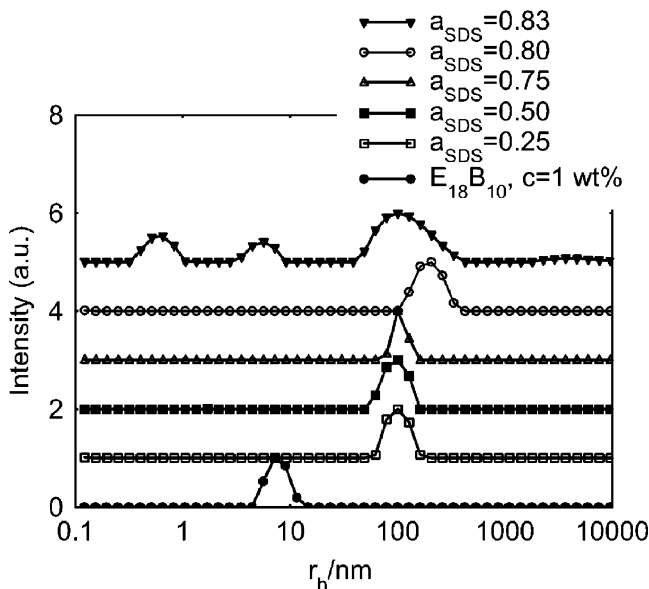


Fig. 7 Distributions of hydrodynamic radius (R_h) in aqueous mixtures of $\text{PEO}_{18}\text{-}b\text{-PBO}_{10}$ with SDS. R_h of the pure polymer aggregates is about 9 nm. The addition of SDS leads to an enormous increase in R_h , which can only be explained by vesicle formation. Copyright Elsevier; reproduced from [55] with permission

schematically. The scheme is reproduced in Fig. 8 and shows that real mixed micelles of SDS and $\text{MPEG}_{53}\text{-}b\text{-PNIPAM}_{113}$ are obtained for intermediate SDS concentrations. At higher SDS content, the surfactant forms micelles inside the MPEG_{53} brush of the BCP micelle. All formed structures are found to change with changes in temperature.

Other interesting systems are $\text{PEO-}b\text{-PMA}$ mixtures with cationic surfactants. Kabanov and coworkers studied these systems by applying a variety of different techniques and found the formation of mixed polymer surfactant complexes [110, 117]. In both studies, they investigated mixtures of $\text{PEO}_{176}\text{-}b\text{-PMA}_{186}$ with the surfactants CTAB, DTAB, TTAB, cetylpyridinium bromide (CPB), and dodecylpyridinium bromide (DPB). In stoichiometric mixture (charge neutrality), aggregates with diameters ranging from 85 to 125 nm were observed. Electron microscopy using staining techniques revealed that the formed structures are vesicles.

The same authors also examined the structural changes in these systems induced by changes in block length of the BCPs. Besides the previously studied $\text{PEO}_{176}\text{-}b\text{-PMA}_{186}$, this work presents data for $\text{PEO}_{210}\text{-}b\text{-PMA}_{35}$ [118]. Turbidity measurements indicate that the BCPs with the shorter PMA block lead to more turbid solutions upon addition of the surfactants. However, the size of the obtained complexes is similar.

In a more recent article, the same group studied the stability of mixtures of $\text{PEO}_{210}\text{-}b\text{-PMA}_{97}$ with hexadecyltrimethylammonium bromide (HTAB). For an

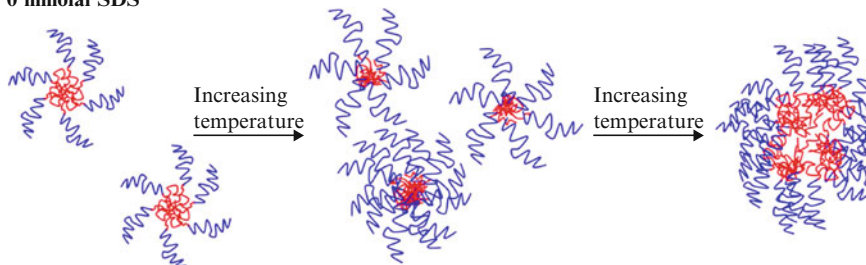
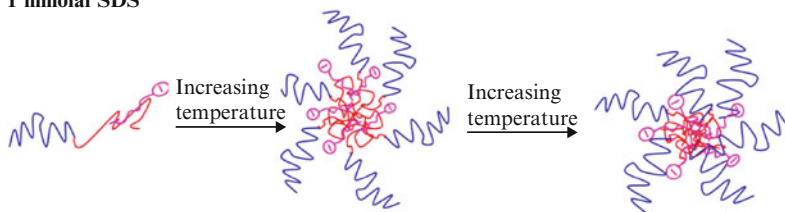
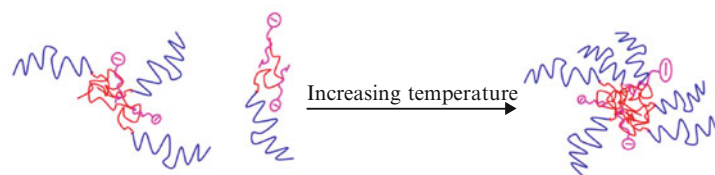
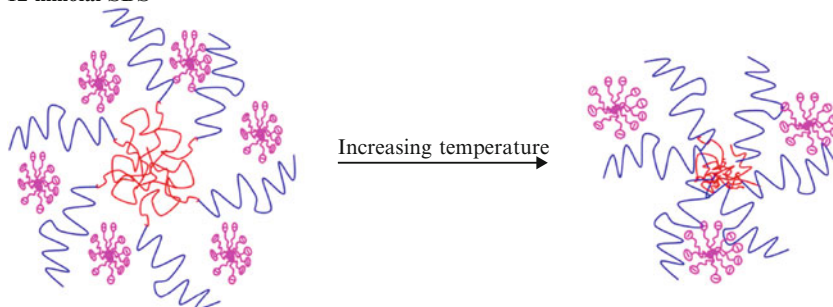
0 mmolal SDS**1 mmolal SDS****6 mmolal SDS****12 mmolal SDS**

Fig. 8 Effect of SDS addition and temperature on the assembly and contraction of polymer surfactant complexes in aqueous solutions of the diblock copolymer MPEG₅₃-*b*-PNIPAM₁₁₃. Copyright Elsevier; reproduced from [111] with permission

electro-neutral mixture, they observed stable aggregates with an effective diameter of 80 nm by DLS [119]. The identical polymer was also used to investigate the anisotropy of the formed complexes and their change upon addition of aliphatic alcohols [120].

A study systematically changing the degree of charge of mixed PEO₁₇₀-*b*-PMA₁₈₀/CTAC micelles was published by Li and Nakashima [121]. In this study, the

authors found two main factors that have an impact on the size of the obtained mixed polymer/surfactant micelles. The first parameter is the polymer concentration, and the second is the degree of charge reached upon addition of the cationic surfactant CTAC. The most important experimental techniques used in this work were DLS and fluorescence spectroscopy employing pyrene and other probe molecules.

At charge neutrality, the authors increased the polymer concentration and found the formation of stable micelles above a polymer weight concentration of 0.01 g/L. The hydrodynamic radius of the obtained mixed micelles was approximately 38 nm and remained constant upon further increase of the concentration. Hence, the authors concluded that the cac for the totally charge-neutral polymer surfactant mixture is close to 0.01 g/L (see Fig. 3b of [121]). For lower ratios of polymer to CTAC (incomplete charge neutralization) the found micelles are larger, growing up to $R_h = 100$ nm for the lowest CTAC concentration used. The fluorescence investigation revealed that the probes are incorporated in a region of the mixed micelles that exhibits a polarity comparable to, e.g., ethyl acetate.

A further BCP studied by the Kabanov group was PS-*b*-poly(acrylic acid) (PS-*b*-PAA). In all cases the PS block had a length of 86 monomer units. The PAA block length was varied from 100 up to 900 acrylate units. These polymers precipitated upon addition of CPB [122].

The aforementioned group has also studied the interaction of amphiphilic diblock copolymers with surfactants carrying the same charge as the polyelectrolyte block [123]. The ionic block in this study was poly(*N*-alkyl-4-vinylpyridinium bromide) and the cationic surfactants added were CTAB, DTAB, CPB, and DPB. It was shown that the surfactants form different structures with the charged amphiphilic diblock copolymers. The type of structure formed depends on the surfactant concentration. At low surfactant concentration ($\leq cmc$), hydrophobic clusters are formed that consist of the surfactant alkyl chains and the hydrophobic block of the copolymer. At high surfactant concentration, a change in complexation character is reported [123].

Poly(α -methylstyrene)-*b*-poly(*N*-ethyl-4-vinylpyridinium) copolymers (PMeS-*b*-PE4VP) were also scrutinized by Kabanov et al. [124]. The publication focused on the interaction of PMeS₁₂₀-*b*-PE4VP₂₉₀ with the two-tail surfactant sodium bis(2-ethylhexyl)sulfosuccinate (AOT). The formed complexes were found to precipitate from aqueous solutions, but could be solubilized in most common organic solvents.

3.2 Nonionic Surfactants

Co-micellization of diblock copolymers with nonionic surfactants has not been as intensely studied as the other previously discussed cases. Some results for a mixture of PB₄₂-*b*-PEO₆₀ with the nonionic surfactant C₁₂E₅ will be presented [125].

DLS experiments were performed for several mixtures of the polymer with increasing amounts of C₁₂E₅. In the following the surfactant concentration is given as

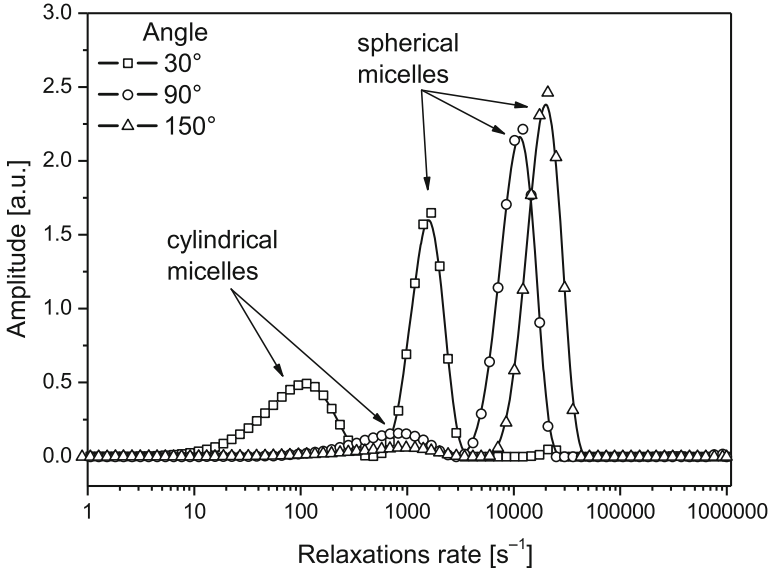


Fig. 9 Relaxation rate distribution for mixed solutions of B₄₂-b-EO₆₀ and C₁₂E₅ with molar ratio $r_m = 2$ for three different scattering angles. The two modes reveal the coexistence of worm-like and spherical aggregates

r_m . r_m is the molar ratio of the total surfactant concentration to the total copolymer concentration as given by:

$$r_m = \frac{C_{C_{12}E_5}}{C_{PB_{42}-b-PEO_{60}}}. \quad (7)$$

The measured intensity time correlation functions were analyzed by inverse Laplace transformation [126, 127], leading to the relaxation rate distributions shown in Figs. 9 and 11.

The results shown in Fig. 9 were obtained for a r_m value of 2. The computed distribution is found to be bimodal. This was also the outcome for pure aqueous PB₄₂-b-PEO₆₀ solutions [29] (see Fig. 5). In Fig. 10 the z -averaged relaxation rates for both modes are plotted against the squared magnitude of the scattering vector q^2 . Both modes show a linear dependence on q^2 that is typical for center of mass diffusion. From the slopes of the linear fit, the diffusion coefficients and hydrodynamic radii were computed, leading to apparent hydrodynamic radii $R_h = 175$ and 11 nm, respectively.

In Fig. 11 the situation is different. The distribution functions shown are only mono-modal and were obtained for a higher surfactant concentration ($r_m = 7$). This clearly indicates that the large BCP aggregates were decomposed and that smaller mixed micelles with a narrow size distribution were obtained. This observation is similar to the effect observed upon addition of SDS and C₁₂TAB [29, 30] and suggests a behavior of the R_h value of the polymer micelles as depicted in Fig. 6. The hydrodynamic radius computed from the data in Fig. 11 is 13.4 nm. This value is

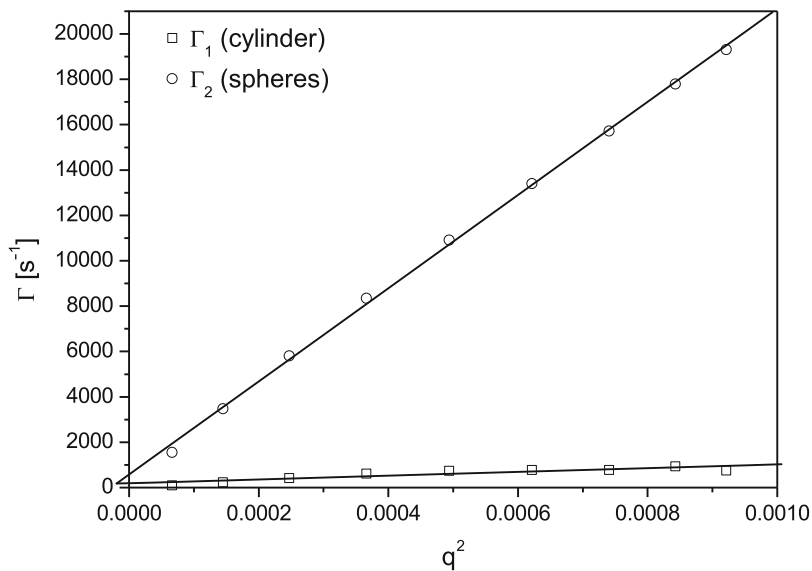


Fig. 10 The z -averaged relaxation rates (Γ) as a function of q^2 for the two modes shown in Fig. 9

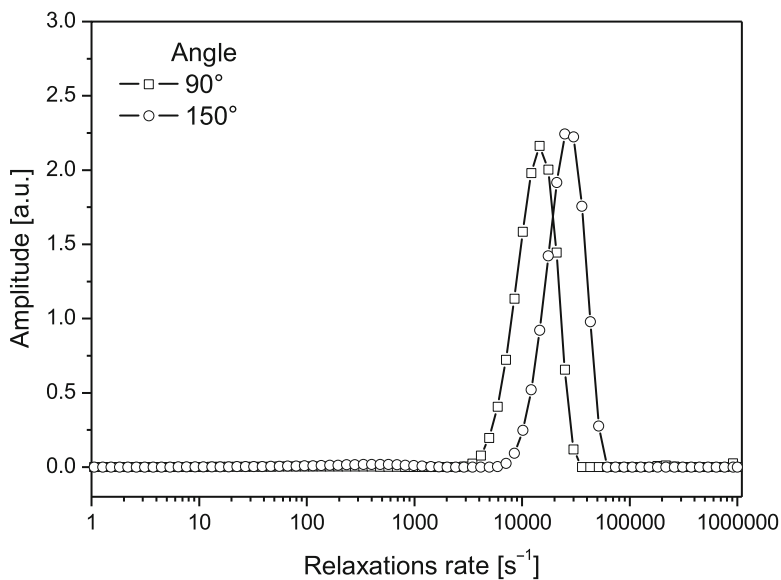


Fig. 11 Relaxation rate distribution for mixed solutions of B_{42} - b -EO₆₀ and C₁₂E₅ with molar ratio $r_m = 7$ for three different scattering angles. Only one mode could be detected (corresponding to spherical micelles)

close to the previously reported radii for mixed micelles with SDS and C₁₂TAB. The headgroup area of the three surfactants is similar and, hence, has a similar influence on the packing of the BCP molecules. In all cases, the polymer content of the finally obtained mixed micelles is rather high and the behavior of the PB-*b*-PEO polymers differs significantly from the comportment of Pluronics. These results are in good agreement with a recent study by Shimoni and Danino [109]. This group studied the structure formation in mixtures of PEO₁₁₄-*b*-PB₁₀₂ with the nonionic surfactant Triton X-100.

A system analogous to the PB-*b*-PEO polymers are poly(isoprene)-*b*-PEO copolymers (PI-PEO). This type of copolymer was studied by Kunieda and coworkers in mixtures with the nonionic surfactants C₁₂E₃, C₁₂E₅, C₁₂E₆, C₁₂E₇, and C₁₂E₉ [128]. The starting point in these investigations was the respective pure surfactant solution, and PI-PEO (C₂₅₀EO₇₀) was subsequently added. Therefore, only the region of the phase diagram with high polymer content should be comparable to the studies of the PB-PEO/surfactant mixtures.

However, for this region of the phase diagram the authors found evidence for the formation of spherical composite micelles with the different C₁₂E_{*n*} surfactants. This is very similar to the behavior of the PB-PEO system in the presence of ionic and nonionic surfactants. For the surfactants C₁₂E₇ and C₁₂E₉, Kunieda et al. report the presence of two distinct micellar species, one copolymer-rich and the other only containing surfactant. This observation is in agreement with the findings for the mixture of PB₄₀-PEO₆₂ with SDS, where excess surfactant micelles were also found using SANS [29].

An interesting type of diblock copolymer is the group of PEO-poly(dimethylsiloxane) polymers [129]. Recently, the phase behavior of these polymers was investigated as a function of added nonionic surfactant (C₁₂E₅). Mixing of these two compounds in water induces the formation of several liquid crystalline phases [130].

3.2.1 Systems with More Components

One of the most striking effects with respect to BCP-surfactant interaction is certainly the efficiency-boosting effect of BCPs in microemulsions [41–44].

This effect was studied for several surfactants of the C_{*i*}E_{*j*} type by adding poly(ethylene propylene)-*b*-PEO (PEP_{*x*}-PEO_{*y*}) copolymers to the respective microemulsion. The phase behavior of a ternary system of oil, water, and C_{*i*}E_{*j*} is very complex and can be tuned using temperature since the hydration of the ethylene oxide part of the surfactant, and therefore the packing parameter, changes with temperature [37–40, 131].

The easiest way to represent the changes in the phase behavior of these systems is to monitor the changes in a so-called fish diagram. This specific cut through the phase prism is schematically shown in Fig. 12.

Efficiency boosting mainly leads to two changes in the fish diagram. The X-point moves to the left (to lower total surfactant concentration) and the three-phase region becomes smaller (fish body). This was shown by Stubenrauch and coworkers for the system H₂O-*n*-octane-C₈E₃ [132].

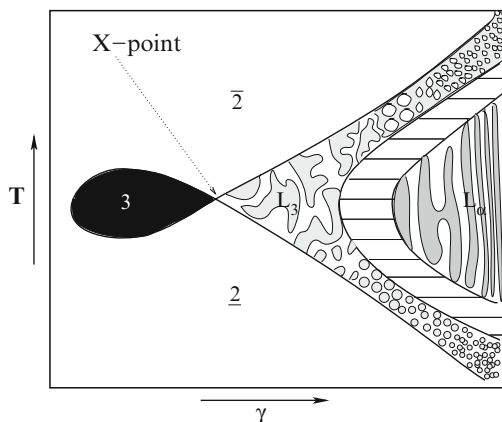


Fig. 12 Scheme of a cut through the temperature-dependent phase prism of microemulsions based on $C_{12}E_6$ surfactants. This type of cut is known as a fish diagram. To compare the phase behavior of different systems it is usually sufficient to investigate the changes of the position of the *X-point* (fish tail point). γ denotes the total surfactant mass fraction. In the case of BCP-containing microemulsions, γ also includes the BCP mass. The black area (fish body) indicates the three phase region where an excess water and an excess oil phase coexist with a bicontinuous microemulsion. At the fish-tail point the system becomes monophasic and first a bicontinuous structures appears (L_3). L_α then indicates the formation of a lamellar phase at higher surfactant content. Above and below the fish 2 phase regions occur

Upon addition of PEP₅-PEO₅, the X-point moves strongly the left without significantly changing the temperature dependence. The effect becomes more pronounced with increasing polymer concentration. When 15% of the total amount of surface active components is polymer, γ can be as low as 0.02 to reach a single phase microemulsion. In the absence of the BCP, the surfactant weight fraction has to be 10 times higher for a complete solubilization of both solvents in a microemulsion. In the same article, a very similar behavior was reported for H₂O-*n*-decane-C₁₀E₄ with the same BCP. However, for this microemulsion the efficiency boosting by PEP₅-PEO₅ also leads to a growing lamellar phase (L_α), which finally extends to the X-point.

The size of the used BCP does not significantly influence the efficiency-boosting effect, but longer polymer blocks are able to suppress the formation of the liquid crystalline phases [132]. The system H₂O-*n*-decane-C₁₀E₄ with PEP₅-PEO₅ was also studied by SANS [133].

4 Other Systems

There is of course a high number of other polymer structures available that also exhibit amphiphilicity and it is beyond the scope of this article to summarize all of these works. A few interesting examples will be mentioned. However, the selection is of course biased by the interests of the author.

4.1 Amphiphilic Poly(*p*-phenylenes)

The aggregation behavior of amphiphilically substituted poly(*para*-phenylenes) (PPP) was studied in our group [48, 134]. In these oligomers, each benzene ring of the aromatic backbone is substituted with an alkyl chain ($C_{12}H_{25}$) and an oxyethylene chain in *para* position to the alkyl substituent. This amphiphilic substitution scheme generates a boundary between the hydrophilic and hydrophobic substituents in a plane parallel to the major axis of the PPP. Amphiphilically substituted PPPs represent a relatively new class of materials. Applications of these and similar backbone polymers in photo- and electroluminescent devices might arise from their peculiar electronic structure. Moreover, their structure suggests an interesting self-assembly behavior, but to our knowledge only a few systems of this type have been studied so far [135–140].

In the case discussed here, the PPP oligomers were uncharged and due to the used substitution scheme similar to nonionic surfactants of the C_mE_n type. However, the oligomers were found to be insoluble in water. They could only be solubilized in the presence of surfactants (e.g., C_8E_4). Under these conditions the rather small oligomers self-assemble into huge rod-like mixed oligomer surfactant aggregates with a length between 300 and 800 nm, as estimated on the basis of DLS data [141]. Using SANS and solvent contrast variation, it was possible to calculate a PPP to surfactant ratio of 1:3 in these fiber structures [142]. This mixed self-assembled system is a good example of structures only arising from the interaction of a polymer with a surfactant.

During the last 6 years there has been growing interest in BCPs comprising bio-inspired blocks, which are currently of great interest [144–148]. Most of the published works only treat the structure formation of pure solutions of these polymers. Not much is known about the interaction with surfactants. A recent study of the BCP PS₃₈₈-poly(L-lysine)₁₃₈ is the only available work (at least to our knowledge) related to the interaction of surfactant with biohybrid copolymers [149]. In this study, the nonionic surfactant $C_{12}E_6$ was added to solubilize the BCP. This shows that surfactant can also be used in these slightly more complex BCP systems to change the packing and the curvature of the formed structures.

5 Summary and Outlook

Mixed BCP/surfactant systems are of growing interest, which manifests in the high number of publications treating this subject. However, it is still difficult to find systematic studies of the interplay between the two components and it is very important to vary parameters like the headgroup area and the alkyl chain length of the surfactant, and also the block length of the BCPs, over a wider range of values.

In summary, it can be said that these systems seem to follow the same principles as do “classical” surfactant/co-surfactant mixtures. Packing parameters and the natural curvature of the mixed films govern the formed structures. Hence, to some

extent the size and shape can be controlled by mixing BCPs with surfactants. Therefore, the answer to the question in the title is a “partial yes”.

Some differences between BCP/surfactant systems and surfactant/co-surfactant mixtures arise from the large difference in size and from the polymer-specific chain entropy contributions to the free energy of the systems. Moreover, in contrast to “simple” surfactant-based samples, the polydispersity of the polymer chains is also an important issue for structure formation. Polydispersity might lead to coexistence of different structures (e.g., spheres and worm-like structures) in the same polymer solution. This is due to the fact that small differences in the degree of polymerization of one of the blocks might lead to different packing parameters for a part of the size distribution.

For triblock copolymers of the Pluronics type, the interaction is now well established. These BCPs behave very similarly when mixed with different surfactants. The behavior is qualitatively independent of the block lengths and also independent of the type of surfactant used. At high surfactant concentration, a complete decomposition of the polymer micelles is usually observed. In the final state, the mixed micelles only contain a single polymer molecule. This behavior is caused by the interaction of the hydrophobic PPO block with the alkyl tails of the different surfactants. It is also a common feature of these mixed systems that low surfactant concentrations lead to a decrease of the cmt of the different Pluronics. However, for other triblocks the available number of studies is rather small and it is not necessarily possible to transfer the outcome of the studies on the behavior of Pluronics to other systems.

For diblock copolymers, the found behavior is even more diverse. This arises from the large variety of the different blocks having different T_g , charge, etc. However, screening the available results at least allows the identification of some similarities in the group of BCPs made of PEO and an apolar chain (e.g., PB or PS). In this case, the decomposition of the BCP micelles often leads to rather monodisperse mixed micelles containing more than one BCP molecule. Above a certain threshold in the surfactant concentration, additional surfactant leads to the formation of small surfactant micelles coexisting with the mixed ones.

Also, the group of double hydrophilic BCPs (e.g. PEO–PMA) shows some universality when oppositely charged surfactants are added. In the charge-neutral state, stable colloidal structures are produced that also exhibit low polydispersities.

Due to the high number of possible variables there is still a lot of work to do in this area. Surprisingly, only a very small number of publications has investigated the interaction of diblock copolymers with nonionic surfactants.

Concerning the BCPs used, a systematic comparison of different hydrophobic blocks is still missing (variation of the hydrophobicity and T_g). In this context, a promising system with a low T_g for the hydrophobic block is polyisobutylene-*b*-PMA, which was recently characterized by Pergushov and coworkers [143]. These authors have already investigated the micellization of such copolymers by means of SANS and DLS. It will be certainly interesting to study this system in mixtures with surfactant because fast equilibration of the mixed micellar structures can be expected due to the low T_g ($T_g \approx 208$ K).

Moreover, BCPs with bio-inspired blocks have recently received growing interest [144–148, 150]. However, for these systems very few data are available at present concerning their co-micellization with surfactants [149]. But these new materials will certainly be of great interest in the future.

Acknowledgements The author wishes to thank H. von Berlepsch for the Cryo-TEM image. The presented experiments were funded by the Deutsche Forschungsgemeinschaft (Sfb 481/TP A15). In addition financial support from the Marie-Curie RTN “POLYAMPHI” is gratefully acknowledged.

References

1. Otsuka H, Nagasaki Y, Kataoka K (2001) *Curr Opin Interf Sci* 6:3
2. Hamley IW, Mai SM, Ryan AJ, Fairclough JPA, Booth C (2001) *Phys Chem Chem Phys* 3:2972
3. Förster S (1997) *Ber Bunsenges Phys Chem* 101:1671
4. Chu B (1995) *Langmuir* 11:414
5. Allouche J, Tyrode E, Sadtler V, Coplin L, Salager JL (2003) *Ind Eng Chem Res* 42:3982
6. Bryskhe K, Jansson J, Topgaard D, Schillén K, Olsson U (2004) *J Phys Chem B* 108:9710
7. Glatter O, Scherf G, Schillén K, Brown W (1994) *Macromolecules* 27:6046
8. Alexandridis P, Athanassiou V, Fukuda S, Hatton TA (1994) *Langmuir* 10:2604
9. Wang Q, Yu G, Deng Y, Price C, Booth C (1993) *Eur Polym J* 29:665
10. Wanka G, Hoffmann H, Ulbricht W (1990) *Colloid Polym Sci* 268:101
11. Schreiber A, Bock H, Schoen M, Findenegg GH (2002) *Molecular Phys* 100:2097
12. Feng P, Bu X, Pine DJ (2000) *Langmuir* 16:5304
13. Hentze HP, Krämer E, Berton B, Förster S, Antonietti M, Dreja M (1999) *Macromolecules* 32:5803
14. Bibette J (1991) *J Colloid Interface Sci* 147:474
15. Bogomolov V, Gaponenko SV, Germanenko IN, Kapitonov AM, Petrov EP, Gaponenko NV, Prokofiev AV, Ponyavina AN, Silvanovich NI, Samoilovich SM (1997) *Phys Rev E* 55:7619
16. Wang DC, Gast AP (1999) *J Phys Condens Matter* 11:10133
17. Palberg T (1999) *J Phys Condens Matter* 11:R323
18. Bronstein LM, Sidorov SN, Valetsky P, Hartmann J, Cölfen H, Antonietti M (1999) *Langmuir* 15:6256
19. Bronstein L, Krämer E, Berton B, Burger C, Förster S, Antonietti M (1999) *Chem Mater* 11:1402
20. Bronstein LM, Chernyshov DM, Timofeeva GI, Dubrovina LV, Valetsky PM, Khoklov AR (2000) *J Colloid Interface Sci* 230:140
21. Bronstein LM, Chernyshov DM, Timofeeva GI, Dubrovina LV, Valetsky PM, Obolonkova ES, Khoklov AR (2000) *Langmuir* 16:3626
22. Hellweg T, Dewhurst CD, Brückner E, Kratz K, Eimer W (2000) *Colloid Polymer Sci* 278:972
23. Yang CS, Awschalom DD, Stucky GD (2002) *Chem Mater* 14:1277
24. Hecht E, Mortensen K, Gradzielski M, Hoffmann H (1995) *J Phys Chem* 99:4866
25. Hoffmann H (1995) *Tenside Surf Det* 32:462
26. Li Y, Xu R, Bloor DM, Holzwarth JF, Wyn-Jones E (2000) *Langmuir* 16:10515
27. Bronstein LM, Chernyshov DM, Vorontsov E, Timofeeva GI, Dubrovina LV, Valetsky PM, Kazakov S., Khokhlov AR (2001) *J Phys Chem B* 105:9077
28. Egger H, Nordskog A, Lang P (2000) *Macromol Symp* 162:291
29. Nordskog A, Egger H, Findenegg GH, Hellweg T, Schlaad H, von Berlepsch H, Böttcher C (2003) *Phys Rev E* 68:11406/1–14

30. Nordskog A, Fütterer T, Schlaad H, Heinemann A, von Berlepsch H, Böttcher C, Hellweg T (2004) *Phys Chem Chem Phys* 6:3123
31. Jansson J, Schillén K, Olofsson G, da Silva RC, Loh W (2004) *J Phys Chem B* 108:82
32. Chen D, Li Z, Yu C, Shi Y, Zhang Z, Tu B, Zhao D (2005) *Chem Mater* 17:3228
33. Israelachvili JN (1991) *Intermolecular and surface forces*, 2nd edn. Academic, London
34. Hellweg T, von Klitzing R (2000) *Physica A* 283:349
35. Menge U, Lang P, Findenegg G (2000) *Colloids Surf A* 163:81
36. Regenbrecht M, Akari S, Förster S, Möhwald H (1999) *J Phys Chem B* 103:6669
37. Hellweg T (2002) *Curr Opin Colloid Interface Sci* 7:50
38. Strey R (1994) *Colloid Polym Sci* 272:1005
39. Strey R (1996) *Curr Opin Colloid Interface Sci* 1:402
40. Langevin D (1992) *Annu Rev Phys Chem* 43:341
41. Jakobs B, Sottmann T, Strey R, Allgaier J, Willner L, Richter D (1999) *Langmuir* 15:6707
42. Endo H, Allgaier J, Gompper G, Jakobs B, Monkenbusch M, Richter D, Sottmann T, Strey R (2000) *Phys Rev Lett* 85:102
43. Mihailescu M, Monkenbusch M, Endo H, Allgaier J, Gompper G, Richter D, Jakobs B, Sottmann T, Farago B (2001) *J Chem Phys* 115:9563
44. Endo H, Mihailescu M, Monkenbusch M, Allgaier J, Gompper G, Richter D, Jakobs B, Strey R, Grillo I (2001) *J Chem Phys* 115:580
45. Landh T (1994) *J Phys Chem* 98:8453
46. Bryskhe K, Schillén K, Löfroth JE, Olsson U (2001) *Phys Chem Chem Phys* 3:1303
47. Demina T, Grozdova I, Krylova O, Zhirnov A, Istratov V, Frey H, Kautz H, Melik-Nubarov N (2005) *Biochemistry* 44:4042
48. Fütterer T, Hellweg T, Findenegg GH (2003) Particle characterization by scattering methods in systems containing different types of aggregates. Aggregation of an amphiphilic poly(paraphenylene) in micellar surfactant solutions. In: Case F, Alexandridis P (eds) *Mesoscale phenomena in fluid systems*. ACS Symposium Series, vol 861. American Chemical Society, Washington, DC, pp 117–142
49. Denkova AG, Mendes E, Coppens MO (2009) *J Phys Chem B* 113:989
50. Son JG, Bulliard X, Kang H, Nealey PF, Char K (2008) *Adv Mater* 20:3643
51. Hecht E (1996) Aggregationsverhalten von Blockcopolymeren des poloxamer-typs und ihre wechselwirkung mit tensiden. PhD thesis, Universität Bayreuth
52. Beezer AE, Loh W, Mitchell JC, Royall PG, Smith DO, Tute MS, Armstrong JK, Chowdhry BZ, Leharne SA, Eagland D, Crowther NJ (1994) *Langmuir* 10:4001
53. Alexandridis P, Holzwarth JF, Hatton TA (1994) *Macromolecules* 27:2414
54. Brown W, Schillén K, Hvídt S (1992) *J Phys Chem* 96:6038
55. Kellarakis A, Chaibundit C, Krysmann MJ, Havredaki V, Viras K, Hamley IW (2009) *J Colloid Interface Sci* 330:67
56. Almgren M, van Stam J, Lindblad C, Li P, Stilbs P, Bahadur P (1991) *J Phys Chem* 95:5677
57. Yang L, Alexandridis P, Steytler DC, Kositzka MJ, Holzwarth JF (2000) *Langmuir* 16:8555
58. Kositzka MJ, Rees GD, Holzwarth A, Holzwarth JF (2000) *Langmuir* 16:9053
59. Hecht E, Hoffmann H (1995) *Colloids Surf A* 96:181
60. de Lisi R, Lazzara G, Milioto S, Muratore N (2004) *Macromolecules* 37:5423
61. de Lisi R, Lazzara G, Milioto S, Muratore N (2004) *Langmuir* 20:9938
62. de Lisi R, Lazzara G, Milioto S, Muratore N (2004) *J Phys Chem B* 108:18214
63. de Lisi R, Milioto S, Muratore N (2002) *Macromolecules* 35:7067
64. Li Y, Xu G, Zhu Y, Wang Y, Gong H (2009) *Colloids Surf A* 334:124
65. Wanka G, Hoffmann H, Ulbricht W (1994) *Macromolecules* 27:4145
66. Hecht E, Mortensen K, Hoffmann H (1995) *Macromolecules* 28:5465
67. Mahajan RK, Vohra KK, Aswal VK (2008) *Colloids Surf A* 326:48
68. Hecht E, Hoffmann H (1994) *Langmuir* 10:86
69. Li Y, Xu R, Couderc S, Bloor DM, Holzwarth JF, Wyn-Jones E (2001) *Langmuir* 17:5742
70. Jansson J, Schillén K, Nilsson M, Söderman O, Fritz G, Bergmann A, Glatter O (2005) *J Phys Chem B* 109:7073

71. Brunner-Popela J, Mittelbach R, Strey R, Schubert KV, Kaler EW, Glatter O (1999) *J Chem Phys* 110:10623
72. Li X, Wettig SD, Verrall RE (2004) *Langmuir* 20:579
73. Egger H, Hellweg T, Findenegg GH (2003) *Phys Chem Chem Phys* 5:3013
74. Helfrich W (1973) *Z Naturforschung* 28c:693
75. Nallet F, Laversanne R, Roux D (1993) *J Phys II France* 3:487
76. Freyssingeas E, Nallet F, Roux D (1996) *Langmuir* 12:6028
77. Minewaki K, Kato T, Yoshida H, Imai M, Ito K (2001) *Langmuir* 17:1864
78. Roux D, Safinya CR (1988) *J Phys France* 49:307
79. Nallet F, Roux D, Milner ST (1990) *J Phys France* 51:2333
80. Dubois M, Zemb T (2000) *Curr Opin Colloid Interface Sci* 5:27
81. Taulier N, Ober R, Gouzy MF, Guidetti B, Rico-Lattes I, Urbach W (2002) *Langmuir* 18:68
82. Hellweg T, Brület A, Lapp A, Robertson D, Kötz J (2002) *Phys Chem Chem Phys* 4:2612
83. Strey R, Schomäcker R, Roux D, Nallet F, Olsson U (1990) *J Chem Soc Faraday Trans* 86:2253
84. Stepanek P, Nallet F, Almdal K (2001) *Macromolecules* 34:1090
85. Farago B, Monkenbusch M, Goecking KD, Richter D, Huang JS (1995) *Physica B* 213 & 214:712
86. Takeda T, Kawabata Y, Seto H, Komura S, Gosh SK, Nagao M, Okuhara D (1999) *J Phys Chem Solids* 60:1375
87. Yang BS, Lal J, Mihailescu M, Monkenbusch M, Richter D, Huang JS, Kohn J, Russel WB, Prudhomme RK (2002) *Langmuir* 18:6
88. Caillé A (1972) *C R Acad Sci Paris* 274b:891
89. Dey S, Adhikari A, Mandal U, Ghosh S, Bhattacharyya K (2008) *J Phys Chem B* 112:5020
90. Singh PK, Kumbhakar M, Pal H, Nath S (2008) *J Phys Chem B* 112:7771
91. Singh PK, Satpati AK, Kumbhakar M, Pal H, Nath S (2008) *J Phys Chem B* 112:11447
92. Singh PK, Kumbhakar M, Pal H, Nath S (2009) *J Phys Chem B* 113:1353
93. Ivanova R, Lindman B, Alexandridis P (2000) *Langmuir* 16:3660
94. Alexandridis P, Ivanova R, Lindman B (2000) *Langmuir* 16:3676
95. Sotmann T, Strey R (1997) *J Chem Phys* 106:8606
96. Couderc S, Li Y, Bloor DM, Holzwarth JF, Wyn-Jones E (2001) *Langmuir* 17:4818
97. Couderc-Azouani S, Sidhu J, Thurn T, Xu R, Bloor DM, Penfold J, Holzwarth JF, Wyn-Jones E (2005) *Langmuir* 21:10197
98. Aramaki K, Hossain MK, Rodriguez C, Uddin MH, Kunieda H (2003) *Macromolecules* 36:9443
99. Löf D, Tomsic M, Glatter O, Fritz-Popovski G, Schillén K (2009) *J Phys Chem B* 113:5478
100. Schillén K, Jansson J, Löf D, Costa T (2008) *J Phys Chem B* 112:5551
101. Löf D, Niemiec A, Schillén K, Loh W, Olofsson G (2007) *J Phys Chem B* 111:5911
102. Löf D, Schillén K, Torres MF, Müller AJ (2007) *Langmuir* 23:11000
103. Taboada P, Mosquera V, Attwood D, Yang Z, Booth C (2003) *Phys Chem Chem Phys* 5:2625
104. Taboada P, Barbosa S, Mosquera, V (2004) *Langmuir* 20:8903
105. Cabane B (1977) *J Phys Chem* 81:1639
106. Brown W, Fundin J, da Graca Miguel M (1992) *Macromolecules* 25:7192
107. Veggeland K, Nilsson S (1995) *Langmuir* 11:1885
108. Fütterer T, Nordskog A, Hellweg T, Findenegg GH, Foerster S, Dewhurst CD (2004) *Phys Rev E* 70:041408
109. Shimon K, Danino D (2009) *Langmuir* 25:2736
110. Kabanov AV, Bronich TK, Kabanov VA, Yu K, Eisenberg A (1998) *J Am Chem Soc* 120:9941
111. Pamies R, Zhu K, Kjoniksen AL, Knudsen KD, Nyström B (2008) *J Colloid Interface Sci* 326:76
112. Castro E, Taboada P, Mosquera V (2005) *J Phys Chem B* 109:5592
113. Crothers M, Attwood D, Collett JH, Yang Z, Booth C, Taboada P, Mosquera V, Ricardo NMPS, Martini LGA (2002) *Langmuir* 18:8685
114. Debye P, Anacker EW (1951) *J Phys Colloid Chem* 55:644
115. Castro E, Taboada P, Barbosa S, Mosquera V (2005) *Biomacromolecules* 6:1438

116. Pispas S, Hadjichristidis N (2003) *Langmuir* 19:48
117. Bronich TK, Kabanov AV, Kabanov VA, Yu K, Eisenberg A (1997) *Macromolecules* 30:3519
118. Bronich TK, Popov AM, Eisenberg A, Kabanov VA, Kabanov AV (2000) *Langmuir* 16:481
119. Solomatin SV, Bronich TK, Eisenberg A, Kabanov VA, Kabanov AV (2004) *Langmuir* 20:2066
120. Solomatin SV, Bronich TK, Eisenberg A, Kabanov VA, Kabanov AV (2005) *J Phys Chem B* 109:4303–4308
121. Li Y, Nakashima K (2003) *Langmuir* 19:548–553
122. Lysenko EA, Bronich TK, Eisenberg A, Kabanov VA, Kabanov AV (1998) *Macromolecules* 31:4511
123. Bakeev KN, Ponomarenko EA, Shishkanova TV, Tirrell DA, Zezin AB, Kabanov VA (1995) *Macromolecules* 28:2886
124. Lysenko EA, Bronich TK, Eisenberg A, Kabanov VA, Kabanov AV (1998) *Macromolecules* 31:4516
125. Nordskog A (2003) Strukturveränderung von Blockcopolymermizellen durch Zusatz von Tenside. PhD thesis, Technische Universität Berlin
126. Provencher SW (1982) *Comput Phys Commun* 27:213
127. Provencher SW (1982) *Comput Phys Commun* 27:229
128. Kunieda H, Kaneko M, Lopez-Quintela MA, Tsukahara M (2004) *Langmuir* 20:2164
129. Uddin MH, Rodriguez C, Watanabe K, Lopez-Quintela A, Kato T, Furukawa H, Harashima A, Kunieda H (2001) *Langmuir* 17:5169
130. Uddin MH, Morales D, Kunieda H (2005) *J Colloid Interface Sci* 285:373
131. Kahlweit M, Strey R (1985) *Angew Chem* 97:655
132. Frank C, Sottmann T, Stubenrauch C, Allgaier J, Strey R (2005) *Langmuir* 21:9058
133. Byelov D, Frielinghaus H, Holderer O, Allgaier J, Richter D (2004) *Langmuir* 20:10433
134. Fütterer T, Hellweg T, Findenegg GH, Frahn J, Schlüter AD, Böttcher C (2003) *Langmuir* 19:6537
135. Bo Z, Rabe JP, Schlüter AD (1999) *Angew Chem Int Ed* 38:2370
136. Bo Z, Zang C, Severin N, Rabe JP, Schlüter AD (2000) *Macromolecules* 33:2688
137. Engelking J, Wittemann M, Rehahn M, Menzel H (2000) *Langmuir* 16:3407
138. Engelking J, Ulbrich D, Menzel H (2000) *Macromolecules* 33:9028
139. Bockstaller M, Köhler W, Wegner G, Fytas G (2001) *Macromolecules* 34:6353
140. Bockstaller M, Köhler W, Wegner G, Vlassopoulos D, Fytas G (2001) *Macromolecules* 34:6359
141. Fütterer T, Hellweg T, Findenegg GH, Frahn J, Schlüter AD (2005) *Macromolecules* 38:7443
142. Fütterer T, Hellweg T, Findenegg GH, Frahn J, Schlüter AD (2005) *Macromolecules* 38:7451
143. Pergushov DV, Remizova EV, Gradzielski M, Lindner P, Feldthusen J, Zezin AB, Müller A HE, Kabanov VA (2004) *Polymer* 45:367
144. Börner HG, Schlaad H (2007) *Soft Matter* 3:394
145. Schlaad H, Smarsly B, Losik M (2004) *Macromolecules* 37:2210
146. Schlaad H, Antonietti M (2003) *Eur Phys J E* 10:17
147. Crespo JS, Lecommandoux S, Borsali R, Klok HA, Soldi V (2003) *Macromolecules* 36:1253
148. Lecommandoux S, Achard MF, Langenwalter JF, Klok HA (2001) *Macromolecules* 34:9100
149. Gil GO, Losik M, Schlaad H, Hellweg T (2008) *Langmuir* 24:12823
150. Börner H, Smarsly B, Hentschel J, Rank A, Schubert R, Geng Y, Discher D, Hellweg T, Brandt A (2008) *Macromolecules* 41:1430

Non-ionic Thermoresponsive Polymers in Water

Vladimir Aseyev, Heikki Tenhu, and Françoise M. Winnik

Abstract Numerous non-ionic thermally responsive homopolymers phase separate from their aqueous solutions upon heating. Far fewer neutral homopolymers are known to phase separate upon cooling. A systematic compilation of the polymers reported to exhibit thermoresponsive behaviour is presented in this review, including *N*-substituted poly[(meth)acrylamide]s, poly(*N*-vinylamide)s, poly(oxazoline)s, protein-related polymers, poly(ether)s, polymers based on amphiphilic balance, and elastin-like synthetic polymers. Basic properties of aqueous solutions of these polymers are briefly described.

Keywords Amphiphilic · LCST · Polymer · Solution · Thermoresponsive · Water

Contents

1	Scope of the Review	31
2	Synthesis	32
3	Polymers in Aqueous Media: Selected Reviews	33
4	Thermal Responsiveness versus Hydrophobic Association	39
4.1	Sensitivity and Responsiveness	39
4.2	The LCST-Type Transition	41
4.3	Phenomenological Classification	43
4.4	The Hydrophobic Interaction	43

V. Aseyev (✉) and H. Tenhu
Laboratory of Polymer Chemistry, Department of Chemistry, University of Helsinki,
PB 55, FIN-00014 HY, Helsinki, Finland
e-mail: vladimir.aseyev@helsinki.fi; heikki.tenhu@helsinki.fi

F.M. Winnik
Department of Chemistry and Faculty of Pharmacy, University of Montreal, CP 6128 succursale
Centre-Ville, H3C 3J7, Montreal, QC, Canada
e-mail: francoise.winnik@umontreal.ca

4.5	Cooperativity of the LCST Transition	44
4.6	Elastin-Like Polymers	46
5	Self-Organization versus Steric Stabilization	47
5.1	Colloidal Stability	47
5.2	Hydrophobic Self-Association	48
5.3	Protein-Like Copolymers	50
5.4	Mesoglobules of Homopolymers	50
6	List of Thermoresponsive Homopolymers	51
7	Some Generalizations	69
7.1	Structural Effects	69
7.2	Structural Isomers of PiPAAm	70
7.3	Hysteresis	71
7.4	Effect of Macromolecular Architecture	72
7.5	Cyclic Polymers	73
7.6	Telechelic Amphiphilic Polymers	74
7.7	Cononsolvency	75
8	Postscript	76
	References	76

Abbreviations

ρ	Average density
η	Viscosity
A_2	Second osmotic virial coefficient
Ac	Acetate
Ad	Adenine
Al	Alcohol
c	Polymer concentration
CAC	Critical aggregation concentration
CMC	Critical micellization concentration
CMT	Critical micellization temperature
C_p	Partial heat capacity
DLS	Dynamic light scattering
DLVO	Derjaguin–Landau–Verwey–Overbeek theory
DSC	Differential scanning calorimetry
ELP	Elastin-like polymer
Es	Ester
Eth	Ether
LCST	Lower critical solution temperature
k_B	Boltzmann constant
M_n	Number average molar mass
M_w	Weight average molar mass
Oz	Oxazoline
PDI	Polydispersity index
SANS	Small angle neutron scattering
SLS	Static light scattering

t	Time
T_{Θ}	Theta temperature
T_{cp}	Cloud-point temperature
T_{dem}	Demixing temperature
T_g	Glass transition temperature
T_{max}	Temperature of the maximum heat capacity
TM-DSC	Temperature-modulated differential scanning calorimetry
UCST	Upper critical solution temperature

Note that in order to keep style and consistency we abbreviate poly(*N*-isopropylacrylamide) as PiPAAm, though other abbreviations are typically used (PNIPAM, pNIPAAm, etc.). We also use such abbreviations as Ac for acetate, Ad for adenine, Al for alcohol, Eth for ether, Es for ester, Oz for oxazoline.

1 Scope of the Review

Numerous supramolecular structures of varying complexity are formed in nature upon self-assembly of biomacromolecules via non-covalent interactions in aqueous media. Many of such molecules are amphiphilic, i.e. they consist of hydrophilic and hydrophobic moieties. Thus, ionic or highly polar groups provide the overall solubility of the molecules in water. Formation of hydrogen bonds between the hydrophilic polar groups of a macromolecule and water molecules contributes favourably to the free energy of mixing. Synthetic amphiphilic macromolecules also form self-assembled structures in aqueous media. They are widely used in industrial applications as emulsifiers and viscosity modifiers. Their newer applications include various nanocontainers, nanoreactors, etc. Their ultimate self-organization derives from the relative contribution of non-covalent interactions, such as hydrogen bonding, van der Waals interactions, ionic interactions, metal–ligand interactions, hydrophobic interactions, and the entropy contribution. One can also induce self-assembly or trigger transitions between different geometries of the assemblies by adjusting the solvent quality. Such polymeric systems serve as stimuli-responsive materials, for which specific properties can be tuned by an appropriate stimulus. Among the possible stimuli are temperature, pH, electric and magnetic fields, ions, reactants, visible and UV radiation, and mechanical stress. These materials are also known as smart, intelligent, or environmentally responsive materials.

The last few years have seen the development of new interdisciplinary branches of science that have led to ordered supramolecular architectures based on well-defined polymers assembled via non-covalent interactions. Our analysis of the literature (using SciFinder Scholar software [1]) reveals a faster-than-linear growth of the number of publications on this topic during the last decade. Thus, the annual number of publications (journals, patents and reviews) on “self-assembling polymer” (as a keyword) increased fivefold, reaching almost 1000 articles per year. The number of publications on “stimuli-responsive polymers” or on “thermo-responsive polymers” in 2008 was about 100, which is six to seven times higher than the

number published in 1998. The most widely studied water-soluble thermoresponsive polymer, poly(*N*-isopropylacrylamide), PiPAAm, was the subject of about 700 publications in 2008 (word search), which is about four times higher than in 1998. The number of reviews on “poly(*N*-isopropylacrylamide)” in highly ranked international journals is five to ten per year, and we believe that this number is an underestimated value. In contrast, there are only a few studies on other thermoresponsive polymers. For example, about 17 and about 25 papers per year, respectively, have been published on two of the structural isomers of PiPAAm: poly(2-isopropyl-2-oxazoline) and polyleucine.

The apparent discrepancy between the numbers of publications also reflects differences in the terminology used in various branches of science and in different scientific schools, which may lead to miscommunication between scientists. Thus, the terms “thermoresponsive” and “thermosensitive” or “lower critical solution temperature” and “cloud point” are used interchangeably, although their meanings are not necessarily identical. The latter case is particularly unfortunate because it prevents quantitative comparison of the literature values. Another factor to consider is that the number of publications on applications of PiPAAm is growing much faster than the number of reports on its fundamental properties. The upcoming years may witness the disappearance of the gap between synthetic and natural water-soluble polymers, that is, between chemistry, biology, medicine and physics. The design, synthesis, characterization and controlled self-organization of well-defined polymer-based nanomaterials will be key research areas in the next decades.

Due to the large number of existing reviews on stimuli-responsive materials, we limit this publication to articles focussed on dilute aqueous solutions of neutral thermoresponsive linear homopolymers and refer our readers to the most recent publications covering other related cases, e.g. copolymers, various gels, self-organization of block and graft copolymers with highly hydrophobic blocks, applications, etc. Unfortunately, the number of intelligent copolymers currently available is so vast, that the self-organization in aqueous solutions of each one of them cannot be deduced de-novo on the basis of our current understanding of basic self-assembly principles. We trust that the understanding of these principles for homopolymers is the first step to the further understanding of more complex systems. For this reason, in this publication we review homopolymers that either exhibit a lower critical solution temperature (LCST) or those few polymers for which solubility in water decreases upon cooling.

2 Synthesis

The synthesis of well-defined polymers and of complex polymer architectures has been greatly facilitated by recent developments in controlled radical polymerization, which has opened up new possibilities in the design and also in the preparation of functional nanostructures based on supramolecular assembly. Controlled radical polymerization is an attractive alternative to anionic polymerization for preparing polymeric building blocks of well-defined size and a low polydispersity index

(PDI). It allows the precision synthesis of a variety of novel well-defined polymer architectures having exciting structure–property–function relationships (such as block and graft copolymers, stars, brushes and bottle-brush structures) starting from a vast array of commercial functional monomers. Thus, controlled radical polymerization has been investigated extensively for poly(*N*-alkyl)acrylamides by using atom transfer radical polymerization (ATRP) [2–15], reversible addition fragmentation chain transfer (RAFT) [16–22], nitroxide-mediated polymerization (NMP) [23–26] and degenerative chain transfer polymerization (DTP) [19, 27–29]. In this review, discussion of polymer synthesis has been kept to a minimum. Interested readers are referred to other reviews or books listed in Table 1. The syntheses of various thermoresponsive homopolymers, block copolymers and end-functionalized polymers have been reviewed recently by Aoshima and Kanaoka [30].

3 Polymers in Aqueous Media: Selected Reviews

The years 2006–2008 were the most productive in terms of the number of reviews on amphiphilic polymers. Over ten detailed reviews on thermoresponsive water-soluble polymers were published in English in 2006 [1]. In Table 1 we list the reviews to date that are the most related to the scope of the current review and, from our point of view, those that fully cover all aspects of thermoresponsive polymers. The key phrases in the table are not just the key words given by the authors, but rather the highlights of the contents.

Table 1 The most recent reviews devoted to the water-soluble thermoresponsive polymers

Title	Authors	Key phrases	Year Ref.
<i>Synthesis of water-soluble polymers</i>			
Synthesis of stimuli-responsive polymers by living polymerization: poly(<i>N</i> -isopropylacrylamide) and poly(vinyl ether)s	Aoshima S, Kanaoka S	Synthesis of various functionalized <i>N</i> -isopropylacrylamide- and vinyl ether-based polymers; grafting onto various substrates; detailed review of thermoresponsive polymers, block and graft copolymers; synthesis of PiPAAm of various shapes; ionic and neutral block copolymers; self-assembly; stimuli-responsive polymers; new initiating systems and synthetic methodologies	2008 [30]
RAFT-synthesized diblock and triblock copolymers: thermally induced supramolecular assembly in aqueous media	McCormick CL, Sumerlin BS, Lokitz BS, Stempka JE	Stimuli-responsive block copolymers via RAFT; micelles and vesicles; postpolymerization modification utilizing crosslinking and copper-catalysed azide–alkyne click chemistry	2008 [21]

(continued)

Table 1 (continued)

Title	Authors	Key phrases	Year	Ref.
RAFT radical polymerization and the synthesis of water-soluble (co)polymers under homogeneous conditions in organic and aqueous media	Lowe AB, McCormick CL	Stimuli-responsive polymers; controlled-structure (co)polymers; detailed list of monomers and chain transfer agents; RAFT mechanism; limitations of homogeneous aqueous RAFT; modification of gold surfaces; control over the copolymer structure for subsequent self-assembly in response to changes in temperature	2007	[31]
Controlled/living radical polymerization: features, developments, and perspectives	Braunecker WA, Matyjaszewski K	Structure–reactivity correlations and rules for catalyst selection in ATRP; chain transfer agents in RAFT; mediating agent in stable free-radical polymerization; nitroxide-mediated polymerization; degenerative transfer polymerization	2007	[3]
Carbocationic polymerizations	Goethals EJ, Du Prez F	Living/controlled polymerizations; vinyl ethers; disubstituted olefins and styrenics; pseudo-cationic polymerization; block copolymers; telechelic polymers	2007	[32]
<i>Supramolecular structures formed by amphiphilic polymers</i>				
Polymer-assisted fabrication of nanoparticles and nanocomposites	Rozenberg BA, Tenne R	Principles of nanoparticle stabilization against aggregation; interaction forces; polymeric surfactants; polymer adsorption; nanotechnology; properties of nanoparticles and nanocomposites	2008	[33]
Supramolecular assemblies of block copolymers in aqueous media as nanocontainers relevant to biological applications	Harada A, Kataoka K	Physicochemical aspects of self-assembly of hydrophilic–hydrophobic block copolymers; Pluronics; block copolymers with a peptide or ionic segment; micelles with cross-linking in the core or in the corona; drug delivery systems; capillary electrophoresis; surface modification; non-viral gene vectors	2006	[34]
Block copolymers in nanoscience	Lazzari M, Lin G, Lecommandoux S	A collection of reviews on block copolymer self-assemblies, from synthesis to applications; vesicles and micelles; stimuli-responsive assemblies; polypeptide-based block copolymers; nanotubes and nanofibres; applications	2006	[35]

(continued)

Table 1 (continued)

Title	Authors	Key phrases	Year	Ref.
Solution self-assembly of tailor-made macromolecular building blocks prepared by controlled radical polymerization techniques	Lutz JF	Synthesis; macrosurfactants, polysoaps, polyelectrolytes as building blocks; preparation of spherical, cylindrical, multicompartment, and schizophrenic micelles, polymer vesicles, polyion complexes; bottom-up self-assembly; stimuli-sensitive colloids	2006	[36]
Block copolymers in solution: fundamentals and applications	Hamley IW	Monograph; from basic physical chemistry to applications; theory, modelling and experiment; dilute and concentrated solution; neutral and polyelectrolyte block copolymers; variety of phase transitions; phase diagrams; adsorption; applications	2005	[37]
Block copolymer micelles	Gohy JF	Micelles from AB and ABC block copolymers in organic and aqueous solvents; preparation, control of micellar morphology; new trends in the field	2005	[38]
Linear and non-linear triblock terpolymers. Synthesis and self-assembly in selective solvents and in bulk	Hadjichristidis N, Iatrou H, Pitsikalis M, Pispas S, Avgeropoulos A	Linear, star-shaped miktoarm, and cyclic ABC terpolymers; self-organization in aqueous and organic solvents; microphase separation in the bulk: theory and experiment	2005	[39]
Phase behaviour and morphologies of block copolymers	Abetz V, Simon PFW	Linear, star, cyclic, and other topologies of block copolymers; phase diagrams: theory and experiment; microphase separation; crossing the boundaries between different phases; blends; superlattice	2005	[40]
Micellization of block copolymers	Riess G	Synthesis and self-assembly in solution and on solid surfaces; theories and computer simulations; AB and ABA block copolymers; micellar architectures; co-micellization; colloidal nanostructures; controlled drug delivery; polyion micellar complexes; metal nanoparticles; surface modification	2003	[41]

(continued)

Table 1 (continued)

Title	Authors	Key phrases	Year	Ref.
<i>Stimuli-responsive polymers and self-assembly</i>				
Complex coacervate core micelles	Voets IK, de Keizer A, Cohen Stuart MA	Co-assembly of neutral-ionic blocks, graft, random copolymers with oppositely charged species in aqueous solution; synthetic (co)polymers of various architectures; biopolymers; multivalent ions; metallic nanoparticles; surfactants; polyelectrolyte block copolymer micelles; metallo-supramolecular polymers	2009	[42]
Smart polymers: applications in biotechnology and biomedicine	Galaev I, Mattiasson B (eds)	A collection of reviews on stimuli-responsive polymeric materials and their application	2008	[43]
Protein-based smart polymers	Rodríguez-Cabello JC, Reguera J, Prieto S, Alonso M	ELPs and block copolymers, adjustable demixing temperature, TM-DSC splits the dehydration of the polymer and simultaneous β -spiral formation, self- assembling, filaments and fibrils, pH- and photoresponse, applications	2008	[44]
Smart polymers and their applications as biomaterials	Aguilar MR, Elvira C, Gallardo A, Vázquez B, Román JS	pH- and thermally responsive polymers; PiPAAM neutral and charged copolymers; hydrogels; polymers with amphiphilic balance: Pluronics or Plooxamer, Tetronics; thermoresponsive biopolymers; dual stimuli-responsiveness	2007	[45]
Thermosensitive water-soluble copolymers with doubly responsive reversibly interacting entities	Dimitrov I, Trzebicka B, Müller AHE, Dworak A, Tsvetanov CB	Large collection of water-soluble copolymers; controlled synthesis; self-assembly; hydrogels; doubly thermoresponsive polymers; combinations of stimuli: thermoresponsive and zwitterionic properties, LCST and UCST properties, thermo- and pH-responsive properties, magnetic field and thermoresponsive properties, thermo- and light-sensitive polymers; solvent-sensitive PEO conjugates	2007	[46]
Design of rapidly assembling supramolecular systems responsive to synchronized stimuli	Choi HS, Yui N	Thermoreversible supramolecular assembly; fast gelation and slow dissociation; intermolecular ionic interactions; stimuli-sensitive hydrogels	2006	[47]

(continued)

Table 1 (continued)

Title	Authors	Key phrases	Year	Ref.
Towards smart nano-objects by self-assembly of block copolymers in solution	Rodríguez-Hernández J, Chécot F, Gnanou Y, Lecommandoux S	Nanoparticles, their preparation and morphologies; responses to changes in pH, temperature, ionic strength, etc.; stabilization of self-assembled morphologies in dilute solution via various mechanisms; applications in the biomedical field	2005	[48]
Stimuli-reponsive polymers and their bioconjugates	Gil ES, Hudson SM	One of the most cited reviews; classification of stimuli-responsive polymers; temperature-responsive; pH-responsive; smart polymers; homo and block copolymers; intelligent polymers; hydrogels; micelles; bioconjugates; drug delivery	2004	[49]
Self-assembly of block copolymers derived from elastin-mimetic polypeptide sequences	Wright ER, Conticello VP	Phase behaviour in aqueous solution; thermo-reversible self-assembly of elastin-mimetic diblock and triblock copolymers into protein-based nanoparticles and nanotextured hydrogels	2002	[50]
Structural properties of self-assembled polymeric aggregates in aqueous solutions	Mortensen K	SANS; block copolymer micelles; polymeric surfactants; PEO/PPO-based Pluronics or Poloxamers	2001	[51]
Water soluble poly- <i>N</i> -vinylamides: synthesis and physicochemical properties	Kirsh YE	<i>N</i> -Vinylamides, <i>N</i> -vinylpyrrolidone, <i>N</i> -vinyl lactams, monomers and polymers, synthesis and properties in aqueous solutions, hydration phenomena	1998	[52]
<i>Colloidal stability of thermoresponsive polymers above LCST</i>				
Conformation-dependent design of sequences in copolymers	Khokhlov AR (ed)	A collection of reviews on temperature-responsive polymers; polymer and biopolymer physics and chemistry; colloidal stability; protein-like copolymers	2006	[53]
Folding and formation of mesoglobules in dilute copolymer solutions	Zhang G, Wu C	PiPAAM; amphiphilic linear, grafted, and segmented copolymers; ionomers; hydrophilically and hydrophobically modified PiPAAM; viscoelastic effect	2006	[54]
Temperature dependence of the colloidal stability of neutral amphiphilic polymers in water	Aseyev V, Tenhu H, Winnik FM	PiPAAM; PVLC; PMVEth; microgels; graft and block copolymers; colloidal stability of homopolymers beyond the phase separation boundary; mesoglobules	2006	[55]

(continued)

Table 1 (continued)

Title	Authors	Key phrases	Year	Ref.
<i>Applications</i>				
The development of microgels and nanogels for drug delivery applications	Oh JK, Drumright R, Siegwart DJ, Matyjaszewski K	Heterogeneous polymerization; preparation of hydrogels by means of photolithographic and micro-molding methods, continuous microfluidics, modification of biopolymers, and heterogeneous free radical and controlled/living radical polymerizations; reverse micelles	2008	[56]
Responsive polymers in controlled drug delivery	Bajpai AK, Shukla SK, Bhanu S, Kankane S	Responsive stimuli-sensitive materials; polymer blends; interpolymer complexes; classifications of interpenetrating networks; block copolymers; drug delivery profiles and systems	2008	[57]
Polymeric nanocarriers: new endeavours for the optimization of the technological aspects of drugs	Sosnik A, Carcaboso ÁM, Chiappetta DA	A comprehensive and updated patent compilation of the most recent inventions relying on polymer-based nanoparticulated carriers; polymeric nanoparticles, dendrimers, polymeric micelles, and polymersomes	2008	[58]
Smart polymers: physical forms and bioengineering applications	Kumar A, Srivastava A, Galaev IY, Mattiasson B	A reversible collapse of linear, free chains in solution; bioseparation; protein folding; covalently crosslinked reversible gels; chain-adsorbed or surface-grafted forms; smart surfaces and membranes; microfluidics and actuators	2007	[59]
Functional copolymers of <i>N</i> -isopropylacrylamide for bioengineering applications	Rzaev ZMO, Dinçer S, Pişkin E	<i>N</i> -Isopropylacrylamide-based random, block and graft copolymers; ionic and neutral blocks; bioconjugates	2007	[60]
Physical stimuli-responsive polymeric micelles for anti-cancer drug delivery	Rapoport N	Core-shell micelles; drug loading; internal and external stimuli; pH, temperature, ultrasound, light-responsive polymeric micelles	2007	[61]
Functionalized micellar systems for cancer-targeted drug delivery	Sutton D, Nasongkla N, Blanco E, Gao J	Nanomedicine; micelle pharmacokinetics; multifunctional polymeric micelles; responsive drug release; <i>N</i> -isopropylacrylamide-based core-shell micelles; Pluronics	2007	[62]
Molecular design of functional polymers for gene therapy	Jeong JH, Kim SW, Park TG	Cationic polymers; poly[2-(dimethylamino)ethyl methacrylate]; nonviral carriers; polyplexes	2007	[63]

(continued)

Table 1 (continued)

Title	Authors	Key phrases	Year	Ref.
Poly(2-oxazolines) in biological and biomedical application contexts	Adams N, Schubert US	Various architectures and chemical functionalities prepared by living, cationic ring-opening polymerization; amphiphilic polyoxazolines; block copolymers; poly(2-oxazoline)-based lipopolymers; poly(oxazoline)-based vectors; stimuli-responsive systems	2007	[64]
Polymeric micelles to deliver photosensitizers for photodynamic therapy	van Nostrum CF	Pluronics; poly(ethylene glycol)–lipid conjugates; pH-sensitive PiPAAM-based micelles; polyion complex micelles; drug loading; biodistribution studies; therapeutic efficiency	2004	[65]

4 Thermal Responsiveness versus Hydrophobic Association

4.1 Sensitivity and Responsiveness

Any flexible macromolecule in solution is sensitive to temperature changes, which typically result in a variation of the coil size. In a given solvent, excluded volume interactions and elastic forces determine the swelling of a neutral linear macromolecule [66, 67]. If the thermal energy $k_B T$ of the repeating units is high, excluded volume interactions prevail over the attraction between the repeating units and, consequently, the macromolecule swells. This is the case for a thermodynamically good solvent, in which a linear homopolymer adopts the conformation of a very loose extended coil. The constraints limiting chain expansion are the C–C covalent bonds and the entropy of the coil. The latter decreases with the coil swelling, due to the lesser number of possible conformations.

It is worth stressing here that thermal sensitivity is a general phenomenon for polymers in solution: the solubility of all polymers in any solvent depends on temperature. For that reason, Allan Hoffman defined intelligent stimuli-responsive polymers as polymers that respond to a small physical or chemical stimulus with large property changes [68–70]. The coil–globule transition is a typical polymer response to a change in its solution temperature.

The internal energy of the segmental interactions, which represents the excluded volume effect, can be expanded as a power series of the segment density ρ :

$$U = V k T (\rho^2 A_2 + \rho^3 A_3 + \dots).$$

The second osmotic virial coefficient of the expansion, A_2 , is a measure of the thermodynamic quality of the solvent for the polymer and accounts for binary

interactions between the repeating units of the chain and depends on the temperature and the form of the interaction potential between the segments. Under theta conditions, i.e. when $T = T_\Theta$, the polymer adopts an ideal Gaussian coil conformation and its repeating units can be described simply as non-interacting molecules of an ideal gas connected in a chain. Consequently, a polymer solution is in a Θ -state when $A_2 = 0$ and the molar mass of the polymer is infinitely high [71].

The mean-field theory adequately predicts the coil-to-globule transition of a single polymer chain in organic solvents upon cooling below T_Θ [72]: the thermal energy of the repeating units becomes lower than the minimum of the potential corresponding to the van der Waals interactions, the solvent turns into a thermodynamically poor one (i.e. $A_2 < 0$) and condensation of the repeating units takes place. A single macromolecule of infinite molecular weight undergoes the transition at T_Θ . However, for real polymers of finite molecular weight, e.g. polystyrene dissolved in cyclohexane, the transition of the chain occurs at $T < T_\Theta$ [73–75]. Light scattering and osmotic pressure are typical experimental methods used to determine A_2 . These methods require dilute solutions and extrapolation to zero polymer concentration. If there are many chains in the solution, the attraction between the repeating units causes intermolecular aggregation. Hence, T_Θ is experimentally defined for a given polymer/organic solvent system when $M \rightarrow \infty$ and $c \rightarrow 0$.

This type of transition is conveniently represented as a phase diagram in which the phase separation boundary, or binodal, indicates the temperature for which a given polymer–solvent mixture passes from a one-phase system to a two-phase system that consists of a polymer-rich phase and a polymer-poor phase. In other words, the binodal corresponds to the temperature at which the coil–globule transition takes place followed by polymer precipitation (see Fig. 1a). The shared maximum of the

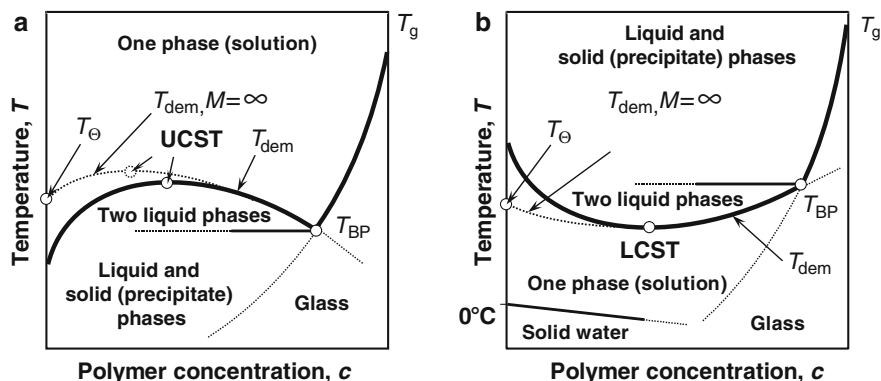


Fig. 1 Possible phase diagrams for polymers showing either (a) UCST (e.g. PS in cyclohexane) or (b) LCST type II (e.g. PiPAAm in aqueous medium) phase separation behaviour. T_{dem} is the demixing temperature, T_Θ is the theta temperature, and T_{BP} is the temperature corresponding to the Berghmans point [76]. For both polymers, T_g in their solid state is well above T_{dem} . For this UCST-type polymer, T_g cannot be lower than T_{BP} . At temperatures below T_{BP} , the polymer is frozen in, and phase morphology is preserved [77]. For the LCST-type polymer shown, partial vitrification takes place at $T_{\text{BP}} < T < T_g$ [78]

spinodal and binodal is the upper critical solution temperature (UCST). Polystyrene (PS) in cyclohexane is a classic polymer/organic solvent system known to show a UCST behaviour [79–81]. In accordance with the Flory theory, the solubility of PS in cyclohexane decreases and its UCST shifts towards lower polymer concentrations on increasing the polymer molar mass.

Non-ionic polymers can also undergo a coil–globule transition in aqueous solutions [82–99]. However, their transition significantly differs from the transition of polymers in organic media. Hydrogen bonds and hydrophobic and hydrophilic interactions contribute much more to the solubility of a polymer in water than do short range van der Waals interactions, which prevail in solutions of polymers in organic solvents. For water-soluble polymers, the experimental value of A_2 reflects the balance of these interactions. In analogy with polymers in organic media, for a single thermoresponsive macromolecule of infinite molar mass, the Θ -condition is realized in water at $T = T_\Theta$ when $A_2 = 0$, $M = \infty$ and $c = 0$. Consequently, the collapse of an amphiphilic homopolymer can be classified as a coil–globule transition if $A_2 < 0$ in the globular state.

The majority of non-ionic water-soluble polymers undergo phase separation upon heating. The phase separation of these polymers can be described by a phase diagram with an LCST, which reflects a local structural transition involving water molecules surrounding specific segments of the polymer in solution. There are only a few reports on neutral water-soluble polymers, whose properties drastically change upon cooling their aqueous solutions. To the best of our knowledge, the UCST-type separation originating from the coil–globule transition has not been reported, though a decrease of the A_2 value has been observed.

For further reading, readers are encouraged to consult the book by Koningsveld, Stockmayer and Nies, which contains an extensive list of phase diagrams for various binary polymer–solvent mixtures [100]. The book also contains a detailed review of the general thermodynamic principles of the phase equilibrium.

4.2 The LCST-Type Transition

The LCST was first described by Heskins and Guillet for an aqueous solution of PiPAAm [101]. When the temperature of a solution is raised above the phase separation temperature (a point on the binodal, also known as the demixing, T_{dem} , or the cloud-point temperature, T_{cp} , depending on the experimental technique used), the hydrophobic backbone and other nonpolar groups of the polymer tend to associate. This causes intra- and intermolecular aggregation leading to collapse of the individual polymer chains (microphase separation) and precipitation of the polymer (macrophase separation). The LCST depends upon pressure [97, 98] and the polydispersity of the polymer. The solution demixing is reversible when the temperature drops below T_{dem} ; however, the rate of polymer redissolution is often slower and the chain expansion takes place at a lower T , which results in a so-called

thermal hysteresis [95]. Studies on kinetics of the demixing and remixing processes of PiPAAM/water solutions show that all molecular changes are reversible if the temperature remains less than ca. 6–8 K above the LCST for less than a few minutes, and that the PiPAAM chains reswell into coils in less than a few seconds [102]. If a PiPAAM/water solution is annealed at higher temperatures, the time of remixing may increase up to 1 day or even more [78].

The most common experimental techniques for constructing a phase diagram are turbidity detection (T_{cp}) or microcalorimetry (T_{dem}). Change in turbidity of solutions can be slow or abrupt, depending on the polymer, its concentration in solution, and the heating/cooling rate. The temperature at which the transition is detected can vary by as much as 30°C for a given polymer, depending on these parameters. For the same experimental settings, the temperature of the endotherm onset, T_{dem} , usually coincides with T_{cp} , whereas the endotherm maximum, T_{max} , is slightly higher than T_{cp} (see Fig. 2) [103]. Unfortunately, different experimentalists define the position of T_{cp} on the transmittance versus temperature curve in different ways, even for the equilibrium heating/cooling (i.e. for the zero rates). Chytrý and Ulbrich have listed existing definitions of T_{cp} obtained using a UV–Vis spectrometer [104]:

1. The temperature of the first appearance of cloudiness (shown in Fig. 2)
2. The temperature of the intersection of the baseline (reading of absorbance of unheated solution) with the tangent to the cloud curve drawn in the inflection
3. The temperature at the inflection point
4. The temperature of different stages (expressed in percentages) of absorbance increase or transmittance decrease, e.g. 10% drop in transmittance

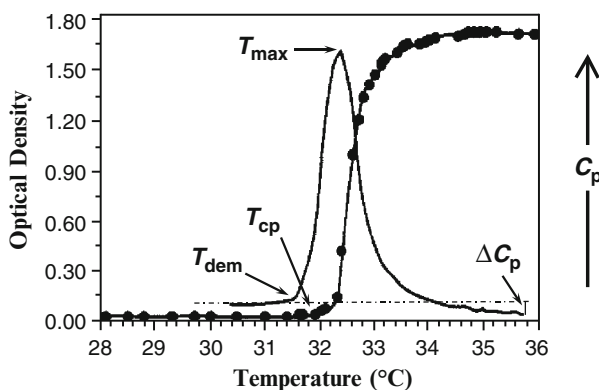


Fig. 2 Typical microcalorimetric endotherm at a heating rate of 15°C/h (solid line) and turbidity curve at a heating rate of 24°C/h (circles) obtained on an aqueous poly(*N*-isopropylacrylamide) solution ($M_w = 414,000$ g/mol, PDI = 2.8, $c = 0.04$ wt%). T_{max} , temperature of the maximum heat capacity; ΔC_p , difference in the heat capacity before and after the transition; T_{dem} , demixing temperature; T_{cp} , temperature of the first appearance of cloudiness. Reprinted with permission from the American Chemical Society [105]

For solutions of most polymers in organic and aqueous media, the phase separation temperature depends on the polymer mass fraction and, in some cases, on the polymer molar mass. Taking into account differences in the experimental parameters (e.g. heating/cooling rate) and the diversity of approaches used to define the phase separation temperature, the reader has certainly realized by now that it is not possible to quantitatively compare experimental data on apparently similar or identical polymeric systems reported by different researchers.

4.3 Phenomenological Classification

To facilitate the description of the phase separation phenomenon of aqueous polymer solutions, Berghmans and Van Mele proposed the following phenomenological classification of their miscibility with water. Type I polymers [e.g. poly(*N*-vinylcaprolactam), PVCL] are species that follow the classic Flory–Huggins behaviour [106, 107]: their LCST (i.e. the absolute minimum in the phase diagram) shifts upon increasing the polymer molar mass towards lower polymer concentrations. Type II polymers (e.g. PiPAAm [78, 108]) are polymers for which the minimum of the demixing curves is hardly affected by chain length (see Fig. 1b). For Type II polymers, the architecture has a negligible effect (e.g. the LCST of star PiPAAs is similar to that of linear polymer [109]), except for polymers with hydrophobic or hydrophilic end-groups [110–112] and polymers with a high number of arms [113] or spherical brushes [114, 115]. Type III polymers [e.g. poly(methylvinylether), PMVEth] exhibit a bimodal phase diagram, presenting two critical points for low and high polymer concentrations corresponding to the Type I and Type II behaviours, respectively [116–119].

4.4 The Hydrophobic Interaction

Water-soluble neutral polymers consist of hydrophilic groups (e.g. amide groups, ether groups), which are able to interact strongly with water molecules and induce water solubility, and hydrophobic groups (e.g. vinyl backbone). The formation of hydrogen bonds between polar groups of the polymers and the water molecules is the initial driving force for dissolution. The word “hydrophobic” can be misleading. It implies that the dissolved substance dislikes water, whereas, in fact, the interaction between a hydrophobic molecule and water is attractive due to the dispersion forces. However, the attraction between the water molecules is much stronger than the van der Waals forces: water molecules simply “love” themselves too much to let nonpolar substances interfere with their association. The hydrophobic parts of the amphiphilic macromolecule organize the surrounding water molecules, leading

to the formation of an ordered hydration layer. The restructuring of water is entropically unfavourable, and thus the hydrophobic substances are only sparingly water-soluble, while trying to minimize the entropic loss of the system [120, 121]. This feature of hydrophobic molecules in water is known as the hydrophobic effect [122–129] and it gives rise to the hydrophobic interaction, i.e. to a strong solvent-mediated “attraction” between hydrophobic molecules in order to minimize the contact surface between hydrophobes and water. Therefore, an amphiphilic water-soluble polymer experiences both repulsive and “attractive” forces. The sum of these forces determines the solubility of the amphiphile in water and thus the value and the sign of the experimentally obtained A_2 in solution. For readers interested in understanding the unique properties of liquid water and its solutions, we recommend the most recent book by Arie Ben-Naim [129].

The LCST transition in aqueous systems reflects first of all a local structural transition involving water molecules surrounding the polymer. At low temperature, the polymer is hydrophilic and the water molecules are bound to its polar groups and to each other via hydrogen bonds. Infrared spectroscopy studies on PiPAAm showed the existence of the amide I ($\text{C}=\text{O}\cdots\text{HN}$, $\text{C}=\text{O}\cdots\text{H}_2\text{O}$) and the amide II ($\text{N}-\text{H}\cdots\text{O}=\text{C}$, $\text{N}-\text{H}\cdots\text{OH}_2$) hydrogen bonds as well as non-hydrogen-bonded $\text{C}=\text{O}$ and $\text{N}-\text{H}$ groups [130–135]. The polymer molecules adopt an extended coil conformation. The relative magnitude of the hydrophobic effect increases with temperature. At higher temperatures, water molecules are released in bulk, allowing associative contacts between the newly exposed hydrophobic monomer units [136]. Thus, during the demixing of PiPAAm, the bound water molecules are liberated, resulting in the formation of intramolecular hydrogen bonds between the carbonyl and amine functions of the *N*-isopropylamide side residues [137]. A negative total entropy change upon heating controls the system over the enthalpy of the hydrogen bonding, and the change in the free energy of the mixing becomes positive, causing chain contraction and, eventually, phase separation. In some cases, it leads to a sol-gel transition: a sol state (a random coil conformation) below $T_{\text{sol-gel}}$ and gelation above $T_{\text{gel-sol}}$.

4.5 Cooperativity of the LCST Transition

The high-temperature collapse of a non-ionic single chain in water has been described using concentration-dependent interaction parameters. Although the average radius of gyration of a chain decreases at high temperature according to phenomenological parameters, the molecular origin of the temperature inversion can only be understood if one considers the molecular property of polymer–water interaction. Tanaka F et al. developed a description of the phase separation with a closed loop miscibility gap that takes place in aqueous solutions of poly(ethylene oxide) (PEO) [138]. The authors explicitly included the hydration [139] in order

to find the molecular origin of the high-temperature collapse. In this description, the model assumed random and independent hydrogen bonding (referred to as H-bonding) between PEO and water molecules along the chain. It was adequate to describe the experimental phase diagrams of PEO. This hydration mechanism was, however, unable to describe the sharp collapse of PiPAAm chains. The concept of cooperative hydration has allowed the theoretical derivation of the flat cloud-point curves of the LCST type observed in aqueous PiPAAm solutions [140]. The cooperativity in hydration is caused by a positive correlation between neighbouring bound water molecules due to the presence of the large hydrophobic isopropyl side groups. If a water molecule succeeds in forming an H-bond with an amido group on a chain, a second water molecule can form an H-bond with the chain more easily than the first one because the first molecule causes some displacement of the isopropyl group, thus creating more access space for the next molecule. As a result, consecutive sequences of bound water appear along the chain, which leads to a pearl-necklace-type chain conformation [140, 141]. When the solution is heated, each sequence is dehydrated as a whole, resulting in the sharp collapse of the chain. This concept of cooperative hydration has successfully been applied to describe theoretically the phenomenon of co-nonsolvency of PiPAAm in a mixed solvent of water and methanol or other alcohols [142]. The concept of cooperative hydration has also allowed derivation of a unified model of the association-induced LCST phase separation in aqueous solutions of telechelic PEO and PiPAAm (Fig. 3) [143].

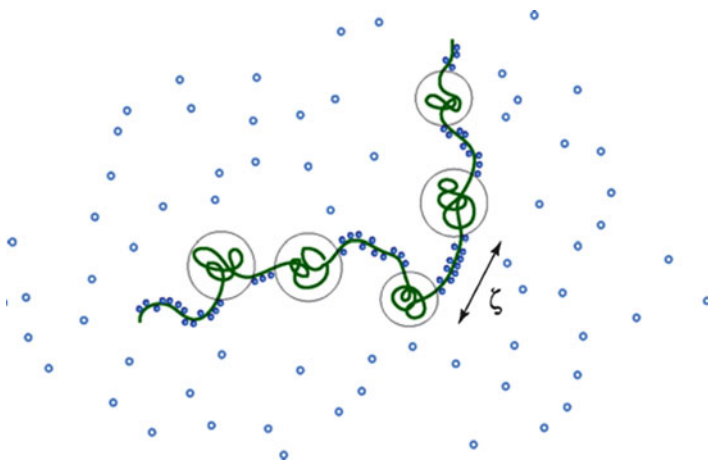


Fig. 3 Sequential hydrogen bonds formed along the polymer chain due to the cooperative interaction between the nearest neighbouring bound water molecules. The average length of sequences sharply reduces as temperature approaches T_{cp} from below. The random-coil parts (*thin circles*) are collapsed near T_{cp} . Reprinted with permission from the American Chemical Society [140]

4.6 Elastin-Like Polymers

Protein-based polymers are composed of repeating peptide sequences, where the repeating unit can be as few as two or as many as hundreds of residues [144]. Among them, elastin-like polymers (ELPs) are multiblock synthetic copolymers consisting of the pentapeptides VPGXG, where V stands for L-valine, P for L-proline, G for glycine, and X represents any natural amino acid except proline [145, 146]. ELPs are water-soluble at temperatures lower than their demixing temperature and precipitate at higher temperatures. However, ELPs are usually described in the literature not as LCST type polymers but as polymers that exhibit an inverse solubility temperature (ITT) in water. The T_{dem} of ELPs depends on their composition. The hydrophobicity scale for the amino acid residues X and T_{cp} of the corresponding ELPs is presented in [144]. The design of ELPs with a desired T_{dem} within $T_{\text{dem}} = 0 - 100^{\circ}\text{C}$ has recently been reviewed [44, 147].

Strictly speaking, the mechanism of the reversible temperature-modulated phase transition of ELPs differs from the transition of the thermosensitive polymers such as PiPAAm. First of all this is because some of the ELPs may either be non-ionic or weakly charged. However, a number of common features of aqueous solutions of ELPs and of PiPAAm are evident. For example, kinetic studies on solutions of poly(VPGVG) showed that the phase separation process is faster than the process of redissolution. This behaviour is similar to the thermal hysteresis reported for PiPAAm [78, 95, 102] and has been verified using temperature-modulated differential scanning calorimetry (TM-DSC) [44, 78, 148], a technique capable of separating phenomena that overlap thermally but present a different time response. TM-DSC uses a periodically alternating heating programme superimposed on the constant heating rate and allows differentiating between overlapping phenomena. Thus, the endothermic peak for aqueous poly(VPGXG) solutions was found to be a sum of two processes. The first endothermic process corresponds to the destruction of the ordered hydrophobic hydration structures surrounding the polymer chain. The other, exothermic, process arises from the chain folding into a β -spiral structure. The hydrophobically driven association of β -spirals results in the formation of filaments composed of three-stranded dynamic polypeptide β -spirals that grow to several hundred nanometers in length and gradually segregate from the solution. The phase-separated poly(VPGXG) above T_{dem} contains 63 wt% of water and 37 wt% of polymer [44], which is surprisingly close to the mass fraction of polymeric material within single chain globules and mesoglobules formed by fully amorphous synthetic polymers having high T_{g} , such as PiPAAm [55]. For comparison, the thermal hysteresis reported for PiPAAm was interpreted as partial vitrification of the polymeric material in the polymer-rich phase [78].

5 Self-Organization versus Steric Stabilization

5.1 Colloidal Stability

For polymer solutions, a decrease in the solvent thermodynamic quality tends to decrease the polymer–solvent interactions and to increase the relative effect of the polymer–polymer interactions. This results in intermolecular association and subsequent macrophase separation. The term “colloidally stable particles” refers to particles that do not aggregate at a significant rate in a thermodynamically unfavourable medium. It is usually employed to describe colloidal systems that do not phase separate on the macroscopic level during the time of an experiment. Typical polymeric colloidally stable particles range in size from ~ 1 nm to ~ 1 μ m and adopt various shapes, such as fibres, thin films, spheres, porous solids, gels etc.

Any system, if left alone, finally adopts its stable state. The time required for that process to occur is determined by the magnitude of the activation energy barriers, which separate the stable and metastable states. A system under a given set of conditions is called thermodynamically metastable if it is in a state corresponding to a local minimum of the appropriate thermodynamic potential for specified constraints imposed upon the system, e.g. constant temperature and pressure [71]. If this system can exist in several states, the state of the lowest free energy is called the thermodynamically stable state. Thus, the coil conformation corresponds to the lowest minimum of the chain free energy and, therefore, is thermodynamically stable. In contrast, the globular conformation of a single chain is a metastable state for the polymer in solution. Globules of single chains tend to associate and adopt a new phase of energy lower than the sum of the energy of individual globules dispersed in the solvent. Colloidally stable particles are thermodynamically metastable.

Standard colloid chemistry strategies have been developed over the years in order to prevent or at least minimize interparticle contacts. We review them briefly here since they help in understanding the properties of the aggregates formed in aqueous solutions of thermosensitive polymers heated above their T_{cp} . In highly dilute polymer solutions, the rate of the globule–globule contacts is slow, which limits macroscopic phase separation. The stability of more concentrated polymer dispersions in water is enhanced either electrostatically or sterically. Electrostatic stabilization is typically realized using either ionic initiators or ionic surfactants or dissociating co-monomers in the polymer syntheses conducted in emulsions. Particles are obtained, which repel each other due to the entropic (osmotic) pressure caused by the counterions between the surfaces. Interactions of the charged surfaces are usually explained by the Derjaguin–Landau–Verwey–Overbeek, (DLVO) theory, which combines short-range attractive van der Waals and long-range electrostatic double-layer forces. The strength of the repulsion force between the particles and the thickness of the electric double layer may be altered by changing the ionic

strength of the aqueous medium [149]. At high electrolyte concentrations, the repulsion between the particles vanishes and the coagulation of the particles is fully diffusion controlled [150, 151].

Stabilizing repulsive forces may also arise from specific chemical and/or physical properties of the particle surface. It is often suggested that the high hydrophilicity of a surface could lead to interparticle repulsion, even if the surface does not possess any electric charge or repulsive polymer layer. This type of repulsion has been ascribed to a force, the hydration or structural force, which arises as a consequence of the specific structure of the hydrogen-bonded water layer on the particle surface. It has been suggested that the overlap of two structurally modified boundary layers gives rise to the hydrophilic repulsion [152–154]. The existence of such hydration forces remains the subject of debates. It has been argued that, in most cases, the short-range non-DLVO forces may simply be repulsive forces, such as the undulation or protruding forces, especially when the surface is rough [155, 156].

Steric stabilization is achieved via grafting the particle surface with water-soluble polymers, e.g. PEO. The repulsive force has an entropic origin; when two grafted surfaces approach each other they experience a repulsive force once the grafted chains begin to overlap and the mobility of the chains decreases [149, 150]. Steric stabilization by non-ionic hydrophilic polymers is independent of the medium ionic strength, assuming that the added electrolyte does not drastically change the thermodynamic quality of the aqueous solvent. PEO has been shown to be an effective steric stabilizer, even at high electrolyte concentrations, as long as the molecular mass of PEO is high [157]. The use of PEO is often also considered advantageous because PEO largely prevents the adsorption of proteins onto polymer surfaces and, thus, increases the biocompatibility of the polymer [158].

5.2 *Hydrophobic Self-Association*

Although we limit the review to thermoresponsive homopolymers, a discussion of the self-association and the colloidal stability of thermoresponsive and non-thermoresponsive amphiphilic copolymers is unavoidable. Thermally responsive polymers, which undergo changes in solubility with changes of the solution temperature, are an alternative to the polymers carrying hydrophobic moieties, i.e. the repeating units that are not soluble in water at $T = 0 - 100^{\circ}\text{C}$ and normal pressure. Similar to the low-molar-mass surfactants, amphiphilic non-thermoresponsive block, graft and telechelic copolymers self-organize into diverse micellar structures in the block-selective solvents above a certain concentration, which is either called the critical micellization concentration (CMC) or the critical aggregation concentration (CAC). The advantages of the amphiphilic block copolymers over the classical detergents lie in the low CAC, in the highly tuneable composition and architecture, as well as in the dependence of the micellization on selective solvents. The shape and the size of these self-assemblies are governed by the balance between

three major forces acting on the system, reflecting the constraints between the core-forming blocks, the interaction between the chains in the corona (steric or electrostatic), and the surface energy between the solvent and the core [159]. The most commonly observed morphologies are spheres, cylinders and vesicles [41, 160–162]. Block, graft and random copolymers are known to form unicore or multicore micelles in selective solvents [163]. In addition, a variety of other structures have been reported, including toroids [164], helices [165], disks [166], nanotubes [167] and multicompartiment micelles [168]. Such complex self-assemblies have rarely been observed for classical low-molar-mass surfactants.

The characteristic feature of neutral thermoresponsive polymers showing the LCST behaviour in water is an increased hydrophobicity at elevated temperatures. This feature may lead to the coagulation of the colloidal dispersion. Therefore, in order to avoid macroscopic phase separation above T_{dem} , the surface of the hydrophobic particles needs to be adjusted, either by using amphiphilic additives (e.g. detergents) or by careful chemical modification of the surface (e.g. using PEO blocks or grafts). In the latter case, the thermoresponsive backbones or segments collapse and associate upon heating, thus leading to the formation of colloiddally stable core-shell structures. The demixing temperature of the modified polymers varies, depending on the fraction of hydrophilic or hydrophobic moieties. The size of the aggregates can be altered either by changing the polymer concentration or its chemical composition in the case of copolymers. PEO-grafted copolymers form less dense particles than homopolymers or block copolymers, due to the unavoidable incorporation of a fraction of the PEO grafts in the aggregated phase [169]. The role of the amphiphilic grafts or blocks on the colloidal stability of microgels or aggregates formed above the LCST has recently been reviewed [55, 170, 171] (see Table 1).

The chains within the polymeric micelles may exhibit retarded mobility (slow kinetics), depending on the T_g of the core-forming blocks, which results in the formation of either equilibrium or non-equilibrium metastable supramolecular structures [160, 172–175]. For thermoresponsive polymers, the formation of the equilibrium morphologies is easily controlled by adjusting the heating rate and the polymer concentration, in comparison to the non-thermoresponsive polymers, upon their direct dissolution in water [54, 55]. If the core-forming block exhibits a high T_g , micellar exchange can become suppressed for the block copolymers [41], so that frozen micelles are formed and no chain exchange between micelles is possible [176]. Polymers containing blocks with high T_g form aggregates with a compact glassy core, and either show very low CAC or cannot be directly solubilized in aqueous media. In the latter case, copolymers are first dissolved in a solvent common for both blocks and then transferred into the aqueous medium.

Actually, the term “micelle” refers to the equilibrium structures and, therefore, the non-equilibrium structures prepared at $T < T_g$ of the core should be called “micelle-like aggregates”. However, the term “micelle” is extensively used in literature. If dynamic systems are aspired, it is therefore advisable to employ amphiphilic block copolymers, which bear a hydrophobic block with a low T_g .

5.3 Protein-Like Copolymers

Protein-like copolymers are a special case of thermosensitive copolymers capable of forming small colloidally stable aggregates in solutions heated above their LCST [177–182]. In globular proteins, the hydrophilic units mainly cover the water-exposed surface of the globule, thus preventing interprotein association, whereas hydrophobic units mainly form the core of the globule. Amphiphilic copolymers can mimic the behaviour of biopolymers and, in certain cases, that of globular proteins. The theoretical model of protein-like copolymers ascribes the term “memory” to amphiphilic copolymers, stating that a polymer chain tends to reassume the conformation in which it was synthesized, due to the unique distribution of repeating units along this chain. The synthesis of protein-like copolymers from typical synthetic monomers is difficult, and only few reports on successful synthesis are available [181, 182]. PiPAAm-*graft*-PEO copolymers in water close to the demixing temperature of the backbone turned out to be able to remember the original conformation in which they had been grafted [183, 184].

5.4 Mesoglobules of Homopolymers

When a homopolymer in solution encounters a situation in which the thermodynamic quality of the solvent is poor, individual chains of the homopolymer undergo a coil-to-globule collapse. The globules associate immediately, and macroscopic phase separation seems unavoidable. However, it has been reported that a number of polymers in water or in organic solvents form equilibrium globules, i.e. single chain globules that remain isolated in solution without immediate association and precipitation. We have presented in a recent review a compilation of homopolymers reported to exhibit this behaviour in water [55], forming stable single chain globules or multimolecular aggregates, termed “mesoglobules” [185, 186]. Mesoglobules of thermosensitive polymers that are formed beyond T_{dem} are spherical in shape and monodispersed in size and typically have a radius on the order of 50–200 nm. Various thermoresponsive polymers and their derivatives form colloidally stable suspensions instead of the expected macrophase separation upon heating of their dilute aqueous solutions above T_{dem} , including homopolymers such as PiPAAm [55, 187], PVLC [55], and poly(methylvinyl ether), PMVEth [55, 188, 189]. The fact that mesoglobules are metastable structures can be demonstrated experimentally. For example, when a phase-separated PiPAAm solution is subjected to centrifugation at 4000 rpm at elevated temperature above T_{cp} , it forms a two-phase system consisting of a transparent liquid and a white gel [190]. Nonetheless, in a wide range of conditions the mesoglobules remain colloidally stable.

The properties of the mesoglobules depend on factors related to the intrinsic properties of the polymers and to experimental protocols. Thus, increasing the

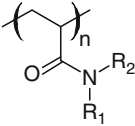
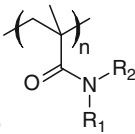
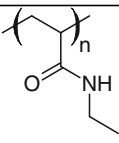
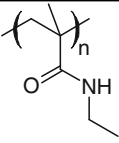
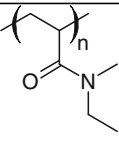
content of hydrophobic comonomer leads to a lowering of T_{dem} of aqueous PiPAAm and concomitant decrease in the size of the mesoglobules [54, 187, 191]. Rapid heating and lowering the polymer concentration have a similar effect. We should add here that the same phenomenon takes place in organic solvents. For example, the precipitation time of PS globules formed by polymers of high molar mass is essentially longer (tens of minutes or even hours) than that of the shorter chains in the solution of the same polymer mass concentration [192]. This suggests a possible general mechanism responsible for the colloidal stability of mesoglobules formed by homopolymers in either organic or aqueous media [55].

Various mechanisms have been proposed to account for the stability of mesoglobules [54, 55, 188, 189]. One such mechanism is the viscoelastic effect, which was introduced by Tanaka H for colloidally stable droplets of PMVEth [188, 189]. Accordingly, a collision of two mesoglobules is not effective as long as the time of their contact is shorter than the time required for establishing a permanent chain entanglement via the chain reptation. Fluorescence spectroscopy allowed us to confirm the contributions of the viscoelastic effect and also of the partial vitrification of the polymer to the mechanism underlying the stability of PiPAAm mesoglobular phases [187]. It also led us to observe directly for the first time that PiPAAm mesoglobules undergo a gradual conversion from fluid-like particles into hard spheres within a narrow temperature window, $T_{\text{dem}} < T < 36^{\circ}\text{C}$, a phenomenon that had been inferred, but not proven, by light scattering data. Mesoglobules grow in size and mass within this temperature range. We suggested that changes in the hydration layer surrounding the PiPAAm chains and the exchange of water–polymer H-bonds for interchain H-bonds are involved in the process. For temperatures higher than T_{dem} , vitrification of the mesoglobule core can occur, enhancing particle stability and the resistance towards merging [78]. The results of our experiments suggest that this process is indeed significant, but only for $T > 36^{\circ}\text{C}$, a temperature $\sim 6 - 7^{\circ}\text{C}$ above T_{dem} . Also, the possibility that electrostatic effects contribute to the stabilization of PiPAAm mesoglobules cannot be excluded [55, 193]. Since our previous review [55], some new fascinating and important evidence has appeared, including experimental [54, 194–203] and theoretical [204–206] aspects of the mesoglobular phase.

6 List of Thermoresponsive Homopolymers

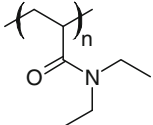
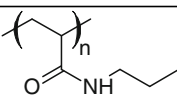
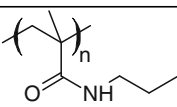
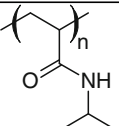
In this section we outline the publications and selected features of neutral thermoresponsive homopolymers exhibiting the LCST phase separation in aqueous media, see Tables 2 and 3, and also those whose properties drastically change upon cooling, see Table 4. We will utilize the definitions for transition temperatures used by the authors. Due to the huge number of polymers of this type, some biopolymers such as polysaccharides will not be described here.

Table 2 Neutral thermoresponsive homopolymers exhibiting LCST-type phase separation behaviour in water

Structure	Properties
I. Polymers bearing amide groups	
<i>N</i> -Substituted poly(acrylamide)s and poly(methacrylamide)s	
 <p>1a</p>	<p>Poly(<i>N</i>-alkyl(meth)acrylamide)s or <i>N</i>-monosubstituted and <i>N</i>-disubstituted poly(acrylamide)s (1a) and poly(methacrylamide)s (1b), where $R_1 = \text{H}$, CH_3, C_2H_5 etc. and $R_2 = \text{CH}_3$, C_2H_5, C_3H_7, etc</p> <p>Homopolymers with $R_1 = \text{H}$, CH_3 and $R_2 = \text{CH}_3$ do not show the LCST behaviour in water in the temperature range of $0 < T < 100^\circ\text{C}$</p>
 <p>1b</p>	<p>Homopolymers with $R_1 = \text{H}$, CH_3, C_2H_5 and $R_2 = \text{C}_2\text{H}_5$, C_3H_7, excluding two pairs of $R_1 = \text{CH}_3$ or C_2H_5 with $R_2 = \text{C}_3\text{H}_7$ (propyl, isopropyl or cyclopropyl), show the LCST behaviour in water in the temperature range of $0 < T < 100^\circ\text{C}$</p> <p>Homopolymers with other R_1 and R_2 are insoluble in water under normal conditions</p>
 <p>2</p>	<p>Poly(<i>N</i>-ethylacrylamide) PEAAM [207–212]</p> <p>$72.8 < \text{LCST} < 85.5^\circ\text{C}$ for $3300 < M_n < 7400$ g/mol upon heating; phase diagram based on T_{cp} ($0 < c < 10$ wt%); LCST of the linear PEAAM is between 1 and 3 wt% and increases with decreasing M [210]; estimated $T_{\text{cp}} = 74^\circ\text{C}$ for $c = 1$ wt% [207]; $T_{\text{max}} = 82^\circ\text{C}$ for $c = 5\text{--}20$ wt% [211]</p> <p>Hysteresis, the effect of the heating/cooling rate on the phase diagram [210]</p> <p>Chemically crosslinked hydrogel shrinks upon heating [207]; $T_{\text{cp}} = 62^\circ\text{C}$ [210]; $T_{\text{max}} = 78.2^\circ\text{C}$ [213]</p> <p>T_{cp} of solutions and gels increases with increasing SDS content and decreases with increasing KCl content or crosslinker [210]</p> <p>Solubility of PEAAM in various solvents [210]</p> <p>$T_g = 138.6^\circ\text{C}$ for $M_w = 204,000$ g/mol, PDI = 3.3 [207]</p> <p>LCST type copolymers with styrene, $20^\circ\text{C} < T_{\text{cp}} < 75^\circ\text{C}$ [207]; other LCST type copolymers of PEAAM [211]</p>
 <p>3</p>	<p>Poly(<i>N</i>-ethylmethacrylamide) PEMAAM [207, 214–217]</p> <p>Structural isomer of PiPAAM</p> <p>$T_{\text{cp}} = 58^\circ\text{C}$ [207]; $T_\Theta = 67^\circ\text{C}$ (phase equilibria) [215]; $T_\Theta = 70.5^\circ\text{C}$ ($M_w \rightarrow \infty$ from $61,000 < M_w < 2,040,000$ g/mol, $1.7 < \text{PDI} < 4.5$, studied using viscometry) [217]; $T_{\text{cp}} = 70^\circ\text{C}$ [214]</p> <p>Thermosensitive microgels functionalized with phenylboronic acid [215]</p>
 <p>4</p>	<p>Poly(<i>N,N'</i>-ethylmethacrylamide) PEMAAM [218–222]</p> <p>Structural isomer of PiPAAM</p> <p>TDSC = 73.8°C ($M_n = 18,100$ g/mol, PDI = 1.12, $c = 0.1$ wt%) [220]; $T_{\text{cp}} = 70^\circ\text{C}$ ($M = 10,000$ g/mol, $c = 0.1$ wt%) [218]; $58 < T_{\text{cp}} < 68.8^\circ\text{C}$ inversely depending on $5400 < M_n < 36,500$ g/mol and $c = 0.05\text{--}5$ wt% [221]; $T_{\text{cp}} = 56^\circ\text{C}$ [210]</p> <p>Tacticity [223]; ATRP and RAFT polymerizations result in PEMAAM of similar stereochemistry [221]</p> <p>Presence of a carboxyl end group instead of an alkyl one elevates T_{cp} by $3\text{--}4^\circ\text{C}$ [221]</p> <p>Block copolymers with PiPAAM and PnPAAM; hysteresis [219]</p>

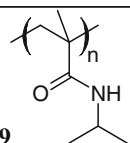
(continued)

Table 2 (continued)

Structure	Properties
<p>5</p> 	<p>Poly(<i>N,N'</i>-diethylacrylamide) PDEAAm [49, 207, 211, 224–237] Phase diagrams and concentration dependences [226, 228–231] $25^{\circ}\text{C} < T_{\text{cp}} < 36^{\circ}\text{C}$ [207, 224, 226]; $T_{\text{cp}} = 29^{\circ}\text{C}$, $M_w = 124,000$ g/mol, $c = 0.2$ wt% [238]; $T_{\text{cp}} = 30.5^{\circ}\text{C}$, $M_w = 91,000$ g/mol, $c = 0.5$ wt% [239, 240]; $T_{\text{cp}} = 32^{\circ}\text{C}$, $M = 10,000$ g/mol, $c = 0.1$ wt% [218]; $T_{\text{max}} = 32^{\circ}\text{C}$ for $c = 5\text{--}20$ wt% [211] Decrease in the T_{cp} with increasing M [226, 231] Chemical crosslinks of PDEAAm decrease T_{cp} for $3\text{--}4^{\circ}\text{C}$ in comparison with the linear polymer [227] Addition of salt decreases T_{cp} [103] Tacticity: syndiotactic and isotactic polymers [223, 230, 235, 236]; isotactic PDEAAm is soluble in water ($T_{\text{cp}} = 31^{\circ}\text{C}$), but syndiotactic PDEAAm is insoluble [223] Copolymers [211, 241–244] and hydrogels [233, 234, 245] $T_g \approx 90^{\circ}\text{C}$, estimated from [211]</p>
<p>6</p> 	<p>Poly(<i>N-n</i>-propylacrylamide) PnPAAm [130, 131, 218, 237, 246–249] Structural isomer of PiPAAm Precise analysis of molecular parameters; for $A_2 = 0$ and $M_w = (13.3\text{--}159) \times 10^4$ g/mol: $T_0 = 22.54 \pm 0.01^{\circ}\text{C}$ [249] $T_{\text{cp}} = 25^{\circ}\text{C}$, $M = 10,000$ g/mol, $c = 0.1$ wt% [218]; $T_{\text{cp}} = 25^{\circ}\text{C}$ ($M = 14,400$ g/mol, PDI = 1.1, $c = 0.1$ wt%) [219]; $T_{\text{cp}} = 24^{\circ}\text{C}$ [246, 247]; $M_w = 361,000$ g/mol: $T_{\text{cp}} = 23.2^{\circ}\text{C}$ ($c = 0.002$ wt%), $T_{\text{dem}} = 23.0^{\circ}\text{C}$, $T_{\text{max}} = 24.5^{\circ}\text{C}$ ($c = 17,100$ unit mol/g) [130] Thermoresponsive gels [130, 250–252]; $T_{\text{cp}} = 25^{\circ}\text{C}$ [247] Syndiotactic PnPAAm with various racemo diad contents: the high cooperativity results from the local formation of ordered structures (presumably helical) in the dehydrated state [253] Block copolymers with PiPAAm and PEMAAm; hysteresis [219]</p>
<p>7</p> 	<p>Poly(<i>N-n</i>-propylmethacrylamide) PnPMMAAm [130, 254–256] $T_{\text{cp}} = 28^{\circ}\text{C}$ [256]; $M_w = 602,000$ g/mol: $T_{\text{cp}} = 27.2^{\circ}\text{C}$ ($c = 0.002$ wt%), $T_{\text{dem}} = 26.9^{\circ}\text{C}$, $T_{\text{max}} = 28.0^{\circ}\text{C}$ ($c = 1.70 \times 10^{-4}$ unit mol/g) [130] Complete resolubilization at 25°C, transition is very slow (h) and takes place in a wide range of T [254, 255] Thermoresponsive gels [130]</p>
<p>8</p> 	<p>Poly(<i>N</i>-isopropylacrylamide) PiPAAm, but generally abbreviated as PNIPAM [45, 49, 55, 86, 101, 130, 207, 257–265] Detailed reviews on synthesis and properties of homo- and copolymers [21, 30, 43, 45, 49, 53, 260] LCST = $27\text{--}32^{\circ}\text{C}$, phase diagram [78, 101, 108, 266]; phase diagram of nanosized gel particles [267]; $M_w = 553,000$ g/mol: $T_{\text{cp}} = 31.2^{\circ}\text{C}$ ($c = 0.002$ wt%), $T_{\text{dem}} = 30.9^{\circ}\text{C}$, $T_{\text{max}} = 32.1^{\circ}\text{C}$ ($c = 2.10 \times 10^{-4}$ unit mol/g) [130] Cooperative hydration [140]</p>

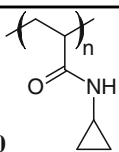
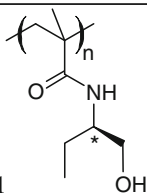
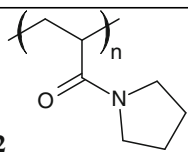
(continued)

Table 2 (continued)

Structure	Properties
	<p>T_{cp} decreases by 2°C when M_n increases from 5400 to 160,000 g/mol [103]; T_{cp} is independent of M if $M > 10^5$ g/mol [78, 266]</p> <p>No intermolecular aggregates are detected at ambient temperature [55]</p> <p>Colloidally stable mesoglobules above 50°C [54, 55, 194–203]</p> <p>Density of polymeric material within a fully collapsed single chain globule or a mesoglobule is 0.3–0.4 g/mL [54, 55, 95, 187], close to 0.40 g/cm³ predicted on the basis of a space-filling model [268]; fractal dimension of the collapsed state is 2.7 [55, 187]</p> <p>Hysteresis understood as limited diffusion of water into the hydrophobic aggregates above the LCST that retards PiPAAM rehydration [95, 269]</p> <p>$T_g = 130^\circ\text{C}$ [270]; $T_g = 140^\circ\text{C}$ [78]</p> <p>Effect of tacticity [271, 272]</p> <p>Effect of salt follows the Hofmeister series [273, 274]</p> <p>Addition of SDS increases T_{cp}: low SDS concentrations – dispersion of colloidal particles, high SDS concentrations – a solution of “necklaces” by SANS [275]; the coil–globule transition in solutions of SDS $T_{cp} = 34^\circ\text{C}$ [276]</p> <p>Addition of a saccharide decreases T_{cp} [277]</p> <p>Oligomers show opposite thermal properties when they are freely dissolved or bound to a gold nanoparticle [278]</p> <p>Brushes grafted to latex particles [279, 280]; polymer-protected gold nanoparticles [281, 282]; various copolymers [45, 49, 55, 259]; drug delivery, tissue engineering [45], thermoresponsive gels [130]</p>
<p>9</p> 	<p>Poly(<i>N</i>-isopropylmethacrylamide) PiPMAAm, but generally named PNIPMAAm [86, 104, 130, 257, 283, 284]</p> <p>For $M_n = 57,000$ g/mol, $M_w/M_n = 1.7$, $c = 2$ wt% and heating rate of 1°C/min, $T_{cp} = 48^\circ\text{C}$ and complete resolubilization upon cooling at 38°C, [284]; for fractions $3000 < M_w < 11,000$ g/mol and $c = 0.05$ wt%, $61 > T_{cp} > 48^\circ\text{C}$ [103]; for $c = 1$ wt% and heating rate of 1°C/min, $T_{cp} = 43^\circ\text{C}$ and complete resolubilization upon cooling at 35°C [86]; $M_w = 420,000$ g/mol: $T_{cp} = 41.2^\circ\text{C}$ ($c = 0.002$ wt%), $T_{dem} = 41.8^\circ\text{C}$, $T_{max} = 42.0^\circ\text{C}$ ($c = 1.81 \times 10^{-4}$ unit mol/g) [130]</p> <p>$T_{cp} = 43\text{--}44^\circ\text{C}$ at normal pressure and $10 < T_{cp} < 50^\circ\text{C}$ at high pressure (0.1–200 MPa) induced coil–globule transition of anthracene-labelled PiPMAAm (50,000 and 140,000 g/mol, PDI = 1.4–1.6, $c < 0.001$ wt%); pressure–temperature phase diagram [97]</p> <p>Kinetics: transition is very slow and takes place in a wide range of T; hysteresis is more pronounced than in the case of PiPAAm [86, 284]</p> <p>Copolymers, effect of NaCl and other cosolutes [103]</p> <p>Thermoresponsive gels [130, 285–288]</p> <p>$T_g = 176^\circ\text{C}$ [289]</p>

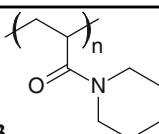
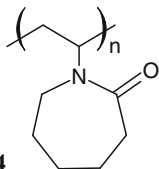
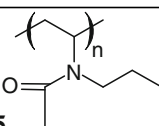
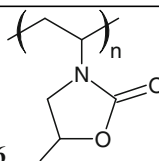
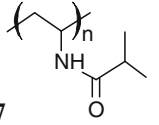
(continued)

Table 2 (continued)

Structure	Properties
	<p>Poly(<i>N</i>-cyclopropylacrylamide) PcPAAM [131] $T_{cp} = 47^{\circ}\text{C}$, $M_w = 211,000$ g/mol, PDI = 4.4, 1 wt% [229]; $T_{cp} = 49^{\circ}\text{C}$, $M_n = 700,000$, 0.5 wt% [131]; $T_{cp} = 57^{\circ}\text{C}$ [207, 229] Thermoresponsive copolymers [290] $T_{cp} = 30^{\circ}\text{C}$ for copolymer with 5 mol% pyrene side groups used for stabilization of carbon nanotubes in water [291] $T_{cp} = 48^{\circ}\text{C}$ for PcPAAM-protected gold nanoparticles [292] Continuous volume change for thermoresponsive gels, $T_{cp} = 40\text{--}50^{\circ}\text{C}$ [247]</p>
	<p>Poly(<i>N</i>-(<i>L</i>)-(1-hydroxymethyl)propylmethacrylamide), abbreviated to P(L-HMPMAm) [293] P(L-HMPMAm) shows optical activity; polymer chains may form packed structures and hence a low hydration state in water $T_{cp} = 30^{\circ}\text{C}$, $M_w = 58,700$ g/mol, 0.4 wt%; above T_{cp}, forms solid precipitates; the turbidity of supernatant is not affected by further heating up to 55°C Upon cooling the turbidity starts to decrease at 21°C; hysteresis is explained by the low hydration state in water due to the compact structure of the polymer Size distributions of P(L-HMPMAm) are bimodal below T_{cp} (6°C) P(DL-HMPMAm) is optically inactive; possesses better solubility in water than P(L-HMPMAm); it exhibits some degree of turbidity at 34°C, but the transmittance does not decrease to 0%; no hysteresis P(DL-HMPMAm) forms a clear coacervate above 34°C; forms no solid precipitate; steric hindrance between the side chains (racemic monomers) results in relatively expanded structures of polymeric chains above 34°C No intermolecular aggregates of P(DL-HMPMAm) below T_{cp} (6°C)</p>
	<p>Poly(<i>N</i>-acryloylpyrrolidine) [207, 237, 294–298] $T_{cp} = 51^{\circ}\text{C}$ for $M_n = 15,000$ g/mol, $c_p = 1$ wt% [294]; $T_{cp} = 52^{\circ}\text{C}$ [237]; $T_{cp} = 56^{\circ}\text{C}$ [298]; no intermolecular aggregates were detected at ambient temperature [294, 297] Hydrophobic end-groups of the RAFT agent decrease T_{cp}: e.g., $T_{cp} = 55\text{--}56^{\circ}\text{C}$ for $M_n = 17,000$ g/mol and PDI = 1.84, whereas $T_{cp} = 48^{\circ}\text{C}$ for $M_n = 5000$ g/mol and PDI = 1.47 ($c_p = 3$ wt%) [297] A small hysteresis between the heating and cooling runs [297] T_{cp} decreases upon increasing NaCl concentration [297] Chemically crosslinked hydrogel shrinks upon heating $T_{cp} \approx 50\text{--}60^{\circ}\text{C}$; collapse is not abrupt [207] Tacticity [223] Self assembling thermosensitive copolymers, e.g., block copolymers with poly(butyl acrylate) [294–297] $T_g = 142^{\circ}\text{C}$ [295]</p>

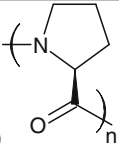
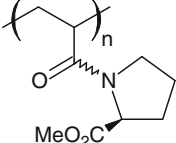
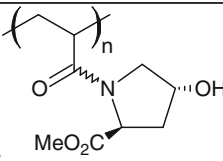
(continued)

Table 2 (continued)

Structure	Properties
13 	Poly(<i>N</i> -acryloylpiperidine) PAOPip [237, 299, 300] PAOPip is soluble below $T_{cp} = 4-6^{\circ}\text{C}$ in the basal buffer (pH 7.0) and completely insoluble above 8°C [237, 299] Purification of thermolabile proteins from a crude solution by affinity precipitation [43] Tacticity [223]
<i>Poly(N-vinyl amide)s</i>	
14 	Poly(<i>N</i> -vinyl caprolactam) PVCL [52, 55, 170, 260, 301–306] Detailed reviews on synthesis and properties on homo- and copolymers [52, 55, 170]; no reports have been found on the controlled radical polymerization Phase diagram: LCST = 31°C , $M_{\eta} = 470,000 \text{ g/mol}$ [307]; LCST 30°C [116]; if $M_w < 10^5 \text{ g/mol}$ then LCST depends on M Intermolecular aggregates are formed by the $M_w < 10^4 \text{ g/mol}$ samples even below T_{cp} [55] $T_{cp} = 38^{\circ}\text{C}$, $M_n = 3200 \text{ g/mol}$, PDI = 2–2.5, $c = 10^{-2} \text{ wt\%}$: coil–globule transition by fluorescence technique [194] Colloidally stable neutral mesoglobules above 50°C [55] T_{cp} decreases with increasing NaCl concentration [308] T_{cp} increases with increasing SDS [308, 309] and cetylpyridinium Chloride concentration [309] $T_g = 190^{\circ}\text{C}$ [107]
15 	Poly(<i>N</i> -vinyl propylacetamide) [307] Phase diagram: LCST = 40°C , $M_{\eta} = 30,000 \text{ g/mol}$
16 	Poly(<i>N</i> -vinyl-5-methyl-2-oxazolidone) [124] $T_{cp} = 40^{\circ}\text{C}$ [124]; $T_{cp} = 65^{\circ}\text{C}$ [303] Effect of cosolute on LCST [124]
17 	Poly(<i>N</i> -vinyl isobutyramide) PViBAm [310–313] Structural isomer of PiPAAm (reversed amide linkage): differences in the properties have been analysed using microcalorimetry [314], pressure-dependent solubility analysis [315] and light scattering [316] $T_{cp} = 35-39^{\circ}\text{C}$ [310, 313] Used to prepare poly(vinylamine) by hydrolysis of the side chain [312, 317] Polymer-protected Pt nanoparticles [318] Copolymers [311, 312, 319, 320]
<i>Protein related polymers</i>	
18 Synthetic polypeptides	Protein-based polymers are composed of repeating peptide sequences ITT-type phase transition: although the transition resembles the LCST type, these polymers usually form helical structures in precipitated state

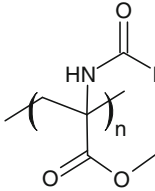
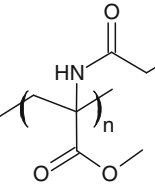
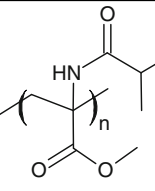
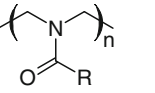
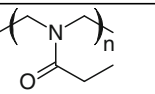
(continued)

Table 2 (continued)

Structure	Properties
	An overview of modern synthesis and self-association of homo- and block/graft copolypeptides can be found in [321–327]; peptide-based amphiphiles [328] Selected examples of neutral homopolypeptides are discussed below
19 Poly(VPGXG): V, L-valine; P, L-proline; G, glycine; X, any natural amino acid except proline	Elastin-like synthetic biopolymers or “elastic protein-based polymers”: consist of repeating pentapeptides [44, 50, 144, 322, 329–344]; ITT-type transition; detailed reviews [44, 144, 331] $0^{\circ}\text{C} < T_{\text{cp}} < 100^{\circ}\text{C}$ depending on X: above T_{cp} a random coil turns into a β -spiral and precipitate T_{cp} is dependent on pH and the ionic strength Hydrophobicity and conformational preferences of the constituent amino acids define the LCST behaviour: T_{cp} of the peptides could be adjusted by replacing valine residues by more hydrophobic isoleucine, leucine or phenylalanine residues [329] Example: $T_{\text{cp}} = 25^{\circ}\text{C}$ for (GVGVP) ₂₅₁ at 0.7 wt% and $M = 100,000$ g/mol [144] TM-DSC on elastin-like biopolymers reveals two simultaneous processes representing chain collapse (endoterm) and β -spiral formation (exoterm); above T_{cp} Elastin-like biopolymers fold and assemble, due to the periodicity of repeating sequences[44, 344] Short chains based on GVGVP pentad sequence: effects of M , chemical composition, and salt concentration on the secondary structure and T_{cp} [329] Methacrylate-functionalized poly(VPGVG) prepared by RAFT [345]
20 	Poly(L-proline) PPro [346, 347] Precipitated polymer is in the ordered crystalline state; theoretically predicted $T_{\Theta} = 100^{\circ}\text{C}$ for $M_n = 53,000$ g/mol using temperature dependence of the second virial coefficient [346] Helical structure of oligoprolines [348, 349]
21 	Poly(<i>N</i> -acryloyl-L-proline methyl ester) PAProMEs [350–355] $T_{\text{cp}} = 14^{\circ}\text{C}$ [350, 351] $T_{\text{cp}} = 17.5^{\circ}\text{C}$ for $M_n = 12,200$ g/mol, $M_w/M_n = 1.26$ [353] $15^{\circ}\text{C} < T_{\text{cp}} < 20^{\circ}\text{C}$, depending on the tacticity $4000 < M_n < 17,000$ g/mol, $M_w/M_n < 1.22$ [352, 353] $15^{\circ}\text{C} < T_{\text{cp}} < 43.5^{\circ}\text{C}$, random copolymers with <i>N,N</i> -dimethylacrylamide [352] Synthesized using RAFT polymerization [352, 353]
22 	Poly(<i>N</i> -acryloyl-4-trans-hydroxy-L-proline methyl ester) PAHProMEs [353] $T_{\text{cp}} = 49.5^{\circ}\text{C}$ for $M_n = 11,000$ g/mol, $M_w/M_n = 1.29$ [353] Synthesized using RAFT polymerization [352, 353]

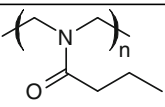
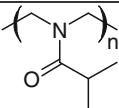
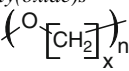
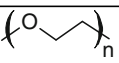
(continued)

Table 2 (continued)

Structure	Properties
<i>Poly(methyl 2-alkylamidoacrylate)s</i>	
	<p>Poly(methyl 2-alkylamidoacrylate)s [356]</p> <p>R₁: poly(methyl 2-acetamidoacrylate), water-soluble</p> <p>R₂: poly(methyl 2-propionamidoacrylate), thermosensitive</p> <p>R₃: poly(methyl 2-isobutyramidoacrylate), thermosensitive</p> <p>R₄: poly(methyl 2-<i>n</i>-butyramidoacrylate), insoluble in water</p>
23	
	<p>Poly(methyl 2-propionamidoacrylate) [356–359];</p> <p>LCST = 49–50°C, $M_n = 670,000$ g/mol, PDI = 2.7: the phase diagram (T_{cp} vs. c, $0.1 < c < 10$ wt%) is flat above 4 wt%; below 4 wt%, T_{cp} decreases with the increasing c; $c = 0.5$ wt%: sharp transition at $T_{cp} = 51^\circ\text{C}$, no hysteresis [356, 357]</p> <p>Shows no endotherm during the phase transition; the difference with the <i>i</i>Pr-containing polymer results from the size of the hydrophobic group [356]</p> <p>T_{cp} decreases with salt concentration in line with the Hofmeister series [356, 357]</p>
24	
	<p>Poly(methyl 2-isobutyramidoacrylate) [357]</p> <p>$T_{cp} = 19^\circ\text{C}$: $c = 0.5$ wt%, sharp transition, no hysteresis [357]</p> <p>Shows endotherm during the phase transition [357]</p>
25	
<i>Poly(oxazoline)s</i>	
	<p>Poly(2-substituted-2-oxazoline)s are polymeric non-ionic tertiary polyamides obtained from 2-substituted oxazolines via living cationic ring-opening polymerization [64, 360–365];</p> <p>Poly(2-methyl-2-oxazoline), PMOz, is soluble in water at $0^\circ\text{C} < T < 100^\circ\text{C}$; polyoxazolines with ethyl, propyl and isopropyl pendants show the LCST behaviour; the transition is sharp with fast responsivity in comparison to PiPAAm; transition is reversible, and shows no noticeable hysteresis; no polyoxazolines with four or more carbon atoms have been reported to be soluble in water [362, 366–370]; poly(2-alkyl-2-oxazoline)s with 1–7 pendants are crystallizable and form oriented crystalline filaments [365, 371–376]; while those with 6–11 reveal glass transition temperatures [365]</p>
26	
	<p>Poly(2-ethyl-2-oxazoline) PEOz [366, 367, 370, 377–383]</p> <p>Phase diagram and LCST [377, 383]</p> <p>$T_{cp} > 100^\circ\text{C}$ ($M_n < 10,000$ g/mol) [383]; $T_{cp} > 90^\circ\text{C}$ ($M_n = 8000$ g/mol, PDI = 1.02, $c = 1$ wt%) [366, 367]; $T_{cp} = 90.6^\circ\text{C}$ ($M_n = 6700$ g/mol, PDI = 1.15, $c = 5$ g/l) and $T_{cp} = 69.3^\circ\text{C}$ ($M_n = 37,300$ g/mol, PDI = 1.6, $c = 5$ g/l) [382]; $78^\circ\text{C} > T_{cp} > 66^\circ\text{C}$ (9200 g/mol $< M_n < 40,000$ g/mol, $c = 5$ g/l) [383]; $60^\circ\text{C} < T_{cp} < 78^\circ\text{C}$ ($M > 20,000$ g/mol) [370, 377–379]</p>
27	

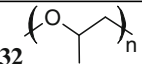
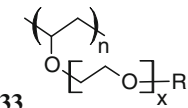
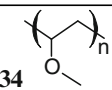
(continued)

Table 2 (continued)

Structure	Properties
	<p>Effect of crosslinks: $T_{cp} = 68^{\circ}\text{C}$ of PEOz hydrogel is lower than the $T_{cp} = 73^{\circ}\text{C}$ of the linear polymer with comparable molecular mass [381]; this is similar to PiPAAm hydrogels [382]</p> <p>Effect of salt [377]</p> <p>- At pH < 3.5 forms a H-bonded complex with poly(methacrylic acid) PMAA [385], this is similar to PiPAAm/PMAA complexation (pH < 6.3) [386]</p> <p>$T_g = 60^{\circ}\text{C}$ [371]; $T_m = 149^{\circ}\text{C}$ for $M_n = 14,920$ g/mol, PDI = 1.2 [365]</p>
<p>28</p> 	<p>Poly(2-<i>n</i>-propyl-2-oxazoline) PnPOz</p> <p>Structural isomer of PiPAAm (reversed amide linkage with N in the main chain and propyl instead of isopropyl pendant)</p> <p>$T_{cp} = 23.8^{\circ}\text{C}$ ($M_n = 12,000$ g/mol, PDI = 1.04, $c = 1$ wt%) [366];</p> <p>$T_{cp} = 25^{\circ}\text{C}$ ($M_n = 3068$ g/mol, PDI = 1.13, $c = 2$ wt%) [387];</p> <p>$T_{cp} = 42.9^{\circ}\text{C}$ ($M_n = 3100$ g/mol, PDI = 1.1, $c = 5$ g/l) and</p> <p>$T_{cp} = 22.5^{\circ}\text{C}$ ($M_n = 18,000$ g/mol, PDI = 1.46, $c = 5$ g/l) [382]</p> <p>$T_g = 40^{\circ}\text{C}$ [371]; $T_m = 145^{\circ}\text{C}$ for $M_n = 12,160$ g/mol, PDI = 1.3 [365]</p>
<p>29</p> 	<p>Poly(2-isopropyl-2-oxazoline) PiPOz [64, 366, 388–390]</p> <p>Structural isomer of PiPAAm (reversed amide linkage with N in the main chain)</p> <p>$T_{cp} = 36^{\circ}\text{C}$ ($M_n = 16,700$ g/mol) [370]; $T_{cp} = 38.7^{\circ}\text{C}$ ($M_n = 9700$ g/mol, PDI = 1.02, $c = 1$ wt%) [366]; $T_{cp} = 47^{\circ}\text{C}$ ($M_n = 3907$ g/mol, PDI = 1.09, $c = 2$ wt%) [387];</p> <p>$45^{\circ}\text{C} < T_{cp} < 63^{\circ}\text{C}$, T_{cp} decreases with increasing M_n ($1900 < M_n < 5700$ g/mol, PDI ≤ 1.05, $c = 0.1$ wt%) [388]</p> <p>Telechelic and heterotelechelic with hydroxy, amine or acetal groups: T_{cp} is highly concentration-dependent [389]; hydrophobic methyl, <i>n</i>-nonyl, piperidine, piperazine as well as hydrophilic oligo(oxyethylene) end groups decrease the LCST; the effect of the end group polarity on T_{cp} is stronger than with PiPAAm [390]</p> <p>Insoluble aggregates of PiPOz are formed when the precipitated polymer is kept for 24 h above $T_{cp} = 65^{\circ}\text{C}$; precipitated polymer is fibrous [372, 373, 387]</p> <p>$T_g = 70^{\circ}\text{C}$ [372]</p>
II. Poly(ether)s	
Poly(oxide)s	
<p>30</p> 	<p>Polyoxide is a polymer with oxygen atoms in the main chains [124]; polyoxides with $x = 1, 3$ (except PPO), 4, 5, etc. are not soluble in water at any temperature</p>
<p>31</p> 	<p>Poly(ethyleneoxide) or poly(ethylene glycol) PEO or PEG [124, 391–394]</p> <p>One LCST-type critical temperature of $T_{\Theta} = 106^{\circ}\text{C}$ (estimated at 3 MPa) and two critical temperatures corresponding to the UCST behaviour: $T_{\Theta I} = -12 \pm 3^{\circ}\text{C}$ (estimated in supercooled state) and $T_{\Theta II} = 115^{\circ}\text{C}$ (estimated at 3 MPa) [124, 395]</p>

(continued)

Table 2 (continued)

Structure	Properties
	<p>LCST-type behaviour: $T_{cp} = 96^{\circ}\text{C}$ for $M_n = 20,000$ [396], $T_{\theta} = 96 \pm 3^{\circ}\text{C}$ [124]</p> <p>Addition of salt decreases T_{θ} [124, 396–400]: $T_{\theta} = 90^{\circ}\text{C}$, 2 M LiCl; $T_{\theta} = 82^{\circ}\text{C}$, 2 M CaCl_2; $T_{\theta} = 80^{\circ}\text{C}$, 2 M MgCl_2; $T_{\theta} = 76^{\circ}\text{C}$, 2 M NH_4Cl; $T_{\theta} = 73^{\circ}\text{C}$, 2 M SrCl_2; $T_{\theta} = 60^{\circ}\text{C}$, 2 M CsCl; $T_{\theta} = 60^{\circ}\text{C}$, 2 M NaCl; $T_{\theta} = 57^{\circ}\text{C}$, 2 M KCl; $T_{\theta} = 56^{\circ}\text{C}$, 2 M RbCl [397] $T_{\theta} = 35^{\circ}\text{C}$, 0.45 M K_2SO_4 and $T_{\theta} = 45^{\circ}\text{C}$, 0.39 M MgSO_4 [124]</p> <p>Crystallizable, $-65^{\circ}\text{C} < T_g < -20^{\circ}\text{C}$ depending on M and crystalline content [124, 401]</p>
<p>32</p> 	<p>Poly(propyleneoxide) or poly(propylene glycol) PPO [103, 124, 125, 402]</p> <p>$M \leq 400$ g/mol is water-soluble at room temperature; $M = 1200$ g/mol is soluble up to 2 wt%; solubility of $M \geq 2000$ g/mol PPO is less than 0.1 wt% [103, 124, 125]</p> <p>For $c = 0.05$ wt%: $T_{cp} = 15^{\circ}\text{C}$ for $M = 3000$ g/mol and $T_{cp} = 35^{\circ}\text{C}$ for $M = 1200$ g/mol [403]; estimated $T_{\theta} = -53^{\circ}\text{C}$ for $M = \infty$ [124]</p> <p>For $c = 4.15$ g/L, $M_n = 1,000$ g/mol: $35^{\circ}\text{C} < T_{cp} < 40^{\circ}\text{C}$, broad transition with $T_{max} = 40.9^{\circ}\text{C}$ [103], transition enthalpy is 1.4 kcal/mol of repeating units, similar to the values observed for PiPAAm and PMVEth</p> <p>Limited solubility is suggested to result from spiral folding of the chain into tightly coiled disks in aqueous solution [402]</p> <p>Crystallizable, $T_g = -75^{\circ}\text{C}$ for high M [124]</p>
<i>Poly(vinylether)s</i>	
<p>33</p> 	<p>Polyether is a polymer with oxygen atoms in the main or side chain. Among them, thermoresponsive poly(vinylether)s have oxymethylene and/or oxyethylene pendants in their side chains [30, 124, 404–406]</p> <p>Phase separation temperature of vinyl ethers can be controlled by varying the number of the pendant oxyethylene units and/or the hydrophobicity of an ω-alkyl group, R</p> <p>T_{cp} measurements typically reveal an abrupt reversible transition within $\Delta T = 1^{\circ}\text{C}$; no hysteresis</p> <p>Homopolymers of ethyl vinylether and higher alkyl vinylethers are insoluble in water</p>
<p>34</p> 	<p>Poly(methylvinylether) PMVEth [30, 32, 55, 103, 188, 260, 407–416]</p> <p>Bimodal phase diagram [188, 417, 418]</p> <p>Colloidally stable droplets of PMVEth [188]</p> <p>LCST1 = $32\text{--}33^{\circ}\text{C}$ ($c < 30$ wt%) and LCST2 $\approx 28^{\circ}\text{C}$ ($c > 30$ wt%) [116–119, 417, 418]; intermolecular aggregates exist below T_{cp} [55]</p> <p>DSC: broad endothermic peak typically has a low ΔC_p shoulder on the lower temperature side [103, 417, 418]</p> <p>Addition of salt decreases T_{cp} [103, 407]</p> <p>Polymer-protected gold nanoparticles [413]</p> <p>Time-limited colloidal stability; stable droplets [188]; mesoglobules above 50°C; liquid–liquid macrophase separation within a month [55]</p>

(continued)

Table 2 (continued)

Structure	Properties
	Isotactic PMVEth is crystallizable, $-19 < T_g < -40^\circ\text{C}$ [118, 119, 124, 417, 418] Copolymers [30, 414, 419–422]
35	Poly(2-methoxyethylvinylether) PMOVEth [405, 423, 424] $T_{cp} = 63^\circ\text{C}$ [405]; $T_{cp} = 70^\circ\text{C}$ ($M_n = 20,000$ g/mol, PDI = 1.11, 1 wt%) [405] T_{cp} decreases by 5°C as M_n increases from 10,000 to 20,000 g/mol; further increase in M_n hardly affects T_{cp} [405] No hysteresis [405] Gradient, random and block copolymers with PEOVEth [424]
36	Poly(2-ethoxyethylvinylether) PEOVEth [404, 423, 424] $T_{cp} = 20^\circ\text{C}$ ($M_n = 22,000$ g/mol, PDI = 1.13, 1 wt%) [405] No hysteresis [405] Gradient EOVEth-co-MOVEth undergo gradual thermally induced association above $T_{cp} = 20^\circ\text{C}$, forming micelles with a hydrophobic core of EOVE-rich segments. The size of the micelles decreases monotonously with further increasing solution temperature, whereas block copolymers reveal two-step transition, and random copolymers one-step transition [424] Block copolymers with poly(hydroxyethyl vinyl ether), PHOVEth: sol-gel transition at 20.5°C , $c = 17$ wt% [423, 425]
37	Poly(2-(2-ethoxy)ethoxyethylvinylether) [426] Phase diagram $c < 50$ wt% [427]; the T_{cp} curve is flat except in a very dilute region $T_{cp} = 40^\circ\text{C}$ [428]; LCST = $40.0\text{--}40.5^\circ\text{C}$ ($M_n = 20,000$ g/mol, PDI = 1.33 and $M_n = 34,000$ g/mol, PDI = 1.26) [427] Thermoresponsive copolymers [420, 428]
38	Poly(4-hydroxybutylvinylether) [30, 420, 429] $T_{dem} \sim 42^\circ\text{C}$ Derived from a silyloxy-protected pendant counterpart Polymers with shorter or longer $-(\text{CH}_2)_n$ spacers are soluble or insoluble in water, respectively
39	Alkylglycidylethers: poly(methyl glycidyl ether), poly(ethyl glycidyl ether), poly(ethoxyethyl glycidyl ether) [430–432]; $14.6^\circ\text{C} < T_{cp} < 57.7^\circ\text{C}$ is strongly affected by the length and structure of the alkyl chain [430, 431] Anionic ring-opening polymerization Ether bond in the main and side chain Temperature-dependent sol-gel transitions Copolymers of glycidyl methyl ether with ethyl glycidyl ether to adjust T_{cp} [432]

(continued)

Table 2 (continued)

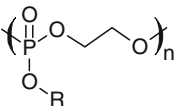
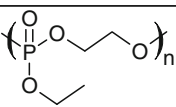
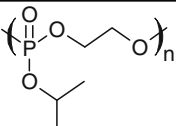
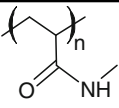
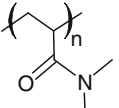
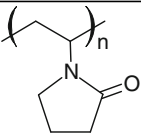
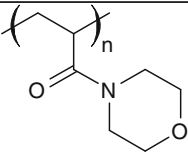
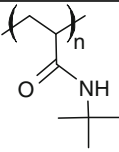
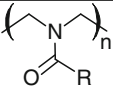
Structure	Properties
III. Polymers bearing phosphate groups	
<i>Poly(phosphoester)s</i>	
<p>40</p> 	<p>Poly(phosphoester)s are polyphosphates obtained through ring-opening polymerization of cyclic phosphoester monomers; poly(2-methoxy-2-oxo-1,3,2-dioxaphospholane), or poly(methyl ethylene phosphate), is not reported to show the LCST behaviour; poly(phosphoester)s are biodegradable and biocompatible [433–438]</p>
<p>41</p> 	<p>Poly(2-ethoxy-2-oxo-1,3,2-dioxaphospholane) or poly(ethyl ethylene phosphate) [437, 439, 440] $T_{cp} = 38^\circ\text{C}$ ($M_w = 14,600$ g/mol, PDI = 1.25, $c = 1$ wt%) [440] Transition is thermoreversible with small hysteresis Gold nanoparticles [438]</p>
<p>42</p> 	<p>Poly(2-isopropoxy-2-oxo-1,3,2-dioxaphospholane) or poly(isopropyl ethylene phosphate) [437, 439, 440] $T_{cp} = 5^\circ\text{C}$ [440] Linear copolymers [437, 440]; addition of NaCl decreases T_{cp}; transition is thermoreversible with small hysteresis Gold nanoparticles [438]</p>

Table 3 Selected examples of thermoresponsive neutral polymers based on amphiphilic balance and showing the type of LCST behaviour

Structure	Properties
<p>43</p> 	<p>Poly(<i>N</i>-methylacrylamide) PMAAm [207] Estimated $T_{cp} > 100^\circ\text{C}$ $T_g = 178.5^\circ\text{C}$, $M_w = 185,000$ g/mol, PDI = 3.6 LCST-type copolymers with styrene, $20^\circ\text{C} < T_{cp} < 100^\circ\text{C}$</p>
<p>44</p> 	<p>Poly(<i>N,N'</i>-dimethylacrylamide) PDMAAm [195, 207, 222, 236, 454–456]; LCST: estimated $T_{cp} > 100^\circ\text{C}$ [207, 454], $T_{cp} \approx 200^\circ\text{C}$ [195] Chemically crosslinked hydrogel shrinks upon heating [207] $T_g = 125.7^\circ\text{C}$, $M_w = 156,000$ g/mol, PDI = 3.4 [207]; $T_g = 122^\circ\text{C}$ [454]; $T_g = 105^\circ\text{C}$ [295] Tacticity [223]; isotactic PDMAAm is highly crystalline and only partially soluble in water [457, 458]; however, in [223] PDMAAm samples are reported to be soluble in water regardless of the tacticity LCST type copolymers with styrene, $20^\circ\text{C} < T_{cp} < 100^\circ\text{C}$ [207] and with 2-methoxyethylacrylate, $9^\circ\text{C} < T_{cp} < 80^\circ\text{C}$ [454]; AB diblock copolymers [455]</p>

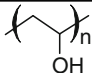
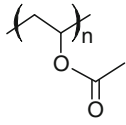
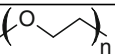
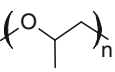
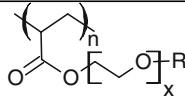
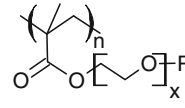
(continued)

Table 3 (continued)

Structure	Properties
45 Poly(<i>N</i> -alkyl(meth)acrylamide)s bearing hydroxyl groups	<i>N</i> -monosubstituted and <i>N</i> -disubstituted poly(acrylamide)s and poly(methacrylamide)s [459] The precursor polymers, e.g. poly(<i>N</i> -2-hydroxypropylmethacrylamide), poly[<i>N,N</i> -bis(hydroxyethyl) acrylamide] and poly(<i>N</i> -[tris(hydroxymethyl)-methyl] acrylamide): the T_{cp} is tailored by varying the acylating agent (acetylation and cinnamoylation) or by varying the extent of acylation
46 	Poly(vinylpyrrolidone) [303, 460, 461] Phase separation and solubility behaviour [124, 461] Estimated and measured $T_{\theta} = 140 \pm 5^{\circ}\text{C}$ [124], $T_{\theta} = 160^{\circ}\text{C}$ [303] Salt and aromatic cosolutes decrease T_{cp} : $M_w = 78,000$ g/mol, $27^{\circ}\text{C} < T_{cp} < 77^{\circ}\text{C}$ [462–465] $T_{\theta} = 28^{\circ}\text{C}$, $M_n = 99,000$ –457,000 g/mol in 0.55 M Na_2SO_4 [461] $T_g = 86 \pm 1^{\circ}\text{C}$ [124]
47 	Poly(<i>N</i> -acryloylmorpholine) pAOM RAFT polymerization [300, 466–468] Well soluble in water; T_{cp} is probably 100°C $36 < T_{cp} < 80^{\circ}\text{C}$ thermosensitive fluoroalkyl-end-capped pAOM homo- and co-oligomers [469, 470] Tacticity [223]
48 	Poly(<i>N</i> - <i>tert</i> -butylacrylamide) [471, 472] LCST: theoretical $T_{cp} = -5^{\circ}\text{C}$; $T_g = 108^{\circ}\text{C}$ $T_{cp} = 27^{\circ}\text{C}$ for random poly[(<i>N</i> - <i>tert</i> -butylacrylamide)- <i>co</i> -acrylamide] with 50:50 molar ratio of <i>N</i> - <i>tert</i> -butylacrylamide/acrylamide 0.2 mm thick film made of chemically crosslinked random poly[(<i>N</i> - <i>tert</i> -butylacrylamide)- <i>co</i> -acrylamide], with 27:73 molar ratio of repeating units, reversibly swells and contracts in the range of 6 – 80°C
49 	Poly(2-substituted-2-oxazoline)s Copolymers with adjusted T_{dem} by changing the comonomer composition and molecular weight [382, 473, 474]; gradient or random copolymers of POz and either iPOz or EOz $23.8^{\circ}\text{C} < T_{cp} < 75.1^{\circ}\text{C}$ [366, 367]; gradient copolymers of iPOz with 2- <i>N</i> -propyl-, 2- <i>N</i> -butyl-, and 2- <i>N</i> -nonyl-2-oxazoline, $9^{\circ}\text{C} < T_{cp} < 46^{\circ}\text{C}$ [387] Block copolymers and thermoresponsive micelles [475]; cylindrical molecular brushes [476]; comb and graft shaped poly(oligoEOz methacrylate)s [477]; polyion complex micelles stabilized with PiPOz [478] Poly(2-ethyl-2-oxazoline)- <i>block</i> -poly(ϵ -caprolactone): thermally reversible sol–gel transition [479, 480]

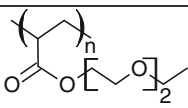
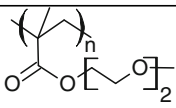
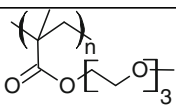
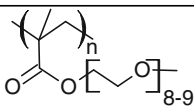
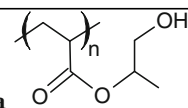
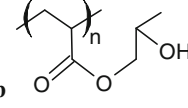
(continued)

Table 3 (continued)

Structure	Properties
	Effect of salt: NaCl lowers the LCST [367] A variety of amphiphilic random, block and star copolymers of 2-methyl-2-oxazoline with 2-oxazoline-bearing pendant hydrophobic moieties (LCST behaviour was not studied) [371, 481–484]
50a  50b 	(50a) Poly(vinylalcohol) PVAL (50b) Poly(vinylacetate) PVAc [303, 485–490] PVAL: estimated $T_{\Theta} = 125^{\circ}\text{C}$ [303] PVAL is obtained from PVAc by alcoholysis, hydrolysis or aminolysis [485]; PVAL–PVAc with the degree of hydrolysis below 83% shows the LCST behaviour between 0 and 100°C ; T_{cp} decreases with increasing Vac content [124, 491–493] Properties of aqueous PVAL–PVAc solutions are affected by the degree of hydrolysis, temperature, pressure, addition of electrolytes; H-bonds are disrupted at $T = 54 - 67^{\circ}\text{C}$ [491] PVAL is highly crystallizable: needs to be heated above 70°C to solubilize PVAL with the degrees of hydrolysis above 87% are not soluble at all For PVAL–PVAc, 50% of Vac, $T_{\Theta} = 25^{\circ}\text{C}$ [494] PVAL–PVAc: $T_{\Theta} = 97^{\circ}\text{C}$ for $M_w = 13,500, 34,400, 74,100 \text{ g/mol}$ [397, 487] $T_g = 70 - 99^{\circ}\text{C}$ [124, 401]
51a  51b 	(51a) Poly(ethyleneoxide) PEO (51b) Poly(propyleneoxide) PEO Copolymers, PEO–PPO–PEO block copolymers, Pluronics or Poloxamer, Tetronics [45, 49, 51, 392, 495–503] PEO37–PPO56–PEO37: micellization at $12 - 18^{\circ}\text{C}$ and $T_{\text{cp}} = 91^{\circ}\text{C}$ of LCST type [499] Hydrophobically end-capped poly(EO- <i>co</i> -PO): T_{cp} is in the range of $18 - 71^{\circ}\text{C}$ depending on the end group, $c = 0.5 \text{ wt\%}$; sharp phase transition within 3°C and small hysteresis; two liquid phases above T_{cp} ; T_{cp} is linearly decreases with increasing concentration of salts (Na_2SO_4 and Na_3PO_4) [504]
52a  52b 	Self-assembling polymers containing PEO in the side chain form a class of thermoresponsive polymers based on amphiphilic balance [49]; R is ω -alkyl group or H Substituting the hydrophilic groups that make the polymer water-soluble with hydrophobic groups, one can convert a polymer, originally soluble in water at all temperatures, into a polymer soluble in water only below a given temperature and vice versa [207] Example: grafted polymethacrylates (molecular brushes) [30, 505–515]

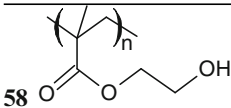
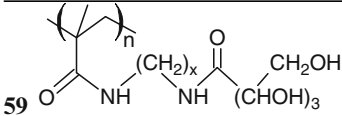
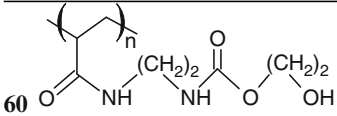
(continued)

Table 3 (continued)

Structure	Properties
	<p>Polymers show reversible cloud points with no hysteresis; T_{cp} of these polymers depends on chemical composition and can be adjusted between $20 < T < 90^{\circ}\text{C}$ T_{cp} is strongly dependent on the lengths of PEO chain T_{cp} is not dependent on c, flat phase diagram Typically $T_g < 0^{\circ}\text{C}$; longer flexible PEO side chains decrease T_g [516]</p>
53 	<p>Poly[2-(2-ethoxyethoxy)ethylacrylate] PEE02A [297] $T_{cp} = 9^{\circ}\text{C}$ for $M_n = 17,500$ g/mol, PDI = 1.66 at $c = 1$ wt%; Copolymers with oligo(ethylene glycol) methyl ether acrylate $9 < T_{cp} < 49.9^{\circ}\text{C}$; no hysteresis</p>
54 	<p>Poly[2-(2-methoxyethoxy)ethylmethacrylate] PME02MA [297, 509, 512] $T_{cp} = 28^{\circ}\text{C}$ for $M_n = 16,700$ g/mol, PDI = 1.72, $c = 3$ wt% [512] T_{cp} in water is around $26\text{--}27^{\circ}\text{C}$, $M_n = 10,000\text{--}37,000$ g/mol, PDI < 1.1, $c = 0.2$ wt% [509]; T_{cp} decreases with increasing the M_n Very weak hysteresis [509, 512] $T_g = -40^{\circ}\text{C}$ [509] Effect of tacticity [509] Block copolymers with PS [509]</p>
55 	<p>Poly[2-(2-methoxyethoxy)ethoxymethylmethacrylate] PME03MA [509] $T_{cp} = 49\text{--}52^{\circ}\text{C}$, $M_n = 10,000\text{--}37,000$ g/mol, PDI < 1.1, $c = 0.2$ wt%; T_{cp} decreases with increasing the M_n Very weak hysteresis $T_g = -47^{\circ}\text{C}$ Effect of tacticity Block copolymers with PS and PME02MA</p>
56 	<p>Poly[oligo(ethyleneglycol)methacrylate] POEGMA with side chains of eight or nine ethylene oxide units [294, 512] $T_{cp} = 83^{\circ}\text{C}$ for $M_n = 15,000$ g/mol, PDI = 1.08, $c = 1$ wt% [294]; $T_{cp} = 90^{\circ}\text{C}$ for $M_n = 10,000$ g/mol, PDI = 1.18, $c = 3$ wt% [512] Very weak hysteresis for homo- and copolymers [294, 512]; Copolymers P(MEO2MA-co-OEGMA): flat phase diagram; measured T_{cp} were in the range of $28\text{--}90^{\circ}\text{C}$; $T_{cp} = 28 + 1.04 \times \text{DPOEGMA}$ [512]; self-assembling block copolymers [294]</p>
57a  57b  mixture of isomers	<p>Poly(2-hydroxypropylacrylate) PHPA, mixture of isomers [207, 517] Strong concentration dependence of T_{cp}: $T_{cp} = 16^{\circ}\text{C}$ at $c = 10$ wt% [207]; $T_{cp} = 18.3^{\circ}\text{C}$ at $c = 1.5$ wt%, $T_{cp} = 21.4^{\circ}\text{C}$ at $c = 1.0$ wt%, $T_{cp} = 26.7^{\circ}\text{C}$ at $c = 0.5$ wt%, $T_{cp} = 33.3^{\circ}\text{C}$ at 0.25 wt% ($M_n = 11,100$ g/mol, PDI = 1.21) [517] For dilute solutions, the phase transition is broad and it is broader upon dissolution than upon precipitation [517]</p>

(continued)

Table 3 (continued)

Structure	Properties
	For dilute solutions, redissolution of PHPA upon cooling occurs at higher temperatures than precipitation upon heating [517], i.e. hysteresis is reversed to the hysteresis observed PiPAAm [95] $T_g = 21.7^\circ\text{C}$ ($M_n = 11,100$ g/mol, PDI = 1.21) [517] Random copolymers [207, 517]
	Poly(2-hydroxyethylmethacrylate) PHEMA [518–524] $M_w/M_n < 1.25$, $c = 0.50$ wt%: for $M_n < 10,900$ g/mol $T_{cp} > 100^\circ\text{C}$, for $10,900 < M_n < 14,300$ g/mol $39 > T_{cp} > 28^\circ\text{C}$, $M_n > 14,300$ g/mol is insoluble; range of transition temperature is very broad $\sim 15^\circ\text{C}$; enhanced water solubility of these PHEMA at pH 2.2 is due to protonation of the terminal morpholine groups derived from the ATRP initiator [518] Copolymers [518], hydrogels [519, 524] Urea raises the degree of swelling of PHEMA gels: $M_\eta = (1 - 50) \times 10^5$: $T_\theta = 10^\circ\text{C}$ in aqueous 4 M urea, $T_\theta = 27.2^\circ\text{C}$ in 6 M urea, and $T_\theta = 52.5^\circ\text{C}$ in 8 M urea [523] Isotactic PHEMA: $T_\theta = 15.3^\circ\text{C}$ for $M_\eta = 39,000 - 816,000$ [522] HEMA copolymers are biocompatible and blood compatibility [525, 526]
	<i>N</i> -substituted polymethacrylamides with alkylaldonamide side chains Phase diagram for the polymer with $x = 10$ and $c > 20$ wt%; thermotropic and lyotropic properties; Physical gel melts upon heating and consequently adopts a birefringent glassy lamellar phase, lamellar phase, and isotropic solution [527]
	Poly(amidohydroxyurethane) PAmHU [528, 529] $T_{cp} = 57^\circ\text{C}$ for $M_n = 18,700$ g/mol, $c_p = 1-3$ w/wt% The molecular architecture of studied polymer suggests a coil-to-micelle demixing scenario PAmHU is crystalline $22^\circ\text{C} < T_{cp} < 57^\circ\text{C}$ of PAmHU/water/ethanol mixture
61 Hyperbranched polyethers	(61a) 1,4-butanediol diglycidyl ether with triols such as trimethylolethane and trimethylolpropane [530] $19.0 < T_{cp} < 40.3^\circ\text{C}$: ($c = 1.0$ wt%) is adjustable depending on the hydrophilic/hydrophobic balance of 1,4-butanediol diglycidyl ether and triols (61b) 1,2,7,8-diepoxyoctane with ethylene glycol, di(ethylene glycol), tri(ethylene glycol), 1,2-propanediol, and glycerol [531] $23.6 < T_{cp} < 67.2^\circ\text{C}$: ($c = 1.0$ wt%) is adjustable depending on the composition $-48.8 < T_g < -29.7^\circ\text{C}$; highly branched polyethers are flexible polymers

(continued)

Table 3 (continued)

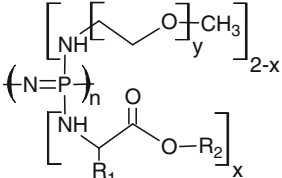
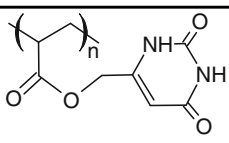

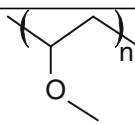
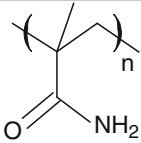
Structure	Properties
62 Oligo(ethylene oxide)-grafted poly lactides	<p>Glycolides with pendent oligoEO monomethyl ether substituents [532]</p> <p>One or two EO units: more hydrophilic than polylactide but insoluble in water</p> <p>Three EO units: $T_{cp} = 19^{\circ}\text{C}$, $M_n = 59,800$ g/mol, $PDI = 1.16$, $c = 1.5\text{wt}\%$</p> <p>Four EO units: $M_n = 10,600$ g/mol, $PDI = 1.12$, $c = 1.5$ wt%: $T_{cp} = 37^{\circ}\text{C}$</p>
63 Methoxy-terminated dendronized polymethacrylates	<p>PG1: $T_{cp} = 62.5\text{--}64.5^{\circ}\text{C}$ ($c < 4$ wt%, M independent, no specific morphologies for aggregates is observed above T_{cp}, aggregation is dependent on heating rate and concentration, and also differs for heating and cooling)</p> <p>PG2: $T_{cp} = 64.2\text{--}65.7^{\circ}\text{C}$ ($c < 2$ wt%, uniform spherical aggregates above T_{cp}, uniformity is independent of heating rate and concentration)</p> <p>$T_g < -80^{\circ}\text{C}$ for both</p> <p>Thermoresponsiveness results from the entire branch-work and not from just a peripheral decoration</p> <p>Change methyl for ethyl groups at the periphery of the polymers has a pronounced effect on LCST [533]</p>
64 Isobutyramide-terminated poly(amidoamine) dendrimers	<p>Dendrimers of generation G3, G4, and G5 (32, 64, and 128 terminal VIBAm groups) showed T_{cp} of 76, 60 and 42°C, respectively, in 10 mM phosphate buffer (1.0 wt%, pH 9.0); phase diagram for $c < 1$ wt%</p> <p>T_{cp} increases with increasing urea concentration</p> <p>T_{cp} decreases with increasing hydrophilicity of generations; this finding was rationalized in terms of densely packed structures, which facilitate the dehydration process (impact of steric hindrance on LCST) [534–536]</p>
65 	<p>Poly(organophosphazene)s with two side groups of poly(ethylene oxide) and amino acid esters, where $R_1 = \text{H}, \text{CH}_3, \text{COOR}_2, \text{CH}_2\text{COOR}_2, \text{CH}_2\text{CH}_2\text{COOR}_2, \text{CH}(\text{CH}_3)\text{CH}_2\text{CH}_3$ and $R_2 = \text{CH}_3, \text{C}_2\text{H}_5, \text{CH}_2\text{C}_6\text{H}_5$ [30, 49, 303, 537–542]</p> <p>$50^{\circ}\text{C} < T_{cp} < 93^{\circ}\text{C}$, depending on the structure of the side groups</p> <p>Biodegradable thermosensitive polymer [543]</p> <p>Reversible sol–gel transition upon heating [540]</p>

Table 4 Neutral thermoresponsive homopolymers, for which the solubility in water decreases upon cooling

Structure	Properties
<p>66</p> 	<p>Poly[6-(acryloyloxymethyl)uracil] [544] UCST type of transition: $T_{cp} \approx 60^\circ\text{C}$ for $c = 0.1$ wt% Since NH and C=O groups of uracil act as donors and acceptors, interpolymer complexes are formed upon decreasing temperature and increasing the strength of the hydrogen bonds Phase transition is shifted to lower temperatures upon addition of urea or adenosine (complementary nucleic acid base to uracil) preventing the complex formation in cold water</p>
<p>67</p> 	<p>Poly(ethyleneoxide) PEO Two critical temperatures corresponding to the UCST behaviour $T_{\Theta I} = -12 \pm 3^\circ\text{C}$, estimated in supercooled state [124] PEO shows UCST behaviour ($T_{cp II} = 115^\circ\text{C}$) above its LCST ($T_{cp} = 106^\circ\text{C}$) under pressure of 3 MPa, between 106 and 115°C PEO demixes (immiscibility island); phase behaviour studied using SANS [395] Hydrostatic pressure lowers both the LCST and the UCST [395]</p>
<p>68</p> 	<p>Poly(methylvinylether) PMVEth Two UCSTs are theoretically predicted for the low and high polymer concentrations using thermodynamic perturbation theory of Wertheim for saturation interactions (i.e. hydrogen bonds) [545–547], adapted to the lattice model [417] One UCST $< -15^\circ\text{C}$ has been experimentally observed at $c > 80\text{wt}\%$ [418]</p>
<p>69</p> 	<p>Poly(methacrylamide) PMAAm [124, 548–551] The second virial coefficient and the intrinsic viscosity were found to increase with increasing temperature; highly concentrated PMAAm solutions form gel upon heating [548] $T_{\Theta} = 6^\circ\text{C}$, $M_w = 320,000\text{g/mol}$ (T dependence of the second virial coefficient) [548]; $T_{\Theta} > 30^\circ\text{C}$, $M_w = 78,000\text{g/mol}$ [549]; $T_{\Theta} > 100^\circ\text{C}$ [550] Effect of salts (perchlorates, thiocyanates, chlorides, sulphates of uni- and bivalent metals); electrophoretic measurements suggests that both anions and cations are bound on the polymer chain; salting-in effect of cations (increasing with increasing surface charge density); the effect of anions is unfavourable to dissolution [551] $T_g > 100^\circ\text{C}$ [124]</p>

(continued)

Table 4 (continued)

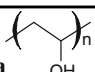
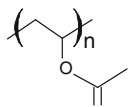
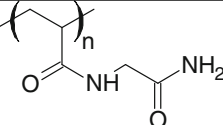
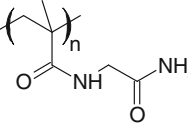
Structure	Properties
70a 	(70a) Poly(vinyl alcohol) PVAI (70b) Poly(vinyl acetate) PVAc [493] PVAI–PVAc gels form upon cooling; prepared by freeze/thaw cycling [552, 553]; the gel–sol transition for physically crosslinked PVA hydrogels is 55–70°C [554]
70b 	Both the LCST and the UCST behaviour in an aqueous mixture of 99–89% hydrolysed PVAI (DP = 1,700, $c > 15$ wt%)
71 	Poly(<i>N</i> -acrylylglycinamide) [124, 555–561] Aggregation of chains occurs in solutions with $c \leq 1$ wt% Physical thermoreversible gels are formed from solutions annealed below room temperature; gels melt upon heating above their T_m T_m increases with molar mass ($23.5^\circ\text{C} < T_m < 78.6^\circ\text{C}$ for $27,600 < M_n < 944,000$ g/mol) and with polymer concentration ($67.4^\circ\text{C} < T_m < 87.0^\circ\text{C}$ for $3 < c < 7$) Effect of added reagents on gelation; $[\eta]$ of PAG solution containing 2 M NaCNS is higher than that of pure aqueous solution $T_g = 182 \pm 2^\circ\text{C}$ [557]
72 	Poly(<i>N</i> -methacrylylglycinamide) [555, 561] Physical thermoreversible gels: gels melt upon heating; Solubilities and properties of PMG and PAG are similar, but higher c and/or M are required for PMG, and T_m of gels are lower than for PAG $T_g = 226^\circ\text{C}$ [561]

Table 5 Structural isomers of PiPAAM

Isomer of PiPAAM	Abbreviation	T _{cp} (°C)
Poly(<i>N</i> -ethylmethacrylamide)	PNEMAAM	67–71
Poly(<i>N,N</i> -ethylmethylacrylamide)	PNNEMAAM	56–74
Poly(<i>N-n</i> -propylacrylamide)	PnPAAM	23–25
Poly(<i>N</i> -isopropylacrylamide)	PiPAAM	27–33
Poly(<i>N</i> -vinylisobutyramide)	PViBAM	35–39
Poly(2- <i>n</i> -propyl-2-oxazoline)	PnPOz	22–25
Poly(2-isopropyl-2-oxazoline)	PiPOz	36–63
Polyleucine	PLeu	Insoluble
Polyisoleucine	PiLeu	Insoluble

7 Some Generalizations

7.1 Structural Effects

As noted above, only a qualitative analysis can be done in view of the different approaches to defining the T_{cp} , and, in general, the use of T_{cp} or T_{dem} instead of the LCST as a uniform and unique temperature to define the phase transition

of any polymer of a certain molar mass. We highlight in this section important evidence on the structural features of a polymer chain that affect its thermal response in water. Thus, Kano and Kokufuta report that the thermally induced interactions between macromolecules in solution, as well as between polymer chains and solvent molecules, depend on whether the α -carbon in the backbone bears an H atom (AAm) or a methyl group (MAAm) and whether the *N*-propyl pendant group is branched (iP) or linear (nP) [130]. From a comparison of T_{cp} values for PiPAAm and PiPMAAm, one may expect that a methyl group in the main chain in the α -position increases solubility. This agrees with the reported molar fraction of the $C=O \cdots HN$ bonds at temperatures near the demixing temperature: 0.13 for PiPAAm [131] and 0.42 for PiPMAAm [132], and also 0.30 for PnPAAm [131] and 0.40 for PnPMAAm [132]. Based on the H-bonds fraction, Kano and Kokufuta noted that the solubility order ought to be PiPMAAm > PnPMAAm > PnPAAm > PiPAAm, which disagrees with their measurements of T_{dem} (PiPMAAm > PiPAAm > PnPMAAm > PnPAAm) and of the endothermic enthalpy (PnPMAAm > PnPAAm > PiPMAAm > PiPAAm) [130]. Analysis of the highly diverse T_{cp} values collected in Table 2 does not offer any evident conclusions. This certainly calls for further systematic studies on the structural effect of the constituent repeating units.

7.2 Structural Isomers of PiPAAm

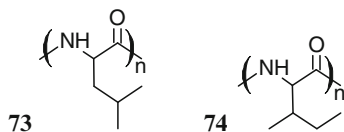
The structural isomers of PiPAAm with corresponding literature values of T_{cp} are given in Table 5.

To the best of our knowledge, the last two structural isomers of PiPAAm are not soluble in water (PLEu [144, 441, 442] and PiLeu [144]). Urry defined Leu as a more hydrophobic residue than iLeu [144]. Small rearrangement of the methyl group from Leu to iLeu results in a 5°C rise on the hydrophobicity scale. PLeu and PiLeu are crystalline polymers. PLeu forms α -helical structures, the so called leucine zippers, consisting of two parallel α -helices. PiLeu forms fewer α -helices, favouring the formation of β -structures (Fig. 4) [144, 443].

A comparison of the isomers suggests that:

1. PnPAAm vs. PiPAAm and PLEu vs. PiLeu: the solubility is higher (i.e. higher T_{cp}) for polymers with an isopropyl pendant in the side chain rather than *n*-propyl.

Fig. 4 Chemical structures of polyisoleucine (73) and polyisoleucine (74)



2. PNEMAAm vs. PNNEMAAm: methyl group in the main chain causes higher solubility.
3. PViBAm vs. PiPAAm: reversed amide linkage (NH group linked to the main chain in the case of PViBAm, vs. C=O for PiPAAm) results in better solubility.
4. PiPOz vs. PiPAAm: tertiary amide linkage and N in the main chain enhances solubility. However, if both N and C=O are in the main chain, solubility decreases (see PLeu vs. PiPAAm).
5. As an overall tendency, a C=O group positioned closer to the end of the pendant group, and N closer to the backbone, results in an increase in the polymer solubility.

Structural differences, together with differences in the synthesis, result in considerable variations of the physical properties of the PiPAAm structural isomers. Thus, PiPOz is a crystalline polymer [389] and is able to crystallize from water as a fibrous material when its solution is annealed for 24 h above $T_{cp} = 65^{\circ}\text{C}$ [373, 387]. Coagulated PiPOz particles exhibit hierarchical structures with two levels of ordering that are micron-sized spherical particles consisting of fibrils with a cross-sectional diameter of about 30–50 nm and a length of several microns [373]. The densely packed microspheres formed in dilute solutions are uniform in size and shape and resemble a ball made of rattan.

7.3 Hysteresis

Hysteresis in the heating/cooling cycles of polymer–water systems featuring an LCST has been ascribed to the limited diffusion of water into the dense hydrophobic aggregates formed above the LCST, which effectively delays the hydration of the aggregates and the eventual resolubilization of the polymer upon cooling below the LCST [95, 269]. In order to increase the rate of response, macroporous hydrogels have been prepared [444, 445]. Macroporous thermoresponsive hydrogels allow molecules of water to enter freely within the polymer matrix, and to leave it quickly, in response to a temperature change. Pore forming agents, foaming reagents or solvent mixtures are typically used to prepare macroporous hydrogels. An alternative synthetic procedure, cryogelation, has been introduced recently for bioseparation [445–448]. Since the pore surface can be functionalized to recognize target molecules, hydrogels are suitable media for the reversible immobilization or separation of biomacromolecules. Thus, macroporous PiPAAm-based hydrogels were used for the reversible adsorption of bovine serum albumin [449, 450] and to concentrate its aqueous solutions [451, 452] or to concentrate aqueous solutions of lignin [453]. PEO-grafted PiPAAm [169] or PEO-grafted PVCL [107] have also been used as fast-response polymeric systems, based on the expectation that PEO chains may provide hydrophilic channels, thus facilitating the diffusion of water molecules through the collapsed polymer matrix for temperatures above T_{dem} .

The limited diffusion of water molecules into the collapsed polymer matrix does not explain why the cooling/heating rates are different for the kinetically fast

process of hydrophobic hydration/dehydration. A qualitative analysis of the data listed in Tables 2 and 3 suggests that the phase transition in water of polymers with T_g well below the phase separation boundary show a weak heating/cooling hysteresis, if any at all. This is the case for thermoresponsive poly(vinylether)s, poly(phosphoester)s, as well as acrylate- and methacrylate-based copolymers containing PEO in their side chains. The majority of thermoresponsive *N*-substituted poly(acrylamide)s and poly(methacrylamide)s, for which the phase transition shows hysteresis, have a T_g value above 100°C. In this case, the polymer concentration and the rate of heating/cooling affect the hysteresis. One may assume, consequently, that this type of hysteresis originates in the kinetically slow exothermic process of partial vitrification of the phase-separated polymer, which is also responsible for the stability of the mesoglobular phase [78, 108, 187]. Polyoxazolines with ethyl and *n*-propyl pendant groups also show sharp LCST transitions and faster response to changes in temperature, compared to PiPAAm. Poly(2-ethyl-2-oxazoline) (PEOz) has a $T_g = 60^\circ\text{C}$ [371]. The T_{cp} of PEOz takes place for a temperature higher than T_g . PnPOz ($T_g = 40^\circ\text{C}$ [371]) has a $T_{cp} \approx T_g$. The transitions are reversible, with no hysteresis if solutions are heated/cooled with sufficiently high rates.

As stated above, the hysteresis of ELPs in the course of the ITT transition results from the overlap of two kinetically different processes: a fast endothermic process, which corresponds to the destruction of the ordered hydrophobic hydration, and a second exothermic process arising from the β -spiral chain folding.

7.4 Effect of Macromolecular Architecture

The polymer architecture affects the demixing behaviour of thermoresponsive polymers [562]. On the basis of theoretical studies it is expected that, as a rule, branched macromolecules are more soluble than their linear analogues [563–565]. This prediction was confirmed experimentally in the case of a solution of star-like polystyrene in cyclohexane (an UCST-type phase separation) for which an increase in the degree of branching resulted in a decrease in the temperature of demixing [566, 567]. On the basis of a review of water-soluble polymers of various shapes by Aoshima and Kanaoka [30], it appears that water-soluble polymers do not offer a uniform tendency in their LCST-type phase behaviour.

Xu and Liu recently reported the syntheses of the well-defined 7-arm and 21-arm PiPAAm stars with a β -cyclodextrin core [278, 568] and presented a thorough analysis of the literature on thermoresponsive stars and polymer brushes tethered to curved surfaces, such as latex particles [279, 280, 569], gold nanoparticles [282] and microgels [570]. A unique feature of these architectures is that they form a densely packed spherical core and a less-dense outer shell [159]. As a result of such a non-uniform density distribution, two temperature-induced phase transitions have been observed experimentally in several systems based on PiPAAm [279, 280, 282, 568, 569]. One transition has been ascribed to the phase transition of the inner segments of PiPAAm, whereas the other transition, which is concentration dependent, was assigned to the collapse of the outer PiPAAm segments [282].

The two-step transition can also be explained in terms of the n -clustering that induces the collapse [571]. Attractive many-body interactions between the polymer repeating units take place within the most dense regions in the vicinity of the particle core and result in n -clustering [279, 280, 568, 569]. The collapse of the outer layer occurs at higher temperatures due to the lower local chain density. According to the n -clustering concept, the n -clustering increases with decreasing polymer length, i.e. polymer brushes with short chains should have a lower T_{cp} . This was observed experimentally for surface-adsorbed PiPAAm brushes [279, 280, 569]. Also, the T_{cp} of 7-arm and 21-arm PiPAAm stars increases with increasing the arm length [568]. Solutions of 21-arm PiPAAm stars with relatively long arms exhibit a bi-modal DSC curve, which the authors explained on the basis of the two-layer brush concept used to account for the two-step collapse of PiPAAm brushes grafted on the gold nanoparticles.

7.5 Cyclic Polymers

There have been a few recent reports on the synthesis of macrocyclic PiPAAmS aimed at exploring the effect of topological constraints on the solution properties of PiPAAm. The polymers were obtained by “click” intramolecular coupling of linear heterofunctional α -azido- ω -alkynyl-PiPAAm samples synthesized via RAFT [572] or via ATRP [573, 574] polymerizations. The phase separation of cyclic PiPAAmS (c -PiPAAm) and their linear counterparts (l -PiPAAm) in aqueous solution was monitored by microcalorimetry and turbidimetry. Qiu et al. reported that the T_{dem} values of c -PiPAAmS were systematically higher than those of the corresponding l -PiPAAm precursors [572]. As the size of PiPAAm increases, the gap in T_{dem} between linear and cyclic PiPAAmS becomes narrower, implying that as the ring size becomes larger, the effect of topological constraint on the LCST of cyclic polymers becomes smaller. It should be noted that the T_{dem} values reported by Ye et al. [573] followed slightly different trends, which may be attributed to differences in measurement protocols or in the detailed chemical structure of the coupling groups. The ring size of the cyclic polymers also exerts a marked effect on the enthalpy change during the phase transition. The enthalpy of the phase transition (ΔH) for l -PiPAAmS (6000–19,000 g/mol) remains constant (6.06 and 6.40 kJ/mol per NIPAM unit), which is consistent with the reported ΔH values of 5.5–7.5 kJ/mol per repeating unit upon phase transition for linear PiPAAm. In contrast, the phase transition enthalpies of c -PiPAAmS are significantly lower than those of ordinary l -PiPAAm, with ΔH values of 3.86, 4.47 and 5.38 kJ/mol for c -PiPAAm of molecular weight 6000, 12,000 and 19,000 g/mol, respectively. In addition, the density of the mesoglobules formed by c -PiPAAm was lower than that of l -PiPAAm mesoglobules [573]. The density difference was attributed to the lack of chain interpenetration and entanglements in the c -PiPAAm mesoglobules. The hydration and dynamic behaviour of c -PiPAAm in water was investigated by means of high frequency dielectric relaxation measurements. Additional cooperativity in the molecular motions

of the amide functional groups of each monomer unit in the polymer chains with a cyclic topology was observed, compared to *l*-PiPAAm of similar molecular weight. This enhanced cooperativity may contribute to the increase in the LCST of aqueous solutions of *c*-PiPAAm, compared to that of *l*-PiPAAm, in the 10 g/L concentration domain probed [575].

7.6 Telechelic Amphiphilic Polymers

Polymers that carry a hydrophobic group at one chain end tend to form core-shell structures in which the hydrophobic core is insulated from the water by a brush-like corona of PiPAAm chains [576]. Flower-like micelles, consisting of loops of hydrated polymer chains having both end groups entrapped in the micellar core, form in solutions of PiPAAm carrying a hydrophobic group at each chain end [577, 578]. The introduction of hydrophobic end-chains affects the phase behaviour of PiPAAm solutions in two ways. First, the miscibility of the polymer in water becomes poorer as a result of direct interactions between water and the alkyl chains. Second, the mixing entropy of the polymer chains is reduced due to the increase of their apparent molecular weight via micelle formation. Both factors favour phase separation, so that LCST tends to shift downwards. However, association of the end chains does not affect the hydration of the main chains, except for segments near the micellar core, because they remain exposed to water even when association takes place. Therefore, the telechelic PiPAAm/water system is an interesting example of the coexistence, without competition, of two phenomena: end-chain association and hydration. These phenomena were monitored experimentally by microcalorimetry, light scattering [579, 580] and small angle neutron scattering (SANS) [581]. A theoretical study of systems featuring coexisting LCST behaviour and hydrophobic association via hydrophobic end groups was described by Okada et al. for systems with “random” hydration (such as PEO) and “cooperative” hydration (such as PiPAAm) [143].

There have been only a few reports so far on the preparation of telechelic or semi-telechelic hydrophobically modified poly(oxazolines). Volet et al. have described the synthesis and solution properties of semi-telechelic poly(2-methyl-2-oxazolines) (PMOz) bearing an *n*-dodecyl- or an *n*-octadecyl group at one chain end [475]. Telechelic PMOz with a perfluorooctyl group at one end and a hydrocarbon group 6–18 carbons long were prepared with a view towards the creation of multidomain micelles containing segregated fluorinated and hydrocarbon hydrophobic compartments [582]. Hydrophobically end-modified poly(2-ethyl-2-oxazolines) (PEOz) and poly(2-isopropyl-2-oxazolines) (PiPOz) bearing an *n*-octadecyl chain on both termini or on one chain end only were prepared by cationic ring-opening polymerization of 2-ethyl-2-oxazoline and 2-isopropyl-2-oxazoline, respectively, and subsequent end-group modification [583]. The polymers had M_n ranging from 7000 to 13,000 g/mol, a size distribution $M_w/M_n < 1.20$, and end-group functionality >0.97 . All polymers, except the semi-telechelic sample C₁₈-PiPOz ($M_n = 13,000$ g/mol),

formed core-shell micelles in cold water with a hydrodynamic radius (R_h) of 7–12 nm and a core radius (R_c), determined by analysis of small angle X-ray scattering (SAXS) data, of ~ 1.3 nm. Aqueous solutions of all polymers underwent a heat-induced phase transition detected by an increase in solution turbidity at T_{cp} of 32–62°C, depending on the polymer structure and size. Temperature-dependent light scattering measurements and fluorescence depolarization studies with the probe diphenylhexatriene revealed that extensive intermicellar bridging takes place in solutions heated in the vicinity of T_{cp} , leading to microgels ($R_h \geq 1 \mu\text{m}$). Further heating caused these assemblies to shrink into objects with R_h of about 300–700 nm, depending on the size and structure of the polymer. Upon heating aqueous semi-telechelic PiPOz at 65°C for 24 h, extensive crystallization occurred, as already noticed for aqueous solutions of the unmodified PiPOz [584]. Interestingly, telechelic PiPOz samples were shown to resist crystallization from hot water. This resistance to crystallization was taken as an indication that the loops formed by polymer chains captured in the flower micelles that exist in cold water, retain their conformation in the aggregates formed upon heating telechelic PiPOz samples above their phase transition temperature. This behaviour is rather unique because other end-modifications of the PiPOz chains reported so far, for example grafting onto polysaccharides [585], do not hinder its crystallization from hot water.

7.7 Cononsolvency

The PiPAAm chain exhibits peculiar conformational changes in water upon addition of a second water-miscible solvent such as methanol, tetrahydrofuran or dioxane. Although the second solvent is a good solvent for the polymer, the polymer chain collapses in certain compositions of the mixed solvent, followed by the eventual reswelling when the second solvent is the major component [586, 587]. The tendency for phase separation is also strongly enhanced by the presence of the second solvent. For instance, the LCST of aqueous PiPAAm solutions shifts to a lower temperature when methanol is added. The temperature drop is the largest, from 31°C down to 7°C, for a specific molar fraction, 0.35, of methanol. This enhanced phase separation in mixed good solvents is known as cononsolvency. Crosslinked PiPAAm gels are also known to collapse sharply in water in the presence of methanol, at a specific molar fraction of around 0.3, and gradually recover their swollen state with increasing methanol content [588]. There have been efforts to understand cononsolvency by the combination of three parameters [587] and also by the formation of stoichiometric compounds between the solvent molecules [589]. Without considering direct hydrogen bonds between polymer and solvent, however, it is difficult to explain the sharp LCST behaviour. Tanaka F et al. recently derived a polymer expansion factor for PiPAAm in mixed water and methanol as a function of the solvent composition on the basis of competitive hydrogen bonds between PiPAAm/water and PiPAAm/methanol [142]. This approach allowed them to model the sharp re-entrant coil-to-globule-to-coil transition of PiPAAm in mixed water/methanol.

8 Postscript

Arieh Ben-Naim wrote in his latest book that: “The field of aqueous solutions has become so huge that it is impossible to review the whole field in a single book” [129]. He added that “the behaviour of water and of aqueous solutions of simple solutes is reasonably well understood”. This review led us to conclude that the solutions of amphiphilic polymers in water still present mysteries, in spite of the staggering number of publications on this topic. The literature provides mechanisms responsible for the phase behaviour of aqueous amphiphilic polymer solutions, yet most existing theoretical approaches still require proper experimental validation. It is our hope that the systematic presentation of the experimental data collected for a great variety of amphiphilic thermoresponsive polymers contained in this review will help experimentalists and theoreticians in their quest towards a rational understanding of the phenomena involved and the intricate relationships among them.

References

1. CAS (2007) SciFinder Scholar software. <http://www.cas.org/support/academic/sf/index.html>. American Chemical Society. Accessed 2 March 2010
2. Matyjaszewski K, Davis TP (eds) (2002) Handbook of radical polymerization. Wiley, New York
3. Braunecker WA, Matyjaszewski K (2007) Prog Polym Sci 32:93
4. Pyun J, Matyjaszewski K (2001) Chem Mater 13:3436
5. Kato M, Kamigaito M, Sawamoto M, Higashimura T (1995) Macromolecules 28:1721
6. Wang J, Matyjaszewski K (1995) J Am Chem Soc 117:5614
7. Zhang X, Matyjaszewski K (1999) Macromolecules 32:1763
8. Lee SB, Russell AJ, Matyjaszewski K (2003) Biomacromolecules 4:1386
9. Beers KL, Boo S, Gaynor SG, Matyjaszewski K (1999) Macromolecules 32:5772
10. Neugebauer D, Matyjaszewski K (2003) Macromolecules 36:2598
11. Teodorescu M, Matyjaszewski K (1999) Macromolecules 32:4826
12. Teodorescu M, Matyjaszewski K (2000) Macromol Rapid Commun 21:190
13. Sheiko SS, Prokhorova SA, Beers KL, Matyjaszewski K, Potemkin II, Khokhlov AR, Moeller M (2001) Macromolecules 34:8354
14. Percec V, Guliashevili T, Ladislav JS, Wistrand A, Stjern Dahl A, Sienkowska MJ, Monteiro MJ, Sahoo S (2006) J Am Chem Soc 128:14156
15. Goto A, Fukuda T (2004) Prog Polym Sci 29:329
16. Chiefari J, Chong YK, Ercole F, Krstina J, Jeffery J, Le TPT, Mayadunne RTA, Meijs GF, Moad CL, Moad G, Rizzardo E, Thang SH (1998) Macromolecules 31:5559
17. Moad G, Chiefari J, Chong YK, Krstina J, Mayadunne RTA, Postma A, Rizzardo E, Thang SH (2000) Polym Int 49:993
18. Moad G, Rizzardo E, Thang SH (2005) Aust J Chem 58:379
19. Perrier S, Takolpuckdee P (2005) J Polym Sci Polym Chem 43:5347
20. Barner-Kowollik C, Davis TP, Heuts JPA, Stenzel MH, Vana P, Whittaker M (2003) J Polym Sci Polym Chem 41:365
21. McCormick CL, Sumerlin BS, Lokitza BS, Stempka JE (2008) Soft Matter 4:1760
22. Mertoglu M, Laschewsky A, Skrabania K, Wieland C (2005) Macromolecules 38:3601
23. Georges MK, Veregin RPN, Kazmaier PM, Hamer GK (1993) Macromolecules 26:2987
24. Hawker CJ, Bosman AW, Harth E (2001) Chem Rev 101:3661

25. Fischer H (2001) *Chem Rev* 101:3581
26. Solomon DH (2005) *J Polym Sci Polym Chem* 43:5748
27. Otsu T, Yoshida M (1982) *Makromol Chem* 3:127
28. Otsu T (2000) *J Polym Sci Polym Chem* 38:2121
29. Charmot D, Corpart P, Adam H, Zard SZ, Biadatti T, Bouhadir G (2000) *Macromol Symp* 150:23
30. Aoshima S, Kanaoka S (2008) *Adv Polym Sci* 210:169
31. Lowea AB, McCormick CL (2007) *Prog Polym Sci* 32:283
32. Goethals EJ, Du Prez F (2007) *Prog Polym Sci* 32:220
33. Rozenberg BA, Tenne R (2008) *Prog Polym Sci* 33:40
34. Harada A, Kataoka K (2006) *Prog Polym Sci* 31:949
35. Lazzari M, Lin G, Lecomandoux S (2006) *Block copolymers in nanoscience*. Wiley-VCH, Weinheim
36. Lutz JF (2006) *Polym Int* 55:979
37. Hamly IW (2005) *Block copolymers in solution: fundamentals and applications*. Wiley, Chichester
38. Gohy JF (2005) *Adv Polym Sci* 190:65
39. Hadjichristidis N, Iatrou H, Pitsikalis M, Pispas S, Avgeropoulos A (2005) *Prog Polym Sci* 30:725
40. Abetz V, Simon PFW (2005) *Adv Polym Sci* 189:125
41. Riess G (2003) *Prog Polym Sci* 28:1107
42. Voets IK, de Keizer A, Cohen Stuart MA (2009) *Adv Colloid Interface Sci* 147–148:300
43. Galaev I, Mattiasson B (eds) (2008) *Smart polymers: applications in biotechnology and biomedicine*, 2nd edn. CRC, Boca Raton, FL
44. Rodríguez-Cabello JC, Reguera J, Prieto S, Alonso M (2008) In: Galaev I, Mattiasson B (eds) *Smart polymers: applications in biotechnology and biomedicine*, 2nd edn. CRC, Boca Raton, FL
45. Aguilar MR, Elvira C, Gallardo A, Vázquez B, Román JS (2007) In: Ashammakhi N, Reis R, Chiellini E (eds) *Topics in tissue engineering*, E-book, Expertissues, vol 3
46. Dimitrov I, Trzebicka B, Müller AHE, Dworak A, Tsvetanov CB (2007) *Prog Polym Sci* 32:1275
47. Choi HS, Yui N (2006) *Prog Polym Sci* 31:121
48. Rodríguez-Hernández J, Chécot F, Gnanou Y, Lecommandoux S (2005) *Prog Polym Sci* 30:691
49. Gil ES, Hudson SM (2004) *Prog Polym Sci* 29:1173
50. Wright ER, Conticello VP (2002) *Adv Drug Deliv Rev* 54:1057
51. Mortensen K (2001) *Polym Adv Technol* 12:2
52. Kirsh YE (1998) *Water soluble poly-N-vinylamides: synthesis and physicochemical properties*. Wiley, Chichester
53. Khokhlov AR (ed) (2006) *Adv Polym Sci*, pp 195–196
54. Zhang G, Wu C (2006) *Adv Polym Sci* 195:101
55. Aseyev V, Tenhu H, Winnik FM (2006) *Adv Polym Sci* 196:1
56. Oh JK, Drumright R, Siegwart DJ, Matyjaszewski K (2008) *Prog Polym Sci* 33:448
57. Bajpai AK, Shukla SK, Bhanu S, Kankane S (2008) *Prog Polym Sci* 33:1088
58. Sosnik A, Carcaboso ÁM, Chiappetta DA (2008) *Recent Pat Biomed Eng* 1:43
59. Kumar A, Srivastava A, Galaev IY, Mattiasson B (2007) *Prog Polym Sci* 32:1205
60. Rzaev ZMO, Dinçer S, Pişkin E (2007) *Prog Polym Sci* 32:534
61. Rapoport N (2007) *Prog Polym Sci* 32:962
62. Sutton D, Nasongkla N, Blanco E, Gao J (2007) *Pharm Res* 24:1029
63. Jeong JH, Kim SW, Park TG (2007) *Prog Polym Sci* 32:1239
64. Adams N, Schubert US (2007) *Adv Drug Deliv Rev* 59:1504
65. van Nostrum CF (2004) *Adv Drug Deliv Rev* 56:9
66. Flory PJ (1949) *J Chem Phys* 17:303
67. Flory PJ (1953) *Principles of polymer chemistry*. Cornell University Press, Ithaca, NY
68. Hoffman AS (1995) *Artif Organs* 19:458

69. Chen G, Hoffman AS (1995) *Nature* 373:49
70. Chen G, Hoffman AS (1995) *Macromol Chem Phys* 196:1251
71. McNaught AD, Wilkinson A (1997) *Gold book. Compendium of chemical terminology: IUPAC recommendations*, 2nd edn. Blackwell Scientific Publications, Oxford; XML on-line corrected version: <http://goldbook.iupac.org> (2006) created by Nic M, Jirat J, Kosata B, updates compiled by Jenkins A. Accessed 17 November, 2009
72. Grosberg AY, Khokhlov AR (1994) *Statistical physics of macromolecules*. AIP Press, New York
73. Sanchez JC (1979) *Macromolecules* 12:980
74. Yamakawa H (1993) *Macromolecules* 26:5061
75. Yamakawa H, Abe F, Einaga Y (1994) *Macromolecules* 27:5704
76. Arnauts J, Berghmans H (1987) *Polym Commun* 28:66
77. Callister S, Keller A, Hikmet RM (1990) *Makromol Chem Macromol Symp* 39:19
78. Van Durme K, Van Assche G, Van Mele B (2004) *Macromolecules* 37:9596
79. Swislow G, Sun ST, Nishio I, Tanaka T (1980) *Phys Rev Lett* 44:796
80. Sun ST, Nishio I, Swislow G, Tanaka T (1980) *J Chem Phys* 73:5971
81. Nishio I, Swislow G, Sun ST, Tanaka T (1982) *Nature (UK London)* 300:243
82. Yu J, Wang Z, Chu B (1992) *Macromolecules* 25:1618
83. Chu B, Ying Q, Grosberg AY (1995) *Macromolecules* 28:180
84. Chu B, Wu C (1996) *Vysokomol Soed Ser A* 38:574
85. Fujishige S (1987) *Polym J* 19:297
86. Fujishige S, Kubota K, Ando I (1989) *J Phys Chem* 93:3311
87. Kubota K, Fujishige S, Ando I (1990) *J Phys Chem* 94:5154
88. Ricka J, Meewes M, Nyffenegger R, Binkert Th (1990) *Phys Rev Lett* 65:657
89. Meewes M, Ricka J, de Silva M, Nyffenegger R, Binkert Th (1991) *Macromolecules* 24:5811
90. Tiktopulo EI, Bychkova VE, Ricka J, Ptitsyn OB (1994) *Macromolecules* 27:2879
91. Tiktopulo EI, Uversky VN, Lushchik VB, Klenin SI, Bychkova VE, Ptitsyn OB (1995) *Macromolecules* 28:7519
92. Napper DH (1995) *Macromol Symp* 98:911
93. Wu C, Zhou S (1995) *Macromolecules* 28:8381
94. Wu C, Zhou S (1995) *Macromolecules* 28:5388
95. Wang X, Qiu X, Wu C (1998) *Macromolecules* 31:2972
96. Wu C, Wang X (1998) *Phys Rev Lett* 80:4092
97. Meersman F, Wangm J, Wu Y, Heremans K (2005) *Macromolecules* 38:8923
98. Kirpach A, Adolf D (2006) *Macromol Symp* 237:7
99. Baysal BM, Karasz FE (2003) *Macromol Theor Simul* 12:627
100. Koningsveld R, Stockmayer WH, Nies E (2001) *Polymer phase diagrams. A textbook*. Oxford University Press, Oxford, New York
101. Heskins M, Guillet JE (1968) *J Macromol Sci Pure* 2:1441
102. Yushmanov PV, Furó I, Iliopoulos I (2006) *Macromol Chem Phys* 207:1972
103. Schild HG, Tirrell DA (1990) *J Phys Chem* 94:4352
104. Chytrý V, Ulbrich K (2001) *J Bioact Compat Polym* 16:427
105. Schild HG, Tirrell DA (1991) *Langmuir* 7:665
106. Meeussen F, Nies E, Berghmans H, Verbrugghe S, Goethals E, Du Prez F (2000) *Polymer* 41:8597
107. Van Durme K, Verbrugghe S, Du Prez FE, Van Mele B (2004) *Macromolecules* 37:1054
108. Afroze F, Nies E, Berghmans H (2000) *J Mol Struct* 554:55
109. Zheng Q, Pan CY (2006) *Eur Polym J* 42:807
110. Xia Y, Burke NAD, Stöver HDH (2006) *Macromolecules* 39:2275
111. Plummer R, Hill DJT, Whittaker AK (2006) *Macromolecules* 39:8379
112. Schilli CM, Müller AHE, Rizzardo E, Thang SH (2003) *RAFT polymers: novel precursors for polymer-protein conjugates*. In: Matyjaszewski K (ed) *Advances in controlled/living radical polymerization*. ACS symposium series, vol 854. ACS, Washington DC
113. Luo S, Xu J, Zhu Z, Wu C, Liu S (2006) *J Phys Chem B* 110:9132
114. Lu Y, Wittemann A, Ballauff M, Drechsler M (2006) *Macromol Rapid Commun* 27:1137

115. Deike I, Ballauff M, Willenbacher N, Weiss A (2001) *J Rheol* 45:709
116. Schäfer-Soenen H, Moerkerke R, Berghmans H, Koningsveld R, Dušek K, Šolc K (1997) *Macromolecules* 30:410
117. Moerkerke R, Meeussen F, Koningsveld R, Berghmans H, Mondelaers W, Schacht E, Dušek K, Šolc K (1998) *Macromolecules* 31:2223
118. Meeussen F, Bauwens Y, Moerkerke R, Nies E, Berghmans H (2000) *Polymer* 41:3737
119. Swier S, Van Durme K, Van Mele B (2003) *J Polym Sci Polym Phys* 41:1824
120. Tanford C (1966) *Physical chemistry of macromolecules*. Wiley, New York
121. Israelachvili JN (1992) *Intermolecular and surface forces*, 2nd edn. Academic, London
122. Tanford C (1973) *The hydrophobic effect: formation of micelles and biological membranes*. Wiley, New York
123. Franks F, Reid DS (1975) In: Franks F (ed) *Water. A comprehensive treatise*. Plenum, New York
124. Molyneux P (1985) *Water-soluble synthetic polymers: properties and behavior*. CRC, Boca Raton, FL
125. Molyneux P (1975) In: Franks F (ed) *Water. A comprehensive treatise*. Plenum, New York
126. Chandler D (2005) *Nature* 437:640
127. Southall NT, Dill KA, Haymet ADJ (2002) *J Phys Chem B* 106:521
128. Ben-Naim A (1974) *Water and aqueous solutions: introduction to a molecular theory*. Plenum, New York
129. Ben-Naim A (2009) *Molecular theory of water and aqueous solutions. Part I: understanding water*. World Scientific Publishing, Singapore
130. Kano M, Kokufuta E (2009) *Langmuir* 25:8649
131. Maeda Y, Nakamura T, Ikeda I (2001) *Macromolecules* 34:1391
132. Maeda Y, Nakamura T, Ikeda I (2001) *Macromolecules* 34:8246
133. Katsumoto Y, Tanaka T, Sato H, Ozaki Y (2002) *J Phys Chem A* 106:3429
134. Ramon O, Kesselman E, Berkovici R, Cohen Y, Paz Y (2001) *J Polym Sci Polym Phys* 39:1665
135. Paz Y, Kesselman E, Fahoum L, Portnaya I, Ramon O (2004) *J Polym Sci Polym Phys* 42:33
136. Widom B, Bhimalapuram B, Koga K (2003) *Phys Chem Phys* 5:3085
137. Onoa Y, Sihikata T (2006) *J Am Chem Soc* 124:10030
138. Matsuyama A, Tanaka F (1990) *Phys Rev Lett* 65:341
139. Matsuyama A, Tanaka F (1991) *J Chem Phys* 94:781
140. Okada Y, Tanaka F (2005) *Macromolecules* 38:4465
141. Ye X, Lu Y, Shen L, Ding Y, Liu S, Zhang G, Wu C (2007) *Macromolecules* 40:4750
142. Tanaka F, Koga T, Winnik FM (2008) *Phys Rev Lett* 101:028302
143. Okada Y, Tanaka F, Kujawa P, Winnik FM (2006) *J Chem Phys* 125:244902
144. Urry DW (1997) *J Phys Chem B* 101:11007
145. Foster JA, Bruenger E, Gray WR, Sandberg LB (1973) *J Biol Chem* 248:2876
146. Mithieux SM, Weiss AS (2005) *Adv Protein Chem* 70:437
147. Renugopalakrishnan V, Lewis R (eds) (2006) *Protein-based nanotechnology*. Kluwer Academic, Dordrecht
148. Reguera J, Lagaron JM, Alonso M, Reboto V, Calvo B, Rodríguez-Cabello JC (2003) *Macromolecules* 36:8470
149. Hunter RJ (2001) *Foundations of colloid science*, 2nd edn. Oxford University Press, Oxford, USA
150. Evans DF, Wennerström H (1999) *The colloidal domain*. Wiley-VCH, New York
151. Sonntag H, Strenge K (1987) *Coagulation kinetics and structure formation*. Plenum, New York
152. Derjaguin BV, Churaev NV (1989) *Colloids Surf* 41:223
153. Besseling NAM (1997) *Langmuir* 13:2113
154. Marcelja S, Radic N (1976) *Chem Phys Lett* 42:129
155. Israelachvili JN, Wennerström H (1996) *Nature* 379:219
156. Leckband D, Israelachvili J (2001) *Q Rev Biophys* 34:105
157. Einarson MB, Berg JC (1992) *Langmuir* 8:2611

158. Sofia SJ, Merrill EW (1997) In: Harris JM, Zaplisky S (eds) Poly(ethylene glycol): chemistry and biological applications. ACS symposium series, vol 680. ACS, Washington DC
159. Halperin A, Tirrell M, Lodge TP (1992) *Adv Polym Sci* 100:31
160. Choucair A, Eisenberg A (2003) *Eur Phys J E* 10:37
161. Foerster S, Antonietti M (1998) *Adv Mater* 10:195
162. Discher DE, Eisenberg A (2002) *Science* 297:967
163. Ciferri A (2000) *Supramolecular polymers*. Marcel Dekker, New York
164. Pochan DJ, Chen Z, Cui H, Hales K, Qi K, Wooley KL (2004) *Science* 306:94
165. Cornelissen J, Fischer M, Sommerdijk N, Nolte RJM (1998) *Science* 280:1427
166. Lodge TP, Hillmyer MA, Zhou Z, Talmon Y (2004) *Macromolecules* 37:6680
167. Raez J, Manners I, Winnik MA (2002) *J Am Chem Soc* 124:10381
168. Kubowicz S, Baussard JF, Lutz JF, Thünemann AF, von Berlepsch H, Laschewsky A (2005) *Angew Chem Int Ed* 44:5562
169. Van Durme K, Van Assche G, Aseyev V, Raula J, Tenhu H, Van Mele B (2007) *Macromolecules* 40:3765
170. Laukkanen A, Tenhu H (2008) In: Galaev I, Mattiasson B (eds) *Smart polymers: applications in biotechnology and biomedicine*, 2nd edn. CRC, Boca Raton, FL
171. Motokawa R, Koizumi S, Annaka M, Nakahira T, Hashimoto T (2005) *Prog Colloid Polym Sci* 130:85
172. Cameron NS, Corbierre MK, Eisenberg A (1999) *Can J Chem* 77:1311
173. Lodge TP (2003) *Macromol Chem Phys* 204:265
174. Cui H, Chen Z, Wooley KL, Pochan DJ (2006) *Macromolecules* 39:6599
175. Won YY, Bates FS (2007) In: Zana R, Kaler EW (eds) *Giant micelles: properties and applications*. CRC, Boca Raton, FL
176. Jain S, Bates FS (2004) *Macromolecules* 37:1511
177. Khokhlov AR, Khalatur PG (1998) *Physica A* 249:253
178. Khalatur PG, Ivanov VI, Shusharina NP, Khokhlov AR (1998) *Russ Chem Bull* 47:855
179. Khokhlov AR, Khalatur PG (2004) *Curr Opin Solid State Matter* 8:3
180. Khalatur PG, Khokhlov A (2006) *Adv Polym Sci* 195:1
181. Siu MH, Liu HY, Zhu XX, Wu C (2003) *Macromolecules* 36:2107
182. Lozinsky VI (2006) *Adv Polym Sci* 196:87
183. Virtanen J, Baron C, Tenhu H (2000) *Macromolecules* 33:336
184. Virtanen J, Tenhu H (2000) *Macromolecules* 33:5970
185. Gorelov AV, Du Chesne A, Dawson KA (1997) *Physica A* 240:443
186. Dawson KA, Gorelov AV, Timoshenko EG, Kuznetsov YA, Du Chesne A (1997) *Physica A* 244:68
187. Kujawa P, Aseyev V, Winnik F, Tenhu H (2006) *Macromolecules* 39:7686
188. Tanaka H (1993) *Phys Rev Lett* 71:3158
189. Tanaka H (1992) *Macromolecules* 25:6377
190. Zhen T, Fang Z, Xu Z (1999) *Macromolecules* 32:4488
191. Wu C, Li W, Zhu XX (2004) *Macromolecules* 37:4989
192. Chuang J, Grosberg AY, Tanaka T (2000) *J Chem Phys* 112:6434
193. Ding H, Wu F, Huang Y, Zhang Z, Nie Y (2006) *Polymer* 47:1575
194. Chee CK, Rimmer S, Soutar I, Swanson L (2006) *React Funct Polym* 66:1
195. Soto RT, Zufferey D, Schmidt N, Fischer F (2007) *Eur Polym J* 43:2768
196. Balu C, Delsanti M, Guenoun P, Monti F, Cloitre M (2007) *Langmuir* 23:2404
197. Guo L, Nie J, Du B, Peng Z, Tesche B, Kleinermanns K (2008) *J Colloid Interface Sci* 319:175
198. Weda P, Trzebicka B, Dworak A, Tsvetanov CB (2008) *Polymer* 49:1467
199. Dybal J, Trchová M, Schmidt P (2009) *Vib Spectrosc* 51:44
200. Starovoytova L, Spěváček J (2006) *Polymer* 47:7329
201. Starovoytova L, Spěváček J, Trchová M (2007) *Eur Polym J* 43:5001
202. Hanyková L, Labuta J, Spěváček J (2006) *Polymer* 47:6107
203. Spěváček J (2009) *Curr Opin Colloid Interface Sci* 14:184
204. Ushakova AS, Govorun EN, Khokhlov AR (2006) *J Phys Condens Matter* 18:915

205. Yoshinaga N, Bicout DJ, Kats EI, Halperin A (2007) *Macromolecules* 40:2201
206. Maresov EA, Semenov AN (2008) *Macromolecules* 41:9439
207. Taylor LD, Cerankowski LD (1975) *J Polym Sci Polym Chem Ed* 13:2551
208. Bae YH, Okano T, Kim SW (1990) *J Polym Sci Polym Phys* 28:923
209. Nichifor M, Zhu XX (2003) *Polymer* 44:3053
210. Xue W, Huglin MB, Jones TGJ (2003) *Macromol Chem Phys* 204:1956
211. Liu HY, Zhu XX (1999) *Polymer* 40:6985
212. Ye W, DeSimone JM (2005) *Macromolecules* 38:2180
213. Lowe JS, Chowdhry BZ, Parsonage J, Snowden MJ (1998) *Polymer* 39:1207
214. Hazot P, Chapel JP, Pichot C, Elaïssari A, Delair T (2002) *J Polym Sci Polym Chem* 40:1808
215. Bohdanecký M, Horský J, Petrus V, Mrkvičková L, Ulbrich K (1993) *Collect Czech Chem Commun* 58:2370
216. Hazot P, Delair T, Elaïssari A, Chapel JP, Pichot C (2002) *Colloid Polym Sci* 280:637
217. Bohdanecký M, Petrus V, Horský J (1995) *Macromolecules* 28:8344
218. Cao Y, Zhu XX, Luo J, Liu H (2007) *Macromolecules* 40:6481
219. Xie D, Ye X, Ding Y, Zhang G, Zhao N, Wu K, Cao Y, Zhu XX (2009) *Macromolecules* 42:2715
220. Cao Y, Zhao N, Wu K, Zhu XX (2009) *Langmuir* 25:1699
221. Xu J, Jiang X, Liu S (2008) *J Polym Sci Polym Chem* 46:60
222. Ali AS, El-Ejmi S, Huglin MB *Polym Int* 1996;39:113
223. Kobayashi M, Okuyama S, Ishizone T, Nakahama S (1999) *Macromolecules* 32:6466
224. Lessard DG, Ousaleem M, Zhu XX, Eisenberg A, Carreau PJ (2003) *J Polym Sci Polym Phys* 41:1627
225. Qiu Y, Park K (2001) *Adv Drug Deliv Rev* 53:321
226. Lessard DG, Ousaleem M, Zhu XX (2001) *Can J Chem* 79:1870
227. Speřváček J, Geschke D, Ilavský M (2001) *Polymer* 42:463
228. Speřváček J, Hanyková L, Ilavský M (2001) *Macromol Chem Phys* 202:1122
229. Idziak I, Avoce D, Lessard D, Gravel D, Zhu XX (1999) *Macromolecules* 32:1260
230. Freitag R, Baltes T, Eggert M (1994) *J Polym Sci Polym Chem* 32:3019
231. Tong Z, Zeng F, Zheng X (1999) *Macromolecules* 32:4488
232. Zheng X, Tong Z, Xie X, Zeng F (1998) *Polym J (Tokyo)* 30:284
233. Pleštil J, Ilavský M, Pospíšil H, Hlavatá D, Ostanvich YM, Degovics G, Kriechbaum M, Laggner P (1993) *Polymer* 34:4846
234. Katayama S, Hirokawa Y, Tanaka T (1984) *Macromolecules* 17:2641
235. Kobayashi M, Ishizone T, Nakahama S (2000) *J Polym Sci Polym Chem* 38:4677
236. Kobayashi M, Ishizone T, Nakahama S (2000) *Macromolecules* 33:4411
237. Hoshino K, Taniguchi M, Kitao T, Morohashi S, Sasakura T (1998) *Biotechnol Bioeng* 60:568
238. Liu S, Liu MJ (2003) *Appl Polym Sci* 90:3563
239. Gan LH, Cai W, Tam KC (2001) *Eur Polym J* 37:1773
240. Cai WS, Gan LH, Tam KC (2001) *Colloid Polym Sci* 279:793
241. Hrouz J, Ilavský M (1989) *Polym Bull* 22:271
242. Percot A, Lafleur M, Zhu XX (2000) *Polymer* 41:7231
243. Bromberg L, Levin G (1996) *J Polym Sci Polym Chem* 34:2595
244. Fang J, Bian F, Shen W (2008) *J Applied Polym Sci* 110:3373
245. Saunders JM, Alava C, Saunders BR (2007) *Macromol Symp* 251:63
246. Inomata H, Goto S, Saito S (1990) *Macromolecules* 23:283
247. Inomata H, Goto S, Saito S (1990) *Macromolecules* 23:4887
248. Ito D, Kubota K (1999) *Polym J* 31:254
249. Ito D, Kubota K (1997) *Macromolecules* 30:7828
250. Jin MR, Wang YX, Zong X, Wang SC (1995) *Polymer* 36:221
251. Norisuye T, Kida Y, Masui N, Tran-Cong-Miyata Q, Maekawa Y, Yoshida M, Shibayama M (2003) *Macromolecules* 36:6202
252. Takekawa M, Kokufuta E (2009) *Colloid Polym Sci* 287:323
253. Mori T, Hirano T, Maruyama A, Katayama Y, Niidome T, Bando Y, Ute K, Takaku S, Maeda Y (2009) *Langmuir* 25:48

254. Anufrieva EV, Krakovyak MG, Gromova RA, Lushchik VB, Ananeva TD, Sheveleva TV (1991) Dokl Akad Nauk SSSR 319:895
255. Anufrieva EV, Krakovyak MG, Gromova RA, Lushchik VB, Ananeva TD, Sheveleva TV (1992) Chem Abstract 116:42434
256. Ito S (1989) Kobunshi Ronbunshu 46:437
257. Schild GH (1992) Prog Polym Sci 17:163
258. Jeong B, Gutowska A (2002) Trends Biotechnol 20:305
259. Hoffman AS, Stayton PS, Bulmus V, et al (2000) J Biomed Mater Res 52:577
260. Schmaljohann D (2006) Adv Drug Deliv Rev 58:1655
261. Luchette P, Abiy N, Mao H (2007) Sens Actuators B 128:154
262. Plate NA, Lebedeva TL, Valuev LI (1999) Polym J 31:21
263. Baltes T, Garret-Flaudy F, Freitag R (1999) J Polym Sci Polym Chem 37:2977
264. Durand A, Hourdet D (2000) Polymer 41:545–557
265. Loos W, Du Prez F (2004) Macromol Symp 210:483
266. De Azevedo RG, Rebelo LPN, Ramos AM, Szydłowski J, de Sousa HC, Klein J (2001) Fluid Phase Equilib 185:189
267. Jung SC, Oh SY, Bae YC (2009) Polymer 50:3370
268. Marchetti M, Prager S, Cussler EL (1990) Macromolecules 23:3445
269. Wang J, Gan D, Lyon L, El-Sayed MA (2001) J Am Chem Soc 123:11284
270. Brandrup J, Immergut EH, Grulke EA (eds) (1999) CRC polymer handbook, 4th edn. Wiley, New York
271. Katsumoto Y, Kubosaki N (2008) Macromolecules 41:5955
272. Nuopponen M, Kalliomäki K, Aseyev V, Tenhu H (2008) Macromolecules 41:4881
273. Freitag R, Garret-Flaudy F (2002) Langmuir 18:3434
274. Zhang Y, Furyk S, Bergbreiter DE, Cremer PS (2005) J Am Chem Soc 127:14505
275. Lee LT, Cabane B (1997) Macromolecules 30:6559
276. Staikos G (1995) Macromol Rapid Commun 16:913
277. Kim YH, Kwon IC, Bae YH, Kim SW (1995) Macromolecules 28:939
278. Shan J, Zhao Y, Granqvist N, Tenhu H (2009) Macromolecules 42:2696
279. Zhu PW, Napper DH (1994) J Colloid Interface Sci 164:489
280. Zhu PW, Napper DH (1996) Colloids Surf A 113:145
281. Zhou J, Ralston J, Sedev R, Beattie DA (2009) J Colloid Interface Sci 331:251
282. Shan J, Tenhu H (2007) Chem Commun 44:4580
283. Chytrý V, Netopilík M, Bohdanecký M, Ulbrich K (1997) J Biomater Sci Polym Ed 8:817
284. Netopilík M, Bohdanecký M, Chytrý V, Ulbrich K (1997) Macromol Rapid Commun 18:107
285. Duracher D, Elaïssari A, Pichot C (1999) J Polym Sci Polym Phys 37:1823
286. Guillermo A, Addad JPC, Bazile JP, Duracher D, Elaïssari A, Pichot C (2000) J Polym Sci Polym Phys 38:889
287. Fomenko A, Pospíšil H, Sedláková Z, Pleštil J, Ilavský M (2002) Phys Chem Chem Phys 4:4360
288. Tirumala VR, Ilavský J, Ilavský MJ (2006) Chem Phys 124:234911
289. Sánchez MS, Hanyková L, Ilavský M, Pradas MM (2004) Polymer 45:4087
290. Kuramoto N, Shishido Y (1998) Polymer 39:669
291. Etika KC, Jochum FD, Theato P, Grunlan JC (2009) J Am Chem Soc 131:13598
292. Roth PJ, Theato P (2008) Chem Mater 20:1614
293. Aoki T, Muramatsu M, Torii T, Sanui K, Ogata N (2001) Macromolecules 34:3118
294. Mertoglu M, Garnier S, Laschewsky A, Skrabania K, Storsberg J (2005) Polymer 46:7726
295. Garnier S, Laschewsky A (2006) Colloid Polym Sci 284:1243
296. Garnier S, Laschewsky A (2005) Macromolecules 38:7580
297. Skrabania K, Kristen J, Laschewsky A, Akdemir Ö, Hoth A, Lutz JF (2007) Langmuir 23:84
298. Ito S, Hirasu O, Yamauchi A (1989) Kobunshi Ronbunshu 46:427
299. Save NS, Jassal M, Agrawal AK (2005) J Appl Polym Sci 95:672
300. Jo YS, van der Vlies AJ, Gantz J, Antonijevic S, Demurtas D, Velluto D, Hubbell JA (2008) Macromolecules 41:1140
301. Solomon OF, Corciovei M, Ciuta I, Boghina C (1968) J Appl Polym Sci 12:1835

302. Inoue T, Chen G, Nakamae K, Hoffman AS (1997) *Polym Gels Netw* 5:561
303. Jeong B, Kim SW, Bae YH (2002) *Adv Drug Deliv Rev* 54:37
304. Verbrugge S, Bernaerts K, Du Prez F (2003) *Macromol Chem Phys* 204:1217
305. Lozinsky VI, Simenel IA, Kurskaya EA, Kulakova VK, Galaev IY, Mattiasson B, Grinberg VY, Grinberg NV, Kokhlov AR (2000) *Polymer* 41:6507
306. Loos W, Verbrugge S, Goethals EJ, Du Prez FE, Bakeeva IV, Zubov VP (2003) *Macromol Chem Phys* 204:98
307. Tager AA, Safronov AP, Berezyuk EA, Galaev IY (1994) *Colloid Polym Sci* 272:1234
308. Dubovik AS, Makhaeva EE, Grinberg VY, Khokhlov A (2005) *Macromol Chem Phys* 206:915
309. Makhaeva EE, Tenhu H, Khokhlov AR (1998) *Macromolecules* 31:6112
310. Akashi M, Nakano S, Kishida A (1996) *J Polym Sci Polym Chem* 34:301
311. Suwa K, Wada Y, Kikunaga Y, Morishita K, Kishida A, Akashi M (1997) *J Polym Sci Polym Chem* 35:1763
312. Suwa K, Morishita K, Kishida A, Akashi M (1997) *J Polym Sci Polym Chem* 35:3087
313. Suwa K, Yamamoto K, Akashi M, Takano K, Tanaka N, Kunugi S (1998) *Colloid Polym Sci* 276:529
314. Kunugi S, Tada T, Tanaka N, Yamamoto K, Akashi M (2002) *Polym J* 34:383
315. Kunugi S, Takano K, Tanaka N, Suwa K, Akashi M (1997) *Macromolecules* 30:4499
316. Kunugi S, Kameyama K, Tada T, Tanaka N, Shibayama M, Akashi M (2005) *Braz J Med Biol Res* 38:1233
317. Akashi M, Yashima E, Yamashita T, Miyauchi N, Sugita S, Marumo K (1990) *J Polym Sci Polym Chem* 28:3487
318. Chen CW, Takezako T, Yamamoto K, Serizawa T, Akashi M (2000) *Colloids Surf A* 169:107
319. Yamamoto K, Serizawa T, Muraoka Y, Akashi M (2000) *J Polym Sci Polym Chem* 38:3674
320. Kunugi S, Tada T, Yamazaki Y, Yamamoto K, Akashi M (2000) *Langmuir* 16:2042
321. Börner HG, Schlaad H (2007) *Soft Matter* 3:394
322. Lutz JF, Börner HG (2008) *Prog Polym Sci* 33:1
323. Klok HA, Lecommandoux S (2006) *Adv Polym Sci* 202:75
324. Schlaad H (2006) *Adv Polym Sci* 202:53
325. Van Domeselaar GH, Kwon GS, Andrew LC, Wishart DS (2003) *Colloids Surf B* 30:323
326. Rodríguez-Cabello JC, Reguera J, Girotti A, Arias FJ, Alonso M (2006) *Adv Polym Sci* 200:119
327. Deming TJ (2007) *Prog Polym Sci* 32:858
328. Löwik DWPM, van Hest JCM (2004) *Chem Soc Rev* 33:234
329. Nuhn H, Klok HA (2008) *Biomacromolecules* 9:2755
330. Rincon AC, Molina-Martinez IT, de Las Heras B, Alonso M, Bailez C, Rodriguez-Cabello JC, Herrero-Vanrell R (2006) *J Biomed Mater Res* 78A:343
331. Mart RJ, Osborne RD, Stevens MM, Ulijn RV (2006) *Soft Matter* 2:822
332. Meyer DE, Chilkoti A (2004) *Biomacromolecules* 5:846
333. Nagarsekar A, Crissman J, Crissman M, Ferrari F, Cappello J, Ghandehari H (2003) *Biomacromolecules* 4:602
334. Kostal J, Mulchandani A, Chen W (2001) *Macromolecules* 34:2257
335. Rodríguez-Cabello JC, Alonso M, Pérez T, Herguedas MM (2000) *Biopolymers* 54:282
336. Urry DW, Luan CH, Harris CM, Parker TM (1997) In: McGrath K, Kaplan D (eds) *Protein-based materials (bioengineering of materials)*. Birkhäuser, Boston
337. Ayad S, Boot-Handford RP, Humphries MJ, Kadler KE, Shuttleworth CA (1998) *The extra-cellular matrix facts book*, 2nd ed. Academic, San Diego
338. Urry DW (1993) *Angew Chem Int Ed* 32:819
339. Kurková D, Kříž J, Schmidt P, Dybal J, Rodríguez-Cabello JC, Alonso M (2003) *Biomacromolecules* 4:589
340. Martino M, Perri T, Tamburro AM (2002) *Macromol Biosci* 2:319
341. Gowda DC, Parker TM, Harris RD, Urry DW (1994) *Synthesis, characterization and medical applications of bioelastic materials*. In: Basava C, Anantharamaiah GM (eds) *Peptides: design, synthesis, and biological activity*. Birkhäuser, Boston

342. McPherson DT, Xu J, Urry DW (1996) *Protein Expr Purif* 7:51
343. San Biagio PL, Madonia F, Trapane TL, Urry DW (1988) *Chem Phys Lett* 145:571
344. Rodríguez-Cabello JC, Reguera J, Alonso M, Parker TM, McPherson DT, Urry DW (2004) *Chem Phys Lett* 388:127
345. Fernández-Trillo F, Duréault A, Bayley JPM, van Hest JCM, Thies JC, Michon T, Weberskirch R, Cameron NR (2007) *Macromolecules* 40:6094
346. Mattice WL, Mandelkern L (1971) *Macromolecules* 4:271
347. Mandelkern L, Mattice WL (1971) *J Am Chem Soc* 93:1769
348. McColl IH, Blanch EW, Hecht L, Kallenbach NR, Barron LD (2004) *J Am Chem Soc* 126:5076
349. Kakinoki S, Hirano Y, Oka M (2005) *Polym Bull* 53:109
350. Yoshida M, Safranji A, Omichi H, Katakai R (1996) *Macromolecules* 29:2321
351. Yoshida M, Asano M, Omichi H, Kamimura W, Kumakura M, Katakai R (1997) *Macromolecules* 30:2795
352. Mori H, Iwaya H, Nagai A, Endo T (2005) *Chem Commun* 38:4872
353. Mori H, Iwaya H, Endo T (2007) *React Funct Polym* 67:916
354. Mori H, Iwaya H, Endo T (2007) *Macromol Chem Phys* 208:1908
355. Mori H, Kato I, Matsuyama M, Endo T (2008) *Macromolecules* 41:5604
356. Mori T, Hamada M, Kobayashi T, Okamura H, Minagawa K, Masuda S, Tanaka M (2005) *J Polym Sci Polym Chem* 43:4942
357. Okamura H, Mori T, Minagawa K, Masuda S, Tanaka M (2002) *Polymer* 43:3825
358. Jun L, Bochu W, Yazhou W (2006) *Int J Pharmacol* 2:513
359. Fischetti L, Barry SM, Hope TJ, Shattock RJ (2009) *AIDS* 23:319
360. Tomalia DA, Sheets DP (1966) *J Polym Sci Polym Chem* 4:2253
361. Seeliger W, Aufderhaar E, Diepers W, Feinauer R, Nehring R, Thier W, Hellmann H (1966) *Angew Chem* 78:913
362. Aoi K, Okada M (1996) *Prog Polym Sci* 21:151
363. Wiesbrock F, Hoogenboom R, Leenen M, van Nispen SFGM, van der Loop M, Abeln CH, Van den Berg AMJ, Schubert US (2005) *Macromolecules* 38:7957
364. Hoogenboom R, Fijten MWM, Schubert US (2004) *J Polym Sci Polym Chem* 42:1830
365. Kempe K, Lobert M, Hoogenboom R, Schubert US (2009) *J Polym Sci Polym Chem* 47:3829
366. Park JS, Kataoka K (2007) *Macromolecules* 40:3599
367. Park JS, Kataoka K (2006) *Macromolecules* 39:6622
368. Kobayashi S, Uyama H (2002) *J Polym Sci Polym Chem* 40:192
369. Kobayashi S (1990) *Prog Polym Sci* 15:751
370. Uyama H, Kobayashi S (1992) *Chem Lett* 21:1643
371. Hoogenboom R (2007) *Macromol Chem Phys* 208:18
372. Demirel AL, Meyer M, Schlaad H (2007) *Angew Chem Int Ed* 46:8622
373. Meyer M, Antonietti M, Schlaad H (2007) *Soft Matter* 3:430
374. Litt M, Rahl F, Roldan LG (1969) *J Polym Sci Polym Phys Ed* 7:463
375. Hoogenboom R, Fijten M, Thijs HML, van Lankvelt BM, Schubert US (2005) *Des Monomers Polym* 8:659
376. Hoogenboom R (2009) *Angew Chem Int Ed* 48:7978
377. Lin PY, Clash C, Pearce EM, Kwei TK, Aponte MA (1988) *J Polym Sci Polym Phys* 26:603
378. Chen FP, Ames AE, Taylor LD (1990) *Macromolecules* 23:4688
379. Chen CH, Wilson J, Chen W, Davis RM, Riffle JS (1994) *Polymer* 35:3587
380. Chiu TT, Thill BP, Fairchok WJ (1986) In: Glass JE (ed) *Water-soluble polymers. Advances in chemistry series*, vol 213. ACS, Washington, DC
381. Wang CH, Hsiue GH (2002) *J Polym Sci Polym Chem* 40:1112
382. Hoogenboom R, Thijs HML, Jochims MJHC, van Lankvelt BM, Fijten MWM, Schubert US (2008) *Chem Commun* 44:5758
383. Christova D, Velichkova R, Loos W, Goethals EJ, Du Prez F (2003) *Polymer* 44:2255
384. Grinberg VY, Dubovik AS, Kuznetsov DV, Grinberg NV, Grosberg AY, Tanaka T (2000) *Macromolecules* 33:8685

385. Lee SC, Chang Y, Yoon Y, Kim C, Kwon IC, Kim YH, Jeong SY (1999) *Macromolecules* 32:1847
386. Burova TV, Grinberg NV, Grinberg VY, Kalinina EV, Lozinsky VI, Aseyev VO, Holappa S, Tenhu H, Khokhlov AR (2005) *Macromolecules* 38:1292
387. Huber S, Jordan R (2008) *Colloid Polym Sci* 286:395
388. Diab C, Akiyama Y, Kataoka K, Winnik FM (2004) *Macromolecules* 37:2556
389. Park JS, Akiyama Y, Winnik FM, Kataoka K (2004) *Macromolecules* 37:6786
390. Huber S, Hutter N, Rainer J (2008) *Colloid Polym Sci* 286:1653
391. Saeki S, Kuwahara N, Nakata M, Kaneko M (1976) *Polymer* 17:685
392. Bromberg LE, Ron ES (1998) *Adv Drug Deliv Rev* 31:197
393. Polverari M, van de Ven TGM (1996) *J Phys Chem* 100:13687
394. Kjellander R, Florin E (1981) *J Chem Soc Faraday Trans I* 77:2053
395. Hammouda B, Ho D, Kline S (2002) *Macromolecules* 35:8578
396. Boucher EA, Hines PM (1978) *J Polym Sci Polym Phys Ed* 16:501
397. Sundararajan PR (2007) Theta temperatures. In: Mark JE (ed) *Physical properties of polymers handbook*, 2nd edn. Springer, New York
398. Napper DH (1970) *J Colloid Interface Sci* 33:384
399. Ataman M, Boucher EA (1982) *J Polym Sci Polym Phys Ed* 20:1585
400. Ataman M (1987) *Colloid Polym Sci* 265:19
401. Van Krevelen DW (1990) *Properties of polymers*. Elsevier, Amsterdam
402. Brackman JC, van Os NM, Engberts JBFN (1988) *Langmuir* 4:1266
403. Saito S, Otsuka T (1967) *J Colloid Interface Sci* 25:531
404. Aoshima S, Yoshida T, Kanazawa A, Kanaoka S (2007) *J Polym Sci Polym Chem* 45:1801
405. Aoshima S, Oda H, Kobayashi E (1992) *J Polym Sci Polym Chem* 30:2407
406. Aoshima S, Oda H, Kobayashi E (1992) *Kobunshi Ronbunshu* 49:933
407. Sawamoto M (1991) *Prog Polym Sci* 16:111
408. Markova D, Christova D, Velichkova R (2003) *Polym Int* 52:1600
409. Horne RA, Almeida JP, Day AF, Yu NT (1971) *J Colloid Interface Sci* 35:77
410. Maeda Y (2001) *Langmuir* 17:1737
411. Aoshima S, Sugihara S, Shibayama M, Kanaoka S (2004) *Macromol Symp* 215:151
412. Schappacher M, Putaux JL, Lefebvre C, Deffieux A (2005) *J Am Chem Soc* 127:2990
413. Bhattacharjee RR, Chakraborty M, Mandal TK (2006) *J Phys Chem B* 110:6768
414. Verdonck B, Gohy JF, Khousakoun E, Jérôme R, Du Prez F (2005) *Polymer* 46:9899
415. Van Durme K, Van Mele B, Bernaerts KV, Verdonck B, Du Prez F (2006) *J Polym Sci Polym Phys* 44:461
416. Confortini O, Du Prez FE (2007) *Macromol Chem Phys* 208:1871
417. Van Durme K, Loozen E, Nies E, Van Mele B (2005) *Macromolecules* 38:10234
418. Van Durme K, Van Assche G, Nies E, Van Mele B (2007) *J Phys Chem B* 111:1288
419. Confortini O, Verdonck B, Goethals EJ (2002) *e-Polymers* 43:1
420. Sugihara S, Hashimoto K, Matsumoto Y, Kanaoka S, Aoshima S (2003) *J Polym Sci Polym Chem* 41:3300
421. Sugihara S, Kanaoka S, Aoshima S (2004) *Macromolecules* 37:1711
422. Zhou Y, Faust R, Richard R, Schwarz W (2005) *Macromolecules* 38:8183
423. Okabe S, Sugihara S, Aoshima S, Shibayama M (2003) *Macromolecules* 36:4099
424. Seno KI, Tsujimoto I, Kikuchi T, Kanaoka S, Aoshima S (2008) *J Polym Sci Polym Chem* 46:6151
425. Ishida M, Sakai H, Sugihara S, Aoshima S, Yokoyama S, Abe M (2003) *Chem Pharm Bull* 11:1348
426. Matsuda Y, Kawata T, Sugihara S, Aoshima S, Sato T (2006) *J Polym Sci Polym Phys* 44:1179
427. Matsuda Y, Miyazaki Y, Sugihara S, Aoshima S, Saito K, Sato T (2005) *J Polym Sci Polym Phys* 43:2937
428. Aoshima S, Sugihara S (2000) *J Polym Sci Polym Chem* 38:3962
429. Sugihara S, Ohashi M, Ikeda I (2007) *Macromolecules* 40:3394
430. Labbe A, Carloti S, Deffieux A, Hirao A (2007) *Macromol Symp* 249–250:392

431. Aoki S, Koide A, Imabayashi S, Watanabe M (2002) *Chem Lett* 31:1128
432. Reinicke S, Schmelz J, Lapp A, Karg M, Hellweg T, Schmalz H (2009) *Soft Matter* 5:2648
433. Wan AC, Mao HQ, Wang S, Leong KW, Ong LK, Yu H (2001) *Biomaterials* 22:1157
434. Wang J, Zhang PC, Lu HF, Ma N, Wang S, Mao HQ, Leong KW (2002) *J Control Release* 83:157
435. Huang SW, Wang J, Zhang PC, Mao HQ, Zhuo RX, Leong KW (2004) *Biomacromolecules* 5:306
436. Wang DA, Williams CG, Yang F, Cher N, Lee H, Elisseff JH (2005) *Tissue Eng* 11:201
437. Wang YC, Li Y, Yang XZ, Yuan YY, Yan LF, Wang J (2009) *Macromolecules* 42:3026
438. Yuan YY, Liu XQ, Wang YC, Wang J (2009) *Langmuir* 25:10298
439. Iwasaki Y, Komatsu S, Narita T, Akiyoshi K, Ishihara K (2003) *Macromol Biosci* 3:238
440. Iwasaki Y, Wachiralarpphaithoon C, Akiyoshi K (2007) *Macromolecules* 40:8136
441. Alter JE, Taylor GT, Scheraga HA (1972) *Macromolecules* 5:739
442. Yakubovich AV, Solov'yov IA, Solov'yova AV, Greiner W (2009) *Eur Phys J D* 51:25
443. Fasman GD (ed) (1989) *Prediction of protein structure and the principles of protein conformation*. Plenum, New York
444. Jilie K, Li M (2008) In: Galaev I, Mattiasson B (eds) *Smart polymers: applications in biotechnology and biomedicine*, 2nd edn. CRC, Boca Raton, FL
445. Okay O (2008) In: Galaev I, Mattiasson B (eds) *Smart polymers: applications in biotechnology and biomedicine*, 2nd edn. CRC, Boca Raton, FL
446. Lozinsky VI, Plieva FM, Galaev IY, Mattiasson B (2002) *Bioseparation* 10:163
447. Lozinsky VI, Galaev IY, Plieva FM, Savina I, Jungvid H, Mattiasson B (2003) *Trends Biotechnol* 21:445
448. Komarova GA, Starodubtsev SG, Lozinsky VI, Kalinina EV, Landfester K, Khokhlov AR (2008) *Langmuir* 24:4467
449. Cheng SX, Zhang JT, Zhuo RX (2003) *J Biomed Mater Res A* 67:96
450. Fänger C, Wack H, Ulbricht M (2006) *Macromol Biosci* 6:393
451. Zhuang Y, Wang G, Yang H, Zhu Z, Fu J, Song W, Zhao H (2005) *Polym Int* 54:617
452. Yang H, Song W, Zhuang Y, Deng X (2003) *Macromol Biosci* 3:400
453. Cai W, Anderson EC, Gupta RB (2001) *Ind Eng Chem Res* 40:2283
454. Hennaux P, Laschewsky A (2003) *Colloid Polym Sci* 281:807
455. Chong YK, Le TPT, Moad G, Rizzardo E, Thang SH (1999) *Macromolecules* 32:2071
456. Aoki T, Kawashima M, Katono H, Sanui K, Igata N, Okano T, Sakurai Y (1994) *Macromolecules* 27:947
457. Butler K, Thomas PR, Tyler GJ (1960) *J Polym Sci* 48:357
458. Xie X, Hogen-Esch TE (1996) *Macromolecules* 29:1746
459. Laschewsky A, Rekaï ED, Wischerhoff E (2001) *Macromol Chem Phys* 202:276
460. Devasia R, Bindu RL, Borsali R, Mougin N, Gnanou Y (2005) *Macromol Symp* 229:8
461. Meza RL, Gargallo L (1977) *Europ Polym J* 13:235
462. Güner A (1996) *J Appl Polym Sci* 62:785
463. Salamova UU, Rzaev ZMO, Altindal S, Masimov AA (1996) *Polymer* 37:2415
464. Kavlak S, Güner A (2000) *J Appl Polym Sci* 78:507
465. Kirci B, Güner A (2001) *Eur Polym J* 37:361
466. Favier A, Charreyre MT, Chaumont P, Pichot C (2002) *Macromolecules* 35:8271
467. Favier A, Ladavière C, Charreyre MT, Pichot C (2004) *Macromolecules* 37:2026
468. Bathfield M, D'Agosto F, Spitz R, Ladavière C, Charreyre MT, Delair T (2007) *Macromol Rapid Commun* 28:856
469. Sawada H, Kawase T, Ikematsu Y, Ishii Y, Oue M, Hayakawa Y (1996) *Chem Commun* 2:179
470. Sawada H, Takahashi K, Mugisawa M, Oya T, Ogino S (2007) *Langmuir* 23:11947
471. Save NS, Jassal M, Agrawal AK (2003) *Polymer* 44:7979
472. de Lambert B, Charreyre MT, Chaix C, Pichot C (2005) *Polymer* 46:623
473. Diehl C, Schlaad H (2009) *Macromol Biosci* 9:157
474. Rueda JC, Zschoche S, Komber H, Schmaljohann D, Voit B (2005) *Macromolecules* 38:7330
475. Volet G, Chanthavon V, Wintgens V, Amiel C (2005) *Macromolecules* 38:5190
476. Zhang N, Huber S, Schulz A, Luxenhofer R, Jordan R (2009) *Macromolecules* 42:2215

- 477. Weber C, Becer CR, Hoogenboom R, Schubert US (2009) *Macromolecules* 42:2965
- 478. Park JS, Akiyama Y, Yamasaki Y, Kataoka K (2007) *Langmuir* 23:138
- 479. Lee SC, Kang SW, Kim C, Kwon IC, Jeong SY (2000) *Polymer* 41:7091
- 480. Kim C, Lee SC, Kang SW, Kwon IC, Jeong SY (2000) *J Polym Sci Polym Phys* 38:2400
- 481. Kotre T, Zarka MT, Krause JO, Buchmeiser MR, Weberskirch R, Nuyken O (2004) *Macromol Symp* 217:203
- 482. Nuyken O, Persigehl P, Weberskirch R (2002) *Macromol Symp* 177:163
- 483. Luedtke K, Jordan R, Hommes P, Nuyken O, Naumann CA (2005) *Macromol Biosci* 5:384
- 484. Jin RH (2004) *J Mater Chem* 14:320
- 485. Hassan CM, Peppas NA (2000) *Adv Polym Sci* 153:37
- 486. Napper DH (1969) *Kolloid Z* 234:1149
- 487. Dieu HA (1954) *J Polym Sci* 12:417
- 488. Sakurada I, Sakagushi Y, Ito Y (1957) *Kobunshi Kagaku* 14:41
- 489. Nord FF, Bier M, Timasheff SN (1951) *J Am Chem Soc* 73:289
- 490. Christova D, Ivanova S, Ivanova G (2003) *Polym Bull* 50:367
- 491. Briscoe B, Luckham P, Zhu S (2000) *Polymer* 41:3851
- 492. Briscoe B, Luckham P, Zhuy S (1999) *Proc R Soc Lond A* 455:737
- 493. Pae BJ, Moon TJ, Lee CH, Ko MB, Park M, Lim S, Kim J, Choe CR (1997) *Korea Polym J* 5:126
- 494. Beresniewicz A (1959) *J Polym Sci* 39:63
- 495. Liu TY, Hu SH, Liu DM, Chen SY, Chen IW (2009) *Nano Today* 4:52
- 496. Malmsten M, Lindman B (1992) *Macromolecules* 25:5440
- 497. Zhang Z, Khan A (1995) *Macromolecules* 28:3807
- 498. Mortensen K, Pedersen S (1993) *Macromolecules* 26:805
- 499. Alexandridis P, Holzwarth JF, Hatton TA (1994) *Macromolecules* 27:2414
- 500. Nijenhuis K (1997) *Adv Polym Sci* 130:1
- 501. Mortensen K (2001) *Colloids Surf A* 183–185:277
- 502. Mortensen K, Batsberg W, Hvidt S (2008) *Macromolecules* 41:1720
- 503. Nixon SK, Hvidt S, Booth C (2004) *J Colloid Interface Sci* 280:219
- 504. Mori T, Shiota Y, Minagawa K, Tanaka M (2005) *J Polym Sci Polym Chem* 43:1007
- 505. Neugebauer D (2007) *Polym Int* 56:1469
- 506. Tao L, Mantovani G, Lecolley F, Haddleton DM (2004) *J Am Chem Soc* 126:13220
- 507. Wang XS, Lascelles SF, Jackson RA, Armes SP (1999) *Chem Commun* 18:1817
- 508. Wang XS, Armes, SP (2000) *Macromolecules* 33:6640
- 509. Han S, Hagiwara M, Ishizone T (2003) *Macromolecules* 36:8312
- 510. Yamamoto S, Pietrasik J, Matyjaszewski K (2007) *Macromolecules* 40:9348
- 511. Lutz JF, Akdemir Ö, Hoth A (2006) *J Am Chem Soc* 128:13046
- 512. Lutz JF, Hoth A (2006) *Macromolecules* 39:893
- 513. Lutz JF, Weichenhan K, Akdemir Ö, Hoth A (2007) *Macromolecules* 40:2503
- 514. Huang X, Du F, Ju R, Li Z (2007) *Macromol Rapid Commun* 28:597
- 515. Kitano H, Hirabayashi T, Gemmei-Ide M, Kyogoku M (2004) *Macromol Chem Phys* 205:1651
- 516. Ishizone T, Han S, Okuyama S, Nakahama S (2003) *Macromolecules* 36:42
- 517. Eggenhuisen TM, Becer C, Fijten MWM, Eckardt R, Hoogenboom R, Schubert US (2008) *Macromolecules* 41:5132
- 518. Weaver JVM, Bannister I, Robinson KL, Bories-Azeau X, Armes SP, Smallridge M, McKenna P (2004) *Macromolecules* 37:2395
- 519. Xu FJ, Kang ET, Neoh ET (2006) *Biomaterials* 27:2787
- 520. Ruckenstein E, Zhang H (2001) *Polym Bull* 47:113
- 521. Peppas NA, Mikos AG (1986) In: Peppas NA (ed) *Hydrogels in medicine and pharmacy*, vol 1. CRC, Boca Raton, FL
- 522. Oh SH, Jhon MS (1989) *J Polym Sci Polym Chem Ed* 27:1731
- 523. Dušek K, Bohdanecký M, Prokopová E (1974) *Eur Polym J* 10:239
- 524. Perera DI, Shanks RA (1995) *Polym Int* 37:133
- 525. Seifert LM, Green RT (1985) *J Biomed Mater Res* 19:1043

526. Okano T, Aoyagi T, Kataoka K, Abe K, Sakurai Y, Shimadada M, Shinohara I (1986) *J Biomed Mater Res* 20:919
527. Loos M, Baeyens-Volant D, Szalai E, David C (1990) *Makromol Chem* 191:2917
528. Melnig V, Ciobanu C, Optoelectron J (2005) *Adv Mater* 7:2809
529. Apostu MO, Melnig V (2006) *J Optoelectron Adv Mater* 8:1044
530. Jia Z, Chen H, Zhu X, Yan D (2006) *J Am Chem Soc* 128:8144
531. Chen H, Jia Z, Yan D, Zhu X (2007) *Macromol Chem Phys* 208:1637
532. Jiang X, Smith MR III, Baker GL (2008) *Macromolecules* 41:318
533. Li W, Zhang A, Feldman K, Walde P, Schlüter AD (2008) *Macromolecules* 41:3659
534. Haba Y, Harada A, Takagishi T, Kono K (2004) *J Am Chem Soc* 126:12760
535. Haba Y, Kojima C, Harada A, Kono K (2006) *Macromolecules* 39:7451
536. Haba Y, Kojima C, Harada A, Kono K (2007) *Angew Chem Int Ed* 46:234
537. Seong JY, Jun YJ, Kim BM, Park YM, Sohn YS (2006) *Int J Pharm* 314:90
538. Sohn YS, Kim JK, Song R, Jeong B (2004) *Polymer* 45:3081
539. Lee BH, Lee YM, Sohn YS, Song SC (2002) *Bull Korean Chem Soc* 23:549
540. Lee BH, Lee YM, Sohn YS, Song SC (2002) *Macromolecules* 35:3876
541. Lee SB, Song S, Jin J, Sohn YS (1999) *Macromolecules* 32:7820
542. Song S, Lee SB, Jin J, Sohn YS (1999) *Macromolecules* 32:2188
543. Lakshmi S, Katti DS, Laurencin CT (2003) *Adv Drug Deliv Rev* 55:467
544. Aoki T, Nakamura K, Sanui K, Kikuchi A, Okano T, Sakurai Y, Ogata N (1999) *Polym J* 31:1185
545. Wertheim MS (1984) *J Stat Phys* 35:19
546. Wertheim MS (1984) *J Stat Phys* 35:35
547. Chapman WG, Jackson G, Gubbins KE (1988) *Mol Phys* 65:1057
548. Silberberg A, Eliassaf J, Katchalsky A (1957) *J Polym Sci* 23:259
549. Eliassaf J (1960) *J Appl Polym Sci* 3:372
550. Titkova LV, Prokopová E, Sedláček B, Petrus V, Dusek K, Bohdanecký M (1978) *Eur Polym J* 14:145
551. Chatterjee SK, Prokopová E, Bohdanecký M (1978) *Eur Polym J* 14:665
552. Nugent MJD, Hanley A, Tomkins PT, Higginbotham CL (2005) *J Mater Sci Mater Med* 16:1149
553. Peppas NA, Stauffer SR (1991) *J Control Release* 16:305
554. Hatakeyema T, Uno J, Yamada C, Kishi A, Hatakeyema H (2005) *Thermochim Acta* 431:144
555. Haas HC, Schuler NW (1964) *J Polym Sci Polym Lett* 2:1095
556. Haas HC, Moreau RD, Schuler NW (1967) *J Polym Sci A-2 Polym Phys* 5:915
557. Haas HC, Chiklis CK, Moreau RD (1970) *J Polym Sci A-1 Polym Chem* 8:1131
558. Haas HC, MacDonald RL, Schuler AN (1970) *J Polym Sci A-1 Polym Chem* 8:1213
559. Haas HC, Manning MJ, Mach MH (1970) *J Polym Sci A-1 Polym Chem* 8:1725
560. Haas HC, MacDonald RL, Schuler AN (1970) *J Polym Sci A-1 Polym Chem* 8:3405
561. Haas HC, MacDonald RL, Schuler AN (1971) *J Polym Sci A-1 Polym Chem* 9:959
562. Furyk S, Zhang YJ, Ortiz-Acosta D, Cremer PS, Bergbreiter DE (2006) *J Polym Sci Polym Chem* 44:1492
563. Zhulina EB, Borisov OV, Birshtein TM (1988) *Vysokomol Soedin Ser A* 30:774
564. Garas G, Kosmas M (1994) *Macromolecules* 27:6671
565. Francois J, Beaudoin E, Borisov O (2003) *Langmuir* 19:10011
566. Numasawa N, Okada M (1999) *Polym J* 31:99
567. Shmakov SL (2001) *Polymer* 43:1491
568. Xu J, Liu S (2009) *J Polym Sci Polym Chem* 47:404
569. Turner K, Zhu PW, Napper DH (1996) *Colloid Polym Sci* 274:622
570. Hu TJ, Wu C (1999) *Phys Rev Lett* 83:4105
571. Wagner M, Brochardwyart F, Hervet H, Degennes PG (1993) *Colloid Polym Sci* 271:621
572. Qiu XP, Tanaka F, Winnik FM (2007) *Macromolecules* 40:7069
573. Xu J, Ye J, Liu S (2007) *Macromolecules* 40:9103
574. Ye J, Xu J, Hu J, Wang X, Zhang G, Liu S, Wu C (2008) *Macromolecules* 41:4416
575. Satokawa Y, Shikata T, Tanaka F, Qiu XP, Winnik FM (2009) *Macromolecules* 42:1400

- 576. Chung JE, Yokoyama M, Suzuki K, Aoyagi T, Sakurai Y, Okano T (1997) *Colloids Surf B* 9:37
- 577. Kujawa P, Watanabe H, Tanaka F, Winnik FM (2005) *Eur Phys J E* 17:129
- 578. Segui F, Qiu XP, Winnik FM (2008) *J Polym Sci Polym Chem* 46:314
- 579. Kujawa P, Segui F, Shaban S, Diab C, Okada Y, Tanaka F, Winnik FM (2006) *Macromolecules* 39:341
- 580. Nojima R, Sato T, Qiu XP, Winnik FM (2008) *Macromolecules* 41:292
- 581. Koga T, Tanaka F, Motokawa R, Koizumi S, Winnik FM (2008) *Macromolecules* 41:9413
- 582. Weberskirch R, Preuschen J, Spiess HW, Nuyken O (2000) *Macromol Chem Phys* 201:995
- 583. Obeid R, Maltseva E, Thünemann AF, Tanaka F, Winnik FM (2009) *Macromolecules* 42:2204
- 584. Obeid R, Tanaka F, Winnik FM (2009) *Macromolecules* 42:5818
- 585. Morimoto N, Obeid R, Yamane S, Winnik FM, Akiyoshi K (2009) *Soft Matter* 5:1597
- 586. Winnik FM, Ringsdorf H, Venzmer J (1990) *Macromolecules* 23:2415
- 587. Schild HG, Muthukumar M, Tirrel DA (1991) *Macromolecules* 24:948
- 588. Hirotsu S (1988) *J Chem Phys* 88:427
- 589. Zhang G, Wu C (2001) *J Am Chem Soc* 123:1376

From Coordination Polymers to Hierarchical Self-Assembled Structures

Yun Yan, Arie de Keizer, Martien A. Cohen Stuart,
and Nicolaas A.M. Besseling

Abstract In this review, novel hierarchical self-assembled structures based on reversible organo-metallic supramolecular polymers are discussed. Firstly, we discuss recent advances in the field of coordination polymers, considering cases in which transition metal ions and bis- or multiligands are used to build up organo-metallic supramolecular polymers. Secondly, we review hierarchical self-assembled structures based on these coordination polymers, such as polyelectrolyte layer-by-layer films, capsules, complex coacervate core micelles and microemulsions, and nanoribbons. Finally, we give a short perspective on the formation of coordination-polymeric hierarchical self-assembled structures. The implications of fundamental and applied research, as well as aspects of new technologies are also discussed.

Keywords Complex coacervate · Coordination polymers · Layer-by-layer · Micelles · Polyelectrolytes · Self-assembly · Supramolecular polymers

Contents

1	Introduction	92
2	Reversible Coordination Polymers	93
2.1	Metal Ions and Ligands Suitable for Forming Coordination Polymers	93
2.2	Structure of Coordination Polymers	95
2.3	Properties of Reversible Coordination Polymers	98

Y. Yan (✉), A. de Keizer, and M.A.C. Stuart
Laboratory of Physical Chemistry and Colloid Science, Wageningen University,
Dreijenplein 6, 6703 HB Wageningen, The Netherlands
e-mail: yunyan@pku.edu.cn; arie.dekeizer@wur.nl; martien.cohenstuart@wur.nl

Y. Yan
College of Chemistry and Molecular Engineering, Peking University, Beijing 100871, China

N.A.M. Besseling
Nano Structured Materials, Department of Chemical Engineering, Delft University of Technology,
Julianalaan 136, 2628 BL Delft, The Netherlands
e-mail: n.a.m.besseling@tudelft.nl

3	Nanostructures Based on Coordination Polymers	102
3.1	Thin Layer-by-Layer Films	102
3.2	Langmuir and Langmuir–Blodgett Films	104
3.3	Micelles	105
3.4	Microemulsions	109
3.5	Nanoribbons	110
4	Conclusions and Perspectives	113
	References	114

1 Introduction

Putting metals into polymers has been a goal for polymer scientists for the past two decades because the valuable physical and chemical properties of many materials can be attributed to metallic elements. Examples include magnetic materials used in data storage, superconductors, electro-chromic materials, and catalysts. Introduction of a metallic element into polymers is therefore expected to endow polymers with desirable optical, electrical, or magnetic properties [1]. Many efforts were made in this field to create macromolecular chains in which metal atoms were covalently built into the polymeric architecture [2, 3]. Very recently, metal-mediated self-assembly has emerged as a powerful easy-to-process procedure for creation of supramolecular metal-containing polymeric structures [4–9]. This approach helps to create self-organized, functional materials whose properties complement those of purely organic systems [7–9].

In this review, the terms “metallo-supramolecules” or “coordination polymers” are used for the polymeric structures formed from metal ions and small polytopic ligands (≥ 2 ligand groups per molecule) in which the metal ions are an integral part of the polymer backbone. Figure 1 illustrates the formation of a linear chain from metal ions and bisligand molecules. In this review, we will not consider block polymeric structures that consist of two or three chemically different polymer chains coordinatively bonded at their chain ends to form one single linear macromolecule [10–13], nor polymers containing coordination bonds in the side chains of a covalent polymer backbone [14–16]. In this framework, two classes of coordination polymers are discussed. First, we will consider irreversible coordination polymers, which are based on the kinetically inert metal–ligand coordination bonds. In this case, the binding constants between ligands and metal ions are very large, and at ambient temperature exchange of ligands in solution is extremely slow. Hence, the chain length

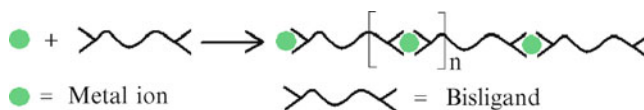


Fig. 1 Formation of coordination polymers from metal ions and bisligands. Note that the polymeric chain is held together by metal–ligand coordination bonds so that metal ions are an integral part of the chain

distribution is effectively frozen. This class of coordination polymers, which is very similar to the covalently synthesized metallo-organic polymers and can be characterized by standard polymer analytical tools, is usually formed in uncoordinating organic solvent. Second, we will discuss reversible coordination polymers, or equilibrium coordination polymers, which are based on kinetically labile coordination bonds in a coordinating solvent (usually water) with medium binding constant. The binding constants are smaller than for the “inert” coordination polymers, and exchange of ligands with solvent molecules occurs. This latter class is of particular interest for constructing functional devices [7–9, 17–19]. The well-defined coordination geometries, the variety of binding strengths, and the ligand exchange kinetics give these coordination polymers stimuli-switchable properties. In addition, judicious choice of the transition metal ions and of the steric and electronic ligand–metal ion interactions add more variables for producing smart materials with useful properties, including strong absorption, high quantum yields, suitable excited state lifetimes, luminescence, and tunable redox states [20–22].

This review focuses on the most interesting reversible coordination polymers and their application in various hierarchical self-assembled structures, including thin films, microcapsules, micelles, microemulsions, and nanoribbons. These structures have in common that they are hierarchical assemblies containing metal-mediated reversible coordination polymers as a main component. The charges carried by the coordination polymers are utilized to interact with oppositely charged components, including nanoparticles, polyelectrolytes, block copolymers, and surfactants. Specific features of these objects, introduced by the coordination polymers, as well as the influence of additional salt are discussed.

2 Reversible Coordination Polymers

2.1 *Metal Ions and Ligands Suitable for Forming Coordination Polymers*

Most transition metal ions can be coordinated into a polymeric structure. These metal ions have empty or unsaturated *d* or *f* atom orbitals (receptors) that can accept electrons from ligand molecules (donors) to form coordination bonds. The first-row transition metal ions, such as, Fe^{2+} , Co^{2+} , Ni^{2+} , and Zn^{2+} , usually form labile coordination bonds with ligands in coordinating solvents such as water [23], whereas those of the second- and third-row transition metal ions often form irreversible coordination bonds [24]. There are also exceptions, such as some lanthanoid ions (e.g., Nd^{3+} and La^{3+}) that can form labile coordination bonds with carboxylic groups [25].

Generally, the ligands required for formation of coordination polymers must have at least two ligand groups, which allow the growth of the chain and form polymeric chains (see Fig. 1). Structures of different polytopic ligand molecules (1–9) are presented in Fig. 2. Bisligands that bear two ligand groups are the most investigated

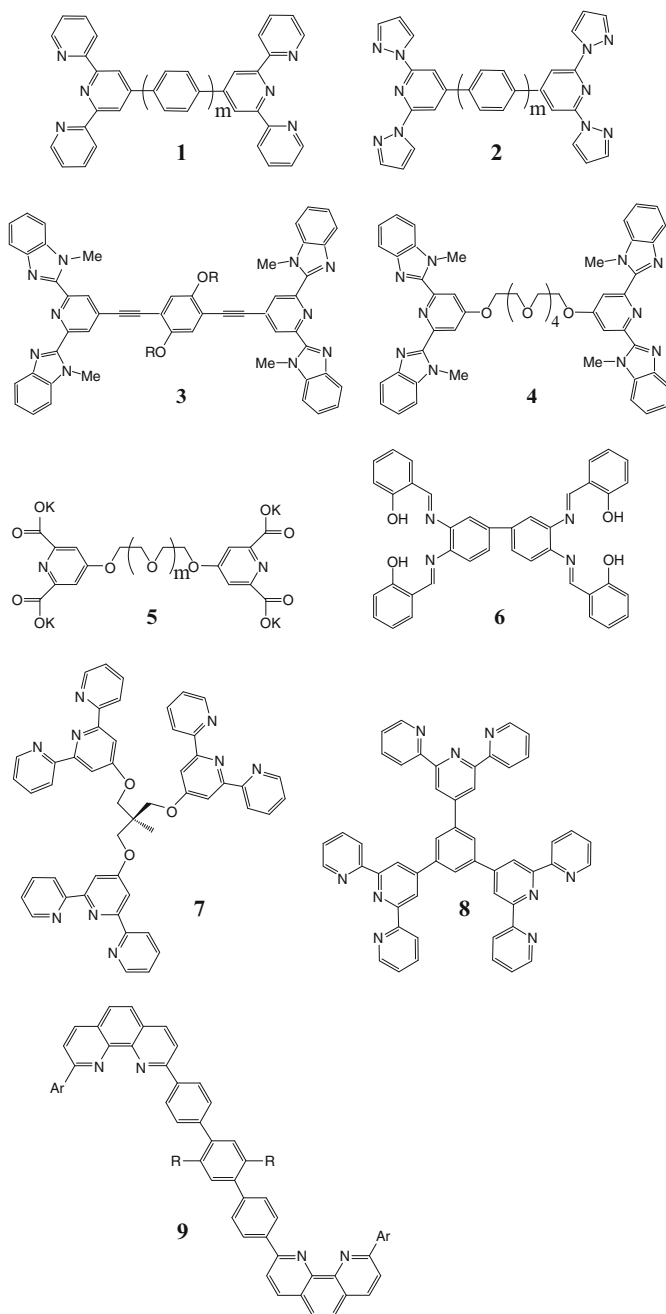


Fig. 2 Structures of the polytopic ligand molecules based on terpyridine (**1**, **7**, **8**), pyrazolopyridine (**2–4**), pyridine-2,6-dicarboxylic acid (**5**), Schiff base (**6**), and phenanthroline (**9**) ligands. Note, that **1–6** and **9** are ditopic ligands (bisligands), and that **7** and **8** are three-head ligands. Structures **4** and **5** are flexible and water-soluble, and the others are all rigid. In molecule **5**, when $m = 3$, it is denoted as L_2EO_4

category, and include examples such as the terpyridine series ligands (**1**) synthesized by Constable [21, 26, 27] and Kurth [22]; the 2,6-bis(benzimidazolyl)-pyridine (BIP) ligands (**2–4**) synthesized by Rowan et al. [28]; the 1,11-bis(2,6-dicarboxypyridin-4-yloxy)-3,6,9-trioxaundecans, abbreviated as L_2EO_4 (**5**), developed by Vermonden et al. [25, 29]; the phenanthroline ligand (**9**, [30, 31]); and the Schiff base ligand (**6**, [32]). As another variation, multiligands with more than two ligand groups (**7**, **8**) were also introduced [33, 34]. The latter enable formation of branched coordination polymers. The steric structure of the multiligands indeed adds additional variables that control the structure of the coordination polymers. If the spacers between the heads are rigid like in molecules **1–3**, **6**, and **9**, the resultant coordination polymers are also rigid. Typical examples are the coordination polymers synthesized by Kurth et al. [22] on the basis of rigid terpyridine ligands and Fe(II) ions. Coordination polymers of this kind are usually soluble only in organic solvent. When flexible spacers are used, like the ethylene oxide (EO) spacers in molecules **4** and **5**, the coordination polymers are flexible, and also rings can be formed in aqueous solution. The formation of rings and chains in aqueous solutions of Zn^{2+} and molecule **5** has been systematically investigated by Vermonden and coworkers [35].

2.2 Structure of Coordination Polymers

The structure of coordination polymers depends both on the coordination geometry of the transition metal ions and on the steric structure of the ligands, as well as on the rigidity of the ligand molecules. Chains, rings, and branched structures can be formed depending on the metal–ligand combination. For example, in the case of rigid assembly between a bisligand and first-row transition metal ions, straight chains are usually formed. Examples include the dynamic coordination polymers based on bisphenanthroline ligands and Cu(I) and Ag(I) ions (Fig. 3a) [30, 31], or those based on the bisterpyridine ligand with rigid benzenyl spacers and Fe(II), Co(II), and Ni(II) ions (Fig. 3b) [8]. Formation of such rigid coordination polymers is usually illustrated as shown in Fig. 3c.

A flexible spacer between the two ligand groups of the bisligand molecule enables formation of ring-like structures. Vermonden et al. [29] have synthesized a series of bisligands with flexible oligo ethylene oxide (EO) as spacers. When four EO units are used, the smallest possible rings of coordination polymer are composed of two metal–ligand coordination centers. More than five EO units enable the formation of rings with only one coordination center (Fig. 4a [35]). However, at high concentrations, chain-like structures occur in these systems. It should be noticed that long chains can be formed only at 1:1 molar mixing ratio between metal ions and bisligand molecules. Excess of either results in additional ends, which restrict the growth of the chain. In the 1:1 mixed L_2EO_4 (where L_2 is the bisligand) and Zn(II) system, rings are the dominant species at L_2EO_4 concentrations lower than about 20 mM, whereas chains govern the system at higher concentrations (Fig. 4b).

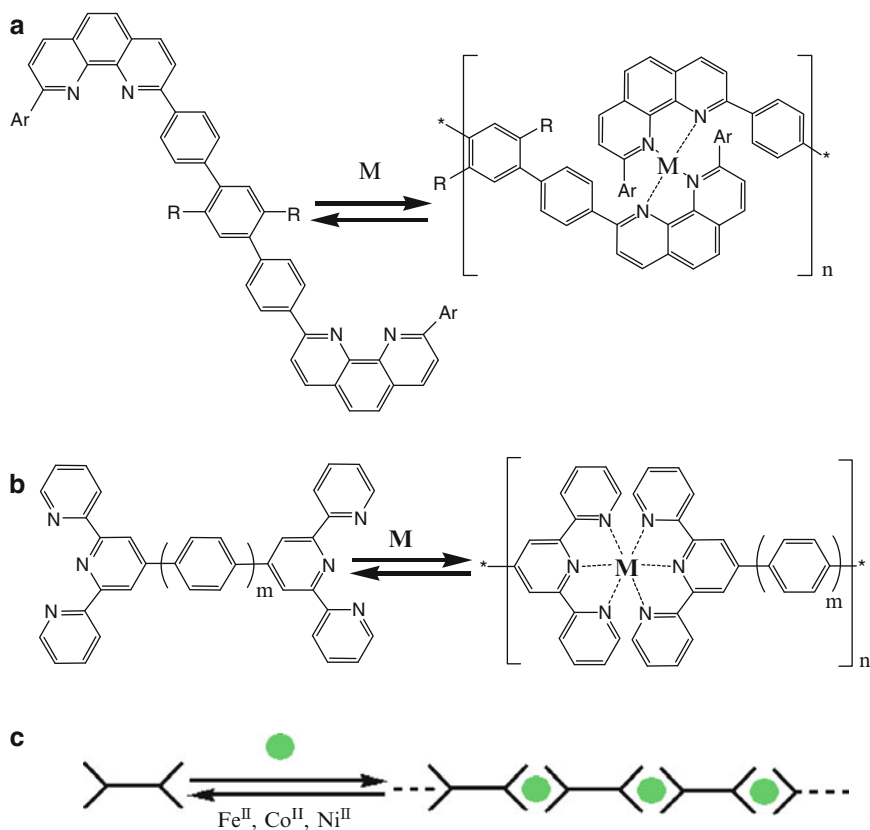


Fig. 3 Dynamic coordination polymers based on (a) the ditopic phenanthroline ligand, and Cu(I) and Ag(I) ions (metals are shown as M); (b) the ditopic terpyridine ligand, and Fe(II), Co(II), and Ni(II) ions. (c) General scheme of formation of such rigid coordination polymers

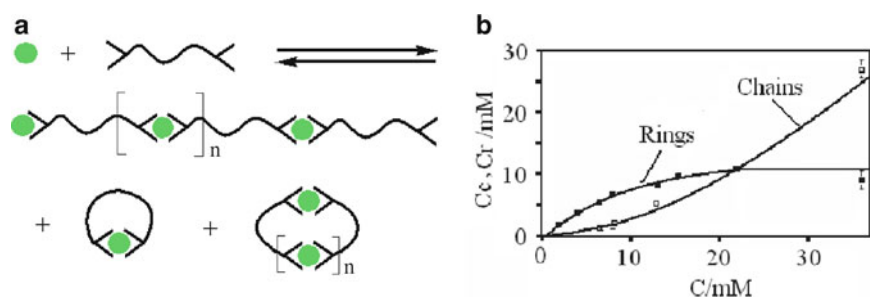


Fig. 4 (a) Formation of rings and chains in solutions of flexible coordination polymers. (b) Concentrations of monomers in rings (C_r) and chains (C_c) as a function of total monomer concentration (C) for metal-to-monomer ratios of 1

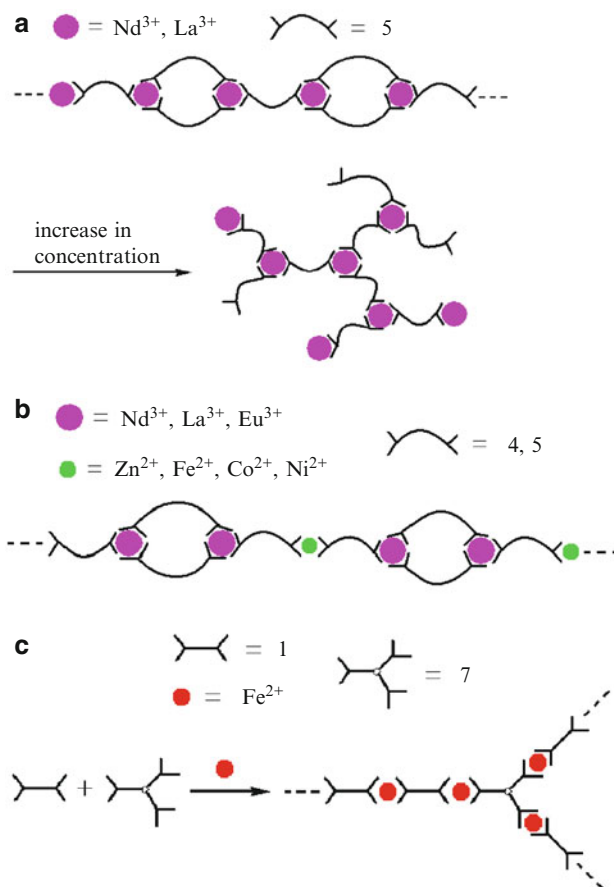


Fig. 5 Different branched structures (a–c) formed by coordination polymers. The metal ions are drawn as solid circles. The numbers in the figures represent the structures in Fig. 2

Interestingly, branched structures are formed when Nd^{3+} or La^{3+} ions are used in combination with these same L_2EO_4 ligands [25]. Since the radii of these ions are much larger than that of Zn^{2+} ions due to presence of half saturated f orbitals, one Nd^{3+} or La^{3+} ion can bind three heads (ligand groups). In this way, the Nd^{3+} or La^{3+} ions act as branching points or as crosslinkers, as illustrated in Fig. 5. Combination of such lanthanide ions and first-row transition metal ions in metal/bisligand and mixed systems lead to the formation of branched coordination polymers [36, 37]. Multiligands constitute another possibility for construction of branched coordination structures. In this case, the multiligands form the crosslinks. Kurth et al. [33] modified the spacer of terpyridine ligands to build star-like three-head ligands (7 and 8 of Fig. 2). It can be imagined that introduction of third-row transition metal ions to multiligands will yield even more complicated network structures. These have not been reported so far. The possible structures of the coordination polymers are summarized in Table 1.

Table 1 Possible structures of coordination polymers formed from metal ions of different rows and ligands of different structures

Metal ions	Bisligands		Multiligands (≥ 3 heads)	Bis + multiligands
	Rigid	Flexible		
1st row	Chain	Chain, Ring	Branched	Branched
2nd, 3rd row	Branched	Branched	Branched	Branched
1st + 2nd or 3rd row	Branched	Branched	Branched	Branched

2.3 Properties of Reversible Coordination Polymers

2.3.1 Formation of Reversible Coordination Polymers

Reversible coordination polymers in a coordinating solvent are equilibrium systems. In the simplest case, in a solution of metal ions M and bisligands L_2 (monomers) where every ligand monomer has two identical ligand groups L connected by a spacer, the metal ions M may bind with one or two ligand groups. Two types of complexes can be formed: a 1:1 complex ML in which a metal ion is coordinated by one ligand group (and one or more solvent molecules), and a 1:2 complex ML_2 in which a metal ion is coordinated by two ligand groups. The equilibrium concentrations of all species in the solution can be described by the binding constants:

$$K_1 = \frac{[ML]}{[M][L]}$$

$$K_2 = \frac{[ML_2]}{[ML][L]}$$

Where $[L]$, $[M]$, $[ML]$, and $[ML_2]$ are the concentrations of free chelating groups, free metal ions, and metal ions coordinated by one and by two chelating groups, respectively. Expressions for the chain-length distributions for open chains and closed rings have been derived by adapting Jacobson and Stockmayer's theory [38] through introducing the probability that a metal ion is coordinated once, or twice, respectively [25].

The length of coordination polymers is highly dependent on the L_2 to M ratio. For first-row transition metal and bisligand systems at high enough concentrations, polymerization is maximal at molar ratio $y = C_{\text{metal}}/C_{\text{ligand}} = 1$. Slight deviations from this ratio result in a dramatic reduction of the average chain length. Figure 6a shows the dependence of the average number of the monomers in one coordination polymer chain of the bisligand terpyridine–Fe(II) system as a function of y for different concentrations [39]. Two features are remarkable in this figure: (1) The curve rises sharply at exactly the mixing ratio of $y = 1$; the higher the concentration, the longer the average chain length that can be achieved. (2) An excess of metal ions

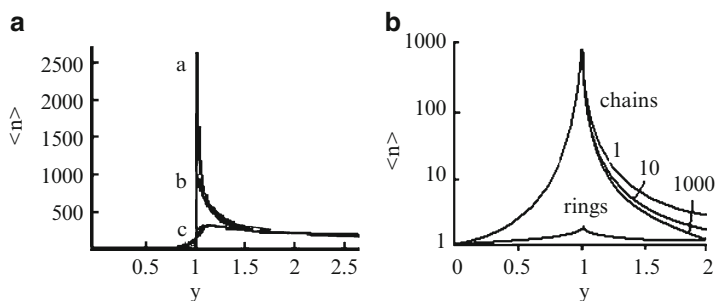


Fig. 6 (a) Prediction of the average number of monomers (bisligands) per chain ($\langle n \rangle$) as a function of the mixing ratio y in the coordination polymer Fe(II)-1 system (one benzenyl ring as the spacer). The monomer concentrations for curves *a*, *b*, and *c* are 10^{-3} , 10^{-4} , and 10^{-5} mol/L, respectively. Adapted from [8]. Reprinted with permission from the Royal Chemical Society. (b) Maximum values of the average length of chains and rings as a function of the metal/monomer ratio y for several ratios K_1/K_2 for the Zn-5 coordination polymer systems. Plots are shown for K_1/K_2 values of 1, 10, and 1000. Adapted from [35]. Reprinted with permission from the American Chemical Society

results in longer assemblies than does an excess of monomers. In practice, it is impossible to achieve an exact 1:1 mixing ratio, so that a slight excess of metal ions is usually used to create coordination polymers.

The average chain length is also affected by the ratio of K_1 to K_2 . The larger the ratio, the more sensitively the chain length decreases with excess metal. As theoretically analyzed by Van der Gucht et al. [35] in the L_2EO_4 -Zn(II) system, the maximum average chain length at the same y ($y > 1$) decreases as the K_1/K_2 value increases from 1 to 1000 (Fig. 6b). Figure 6 demonstrates that it is easier to create a polymeric structure of coordination polymers in systems of lower K_1/K_2 ratio than in the opposite conditions where the mixing ratio between metal ions and ligand molecules is crucial. The dependence of the length of the coordination polymers on mixing ratio and concentration can be used to control the hierarchical assemblies. This was employed by Yan et al. [40] to realize the synergistic formation of complex coacervate core micelles and coordination polymers in mixed systems of metal ions, bisligand, and diblock copolymers. This will be reviewed in further detail in Sect. 3.

2.3.2 Concentration Dependence

A remarkable characteristic of reversible supramolecular polymers, including reversible coordination polymers, is the concentration dependence of the equilibrium chain-length distribution. For covalent polymers, no matter how high or low their concentration, the polymer chain lengths are fixed, and the increase of the specific viscosity with concentration arises from hydrodynamic interactions and entangling of the polymer chains at higher concentrations. In the case of reversible coordination polymers, their structure is different for low and high concentrations. At low concentrations, they exist in the form of oligomers; whereas at high concentrations,

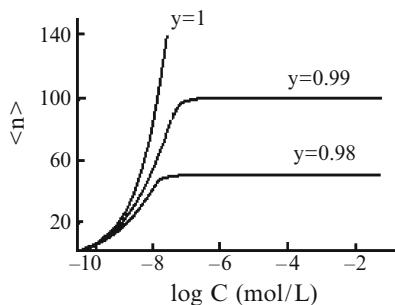


Fig. 7 Predicted average number of monomers per chain ($\langle n \rangle$) as a function of concentration for different mixing ratios y for the Fe(II)-**1** coordination systems (one benzenyl ring as the spacer). Here, the stability constants of Fe(II) and terpyridine are used ($\log[K_2] \ll \log[K_1]$). Adapted from [8]. Reprinted with permission from the Royal Chemistry Society

the degree of polymerization is increased automatically so that they exist in the form of polymers. For a fully reversible coordination polymerization at $y = 1$ and when rings do not form or can be neglected, the polymerization degree can be expressed as $\langle n \rangle \sim C^{0.5}$, where C is the total monomer concentration. According to this relationship, high $\langle n \rangle$ values can be expected at high concentrations when $y = 1$. When $y \neq 1$, the initial increase of the degree of polymerization levels off at higher concentrations at a value of $\langle n \rangle = 1/(1-y)$. This is clearly seen in Fig. 7.

The dependence of the degree of polymerization on the overall concentration for a flexible reversible coordination polymer is more complicated because rings may occur. However, rings are only important when the overall concentration is not much larger than the critical concentration. Otherwise, the behavior is about the same as for systems that cannot form rings at all. The concentration dependence of the rings and chains is illustrated in Fig. 4b, which shows that long chains dominate at high concentrations. The concentration-dependent degree of polymerization was successfully verified by Chen et al. using Monte Carlo simulations [41].

Using La^{3+} and Nd^{3+} ions to construct coordination polymers with the same bisligands **5** (see Fig. 2), the increased concentration results in a shift of the y value at which $\langle n \rangle$ is a maximum (Fig. 8). At low concentrations, the maximum occurs at $y = 0.67$. This indicates that for low concentrations, coordination polymers dominate in which the metal to bisligand ratio is 2:3. Upon increasing the concentration, the maximum shifts towards higher values [25], indicating that the ratio of metal ions to bisligands in the coordination polymers increases.

2.3.3 pH Dependence

Owing to the weakness of the interactions between the ligands and the metal ions as compared to covalent bonds, the response of these coordination polymers to environmental changes is expected. The ligands are generally Lewis bases

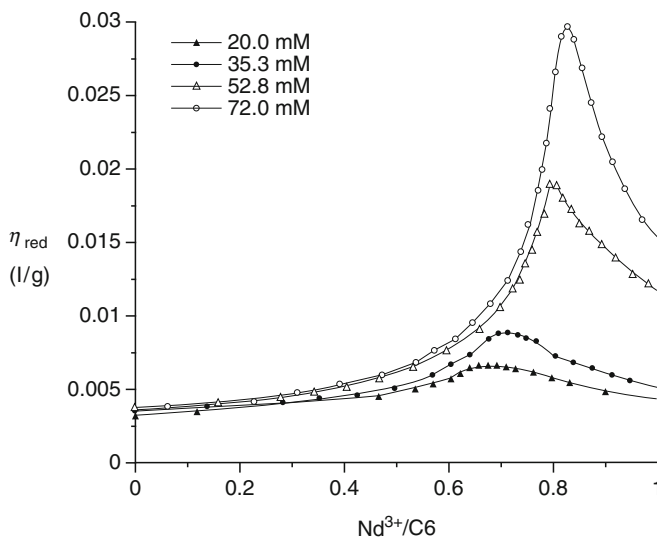


Fig. 8 Shift of the stoichiometry of the coordination polymer in the La-5 system, where six EO units were used as the spacer. Adapted from [25]. Reprinted with permission from Wiley-VCH

and, therefore, protons and metal ions compete for the ligands; thus, the equilibrium is affected by the pH of the solution. The pH can be used to shift the equilibrium, e.g., to tune the length of the coordination polymers into a specific range, so that the polymer is pH-responsive.

2.3.4 Charge Nature

In coordination polymers, metal ions are an integral part of the polymer backbone. The metal ions are always positively charged, but the ligands themselves are generally charge-neutral with only a few exceptions. If the ligands are positively charged [42, 43] or neutral [18–20], e.g., terpyridine ligands, the resultant coordination polymer is positively charged. If the ligand is negatively charged [29], the sign of the net charge carried by each coordination center is determined by the summation of the charges of metal ions and bisligand. In this case, the net charge on the coordination polymers can be negative, neutral, or positive. Neutral coordination polymers are rare [44]. Most reported coordination polymers are either positively [45–48] or negatively charged [25, 35, 37].

Because of their charged nature, coordination polymers resemble covalent polyelectrolytes (Fig. 9). Therefore, they were called metallosupramolecular polyelectrolytes (MEPEs) by Kurth et al. [8, 9]. Because of the charges, the MEPEs interact with polymers, colloids, or other molecules that carry opposite charges [49, 50]. In the following we discuss some typical examples from the literature.



Fig. 9 Illustration of the polyelectrolyte nature of the coordination polymers

3 Nanostructures Based on Coordination Polymers

3.1 Thin Layer-by-Layer Films

According to Kurth et al. [43, 49–55], positively charged MEPEs can be incorporated into thin films by the layer-by-layer (lbl) method. In this method, multilayer fabrication is readily achieved by repeated immersion of the substrate in solutions containing coordination polymers and oppositely charged polyelectrolytes, respectively (Fig. 10a). The thickness of the film can be controlled within nanometer precision. The obtained films are UV-active owing to the presence of coordination polymers. The polarity in the layer is reduced as compared to multilayers of strong polyelectrolytes. This is attributed to the more hydrophobic nature of the film, which strongly alters the diffusion of the ions through the layers. Formation of planar lbl films from coordination polymers and oppositely charged species turns out to be very effective, regardless of the structure of the coordination polymers. Replacing linear coordination polymers with branched ones by replacement of bisligands with terligands does not seem to affect the formation of lbl multilayers [33].

The deposition process is independent of the substrate geometry. In the case of a planar substrate, the above procedure results in planar films. When colloidal particles are used as the substrate, multilayer fabrication is readily achieved by repeatedly dispersing the particles in a solution of coordination polymers, centrifuging them off, and washing them [52, 54]. The alternating negative and positive zeta-potentials of the particles measured after each deposition step are consistent with an alternating particle surface. Removal of the colloidal template core yields multilayer capsules composed of coordination polymers and covalent polyelectrolytes (Fig. 10b). These can be potentially used as microreactors. The multilayers containing coordination polymers are very resistant to metal-ion exchange. Even in the presence of a strong chelating agent that can disassemble the coordination polymer in solution, the multilayers were not influenced [54].

The superior stability against metal-ion exchange of the lbl film made from coordination polymers and oppositely charged covalent polyelectrolytes can be used to immobilize metal ions (Fig. 11) [42, 55, 56]. Since the metal ions themselves cannot be assembled with oppositely charged polyelectrolytes by the lbl method, other assistant interactions are required. For example, by immersion of a negatively charged PSS-covered substrate in a mixed solution containing metal ions and monoligand with an aryl tail, metal ions were immobilized into the lbl film. The π - π interaction between the aryl tail and metal-ligand coordination interaction assembled the metal ions into rod-like supramolecular arrays, which in turn interacted with PSS layers through electrostatic attraction [55, 56].

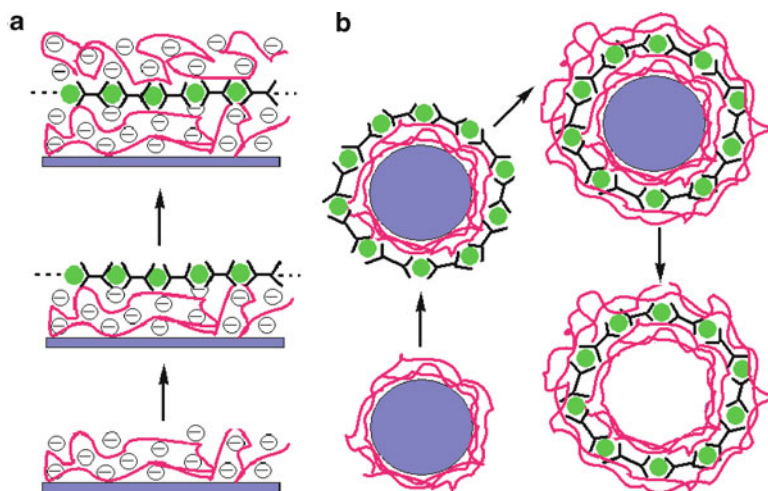


Fig. 10 Layer-by-layer assembly from a positive coordination polymer and an oppositely charged covalent polyelectrolyte, as viewed (a) from the side and (b) from the top

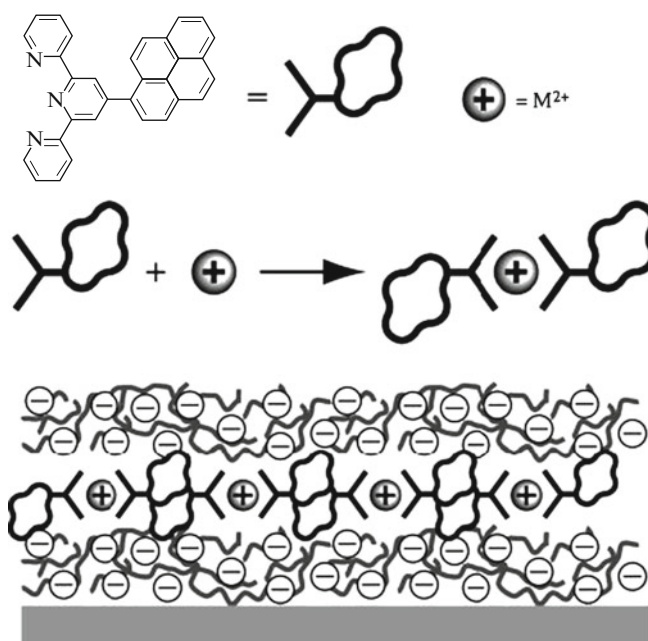


Fig. 11 Immobilization of discrete metallo-units in thin films by combining electrostatic attraction of oppositely charged species with aryl aggregation of metallo-units. Adapted from [56]. Reprinted with permission from Wiley-VCH

3.2 Langmuir and Langmuir–Blodgett Films

The charged nature of the coordination polymers also allow them to interact with oppositely charged amphiphiles, so that the surface chemical properties of the coordination polymers can be tailored. Kurth et al. [57–62] combined an Fe(II)-MEPE and dihexadecyl phosphate (DHP) to prepare a polyelectrolyte–amphiphile complex (PAC, as shown in Fig. 12). This PAC is hydrophobic and dissolves in organic solvents. The organic solution containing PAC can thus spread at the air–water interface to form a Langmuir film. The PAC monolayer collapses at a remarkably high surface pressure of 62 mN m^{-1} and the slope of the isotherm is rather steep, indicating that the PAC monolayer is stiff owing to the strong van der Waals attraction arising from the long DHP chains. Consequently, the resulting Langmuir films can be transferred onto a substrate to form Y-type Langmuir–Blodgett (L–B) layers. At room temperature, 20% water is contained in the film. The release and uptake of water is reversible.

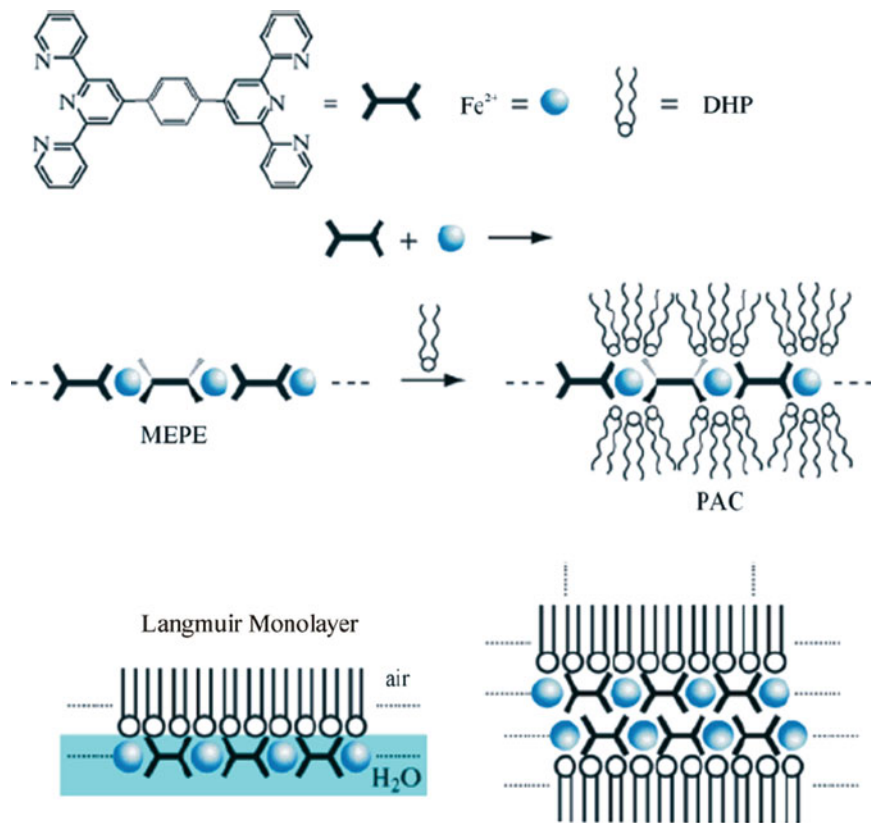
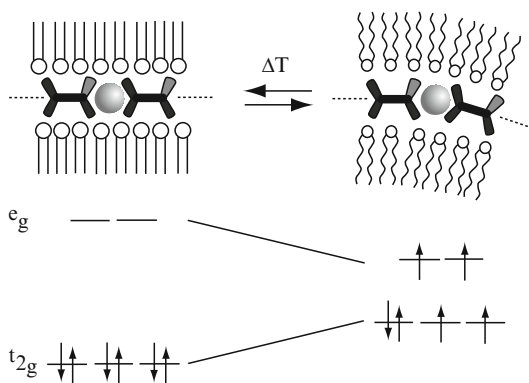


Fig. 12 Formation of Langmuir (bottom left) and L–B (bottom right) films of the polyelectrolyte–amphiphile complex PAC at an air–water interface. Adapted from [60]. Reprinted with permission from the American Chemical Society

Fig. 13 Melting of the amphiphilic matrix in PAC results in a distortion of the coordination geometry of the tightly coupled metal centers, giving rise to a spin-crossover from a diamagnetic low-spin state to a paramagnetic high-spin state. Adapted from [63]. Reprinted with permission from the American Chemical Society



The formation of PACs can be used to tailor the magnetic properties of the coordination polymers [63, 64]. Generally, in the presence of ligand, the crystal field around the metal ions is very strong so that the metal ions are forced into the low spin (LS) state. For Fe(II) ions, there are even numbered unpaired electrons that are forced to pair in the t_{2g} orbitals with low energy. In this case, the Fe(II) incorporated in the coordination polymer is diamagnetic. However, in a PAC, the phase transition of the hydrophobic chains induced by increasing temperature provides enough energy to alter the spin state of Fe(II) from LS to HS (high spin) (Fig. 13). The PAC therefore shows high temperature molecular magnetism, which is linked to the structural arrangement of the amphiphilic matrix.

The PAC as a whole can also be assembled on the basal surface of graphite in the presence of long chain alkanes. The long chain alkanes function as an orientating template on which perfectly ordered straight nanostructures of PACs are formed [61, 65, 66] (Fig. 14). Such straight nanostructure formation is closely related to the rigid skeleton of the Fe(II)-MEPEs. In the case of flexible MEPEs, no such regular structures can be obtained on the graphite. This result clearly shows that the incorporation of coordination polymers in the PAC indeed adds tunable parameters for the molecular assemblies.

3.3 Micelles

3.3.1 Micelle Formation

When the coordination polymer is mixed with an oppositely charged neutral diblock polymer, the electrostatic interaction will drive complex coacervate formation [40]. But, the growth of the complex coacervate will be constrained by the presence of the neutral blocks, and be stabilized at a finite size. In this way, so-called complex coacervate core micelles (C3Ms), or polyion coacervate (PIC) micelles are formed. This micelle formation is analogous to the formation of C3Ms in covalent poly-electrolyte/ block polymer systems [67, 68]. Obviously, the coordination polymer,

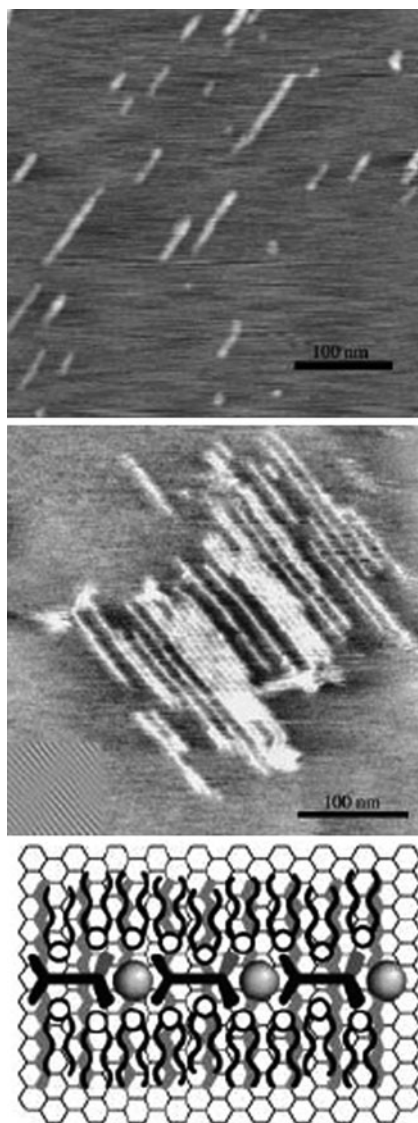
Fig. 14 Adsorption of PACs on the basal plane of graphite.

Top: Representative scanning force microscopy (SFM) image of PAC adsorbed in the

presence of $C_{32}H_{66}$ on the basal plane of graphite.

Middle: SFM image of a sample prepared from about twice the concentration and recorded with harder tapping than usual.

Bottom: Molecular model for the formation of straight rods on the basal graphite surface. Adapted from [61]. Reprinted with permission from Wiley-VCH



which together with the charged block of the diblock copolymer resides in the core of this particle, is acting as a homopolyelectrolyte in this micellar formation. For the Zn-5/P2MVP₄₁-PEO₂₀₅ system, it is striking that even at a concentration as low as 9 ppm, this C3Ms can still be formed [69]. At this concentration, the “coordination polymers” themselves are actually “oligomers” with a very low polymerization degree since the critical concentration is about 20 mM for the coordination polymers (See Fig. 4b) [35]. Similarly sized covalent polyelectrolytes cannot form micelles at all [67]. The formation of micelles with coordination polymers at low concentration must therefore be due to the responsive chain length of the coordination polymers.

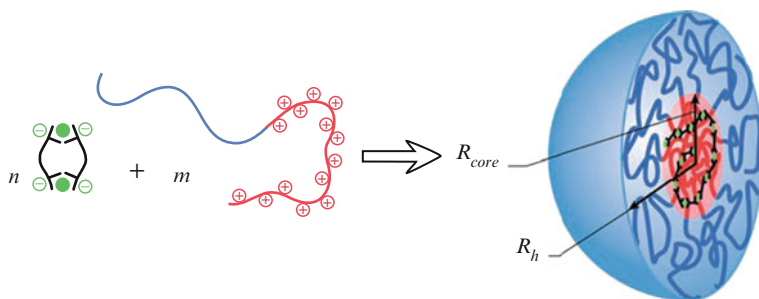


Fig. 15 Formation of C3Ms in mixed systems of Zn-5 (with four EO in the spacer) and diblock copolymer P2MVP₄₁ – PEO₂₀₅. Adapted from [40]. Reprinted with permission from Wiley-VCH

In the presence of oppositely charged block copolymers, the local concentration of coordination complexes is greatly enhanced, so that it is suitable to form polymeric structures (Fig. 15). These long coordination polymers simultaneously promote the formation of complex coacervate core micelles [40].

3.3.2 Critical Micellar Concentration

The low formation concentration of these micelles indicates a low critical micellar concentration (CMC) for such micellar systems. Because no components are surface-active in this micellar system, the CMC cannot be obtained from surface tension measurements, the standard method for conventional surfactant molecules. Instead, the CMC is determined from the variation of the static light scattering intensities with concentration (Fig. 16a) [69, 70]. In contrast to ionic surfactants, the CMC of these C3Ms increases with salt concentration (Fig. 16b). But, the aggregation number decreases with the square root of the salt concentration before the micelles fall apart, which indicates that the decrease of the aggregation number is caused by screening of the electrostatic interaction between the oppositely charged pairs in the core [69]. Kramarenko et al. [71] have predicted theoretically that the increase of salt concentration also results in a decrease of the core–shell interfacial tension, which swells the core. Dynamic light scattering (DLS) indicates that the average hydrodynamic radius of C3Ms does not change significantly with changing salt concentration. However, the presence of metal ions in the C3Ms containing Zn–L₂EO₄ coordination polymer allows high enough electron contrast to see the cores directly by TEM. As can be seen in Fig. 16c, d, TEM indicates that the polydispersity of the C3Ms increases with increasing salt concentration, while the average size stays more or less constant [69].

3.3.3 Stability

Unlike C3Ms formed from covalent polymers, which are stable only in a very narrow range of mixing ratios at around charge-neutral mixing [72–76], the C3Ms made from a coordination polymer and a covalent block copolymer can be stable at a large

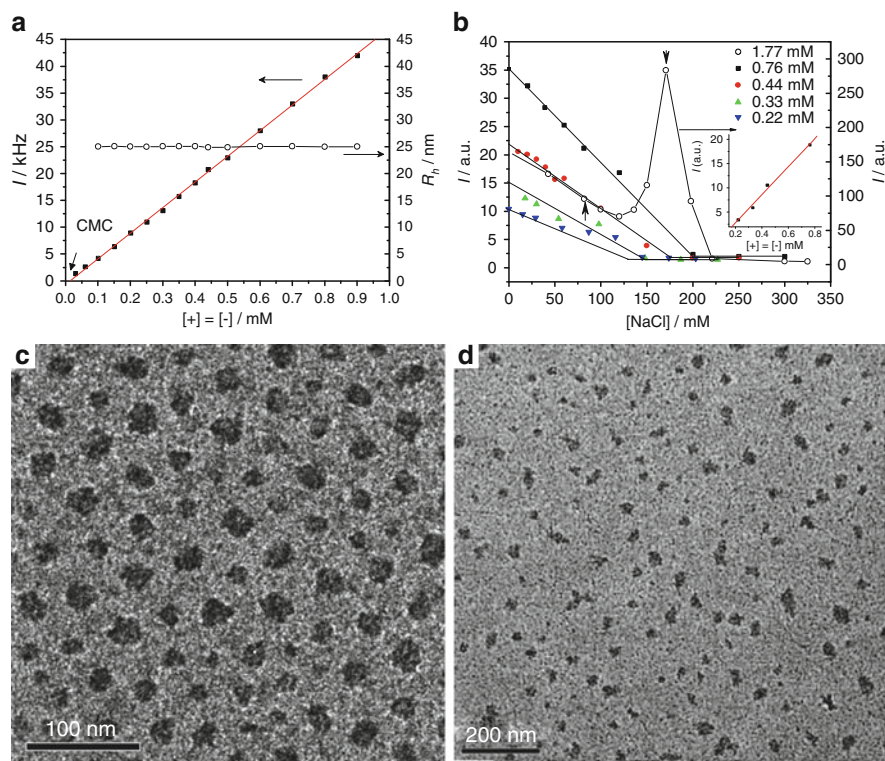


Fig. 16 (a) Scattered light intensity (I , solid squares) and mean hydrodynamic radius (R_h , open circles) versus polymer concentration in P2MVP₄₁-b-PEO₂₀₅/Zn-L₂EO₄ micellar system at $f^- = 0.5$, where f^- is the fraction of negative charge in the solution. (b) Variation of the scattered light intensity for micellar systems of different concentrations with increasing $[\text{NaCl}]$. The scale for the 1.77 mM system is given on the right axis in arbitrary units. The inset is the variation of the scattered light intensity with polymer concentration at 100 mM NaCl. (c) Cryo-TEM image of the micelles at $f^- = 0.5$ where no NaCl is present. (d) Cryo-TEM image for the same micellar system in the presence of 80 mM NaCl. Adapted from [69]. Reprinted with permission from the American Chemical Society

excess of the coordination polymer (Fig. 17a) [69, 77]. This can be explained by the concentration responsiveness of the coordination polymers. At low concentrations, the excess “coordination polymers” actually exist in the form of “oligomers”, which consist of a few monomers only. These oligomers behave like large inorganic ions, which are in such a low concentration that they cannot affect the micelles. Similarly, no obvious influence of excess bisligand on C3Ms can be detected.

However, excess of metal ions may result in a completely different effect. If first-row transition metals are used, excess of metal ions will not produce clear effects on C3Ms, but if the first-row transition metal ions are replaced by those in the second or the third rows, C3Ms can be destroyed by the excess metal ions (Fig. 17b).

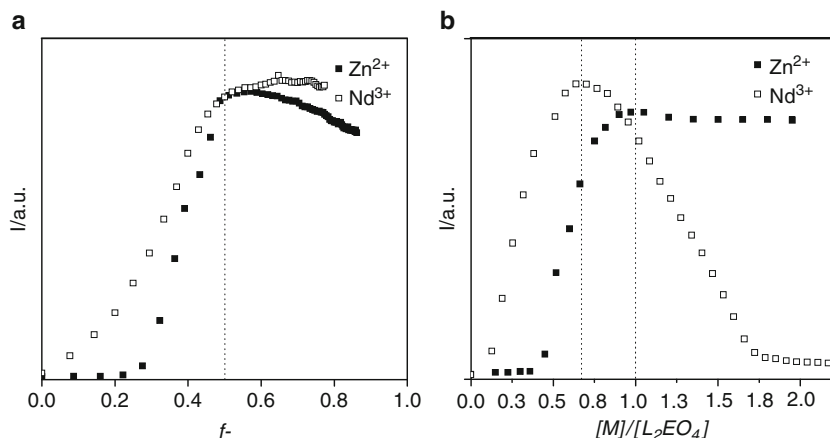


Fig. 17 Variation of the scattered light intensity in a solution of P2MVP₄₁-*b*-PEO₂₀₅ upon addition of (a) Zn- L_2EO_4 (filled squares) and Nd- L_2EO_4 (open squares); (b) zinc ions (filled squares) and neodymium ions (open squares). f^- is the fraction of negative charge in the solution, and $[M]/[L_2EO_4]$ is the molar ratio of metal to bisligand. Adapted from [77]. Reprinted with permission from the American Chemical Society

The reason for this is the formation of positively charged coordination chain ends that exert repulsive forces between the positively charged block of the block copolymers and drive the falling-apart of the C3Ms.

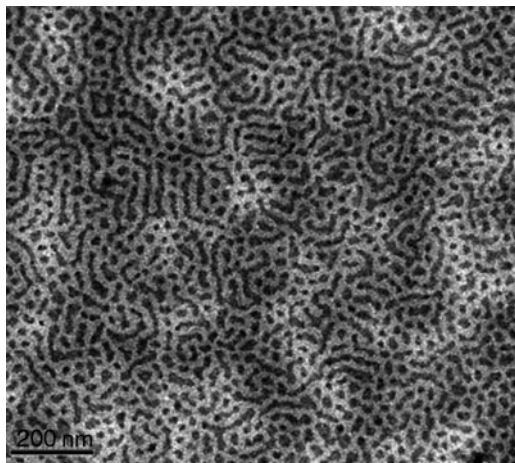
3.3.4 Wormlike Micelles

It is also remarkable that wormlike micelles are sometimes formed, namely when the diblock copolymers are in excess. In cryo-TEM images, these micelles resemble strings of spherical micelles, suggesting that a weak attraction exists between these building blocks. Depending on the overall concentration of the system, wormlike micelles can be found at a negative charge fraction of 0.20–0.35; they always coexist with spherical micelles (Fig. 18). The presence of a modest amount of additional inorganic salt does not suppress the formation of worms. Although the mechanism of how these wormlike micelles are formed is still not fully understood, solid experimental evidence, including results from cryo-TEM, SAXS, angular dependence, and depolarized DLS, has unambiguously confirmed their existence [78, 79].

3.4 Microemulsions

The formation of micelles with coordination polymer has unveiled a new way to produce water-soluble inorganic/organic hybrid self-assembled hierarchical structures. A range of functional metal ions can be incorporated in the core so that these C3Ms

Fig. 18 Wormlike micelles formed in the system of Zn-5 (with four EO in the spacer) and diblock copolymer P2MVP₄₁-PEO₂₀₅ where the negative charge ratio $f^- = [-]/[-] + [+] = 0.33$. Adapted from [78]. Reprinted with permission from the American Chemical Society



can be used as nanocarriers for different medical purposes. Moreover, the loading amount of metal ions in the core is adjustable by swelling the core using the method of fabrication of complex coacervate core microemulsions (C3- μ Es) [80]. The principle of making C3- μ Es is to use a mixture of charged-neutral diblock copolymers (dp) and like-charged homopolymers (hp) instead of only dp , in combination with oppositely charged hp , as illustrated in Fig. 19a. Analogously, by using a mixture of diblock copolymer and homopolymer of like charge in combination with oppositely charged coordination polymer, the amount of metal ions per particle can be tuned. We have successfully increased the loading of Zn^{2+} ions in the Zn-5 C3- μ Es by as much as ten times (Fig. 19b) [81]. When a homopolyelectrolyte of the same charge sign as the coordination polymer is used, one can lower the amount of metal ions in these microemulsion particles by dilution. Hence, the particle size and internal composition can be simply set by varying the compositions of the mixture from which they are formed.

3.5 Nanoribbons

The principle of combining coordination polymers with oppositely charged modules can be used to create a variety of assembled structures. In the case of using a polypeptide as the oppositely charged template, we can even obtain well-defined nanoribbons. For instance, in the charge-neutralized mixture of the Zn- L_2EO_4 coordination complex and an ABA-type polypeptide, micrometer-long ribbons with width of 20 nm and thickness of 2~3 nm were formed (Fig. 20a) [82]. Here, the middle B block is positively charged at $\text{pH} < 6.8$ due to the presence of histidine groups, whereas the outer A block is always charge-neutral. We found that the coordination polymers play a crucial role in the formation of these nanoribbons, because

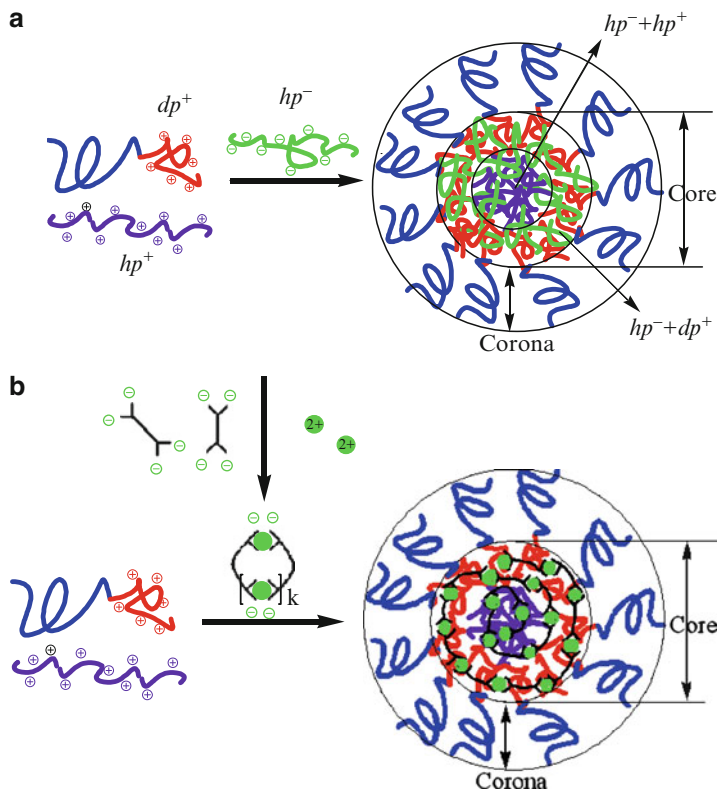


Fig. 19 (a) Formation of a complex coacervate core microemulsion (C3-μE) droplet. The core comprises anionic homopolymer (green, hp^-), cationic homopolymer (purple, hp^+), and cationic block (red, dp^+) of diblock copolymer. The corona consists of the electroneutral hydrophilic blocks (blue) of the diblock copolymer. (b) Formation of C3-μE containing coordination polymers. Adapted from [81]. Reprinted with permission from the Royal Chemical Society

no ribbons can be achieved by other ways of neutralizing the charges on the B block, e.g., by using either covalent polyelectrolyte PANa, or by increasing the pH. We infer that it is the adaptable polymerization degree of the coordination polymers that allows uninterrupted folding and closely packing of the B block of the polypeptide. Cryo-TEM and X-ray data suggest that the nanoribbons are single-stranded, unbundled β -stacks [82]. At pH 5.4, the histidine residues in the middle B block are positively charged. In the presence of an equivalent amount of the negatively charged coordination complex $([Zn-L_2EO_4]^{2-})_n$, the histidine residues in the block form electrostatic complexes. This compensation of the positive histidine charges enables the middle blocks to simultaneously fold into β -sheets and to stack. In this process, linear coordination polymers form simultaneously out of small, ring-shaped oligomers, owing to the interactions with histidine-rich surfaces of the β -stacks. In contrast, covalent polyelectrolytes do not have this adaptability and could therefore interfere with the packing of folded strands, thereby disfavoring the formation of

nanoribbons. If the charge on the histidine groups is removed by increasing the pH to 11, and no coordination polymer is present, the packing of the folded structures is probably not close enough, and only β -turns are provided, which cannot pack into a dense array.

4 Conclusions and Perspectives

We have reviewed recent advances in the development of hierarchical self-assembly structures on the basis of coordination polymers. The judicious combination of reversible coordination polymers with oppositely charged species allows us to fabricate a variety of nanometer-sized self-assembled structures. Formation of films, hollow spheres, micelles, microemulsions, and nanoribbons has been observed. These secondary nanostructures can be used as new functional materials.

The metallocoordination polymer systems are very promising for the fabrication of molecular devices and advanced functional materials. The examples given in this review cover only a small fraction of coordination polymers that have been synthesized. Many more systems with oppositely charged species have not been explored yet. We expect that more coordination polymers and oppositely charged modules with special functional groups will bring unexpected surprises to the field of hierarchical self-assembled structures based on coordination polymers. For instance, modifying the spacer group structure of ligands may produce significant differences in the morphology of the aggregates in the coordination polymer/oppositely charged species mixed systems, as observed by us in recent work. Using coordination polymers formed from different metal ions will endow the mixed systems with interesting optical, electronic, or magnetic responsive properties. If valence-variable metal ions, such as iron, are used, then the mixed systems may display redox-switchable properties.

In addition, multilayers of oppositely charged coordination polymers can be produced via lbl methods. Usually, the lbl method is only applicable for oppositely charged polyelectrolyte systems. By dipping a substrate alternately into positively and negatively charged polyelectrolyte solutions, multilayers can be produced. The charged nature of coordination polymers can also be used in this process. In our laboratory, we have obtained multilayers containing only coordination polymers by alternately dipping a mica or silica wafer into solutions of a positively charged and a negatively charged coordination polymer. When photosensitive components are introduced to the system, the optical properties of the film are expected to be tuned reversibly. It can be imagined that when only coordination polymers are used, the lbl films might show interesting optical, electronic, or magnetic properties. This might open a new vista in the world of advanced functional materials. Compared with the efforts made in the synthesis of various coordination polymers, the hierarchical assembly of them is still a virgin to be explored. We expect in the near future that more interesting work will appear in this field.

Acknowledgment This work has been carried out in the framework of the EU Polyamphi/Marie Curie program (FP6-2002, proposal 505027).

References

1. Manners I (2001) *Science* 294:1664
2. Manners I (1996) *Angew Chem Int Ed Engl* 35:1602
3. Archer RD (2001) *Inorganic and organometallic polymers*. Wiley-VCH, Weinheim
4. Bergman SD, Wudl F (2008) *J Mater Chem* 18:41
5. Rowan ST, Beck JB (2005) *Faraday Discuss* 128:43
6. Burnworth M, Knapton D, Rowan SJ, Weder C (2007) *J Inorg Org Polymer Mater* 17:91
7. Dobrawa R, Würthner F (2005) *J Polym Sci Part A: Polym Chem* 43:4891
8. Kurth DG, Higuchi M (2006) *Soft Matter* 2:915
9. Frieze VA, Kurth DG (2008) *Coord Chem Rev* 252:199
10. Gohy J-F, Lohmeijer BGG, Schubert US (2003) *Chem Eur J* 9:3472
11. Fustin C-A, Guillet P, Schubert US, Gohy J-F (2007) *Adv Mater* 19:1665
12. Chipper M, Meier MAR, Kranenburg, JM, Schubert US (2007) *Macromol Chem Phys* 208:679
13. Chipper M, Meier MAR, Wouters D, Hoeppener S, Fustin C-A, Gohy J-F, Schubert US (2008) *Macromolecules* 41:2771
14. Nguyen P, Gómez-Elipé P, Manners I (1999) *Chem Rev* 99:1515
15. Caruana DJ, Heller A (1999) *J Am Chem Soc* 121:769
16. Yoshida R, Takahashi T, Yamaguchi T, Ichijo H (1997) *Adv Mater* 9:175
17. Kurth DG (2008) *Adv Mater* 9:014103
18. Kurth DG (2002) *Ann NY Acad Sci* 960:29
19. Holliday BJ, Mirkin CA (2001) *Angew Chem Int Ed Engl* 40:2002
20. Barigelletti F, Flamigni L, Balzani V, Collin JP, Sauvage JP, Sour A, Constable EC, Thompson AMW (1994) *J Am Chem Soc* 116:7692
21. Constable EC (2008) *Coord Chem Rev* 252:842
22. Han F-H, Higuchi M, Kurth DG (2008) *Tetrahedron* 64:9108
23. Hogg R, Wilkins RG (1962) *J Chem Soc* 341
24. Marin V, Holder E, Hoogenboom R, Schubert US (2007) *Chem Soc Rev* 36:618
25. Vermonden T, de Vos WM, Marcelis ATM, Sudholter EJR (2004) *Eur J Inorg Chem* 2847
26. Constable EC, Thompson AMW (1981) *J Chem Soc, Dalton Trans* 1991
27. Constable EC, Thompson AMW, Cherryman J, Liddiment T (1995) *Inorg Chim Acta* 235:165
28. Beck JB, Ineman JM, Rowan SJ (2005) *Macromolecules* 38:5060
29. Vermonden T, Branowska D, Marcelis ATM, Sudholter EJR (2003) *Tetrahedron* 59:5039
30. Loeb SJ, Shimizu GKU (1993) *J Chem Soc, Dalton Trans* 3467
31. Velten U, Rehahn M (1996) *Chem Commun* 2639
32. Chen HY, Cronin JA, Archer RD (1994) *Macromolecules* 27:2174
33. Sievers TK, Vergin A, Möhwald H, Kurth DG (2007) *Langmuir* 23:12179
34. Constable EC, Thompson AMWC, Harveson P, Mackol L, Zehnder M (1995) *Chem Eur J* 1:360
35. Vermonden T, van der Gucht J, de Waard P, Marcelis ATM, Besseling NAM, Sudholter EJR, Fleer GJ, Cohen Stuart MA (2003) *Macromolecules* 36:7035
36. Zhao YQ, Beck JB, Rowan SJ, Jamieson AM (2004) *Macromolecules* 37:3529
37. Vermonden T, van Steenbergen MJ, Besseling NAM, Marcelis ATM, Hennink WE, Sudholter EJR, Cohen Stuart MA (2004) *J Am Chem Soc* 126:15802
38. Jacobson H, Stockmayer WH (1950) *J Chem Phys* 18:1600
39. Holyer RH, Hubbard CD, Kettle SFA, Wilkins RG. (1966) *Inorg Chem* 5:622
40. Yan Y, Besseling NAM, de Keizer A, Marcelis ATM, Drechsler M, Cohen Stuart MA (2007) *Angew Chem Int Ed* 46:1807
41. Chen C-C, Dormidontova EE (2004) *J Am Chem Soc* 126:14972

42. Krass H, Papastavrou G, Kurth DG (2003) *Chem Mater* 15:196
43. Kurth DG, López JP, Dong W-F (2005) *Chem Commun* 2119
44. Chow C-F, Fujii S, Lehn J-M (2007) *Angew Chem Int Ed* 46:5007
45. Beck JB, Rowan SJ (2003) *J Am Chem Soc* 125:13922
46. Iyer PK, Beck JB, Weder C, Rowan SJ (2005) *Chem Commun* 319
47. Han FS, Higuchi M, Kurth DG (2007) *Adv Mater* 19:3928
48. Han FS, Higuchi M, Akasaka Y, Otsuka Y, Kurth DG (2008) *Thin Solid Films* 516:2469
49. Schütte M, Kurth DG, Linford MR, Cölfen H, Möhwald H (1998) *Angew Chem Int Ed Engl* 37:2891
50. Kurth DG, Lehmann P, Schütte M (2000) *PNAS* 97:5704
51. Schütte M, Kurth DG (2001) *Macromol Symp* 164:167
52. Caruso F, Schüler C, Kurth DG (1999) *Chem Mater* 11:3394
53. Kurth DG, Schütte M, Wen J (2002) *Colloids Surf A Physicochem Eng Asp* 198:633
54. Kurth DG, Caruso F, Schüler C (1999) *Chem Commun* 1579
55. Krass H, Papastavrou G, Kurth DG (2004) *Macromol Symp* 210:311
56. Krass H, Plummer EA, Haider JM, Barker PR, Alcock NW, Pikramenou Z, Hannon MJ, Kurth DG (2001) *Angew Chem Int Ed* 40:3862
57. Meister A, Förster G, Thünemann AF, Kurth DG (2003) *Chem Phys Chem* 4:1095
58. Lehmann P, Kurth DG, Brezesinski G, Symietz C (2001) *Chem Eur J* 7:1646
59. Kurth DG, Meister A, Thünemann AF, Förster G (2003) *Langmuir* 19:4055
60. Bodenthin Y, Pietsch U, Grenzer J, Geue T, Möhwald H, Kurth DG (2005) *J Phys Chem B* 109:12795
61. Kurth DG, Severin N, Rabe JP (2002) *Angew Chem Int Ed* 41:3681
62. Lehmann P, Symietz C, Brezesinski G, Krass H, Kurth DG (2005) *Langmuir* 21:5901
63. Bodenthin Y, Pietsch U, Möhwald H, Kurth DG (2005) *J Am Chem Soc* 127:3110
64. Bodenthin Y, Schwarz G, Tomkowicz Z, Geue T, Haase W, Pietsch U, Kurth DG (2009) *J Am Chem Soc* 131:2934
65. Severin N, Rabe JP, Kurth DG (2004) *J Am Chem Soc* 126:3696
66. Mao G, Chen D, Handa H, Dong W, Kurth DG, Möhwald H (2005) *Langmuir* 21:578
67. Harada A, Kataoka K (1998) *Macromolecules* 31:288
68. Harada K, Kataoka K (1999) *Science* 283:65
69. Yan Y, de Keizer A, Cohen Stuart MA, Drechsler M, Besseling NAM (2008) *J Phys Chem B* 112:10908
70. Liu G, Liu TB (2005) *J Am Chem Soc* 127:6942
71. Kramarenko EY, Khokhlov AR, Reineker P (2006) *J Chem Phys* 125:194902
72. Cohen Stuart MA, Besseling NAM, Fokkink RG (1998) *Langmuir* 14:6846
73. Van der Burgh S, Fokkink RG, de Keizer A, Cohen Stuart MA (2004) *Langmuir* 20:1073
74. Chelushkin PS, Lysenko EA, Bronich TK, Eisenberg A, Kabanov VA, Kabanov AV (2007) *J Phys Chem B* 111:8419
75. Kabanov AV, Bronich TK, Kabanov VA, Yu K, Eisenberg A (1996) *Macromolecules* 29:6797
76. Solomatin SV, Bronich TK, Bargar TW, Eisenberg A, Kabanov VA, Kabanov AV (2003) *Langmuir* 19:8069
77. Yan Y, Besseling NAM, de Keizer A, Cohen Stuart MA (2007) *J Phys Chem B* 111:5811
78. Yan Y, Besseling NAM, de Keizer A, Cohen Stuart MA, Drechsler M (2007) *J Phys Chem B* 111:11662
79. Yan Y, Harnau L, Besseling NAM, de Keizer A, Ballauff M, Rosenfeldt S, Cohen Stuart MA (2008) *Soft Matter* 4:2207
80. Hof B, de Keizer A, Van der Burgh S, Leermakers FAM, Cohen Stuart MA (2008) *Soft Matter* 4:1473
81. Yan Y, de Keizer A, Cohen Stuart MA, Besseling NAM (2009) *Soft Matter* 5:790
82. Yan Y, Martens AA, Besseling NAM, de Wolf FA, de Keizer A, Drechsler M, Cohen Stuart MA (2008) *Angew Chem Int Ed* 47:4192

Processes of Ordered Structure Formation in Polypeptide Thin Film Solutions

Ioan Botiz, Helmut Schlaad, and Günter Reiter

Abstract An experimental study is presented on the hierarchical assembly of α -helical block copolymers polystyrene–poly(γ -benzyl-L-glutamate) into anisotropic ordered structures. We transformed thin solid films into solutions through exposure to solvent vapor and studied the nucleation and growth of ordered three-dimensional structures in such solutions, with emphasis on the dependence of these processes on supersaturation with respect to the solubility limit. Interestingly, polymer solubility could be significantly influenced via variation of humidity in the surrounding gas phase. It is concluded that the interfacial tension between the ordered structures and the solution increased with humidity. The same effect was observed for other protic non-solvents in the surrounding gas phase and is attributed to a complexation of poly(γ -benzyl-L-glutamate) by protic non-solvent molecules (via hydrogen-bonding interactions). This change of polymer solubility was demonstrated to be reversible by addition or removal of small amounts of protic non-solvent in the surrounding gas phase. At a constant polymer concentration, ordered ellipsoidal structures could be dissolved by removing water or methanol present in the solution. Such structures formed once again when water or methanol was reintroduced via the vapor phase.

Keywords Humidity · Hydrogen bonding · Macromolecular self-assembly · Nucleation · Solvent effects · Supersaturation

I. Botiz

Center for Nanoscale Materials, Argonne National Laboratory, 9700 South Cass Avenue,
Argonne, IL 60439 USA
e-mail: ibotiz@anl.gov

H. Schlaad

Colloid Chemistry, Max Planck Institute of Colloids and Interfaces,
Research Campus Golm, 14424 Potsdam, Germany
e-mail: Helmut.Schlaad@mpikg.mpg.de

G. Reiter (✉)

Physikalisches Institut, Universität Freiburg, 79104 Freiburg, Germany
e-mail: guenter.reiter@physik.uni-freiburg.de

Contents

1	Introduction	118
2	Experimental	119
2.1	Polymers	119
2.2	Preparation and Observation of Thin Film Solutions	120
2.3	“Equilibrium” and “Off-Equilibrium” Experiments	120
2.4	Determining the Concentration of Thin Film Solutions	122
3	Results and Discussions	123
3.1	Nucleation in Solution Films in Dry Air	123
3.2	Nucleation in Solution Films in Ambient Air	126
3.3	Influence of Protic Non-Solvents on Nucleation in Thin Film Solutions	130
3.4	Reversible Influence of Protic Non-Solvents on Nucleation in Thin Film Solutions	131
3.5	Origin of Bimodal and Multimodal Distributions in Size of the Resulting Ordered Objects	135
3.6	Kinetics of Growing Ordered Objects	138
3.7	Origin of the Anisotropic Shape of the Resulting Ordered Objects	139
3.8	Growth in the Out-of-Plane Direction of the Resulting Ordered Objects	142
3.9	Concerted Changes of the Growth Direction: Dependence on Polymer Architecture	143
4	Conclusions	146
	References	147

1 Introduction

Many biological and synthetic macromolecular systems can self-assemble in a hierarchical way, and may even have the ability to undergo a third, fourth, etc. ordering process [1–13]. Structured polymeric materials often exhibit remarkably diverse assemblies of building blocks, frequently arranged in a hierarchical way on multiple length-scales that range from nanometers to macroscopic sizes. As one sub-group of such polymers, rod-coil block copolymers are attracting significant interest for the development of functional surfaces based on novel self-assembled polymeric structures. Rod-coil block copolymers consist of a rigid block, for instance a polypeptide that has internal order and a well-defined shape, and an amorphous block with random (statistical) conformations. Due to the combination of stiff parts that partially interact via directional forces, and a highly flexible coil part, it is expected that such systems are able to generate structures of various shapes, possibly providing interesting properties. Ordered structures on surfaces based on such systems may, for example, be used for purposes such as the development of novel sensors or actuators.

In this context, investigation of the processes of structure formation in thin films of polypeptide block copolymer solutions is the first step towards control of the ways such polymers follow during ordering. By exposure to solvent vapor, thin films can be transformed into solutions while keeping the geometry of a thin film. Combined with microscopy, this approach allows the study of the nucleation and growth of ordered solid structures in solutions by varying systematically and within a single sample the concentration of polymer (c_p), from a “critical concentration” (c_{critical} or polymer solubility) up to very concentrated solutions [14].

The present study focuses mainly on diblock copolymers and star block copolymers based on a coiled polystyrene (PS) part and an α -helical poly(γ -benzyl-L-glutamate) (PBLGlu) part. However, for the purpose of comparison, simpler systems like homopolymers were also investigated. Thin films were analyzed mainly by optical microscopy (OM) and atomic force microscopy (AFM). The central focus was on the process of nucleation and its dependence on environmental parameters like humidity.

2 Experimental

2.1 Polymers

The primary sample investigated was an AB_n heteroarm star block copolymer, denoted $PS_{63}-(PBLGlu_{37})_8$, consisting of eight poly(γ -benzyl-L-glutamate) (PBLGlu = B) blocks on average, attached to the backbone of a single amorphous polystyrene (PS = A) block (see the chemical structure in Fig. 1a). A schematic representation of this polymer is given in Fig. 1b. Figure 1c shows one possible arrangement of the helices in an ordered state. Details about the synthesis and the characterization of this polymer are given elsewhere (see the appendix of [14]). The α -helical secondary structure of PBLGlu – the result of intramolecular hydrogen-bonding interactions – makes PBLGlu a rigid macrodipole with a high overall permanent dipole moment (theoretically 3.5 Debye per repeat unit) caused by the organization of the individual dipoles of the carbonyl groups of the peptide bond such that they point along the helix axis [15–17].

For the purpose of comparison, we also studied a homopolymer of PBLGlu and two diblock copolymers having the same PS block (52 repeat units) and differing PBLGlu blocks (31 and 104 repeat units) [18].

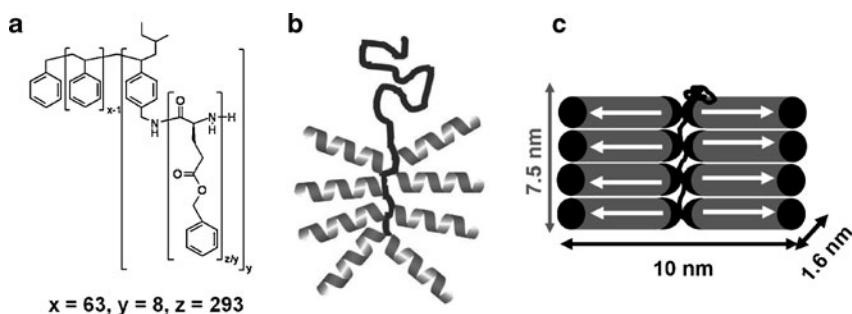


Fig. 1 (a) Chemical structure and (b) representation of $PS_{63}-(PBLGlu_{37})_8$ heteroarm star block copolymer. (c) 3D representation of a possible arrangement of the α -helical PBLGlu block in the ordered state. The arrows indicate the dipole moment of PBLGlu

2.2 Preparation and Observation of Thin Film Solutions

Thin solid films of $\text{PS}_{63}\text{-(PBLGlu}_{37})_8$ with an average thickness of a few tens of nanometres (as determined by ellipsometry) were obtained by spin-casting of chloroform (CHCl_3) polymer solutions onto hydrophilic UV/ozone-cleaned silicon wafers.

Increasing molecular mobility by heating the polymers was not possible because the polymers decomposed before melting. The morphology of none of the spin-coated solid films changed over time, even when the films were heated to 200°C for 60 min. The films were therefore exposed to solvent vapor and turned into concentrated polymer solutions, in order to enable the polymer chains to move, which, in turn, facilitated the structure formation processes. Finally, after structure formation, the dry samples were characterized in detail by OM (Leitz, Metallux 3, Germany) and AFM (Dimension 3000, Nanoscope III, Veeco, USA) in the tapping mode (TM-AFM).

Polished silicon substrates were used because of their excellent reflective properties, which, coupled with an interference phenomenon due to reflected light coming from the film–air and the substrate–film interfaces, gave us the possibility to use OM for our studies. Swelling the spin-coated films in such reflection geometry in a saturated solvent atmosphere allowed us to study processes of structure formation in solutions in real time and direct space by OM. Moreover, using OM for such thin films allowed the variation and direct evaluation of the polymer concentration (c_p) by determining the thickness of the swollen films from the interference colors.

Interference colors were calibrated in order to obtain values of the (solution) film thickness. First, several films with different thicknesses (in steps of about 20 nm between 5 and 200 nm in thickness) were spin-coated from solutions of increasing polymer concentration. The thickness of each film was measured in the dry state by ellipsometry. In parallel, the interference color of each film was determined by OM. Consequently, we obtained a series of distinct interference colors together with the corresponding film thicknesses. The thickness of films having an interference color in between these calibrated colors was interpolated, allowing continuous determination of the thickness of a “film-solution” during swelling and de-swelling. The calibration films used are shown in Fig. 2a. Taking into account that the colors depend somewhat on the setup of the optical microscope (light intensity, sensitivity of the CCD detector), the refractive index (which slightly depends on c_p), and the subjective judgment of the experimenter, we obtained an absolute thickness resolution of about 10 nm. However, relative changes during swelling/de-swelling and during structure formation could be observed with a higher precision of a few nanometers.

2.3 “Equilibrium” and “Off-Equilibrium” Experiments

By exposing thin films to solvent vapor, the swelling of thin films could be done using two different approaches: either by condensation of solvent vapor onto the cooled film surface (denoted as “off-equilibrium” experiments) or by exposure of

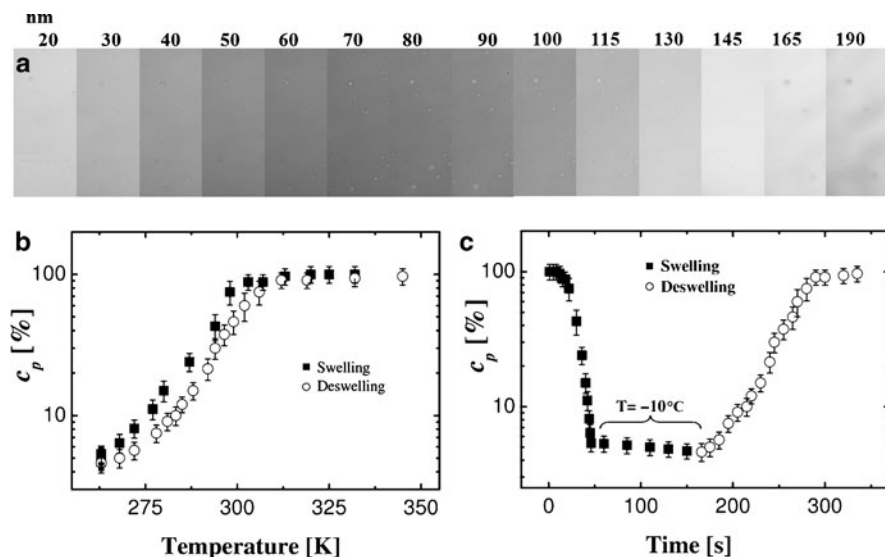


Fig. 2 Swelling and de-swelling of thin films: **(a)** calibration series used in this study (color versus film thickness, ranging from 20 to 190 nm); **(b)** evolution of the polymer concentration during swelling and de-swelling as a function of film temperature; and **(c)** corresponding temporal evolution of the polymer concentration (c_p) during swelling and de-swelling (using chloroform vapor)

thin films to chloroform under conditions without any gradients in temperature (denoted as thermodynamic “equilibrium” experiments). Generally, condensation is controlled by the temperature T_C to which the film surface was cooled below the temperature T_A of the ambient solvent vapor phase, i.e., by the undercooling $\Delta T = T_A - T_C$.

It is important to emphasize that during experiments in ambient air, the polymer molecules were in contact with water molecules from the air. In order to obtain dry air conditions, we used phosphorus pentoxide (P_2O_5) as a desiccant.

To expose thin solid films to solvent vapor, a homebuilt sample chamber was used. It contained two compartments connected via an opening that could be closed when needed. Using two compartments (one for solvent and one for the sample) allowed cooling or heating of both the sample and the solvent independently by using separate Peltier heating/cooling stages for each compartment. The limited temperature range (between about -10 and 65°C) imposed by the Peltier elements did not allow us to use solvents with high boiling points and low volatility [for example *N,N*-dimethylformamide (DMF) with a boiling point of 153°C]. However, solvents such as CHCl_3 or tetrahydrofuran (THF) were well suited.

When performing off-equilibrium experiments, solvent (heated to 50°C in the solvent compartment) was sent into the neighboring compartment, where the sample was initially kept at 35°C . The walls of the sample compartment, however, were not heated. Thus, the sample chamber always stayed approximately at room temperature, with the exception of the sample it contained. After a few minutes, the

sample was in equilibrium with solvent vapor at the temperature of the sample compartment. Under such conditions, not much solvent could be found within the film because its temperature was above the temperature of the vapor phase, which was mainly determined by the temperature of the walls of the sample chamber. Decreasing the sample temperature to a few degrees below the temperature of the surrounding vapor phase led to solvent condensation onto the film and allowed for its swelling. It should be noted that at the same time as condensation of solvent molecules onto the films, small amounts of water from the surrounding air within the chamber were also condensed onto the film, except when precautions (P_2O_5) against humidity were taken.

2.4 Determining the Concentration of Thin Film Solutions

By using an optical microscope, solvent condensation could be followed in real time and direct space via the change of the interference colors of the film. As the amount of polymer in the film stayed constant (this quantity is proportional to the thickness of the dry spin-coated film), a change in film thickness was directly related to the amount of solvent incorporated into the film, i.e., corresponded to swelling by solvent. From the interference colors the thickness (h) of the swollen film could be deduced. The initial film thickness (h_0) was determined by ellipsometry. Accordingly, the polymer concentration c_P in the solution of the swollen film was determined by:

$$c_P = h_0/h \quad (1)$$

In Fig. 2b, a typical temperature-dependence of c_P is shown for a film during swelling/deswelling and for a constant temperature of the solvent reservoir. The corresponding evolution in time is shown in Fig. 2c. Keeping the film at a constant and low temperature led to a slow but steady decrease of the c_P due to continuously condensing solvent molecules (see Fig. 2c for the lowest c_P). Thus, for experiments of long durations, c_P was kept roughly constant by continuously increasing slightly the sample temperature.

Similarly to swelling the film via solvent condensation (i.e., decreasing c_P), c_P could be augmented by increasing the sample temperature and thereby evaporating solvent from the film. A pronounced hysteresis in $c_P(T)$ was observed. At a given temperature, c_P differed between the decreasing and the increasing temperature branch (see Fig. 2b). Finally, at a time chosen to stop the experiment, the sample was dried completely by simply heating the film to relatively high temperatures, for example to 65°C.

In summary, one can distinguish three stages during exposure of thin films to solvent vapor: (1) swelling of films up to (low) c_P ; (2) controlled de-swelling by partial evaporation of the solvent from the swollen films; and finally (3) complete drying of films.

3 Results and Discussions

3.1 Nucleation in Solution Films in Dry Air

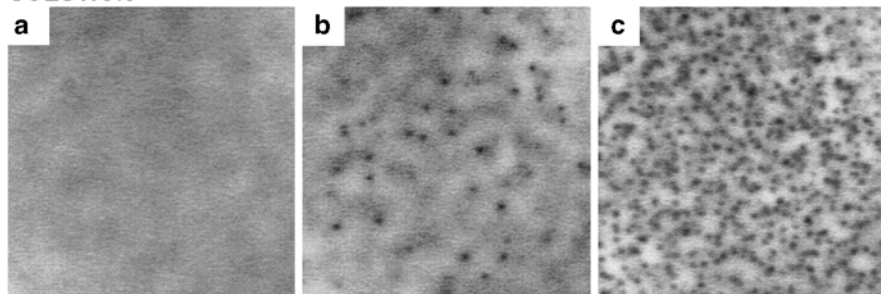
In order to obtain high molecular mobility of polymers, films were swollen until c_p decreased to about 5%. At this concentration, the molecules were distributed homogeneously and the molecular mobility was high. As the viscosity of such an isotropic solution was comparatively low, surface tension was able to smooth the surface of the film quickly within seconds (heterogeneities in film thickness, as observed by OM on spin-coated films, disappeared). This smoothing process was taken as a clear indication for having reached the isotropic phase.

At c_p of about 5%, no changes in time were detectable by OM. The films stayed smooth for many hours. However, when c_p was increased to above 50%, the films started to exhibit local changes in thickness (the corresponding heterogeneities on the film surface could be observed directly under the optical microscope), which were related to the formation of ordered structures within the film. At such increased c_p , the average distance between neighboring molecules became small enough to allow for the formation of nuclei, which led to the growth of ordered structures. This process can be compared to undercooling a polymer melt, thus allowing for nucleation and growth of ordered solid structures. At present, it cannot be decided whether these ordered structures grew from an isotropic solution or from an already (pre)ordered liquid crystalline (LC) phase [19–32]. However, AFM measurements performed after drying the solution film did not indicate any order of the phase surrounding these grown structures.

Figure 3 presents a typical example, which demonstrates that OM is undeniably able to follow in situ both the exposure of films to solvent vapor (i.e. the formation of a solution film by solvent swelling) and the structure formation process. Figure 3a shows the smooth, homogeneous surface of an initially 50 ± 2 nm thick film that had been previously swollen in CHCl_3 vapor (using an off-equilibrium approach) up to a thickness of about $1 \mu\text{m}$ and was subsequently brought back to 95 ± 5 nm, i.e., to c_p of about $53 \pm 5\%$.

After reaching a polymer concentration of $53 \pm 5\%$, the film stayed homogeneous for about 20 min (see Fig. 3a). Later on, isolated “inhomogeneities” started to appear randomly within the film, as observed directly under the optical microscope (see Fig. 3b). Of course, OM has its limitations in resolution (the lateral resolution in this case is about $1 \mu\text{m}$) and the optical contrast is typically weak. This contrast is generated mainly by variations in film thickness and to a minor extent by small differences in the refractive index between the solution and the solid phase. Fortunately, at a concentration of $c_p = 53 \pm 5\%$, the growth process was slow enough to be followed in real time. In addition, the nucleation density was low enough that individual objects were sufficiently separated so that they could be resolved by OM. Thus, structure formation could be clearly detected, starting after approximately 25 min at $53 \pm 5\%$ of polymer. After about 30 min, the surface was extensively covered with isolated objects (Fig. 3c). It is worth emphasizing that OM allowed us to

SOLUTION



DRY

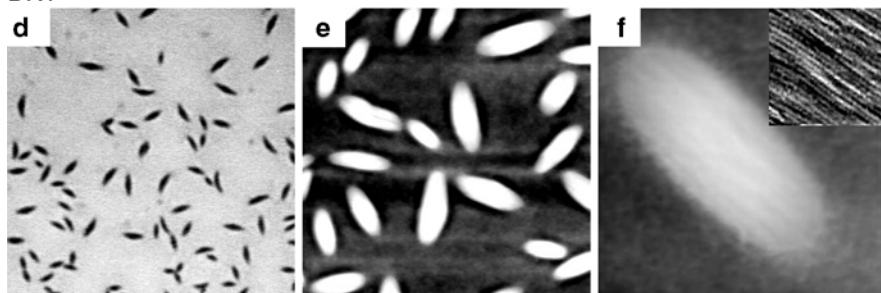


Fig. 3 (a–d) Series of OM and (e, f) AFM topography images showing the temporal evolution of a 50 ± 3 nm thick film at $c_p = 53 \pm 5\%$ after (a) 20, (b) 25, and (c) 30 min. (d–f) Final film morphology after total drying of the film. This film was spin-coated from chloroform solution and swollen under dry air conditions (P_2O_5) using chloroform vapor. The *inset* in (f) represents a phase AFM image magnified in a region on top of the ellipsoidal structure. The sizes of images are (a–c) 100×100 , (d) 35×35 , (e) 5×5 , and (f) $0.8 \times 0.8 \mu m^2$

verify that these structures already existed in solution and were not formed only at a later stage, for example during the drying of the film. After the rapid initial stage of their formation, these objects did not measurably increase in size, even for prolonged times of up to 1 day. This stop in growth can be attributed to the reduction of the concentration of the remaining solution below the critical concentration of supersaturation, due to extraction of the molecules forming the grown objects.

After 30 min at $53 \pm 5\%$ of polymer, the sample was dried and analyzed by OM and AFM. Isolated, randomly distributed ellipsoidal structures embedded in a surrounding film of low degree of order could be identified, as shown in Fig. 3d–e. A detailed morphology of such an ellipsoidal three-dimensional (3D) structure is shown in Fig. 3f. The inset of this figure shows the result of phase-contrast of TM-AFM, which allowed the detection of parallel straight stripes on top of the ellipsoidal structure. These stripes are spaced at an average characteristic distance of molecular dimension: 12 ± 3 nm, which is comparable to about twice the contour length of one block of PBLGlu₃₇ in the α -helix conformation. Intermolecular hydrogen bonding may act normal to the long axis of PBLGlu α -helices, forming long linear stacks of helices (showing as one stripe). This probably explains the existence of parallel straight stripes spaced at a molecular distance and homogeneously covering the whole surface of the grown objects.

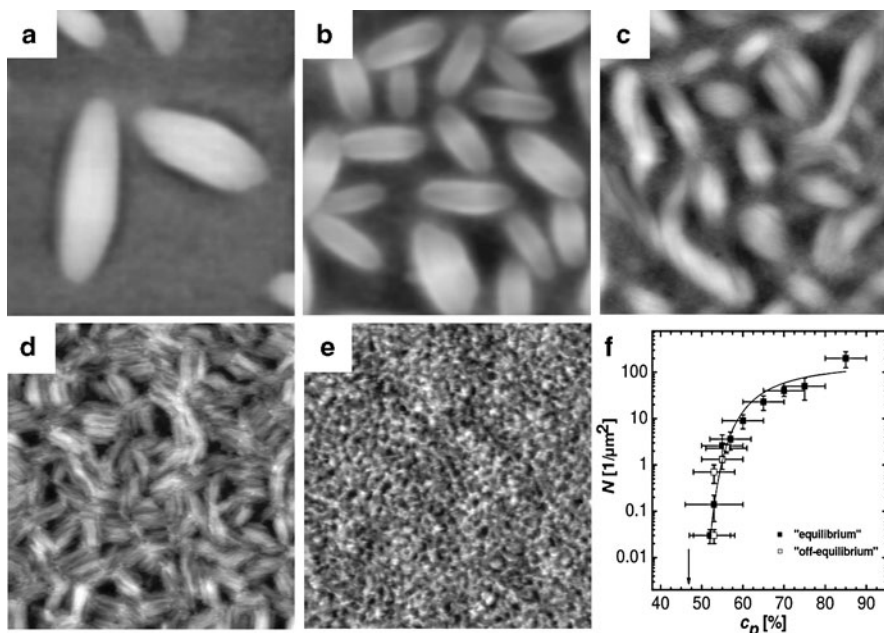


Fig. 4 Series of AFM topography images showing the morphology of 50 ± 3 nm thick films swollen at different c_p : (a) 53, (b) 55, (c) 57, (d) 65, and (e) 85%. The dependence of nucleation density N on c_p is shown in (f). Thin films were spin-coated from chloroform solution and swollen under dry air conditions (P_2O_5) using chloroform vapor. Note that for (a) and (b) off-equilibrium experiments were used, and on-equilibrium for (c), (d), and (e). The arrow in (f) indicates the c_{critical} of $47 \pm 3\%$ (solubility in chloroform), below which no structures could be detected experimentally. The size of all images is $2.5 \times 2.5 \mu\text{m}^2$

Figure 4 presents the experimentally determined dependence of the number density [33–36] $N(c_p)$ of ellipsoidal objects nucleated in thin films swollen in chloroform vapor to variable c_p (ranging from 53 up to 85% of polymer). N , the total number of structures per unit area, was determined by OM and/or AFM after complete drying of the films. These experiments were performed under dry air conditions. As can be seen in Fig. 4a–e, the number of ordered ellipsoidal structures increased with c_p . At the same time, the size of ordered ellipsoidal structures decreased. Figure 4f represents a summary of $N(c_p)$ for all experiments that were performed under dry air conditions. N increased with c_p (see Fig. 4f) because it is less difficult to form a nucleus at higher c_p when molecules are close to each other. However, at large numbers of nuclei per unit volume, the resulting ordered structures will rapidly meet each other (coalesce) during growth due to the short distance between the nucleation sites. Thus, the maximum size of these structures is always smaller than the average distance between the initial nucleation sites. Accordingly, the average size of the structures will be small (see Figs. 4d–e). In order to obtain bigger structures, c_p was decreased until only a few objects nucleated, which then could grow to larger sizes at high nucleation density (see Fig. 4a). Consequently,

in order to be able to employ OM as an observation tool, experiments focused on rather small c_p that were close to a critical concentration c_{critical} . Under such conditions, the formed structures could exceed the micrometer size. Interestingly, all films that were exposed at c_p lower than ca. 53% never showed any indication of nucleation during exposure to chloroform vapor, and no ordered structures were detectable after drying of these films. Thus, one may conclude that the solubility limit in chloroform (represented by c_{critical}) was slightly below 53%. An extrapolation of the $N(c_p)$ curve (Fig. 4f) to 10^{-8} objects per μm^2 (one object per cm^2 , i.e., one object per surface of the whole film) yielded $c_{\text{critical}} = 47 \pm 3\%$ (refer to the black vertical arrow in Fig. 4f). In order to estimate the error bars for this value of c_{critical} , the uncertainty in determining the polymer concentration $\Delta c_p = \pm 5\%$ for each point of the $N(c_p)$ curve has to be taken into account. Two graphical extrapolations, using either the highest or lowest possible values given by Δc_p , to 10^{-8} objects per μm^2 were made, yielding $\Delta c_{\text{critical}} = \pm 3\%$.

The line in Fig. 4f represents a fit to a theoretical description [35, 36] of the nucleation density as given by the following equation:

$$\ln N = \ln P - \frac{Q\beta\sigma^3 v^2}{(kT)^3} \cdot \frac{1}{[\ln(c_p/c_{\text{critical}})]^2} \quad (2)$$

Here, P is an intercept (its exact value depends on the details of the theoretical model chosen) representing the maximum possible number of nuclei for $c_p = 1$, Q characterizes the type of growth, σ represents the interfacial energy between nucleus and solution, β is a shape factor, v represents the volume of the monomeric species, k is the Boltzmann constant, and T is the absolute temperature.

3.2 Nucleation in Solution Films in Ambient Air

The ordering process was also studied under ambient air conditions, i.e., without P_2O_5 as desiccant to eliminate the humidity of the surrounding gas phase. Thus, during an off-equilibrium film-swelling process, some water molecules were also condensed when condensing solvent vapor onto the film surface, and during the equilibrium experiments, thin films were in contact with water molecules contained in surrounding gas phase.

As shown in Fig. 5, OM allowed the structure formation process to be followed in situ and in real time in thin film solutions. Figure 5a shows the smooth, homogeneous surface of an initially 30 ± 3 nm thick film that was initially swollen in chloroform vapor up to a thickness of about 600 nm and then brought back to 100 nm (i.e., at $c_p = 305\%$). At this concentration, the film surface was initially homogeneous (see Fig. 5a). However, it quickly became inhomogeneous due to the appearance of many individual objects protruding from the surrounding film. Structure formation could be clearly observed starting after approximately 6 min at $c_p = 30 \pm 5\%$ (see Fig. 5b). Again, OM allowed verification that these structures already existed in solution.

SOLUTION

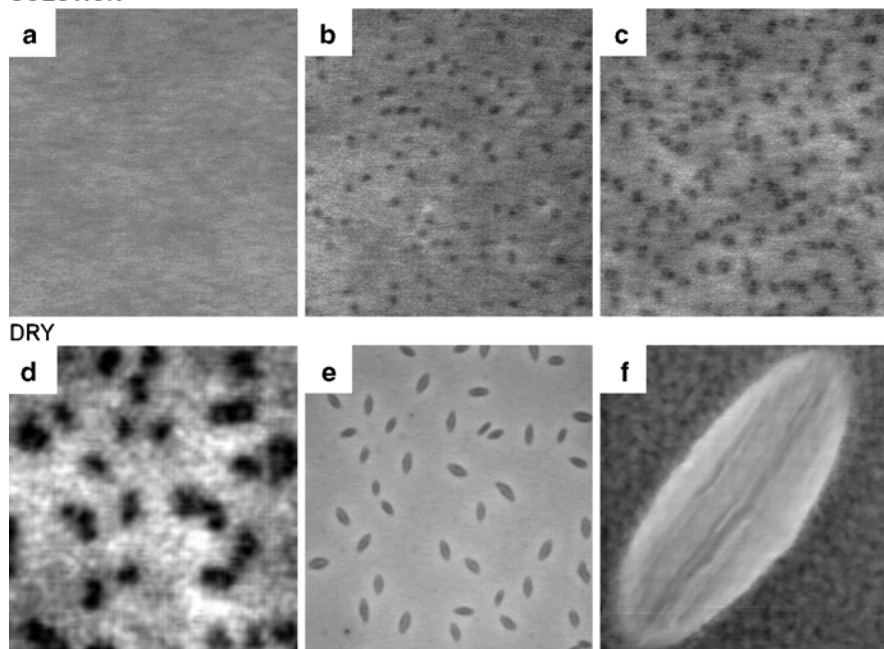


Fig. 5 (a–e) Series of OM and (f) AFM topography images showing the temporal evolution of a thin film during swelling: (a) after 10 s, (b) after 6 min, (c) after 60 min. (d) Magnification of (c). (e) Magnification of the dried film shown in (f). This film was spin-coated from tetrahydrofuran solution and swollen using chloroform vapor at $c_p = 30 \pm 5\%$. The sizes of the images are (a–c) 100×100 , (d, e) 45×45 , and (f) $2.5 \times 2.5 \mu\text{m}^2$

After comparatively rapid formation, the resulting objects did not increase significantly in size, even after prolonged times (see Fig. 5c). It is supposed that the concentration of chains remaining in solution decreased below supersaturation. After 60 min at $c_p = 30 \pm 5\%$, the sample was rapidly dried and analyzed by OM and AFM. The observed isolated structures of ellipsoidal shape were embedded in a film with a low degree of order, as shown in Figs. 5e–f. Note that a magnified area of the still-swollen film (at $c_p = 30 \pm 5\%$) shown in Fig. 5d allowed the observation of protrusions, which corresponded to the ordered ellipsoidal structures shown in Fig. 5e. This was confirmed by subsequent AFM investigations after drying the film.

Systematic experiments revealed that under ambient air, ordered ellipsoidal structures could be obtained at c_p as low as 16–25%. Below c_p of 16–25%, no nucleation and growth of structures could be detected. This raises the question of why structures could be formed in ambient humid air at such low c_p ? As demonstrated for dry air conditions, the concentration below which no structures could be nucleated was as high as 47%. Evidently, the only difference between both experiments is the presence of some water molecules in the surrounding gas phase.

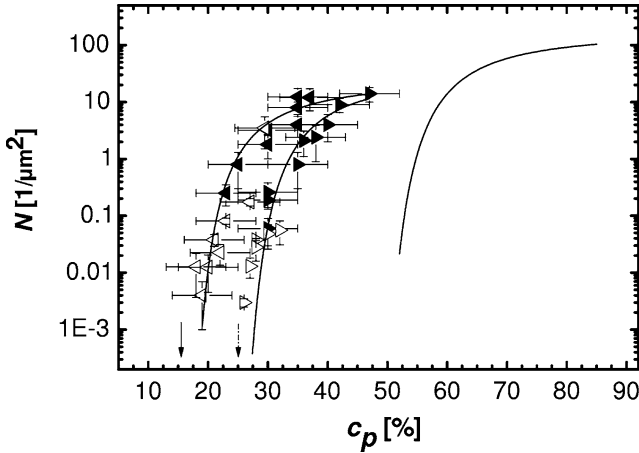


Fig. 6 Representation of nucleation density N versus polymer concentration c_p as determined from off-equilibrium (filled symbols) and equilibrium (empty symbols) experiments carried out under ambient conditions at low humidity (right pointing triangles) and at high humidity (left pointing triangles). The dotted and solid arrows indicate the experimental c_{critical} (solubility in chloroform) of about $25 \pm 3\%$ and $16 \pm 2\%$ determined for less and more humid environments, respectively. Note that below these c_{critical} no structures could be detected experimentally. The lines represent the theoretical fits obtained using (2). The isolated line at high c_p represents a fit for data points presented in Fig. 4f

It has to be concluded that humidity could lower c_{critical} . To rationally explore such a possibility, all results obtained under various ambient air conditions were sorted as a function of the humidity in the laboratory. Such separation allowed us to realize that results obtained in air of ca. 30% humidity (“sunny days”) differed from results obtained under ca. 50% humidity (“rainy days”) (see in Fig. 6 the right- and left-pointing triangles, respectively). As can be seen in Fig. 6, the two series led to different values of c_{critical} of about $25 \pm 3\%$ and $16 \pm 2\%$, respectively, below which no structure formation was detectable. The lines in Fig. 6 represent fits to the data using the theoretical description of (2).

In 1984, Russo and Miller [37] showed that small amounts of water, which can be easily absorbed even from the atmosphere under normal ambient conditions, seriously alter the phase behavior and morphology of PBLGlu homopolymer solutions. This observation is also relevant for the present experiments. When swelling PBLGlu films in humid air, water molecules from the atmosphere obviously entered the polymer solution film. Based on the experiments presented above, it thus can be concluded that water (a non-solvent for the polymer system) facilitates ordering and structure formation, even at low polymer concentrations. In order to verify this statement, complementary experiments were performed on films prepared in air of 100% humidity. Under such conditions, a higher amount of water molecules was expected to condense on the film surface during the film-swelling process. Such conditions of water-saturated air were obtained by including a few droplets of water in the

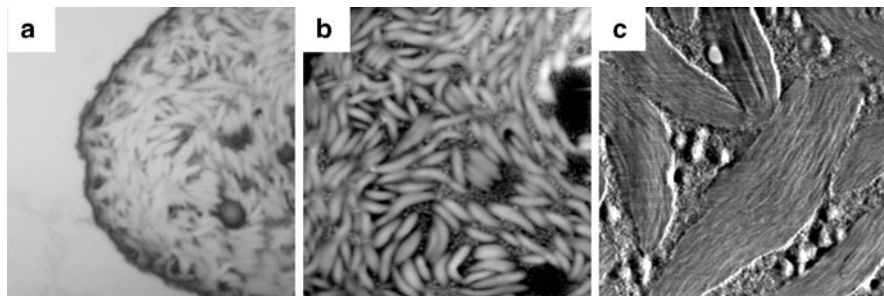


Fig. 7 OM (a) and TM-AFM (b topography, c phase) images showing the morphology of a film made of PS₆₃-(PBLGlu₃₇)₈ and exposed to chloroform vapor at 100% humidity for 50 min at c_p of about 10–15%. Sizes of images are (a) 25×25 , (b) 17.5×17.5 , and (c) $3.5 \times 3.5 \mu\text{m}^2$

sample chamber before the film-swelling process was started. At 100% humidity, a significantly larger amount of water molecules condensed on the film surface during the swelling process compared to the case of ambient air conditions (30–50% humidity).

In the corresponding experiments, $25 \pm 2 \text{ nm}$ thick films were exposed to chloroform vapor under off-equilibrium conditions. The subsequent OM and AFM investigations – performed after drying of the film – revealed (Fig. 7) that the resulting morphology consisted of ellipsoidal ordered structures. By comparing the details of the ellipsoidal structures shown in Fig. 7c with the ones obtained under ambient or dry air conditions, it can be concluded that the morphology is essentially unaffected by the presence of water, at least on the length-scales that are resolved by OM and AFM.

Results of systematic experiments performed for various concentrations of the solution films at 100% humidity are summarized in Fig. 8a (see the upward-pointing triangles). They prove that it was possible to form ellipsoidal ordered structures under 100% humidity conditions even at a very low c_p of about 3–5%. One can determine (by extrapolation) a c_{critical} of about $0.5 \pm 0.4\%$, below which no structure formation will be possible. It should be noted that the way of determining the concentration introduces a large number of uncertainties, particularly for low values of c_p .

The lines in Fig. 8a represent the best fits to the experimental data based on (2). These fits contained three parameters: P , $Q\beta\sigma^3v^2/(kT)^3$ and c_{critical} . The fitted values of c_{critical} were compared to those obtained by graphical extrapolation and are summarized in Table 1. As can be seen, the two sets of values are in reasonable agreement. In Fig. 8b, the fitted values for $Q^{1/3}\beta^{1/3}\sigma v^{2/3}/kT$ are presented as a function of humidity of the surrounding gas phase, with only the interfacial tension σ between ordered structures and the surrounding solution as a variable. This presentation clearly shows that σ varied with humidity: the greater the amount of water (a non-solvent for PBLGlu) in the surrounding gas phase, the higher the value of σ (see Fig. 8b). In Fig. 8c, we show that $Q^{1/3}\beta^{1/3}\sigma v^{2/3}/kT$ and c_{critical} are also correlated and that σ varied inversely with c_{critical} : the lower was c_{critical} , the higher was σ .

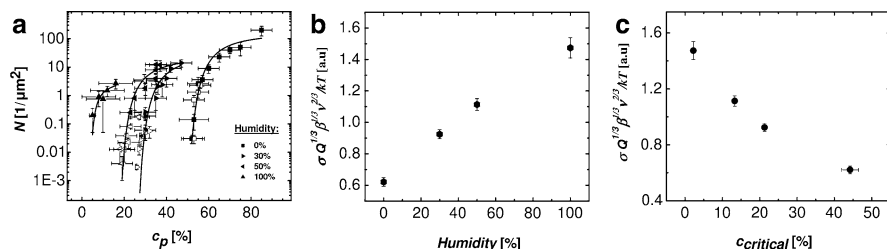


Fig. 8 (a) Representation of nucleation density N versus polymer concentration c_p as determined from off-equilibrium (filled symbols) and equilibrium (empty symbols) experiments carried out: in dry air (squares), at low humidity (right pointing triangles), at high humidity (left pointing triangles) and in water-vapor-saturated air (upwards pointing triangles). (b, c) Variation of interfacial tension σ between the solid ordered structures and solution. The interfacial tension σ increased with an increase in surrounding gas phase humidity (b), and with the decrease of polymer solubility c_{critical} (c)

Table 1 Comparison of c_{critical} values obtained both experimentally (by extrapolation) and by fitting according to (2), for different humidity conditions

Humidity (%)	Extrapolated c_{critical} (%)	Fitted c_{critical} (%)
0	47 ± 3	44.2 ± 2.3
30	25 ± 3	21.3 ± 2
50	16 ± 2	13.3 ± 2
100	0.5 ± 0.4	2.22 ± 1

3.3 Influence of Protic Non-Solvents on Nucleation in Thin Film Solutions

What could be the explanation for such dependence, knowing that water is not a solvent, neither for PBLGlu nor for PS? However, PBLGlu does offer several possible sites that can interact with water via hydrogen-bonding interactions (for example, the polar L-glutamate backbone and the polar ester group).

In the search for a tentative concept to explain the dependence of σ on humidity of the surrounding gas phase, one may assume that protic non-solvent (water) molecules form a complex with PBLG via hydrogen-bonding interactions. This complex is then expected to exhibit a lower solubility c_{critical} . Among the various possibilities for hydrogen bonding, the two hydrogen bonds of type $\text{C}=\text{O} \cdots \text{H}-\text{O}$ between the oxygen atom of the ester carbonyl group and hydrogen atom of water seem to be most favorable. The ester group is located at the exterior of the PBLGlu helix and is not otherwise involved in hydrogen bonding. The secondary amide groups of the PBLGlu backbone, on the other hand, are involved in intramolecular hydrogen bonding, stabilizing the α -helical conformation of PBLGlu, and are hidden inside the core of the helix. Other possibilities of hydrogen-bonding interactions (for example $\text{C}-\text{H} \cdots \text{O}-\text{H}$) cannot be excluded, but will not be considered further.

If this concept is valid, it means that other non-solvents, with similar properties akin to water, should also be able to complex the PBLGlu and to modify its solubility. Furthermore, this concept implies that non-solvents without hydrogen-bonding capabilities should not be able to complex the polymer. If these conclusions were proven, they would represent strong support of our concept of polymer complexation.

In order to test the hypothesis, two series of off-equilibrium experiments were performed by exposing thin films to chloroform vapor mixed with small amounts of (1) methanol and (2) toluene. Methanol is a “strongly hydrogen-bonding” protic non-solvent that can form hydrogen bonds with the polymer. Toluene, although it is a good solvent for PS, does not dissolve PBLGlu (at room temperature). It is an aprotic “poorly hydrogen-bonding” non-solvent [38] for PBLGlu and does not strongly interact with PBLGlu, and certainly does not form hydrogen bonds. Small amounts of methanol or toluene molecules were added to the surrounding gas phase by placing several droplets of these liquids in the sample chamber before swelling of the film. Humidity was avoided either by flushing the sample chamber with nitrogen before the start of the experiment (in the case of methanol, as methanol is absorbed by P_2O_5) or by using P_2O_5 (in the case of toluene).

An example of such off-equilibrium experiments in the presence of methanol will be described. Polypeptide films of 40 ± 3 nm thickness were exposed to chloroform vapor mixed with a small amount of methanol molecules and swollen up to $c_p = 5 \pm 2\%$, which was subsequently increased in two steps to c_p of $30 \pm 5\%$ for 30 min and then to c_p of $45 \pm 5\%$ for 2 min before the film was finally dried.

As can be seen in Fig. 9a–b, ellipsoidal ordered structures were obtained at low c_p of $30 \pm 5\%$. In addition, many smaller ordered structures formed at the higher polymer concentration ($45 \pm 5\%$). It has to be noted that both concentrations were lower than the critical concentration found in experiments performed in dry air without the addition of small amounts of a protic solvent like methanol. This experiment, together with previous and with additional experiments, proved that ordered ellipsoidal morphology does not depend on the type of non-solvent (water or methanol). In Fig. 9c we have summarized the corresponding results. With respect to results obtained in dry air, we observed that methanol did decrease c_{critical} , and toluene did not affect c_{critical} . Accordingly, these results strongly suggest that complexation of PBLGlu by protic non-solvents via hydrogen-bonding interactions causes a decrease in solubility.

3.4 Reversible Influence of Protic Non-Solvents on Nucleation in Thin Film Solutions

In order to investigate whether formation and dissolution of the ordered structures in thin film solutions can be controlled by simply changing the vapor pressure of a protic non-solvent, more complex off-equilibrium experiments were designed. Experiments were performed under dry air conditions and in a vapor

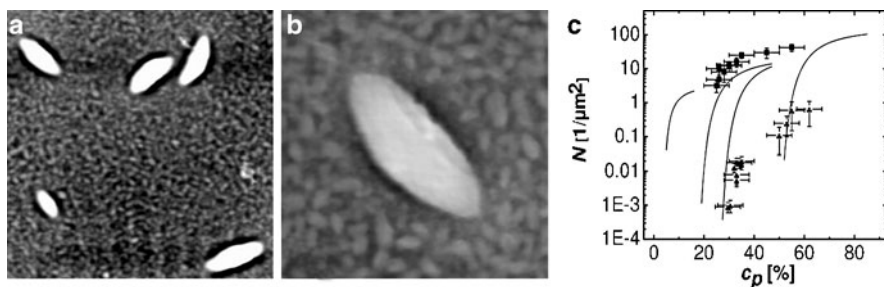


Fig. 9 (a, b) AFM topography images presenting a bimodal distribution of ordered ellipsoidal structures of a 40 ± 3 nm thick film spin-coated from chloroform solution. The film had been exposed using off-equilibrium experiments to a mixture of chloroform and methanol vapor under dry air conditions (obtained by flushing the sample chamber, before film swelling, with a N_2 flow) at $c_p = 30\%$ (for 30 min) and at higher $c_p = 45\%$ (for 2 min). (c) Representation of nucleation density N against polymer concentration c_p as determined from off-equilibrium experiments carried out by exposing thin films to chloroform vapor under dry air conditions and adding methanol (*filled spades*) or toluene (*filled clubs*). Off-equilibrium experiments carried out by exposing thin films to THF vapor under ambient air conditions are indicated by *filled squares*. Note that dry air conditions have been obtained either by using P_2O_5 (in the case of toluene) or by flushing the sample chamber with N_2 flow (in the case of methanol) before the film swelling process. The *lines* are the fits for data points obtained under (from *right to left*): dry, less humid, more humid and highly humid air conditions (see Fig. 13a). Sizes of images are (a) 10×10 , and (b) $3 \times 3 \mu\text{m}^2$

atmosphere with the controlled addition and subsequent removal of water or methanol molecules. Conditions were realized by flushing the sample chamber with N_2 flow before performing the swelling of the film. During formation and dissolution of ordered structures, c_p was kept relatively constant (small fluctuations around this value could not be excluded). The two sets of experiments – either using water or methanol molecules in the surrounding gas phase – yielded similar results. Therefore, only results for the addition and removal of methanol are presented here.

First, a 40 ± 3 nm thick solid film of $\text{PS}_{63}-(\text{PBLGlu}_{37})_8$ heated to a temperature of 35°C was exposed for 10 min to chloroform vapor inside a sample chamber, which was kept approximately at room temperature. The swelling of this film started under dry air conditions. Then, the temperature of the film was lowered until the film was swollen to $5 \pm 2\%$ of polymer.

After 2 min at $c_p = 5 \pm 2\%$, the sample temperature was raised, causing an increase of c_p to $34 \pm 5\%$. The sample was kept at this concentration for about 10 min. The morphology resulting at this stage is shown in Fig. 10a. No isolated objects were observed within the resolution of OM.

After these 10 min, methanol vapor was added in the sample chamber by opening a valve to a supplementary chamber where methanol had been heated to 55°C . After about 5 min, one could observe the appearance of isolated objects. These objects became better developed and more clearly visible after about 9 min (see Fig. 10b).

Then, methanol molecules were removed from the sample chamber (the valve between the two chambers had been closed and the chamber purged with a very weak N_2 flow for 15 min). After 5 min, the isolated objects started to dissolve and almost

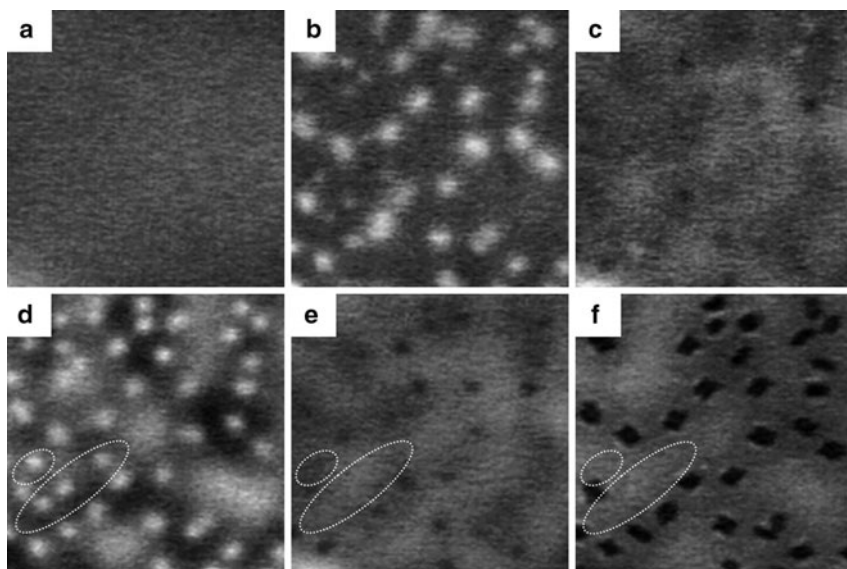


Fig. 10 Structure formation and dissolution in a 40 ± 3 nm thick film of $\text{PS}_{63}\text{-(PBLGlu}_{37})_8$ swollen in chloroform vapor at about $34 \pm 5\%$ of polymer: (a, c, e) no methanol molecules present; (b, d) small amounts of methanol molecules present; (f) totally dried film. Before performing the swelling of the thin solid film, the sample chamber was flushed with N_2 flow in order to create dry air conditions. Regions marked with *dotted lines* show (d) presence, (e) disappearance, and (f) reappearance of structures. Size of all OM images is $50 \times 50 \mu\text{m}^2$

all of them had disappeared after 19 min (see Fig. 10c). Two minutes later, methanol molecules were added again by opening the valve between the two chambers. Isolated objects reappeared after about 2 min and developed into better defined objects during the following 10 min (see Fig. 10d). This procedure of adding and removing methanol was repeated a second time. As expected, the isolated objects dissolved within about 15 min (see Fig. 10e). However, this time, not all objects were dissolved completely. Thus, when adding methanol molecules again, after about 5 min, the previously dissolved objects appeared again, as shown in Fig. 10f (after complete drying of the film). However, not all of the previously visible structures reappeared. Some of them (formed after the second addition of methanol molecules) dissolved completely when methanol molecules were removed and did not reappear again when methanol molecules were added for the third time (compare the regions inside the dotted elliptical forms in Fig. 10d–f).

Detailed features of these isolated objects being formed in film solutions were studied by AFM after completely drying the film solutions. In Fig. 11, two AFM topography images are shown for objects similar to those visible in Fig. 10f. As can be seen, two types of populations of ordered structures were present: ellipsoidal structures, which were most probably formed by nucleation from a single seed, and “double” ellipsoidal structures, which may have been formed from two neighboring seeds. Seeds may have resulted from ordered structures that were only partially

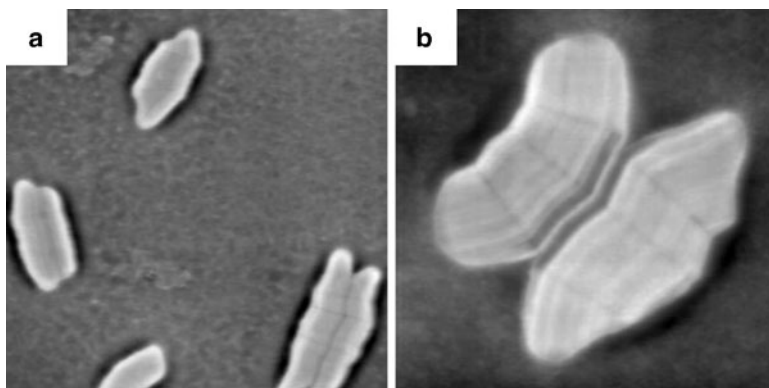


Fig. 11 AFM topography images showing ordered structures obtained in a 40 ± 3 nm thick film of $\text{PS}_{63}\text{-(PBLGlu}_{37})_8$ swollen in chloroform vapor, under dry air conditions (the sample chamber was flushed with N_2 flow before film swelling) and at about 34% of polymer. Note that the two images are from the same film but of slightly different regions on the film surface. Sizes of images are (a) 10×10 , and (b) $4 \times 4 \mu\text{m}^2$

dissolved. From such seeds, a “double” structure (see Fig. 11b) has probably grown when re-adding non-solvent molecules. No such seeds were found when the ordered structures were totally dissolved.

In summary, adding small amounts of water or methanol molecules to the surrounding gas phase can induce nucleation and growth of ellipsoidal ordered structures up to more than $10 \mu\text{m}$ in size. Without such additions, nucleation does not occur at such low polymer concentration. It can be concluded that water or methanol molecules complexed the PBLGlu and, consequently, increased the interfacial tension between the ordered structures and solution, which, in turn, facilitated structure formation by decreasing the polymer solubility. After removal of water or methanol molecules, at constant c_p , these ordered structures dissolved due to the increased polymer solubility.

Ordered structures reappeared at the same c_p when water or methanol molecules were added again to the surrounding gas phase. This structure formation/dissolution cycle can be repeated, which proves the reversibility of the process of structure formation and dissolution.

Finally, all these results support the validity of the concept of complexation of PBLGlu by protic non-solvent molecules via hydrogen-bonding interactions. Such complexes exhibit a lower solubility c_{critical} , which explains the dependence of the interfacial tension σ on the degree of humidity of the surrounding gas phase. Among the various possibilities for hydrogen bonding, the two hydrogen bonds of type $\text{C=O} \cdots \text{H-O}$ between the oxygen atom of the ester carbonyl group and hydrogen atom of water seem to be most favorable (see Fig. 12). The ester group is located at the exterior of the PBLGlu helix and is not otherwise involved in hydrogen bonding. As already indicated, the secondary amide groups of the PBLGlu backbone, on the other hand, are involved in intramolecular hydrogen bonding, stabilizing the α -helical conformation of PBLGlu, and are hidden inside the core of the helix.

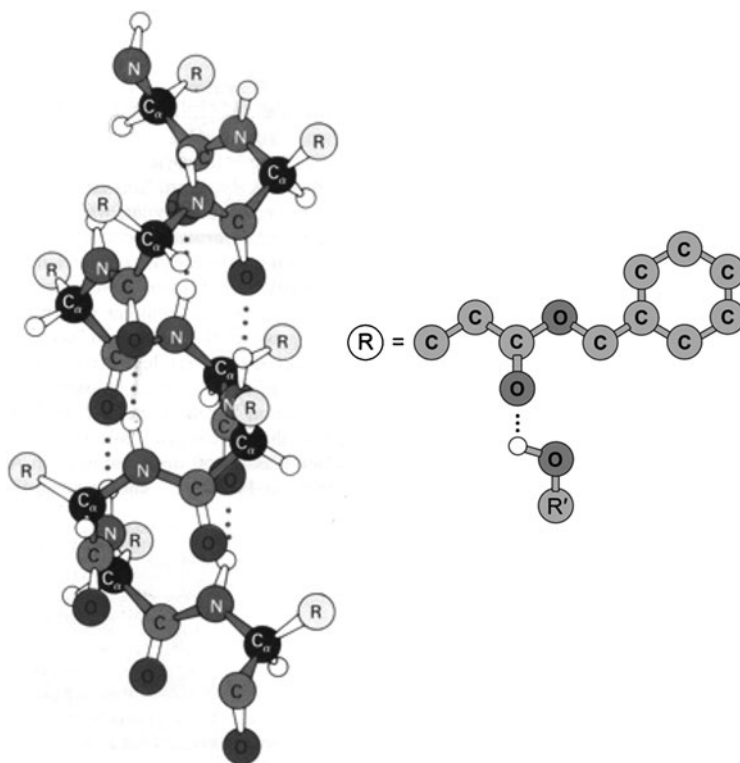


Fig. 12 Representation of a PBLGlu α -helix (taken from [1]) and the coordination of water (or alcohol) molecules to the ester carbonyl group in the side chain via hydrogen bonding

3.5 *Origin of Bimodal and Multimodal Distributions in Size of the Resulting Ordered Objects*

So far, mainly OM has been used to directly observe in real time the nucleation and growth of ordered polypeptide solid ellipsoidal structures in thin solution films. Detailed characterization of these ellipsoidal structures will be given in this section. In particular, more information will be presented on how these structures form at the molecular level, and about the forces that lead to formation of ellipsoidal ordered structures with an aspect ratio of about 2. It will also be explained how two different populations of ordered structures can be generated in a single film.

The chosen experimental approach could not prevent slight fluctuation of c_p around its set value by about 2–3%, including small drifts of c_p . Experimentally, it is often observed (after exposure of the films to solvent vapor and subsequent complete drying) that in a single sample, several types of structures are generated, differing basically only in size. In order to address this behavior, the consequence of an abrupt change in c_p , say, from c_p to $c_p + 15\%$, was examined. Figure 13 shows a

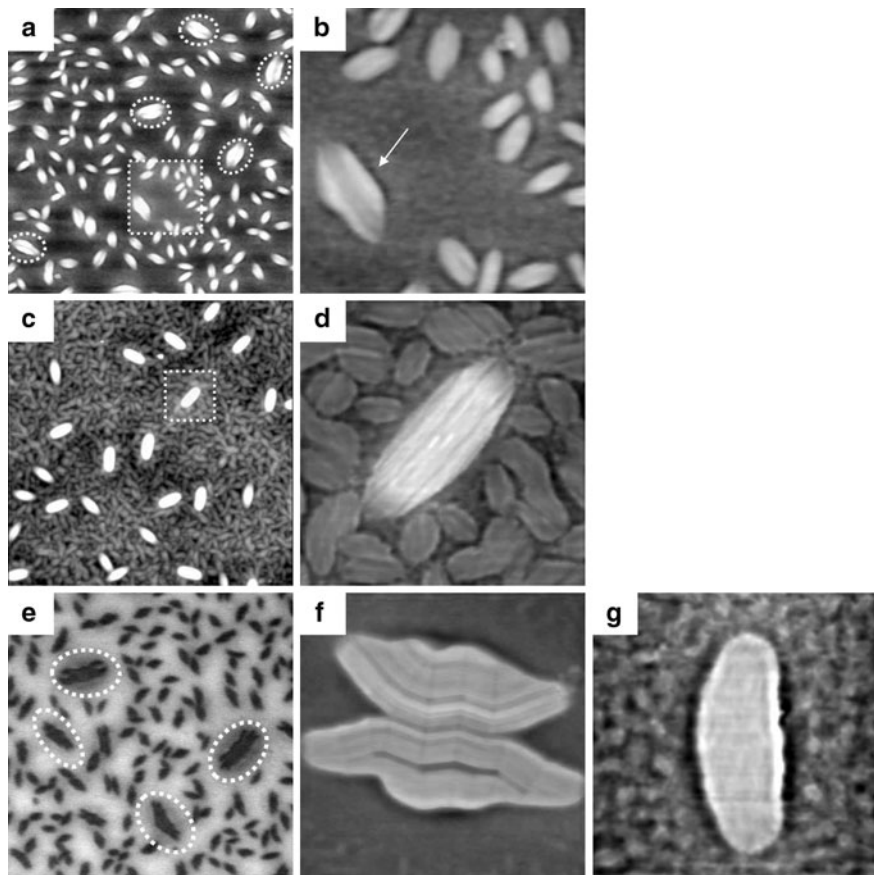


Fig. 13 (a–d, f, g) Series of AFM topography images and (e) an OM micrograph showing different distributions of ordered structures on the film surface. (a, b) Bimodal distribution of a 50 ± 3 nm thick film prepared under dry air conditions (off-equilibrium experiment) at $c_{p1} = 53\%$ (for 10 min) and at slightly higher $c_{p2} = 56\%$ (for 15 min), respectively. (c, d) Bimodal distribution of a 25 ± 2 nm thick film prepared under ambient air conditions (off-equilibrium experiment) at $c_{p1} = 30\%$ (for 15.5 h) and at higher $c_{p2} = 45\%$ (for 7 h), respectively. (e–g) Multimodal distribution of a 40 ± 3 nm thick film prepared under ambient air conditions (off-equilibrium experiment) at $c_{p1} = 18\%$ (for 2 h), at higher $c_{p2} = 25\%$ (for 30 min), and at $c_{p3} = 45\%$ (for 5 min), respectively. The dotted squares indicate a zoomed-in region. Arrow in (b) and dotted regions in (a, e) indicate large objects. The sizes of images are (a) 10×10 , (b) 2.5×2.5 , (c) 9.5×9.5 , (d) 1.25×1.25 , (e) 45×45 , (f) 4.5×4.5 , and (g) $2.25 \times 2.25 \mu\text{m}^2$

series of AFM topography images and an OM micrograph of different distributions of ordered structures observed in films after various experimental conditions.

In a first experiment, a 50 ± 3 nm thick film was exposed to chloroform vapor under dry air conditions (off-equilibrium experiment) at two different concentrations: $c_{p1} \approx 53\%$ and subsequently at a slightly higher concentration, $c_{p2} \approx 56\%$. The experiment was followed in real time under the optical microscope. A spin-coated film

was initially swollen to 5% of polymer and was then concentrated to c_{p1} . After about 10 min, the concentration was again increased (to c_{p2} of ca. 56%) by increasing the film temperature by 0.5°C. After about 15 min at c_{p2} , the sample was completely dried and investigated by AFM.

The two AFM topography images of Fig. 13a, b show the resulting distribution in size of the obtained ordered structures. As can be seen, the ordered structures were of ellipsoidal shape, randomly but evenly distributed over the whole film surface. What is interesting in these images is the fact that there were two distinct distributions of ellipsoidal structures, which could be differentiated according to their size. There were relatively few structures that averaged about 1 μm along their longer axis (referring to the structures inside the dotted ellipses in Fig. 13a and to the structure indicated by the black arrow in Fig. 13b). These larger structures were formed at the lower c_{p1} and could be directly detected by OM. However, the majority of objects were smaller and only slightly exceeded an average size of 500 nm. It may be assumed that the two types of structures appeared at c_{p1} and c_{p2} , respectively.

In a second off-equilibrium experiment (see Fig. 13c, d), this time performed under ambient (humid) air conditions, the ordering process was followed in a 25 ± 2 nm thick film exposed for a long duration (tens of hours) to chloroform vapor. After swelling of the film (up to 5% of polymer), c_p was increased to $c_{p1} = 30\%$ and the sample was kept for 15.5 h. After reaching the concentration c_{p1} , ellipsoidal 3D structures formed rapidly, typically within a few minutes, as confirmed directly by OM (not shown) and later on by AFM (see the white ellipsoidal structures in Fig. 13c). No further changes were detectable for the rest of time (ca. 15 h) at c_{p1} and structures did not grow further.

Finally, the c_{p1} in the film was increased quickly to $c_{p2} = 45\%$ for 7 h before rapidly drying the sample. Subsequent AFM analysis (Figs. 13c, d) showed that the larger ellipsoidal objects detectable by OM were surrounded by smaller structures of similar shape (for each population, both shape and size were rather uniform). These smaller structures were formed at the concentration c_{p2} and contained almost all available material. The ordered structures were separated by narrow depressions containing only very few molecules (depleted regions).

The above and additional experiments (not shown, under both dry and ambient air conditions), proved that the size of the observed objects did not increase measurably beyond the size reached after a few minutes of exposure at c_p , even when the time was increased to more than 10 h. Why did growth not continue?

First, it has to be emphasized that rather low values of c_p , very close to the c_{critical} , were chosen. Under such conditions only few nuclei were formed, which facilitated their observation by OM. As already discussed, once a nucleus has formed, it continues to grow, taking up molecules from the surrounding until c_p of the remaining solution dropped below the c_{critical} (refer to Fig. 13c, d). At this moment, the reservoir of molecules available for insertion into the ordered structures became exhausted and growth stopped.

Accordingly, the bimodal distribution in size observed in Fig. 13c, d can be explained in the following way: The bigger structures were nucleated and grew at

the lower c_{p1} . The comparatively lower number density of objects was determined by the value of c_{p1} (see Fig. 8a). As these objects grew, they finally exhausted the reservoir of available molecules and thus growth came to a halt. However, when the polymer concentration was subsequently increased to a significantly higher value $c_{p2} > c_{\text{critical}}$, a second process of nucleation and growth of structures was initiated. Because the initial distance to c_{critical} was quite large, the resulting number of nuclei was higher because there was a higher probability for nucleation (see e.g. Fig. 8a). This second nucleation and growth process was again stopped, either when the reservoir of available molecules became exhausted (see Fig. 13a, b) or when the growing structures coalesced (see Fig. 13c, d).

Based on this explanation, any multimodal distribution in size can be obtained just by increasing the c_p in an appropriate number of steps. Figure 13e, g present an additional off-equilibrium experiment that was also performed under ambient air (i.e., humid) conditions. The ordering process in a 40 ± 3 nm thick film was again followed in real time during exposure to chloroform vapor at three subsequent values of c_p : $c_{p1} = 18\%$ (for 2 h), a slightly higher value of $c_{p2} = 25\%$ (for 30 min), and $c_{p3} = 45\%$ (for 5 min). Note that c_{p1} was chosen close to the solubility limit, and small concentration fluctuations (caused by temperature fluctuations of ca. 0.1°C) may have crossed c_{critical} temporarily. Thus, growth may have been interrupted by short periods of partial dissolution.

OM had confirmed (see Fig. 13e) that two populations of structures were formed at c_{p1} and c_{p2} . AFM allowed the identification of a third population of structures that formed at c_{p3} (see the multitude of small structures, less than 100 nm^2 , in Fig. 13g). In Fig. 13g, one can see an ellipsoidal structure formed at c_{p2} that is surrounded by the much smaller objects formed at c_{p3} .

Figure 13f presents a structure of about $5\text{ }\mu\text{m}$ formed at c_{p1} . This type of structure is marked by the dotted ellipses in the OM of Fig. 13e. The shape of this structure indicates a “tandem-like” structure, which is most probably the result of the small fluctuations of c_{p1} in between $c_{p1\text{ max}}$ and $c_{p1\text{ min}}$. The nucleus formed initially at $c_{p1\text{ max}}$ and started to grow, but was then partially dissolved when c_{p1} became $c_{p1\text{ min}} < c_{\text{critical}}$, assuming that some seeds could remain. If two such seeds remained close together, a tandem-like structure could grow when the polymer concentration increased again to $c_{p1} > c_{\text{critical}}$. Such a multipart structure may thus be the result of nucleation by self-seeding.

3.6 Kinetics of Growing Ordered Objects

It should be pointed out that in all experiments, the resulting structures were detectable by OM after a few minutes. Certainly, under an optical microscope, such structures can only be detected when their size becomes large enough ($\approx 500\text{ nm}$). So, how fast did these structures grow? In a control experiment, c_p was increased rapidly (within a few seconds) from 5 to 100%. Only small and less well-defined objects of about 100 nm were formed (see Fig. 14). No large ordered structures

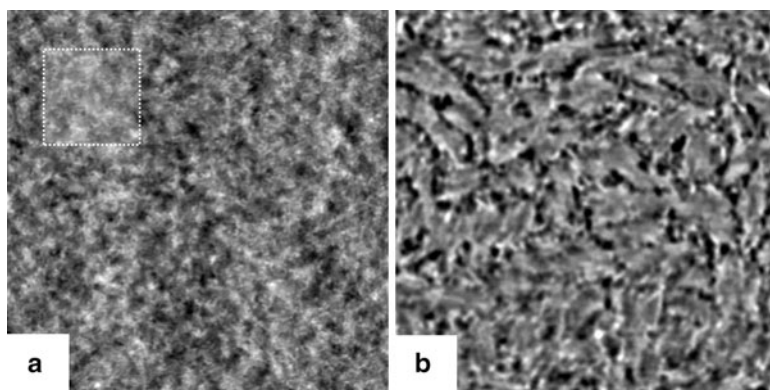


Fig. 14 TM-AFM typical images (**a** topography, **b** phase) showing the surface of a 30 ± 2 nm thick $\text{PS}_{63}\text{-(PBLGlu}_{37})_8$ film after its exposure to chloroform vapor for 5 min and rapid drying. This film was first swollen at about 5% of polymer (the film temperature was decreased from 35 to -5°C). After swelling, the film was then heated very fast (in about 10 s the film temperature was increased from -5 to 65°C) in order to extract all the solvent from the film. No large ordered structures could be observed. The *dotted square* in (**a**) indicates the region that is shown magnified in (**b**). The sizes of images are (**a**) $2 \times 2 \mu\text{m}^2$, and (**b**) $500 \times 500 \text{ nm}^2$

were observed (see Fig. 14a). Consequently, the molecules need more than a few seconds to order themselves on large scales. For example, during spin-casting the solvent evaporates very quickly and, consequently, the molecules are deposited on the substrate in a non-organized fashion. Thus, the time of several seconds during which solvent evaporates is not sufficient for ordering. Similarly, when the c_p was increased rapidly from 5 to 100%, molecules did not have time for ordering at large scales (larger than about 100 nm, see Fig. 14b). During such rapid drying, the molecules pass any polymer concentration c_p (for example 30%) in much less than a second, which is not enough to allow a distinct nucleation and growth process yielding well-defined ordered objects. On the other hand, the above experiments proved that molecules could become ordered into larger ellipsoidal structures within about 2 min when exposed to solvent vapor under constant conditions. Thus, it may be concluded that molecules needed more than a second but less than 2 min to form micrometer-sized ordered structures in solution.

3.7 Origin of the Anisotropic Shape of the Resulting Ordered Objects

As previously shown (Figs. 3 and 5), it was also attempted to follow the kinetics of structure formation. In Fig. 3, at c_p of about 53%, the first indication of the formation of ordered structures became visible after about 25 min. At this concentration, the growth process was sufficiently slow to be followed in real time. In addition,

the nucleation density was low enough so that individual objects were sufficiently separated and could be resolved by OM. These structures, as revealed by AFM analysis after total drying of the film, possessed an anisotropic shape (ellipsoidal, with an aspect ratio of length to width of about 2). A similar anisotropic shape has been observed for all experiments performed with the polymer system of this study. So, why do the observed structures grow laterally faster in one direction and slower along the orthogonal direction?

To answer this question, anisotropic growth has to be related to the intermolecular interactions between the molecules. One has to find out which is the most favorable way for molecules to arrange with respect to these two growth directions. It is known that PBLGlu α -helices possess high dipole moments (about 3.5 Debye per unit and sites for hydrogen-bonding interactions). Thus, the mechanism of structure formation will most probably be based on strong dipole–dipole interactions between rather rigid PBLGlu α -helices. Note that, at larger scales the grown objects have to be electrically neutral, implying that the high dipole–dipole moments have to be compensated for. Directional hydrogen-bonding interactions may contribute to lateral ordering of PBLGlu α -helices (normal to the long axis of the α -helix).

Two possibilities could be causing an asymmetric growth of ellipsoidal structures: (1) anisotropic transport phenomena and/or (2) directional intermolecular interactions. The observed 3D structures were formed in solution, in which molecules can move easily. The large lateral size of the formed objects (much larger than the molecular length-scale) and their random orientation in space (the long axis of the ellipsoidal objects does not exhibit any preferred directions) indicate that anisotropic transport within the solution is probably not responsible for the shape. Therefore, anisotropy in lateral growth may be attributed to specific intermolecular interactions between the α -helices. These interactions will affect the growth rate in various directions.

Figure 15 shows a rather complex morphology, which will help to identify a potential growth mechanism of ordered structures. This morphology resulted from exposure of a 100 ± 5 nm thick film to chloroform vapor under dry air conditions (off-equilibrium experiment) at $c_p = 54 \pm 5\%$ for 25 min. Probably due to the high amount of available molecules in such a thick film and the correspondingly high nucleation density, the shape of the formed structures is not unique, varying from isolated ellipsoidal to “meandering” structures (see Fig. 15a, b).

As an attempt to explain these meandering structures, one may assume that they resulted from coalescence of many initially ellipsoidal structures that coalesced during growth. The initial ellipsoidal structures are indicated in Fig. 15c. These initial structures grew in the plane of the substrate in the fast (f) and the slow (s) direction. After coalescence, growth stopped in one direction.

The clearly visible lines (represented by broken white lines in Fig. 15c, d) are thus supposed to be the result of such coalescence between initial structures during the growth process. The dotted black lines in Fig. 15d indicate the variable directions of the long axis of the initially nucleated structures. The long axis also represents the orientation of parallel stripes building up these objects. These stripes could be

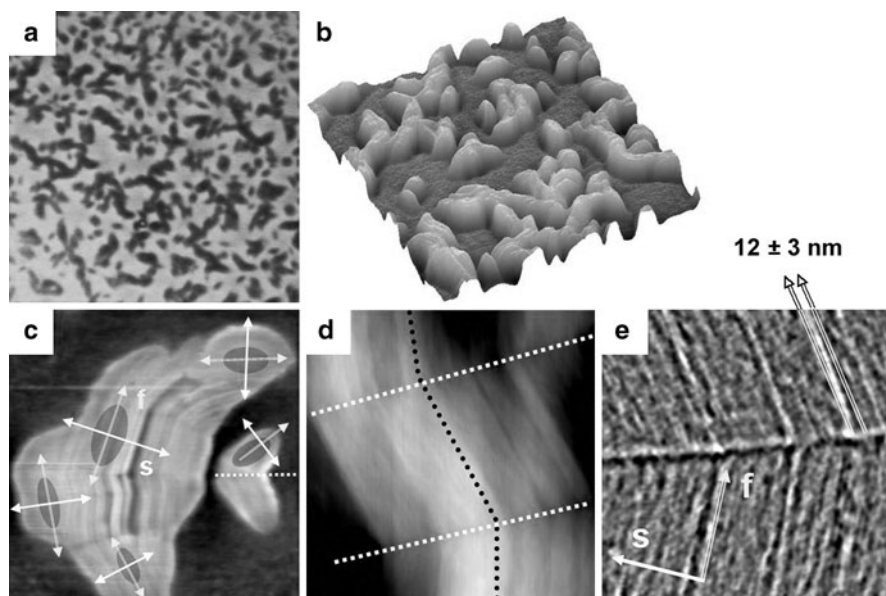


Fig. 15 Series of OM (a) and AFM (b, c, d topography, e phase) images showing the coalescence of ordered structures in a 100 ± 5 nm thick film prepared under dry air conditions (off-equilibrium experiment) at $c_p = 54 \pm 5\%$ for 25 min. The arrows marked *f* indicate the fast-growing direction (along the normal to chain axis of α -helices). The arrows marked *s* indicate the slow-growing direction (parallel to chain axis of α -helices, i.e. normal to main chain axis). The white dotted lines represent a coalescence line, and the black dotted lines indicate the random orientation of initially nucleated structures. The elliptical forms in (c) are the initial ellipsoidal structures. The sizes of images are (a) 100×100 , (b) 19×19 , (c) 5×5 , (d) 1.25×1.25 , and (e) $0.75 \times 0.75 \mu\text{m}^2$

clearly distinguished by examining the surface of the assembled structures by AFM. Their average width (see Fig. 15e), was measured to be 12 ± 3 nm. This size is comparable to the molecular dimension of the investigated molecule, more precisely, to the length of two α -helices in series (see Fig. 1c).

Such long, straight, parallel stripes have been always observed on top of the ellipsoidal structures (see the inset in Fig. 3f). A typical example is also shown at a higher resolution in Fig. 16a. From the height profile presented in Fig. 16b, the average width of the stripes is about 12 ± 3 nm. Taking into account the above considerations, one may conclude that comparatively strong lateral interactions between α -helices (hydrogen-bonding interactions) favor fast growth along the axis normal to α -helical chain, i.e., along the long axis of the ellipsoidal structures. Slow growth then results in the direction along the chain axis of α -helices and will determine the width of the ellipsoidal structures. These observations, together with the average width of the stripes of about 12 ± 3 nm, suggests a model for a possible molecular organization inside the stripes (in the plane direction of the ellipsoidal ordered structures; see Fig. 16c).

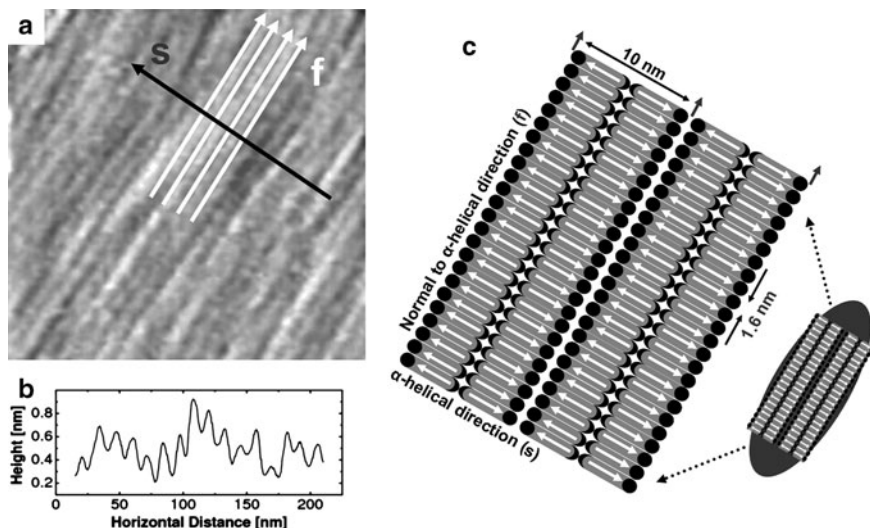


Fig. 16 (a) AFM topography image showing the parallel straight stripes on top of an ellipsoidal structure. (b) Height profile made in the region indicated by the arrow marked *s* in (a). The average distance between the stripes was about 12 ± 3 nm. (c) Representation of a possible arrangement of α -helices inside the parallel stripes observed on top of ellipsoidal structures and indicated in (a) by arrows marked *f*. The white arrows indicate the dipole moments. The size of image (a) is: $250 \times 250 \text{ nm}^2$

3.8 Growth in the Out-of-Plane Direction of the Resulting Ordered Objects

The out-of plane growth is based on interdigitation of α -helices (interdigitation takes place along vertical direction; see later). An interdigitated molecular arrangement can compensate for the high dipole–dipole interaction between α -helices during the course of growth.

Each α -helix carries a considerable permanent dipole moment of about 3.5 Debye per unit. Its value can be approximated by placing 0.5–0.7 positive unit charge near the N-terminus and 0.5–0.7 negative unit charge near the C-terminus of the α -helix. An interdigitated molecular arrangement with alternating directions of the peptide blocks from neighbouring molecules (see Fig. 16c) allows the compensation of these high dipole moments of α -helices. Such an arrangement can also explain, along and normal to the PS chain axis (as indicated in Fig. 1), a 2D growth of structures. It should be noted that PBLGlu α -helices have the tendency to be aligned parallel to the substrate due to the high dipole interactions between PBLGlu α -helices and the hydrophilic substrate. It seems even possible to link PBLGlu α -helices via hydrogen bonds to OH groups of the UV/ozone-treated silicon substrate.

Figure 17 presents a case where clear steps in height inside ordered structures could be observed. A thinner region inside an ordered object (see the dark part in

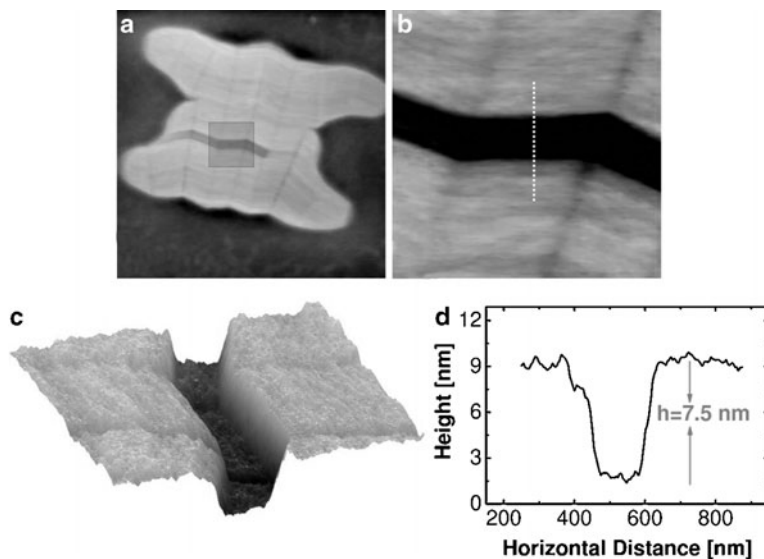


Fig. 17 (a) AFM topography image showing a complex coalesced multistructure. (b) Magnification of *grey square* in (a) showing a defect. (c) 3D representation of the defect shown in (b). (d) Height profile made in the region indicated by the *white broken line* in (b). The sizes of images are (a) 5×5 , (b, c) $1 \times 1 \mu\text{m}^2$

Fig. 17b, c) offered a possibility to visualize how the ordered structures are built up in the direction normal to the surface plane. A cross-section (see height profile in Fig. 17d) yielded a depth of this zone of about 7.5 nm. This value is comparable to the estimated total length of the molecule along the PS chain axis of 7.5 nm (see Fig. 1c). Such steps within the ordered structures, having a mean height about 7.5 nm were observed quite frequently in experiments. Thus, one may assume that the $\text{PS}_{63}\text{-(PBLGlu}_{37})_8$ molecules are stacked with the PS main chain axis normal to the substrate plane.

On the basis of the experiments shown above, one may suppose that the growth in height of the observed ordered structures can be explained by a stratified arrangement, i.e., lamellar layering (see Fig. 18). Such an arrangement of the peptide blocks would avoid the unfavorable contact between the PS segments and the hydrophilic silicon substrate.

3.9 Concerted Changes of the Growth Direction: Dependence on Polymer Architecture

Finally, there is an interesting and so-far unexplained feature that appeared when structures became larger than about $1 \mu\text{m}$. In Figs. 11, 13f, 15c–e and 17a–c, one can detect concerted changes in the growth direction for these large-scale structures.

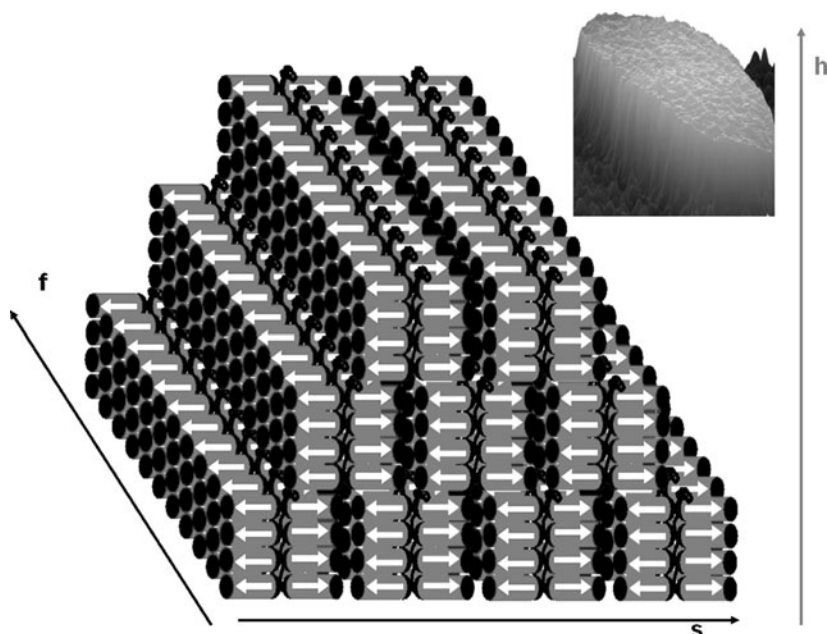


Fig. 18 Possible 3D molecular organization model of $\text{PS}_{63}\text{-(PBLGlu}_{37})_8$ heteroarm star block copolymer. The *inset* represents a 3D AFM topography image showing a typical ellipsoidal solid structure

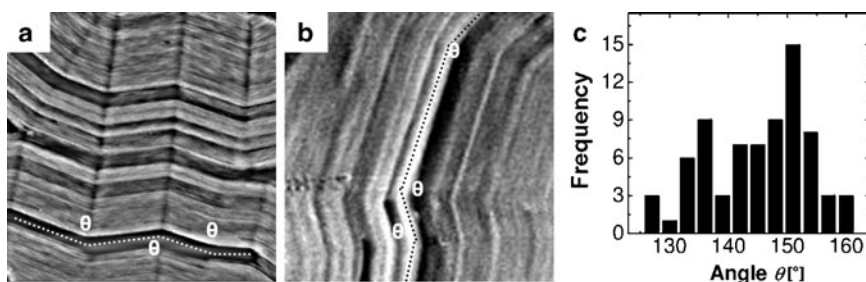


Fig. 19 (a) TM-AFM phase image showing a magnification of the film surface presented in Fig. 13f. (b) TM-AFM phase image showing a magnification of the film surface presented in Fig. 15c. (c) Distribution of orientation angle (θ) showing the number of appearances of a certain orientation angle over 100 measured values. The *white* and *black dotted lines* in (a) and (b) emphasize the orientation angles denoted by θ . Sizes of images are (a) 1×1 , and (b) $1.74 \times 1.74 \mu\text{m}^2$

A multitude of long, parallel straight lines show a simultaneous change in orientation, causing a change of the orientation angles by a well-defined value. Examination of a large number of such large-scale structures yielded an angle (denoted by θ) of about $135\text{--}157^\circ$ between two consecutive domains (see Fig. 19).

The most frequent values were centered around 136° and 151° , with the occurrence of 151° being almost twice as often as that of 136° . It may be concluded

that the large scale structures formed at a c_P close to $c_{critical}$ did not grow in a straight line to big sizes, but that concerted and cooperative discrete changes in orientation angle occurred at distances of the order of $1\ \mu\text{m}$.

One may ask if this effect of changing orientation depends on macromolecular polypeptide architecture. To answer this question, various other polypeptide systems having different architecture were examined. Thin films made of PBLGlu homopolymer, linear $\text{PS}_{52}\text{-PBLGlu}_{104}$ diblock copolymer, linear $\text{PS}_{52}\text{-PBLGlu}_{31}$ and star shaped $\text{PS}_{63}\text{-(PBLGlu}_{37})_8$ were exposed simultaneously to chloroform vapor under ambient air conditions in an “open” system with a continuous but slow evaporation of gas (estimated to be about $0.2\ \text{mL/h}$) from the sample container to the environment. This allowed a slow increase in the polymer concentration c_P .

Under such conditions, the initial polymer concentration c_P in the films was estimated to be about $50 \pm 20\%$. After 195 h, the films were taken out of this sample chamber and dried completely at room temperature. Investigating all four samples by OM and AFM demonstrated a clear ordering process (see Fig. 20). OM

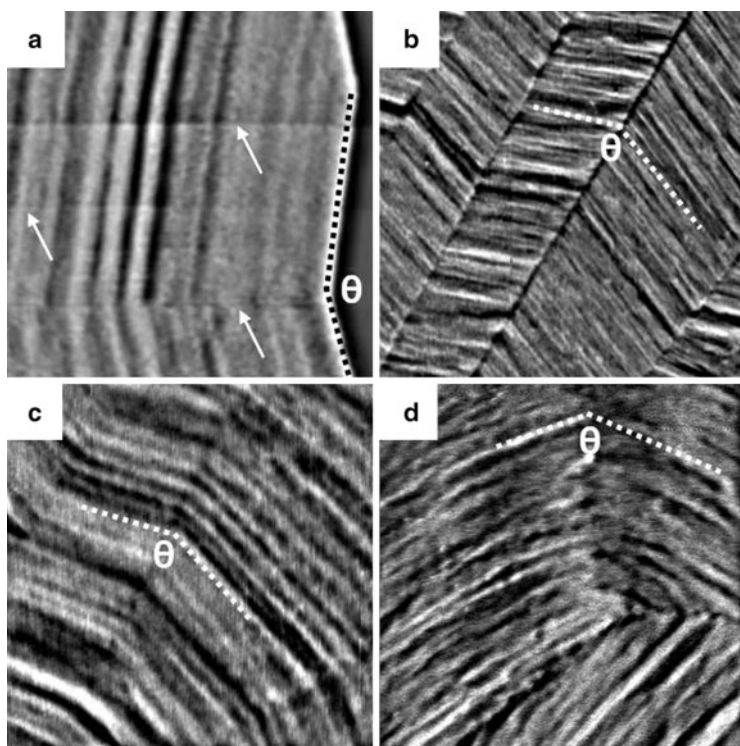


Fig. 20 TM-AFM phase images showing the morphology of (a) a $54 \pm 2\ \text{nm}$ thick film made of $\text{PS}_{63}\text{-(PBLGlu}_{37})_8$ star block copolymer; (b) a $60 \pm 3\ \text{nm}$ thick film made of $\text{PS}_{52}\text{-PBLGlu}_{31}$ diblock copolymer; (c) a $65 \pm 3\ \text{nm}$ thick film made of $\text{PS}_{52}\text{-PBLGlu}_{104}$ diblock copolymer; and (d) a $70 \pm 3\ \text{nm}$ thick film made of PBLGlu homopolymer. All three films were exposed to chloroform vapor for 195 h under ambient air conditions in an “open” system. The white arrows in (a) indicate artifacts (horizontal lines) resulting from removal of some noisy lines acquired during TM-AFM scanning. Sizes of images are (a) 1.75×1.75 , (b, c) 1.5×1.5 , and (d) $0.5 \times 0.5\ \mu\text{m}^2$

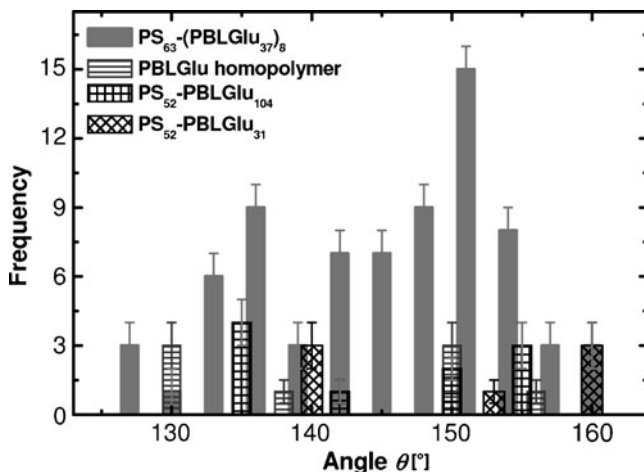


Fig. 21 Orientation angle (θ) distribution showing the number of appearances of a certain orientation angle over 100 measured values for: PS₆₃-(PBLGlu₃₇)₈, PBLGlu homopolymer, PS₅₂-PBLGlu₁₀₄, and PS₅₂-PBLGlu₃₁

(not shown) confirmed that large-scale ordered structures, up to tens of micrometers, were obtained for all systems. As revealed by AFM, all four polymer systems showed micrometer-long, straight parallel stripes that often changed their orientation (see Fig. 20). The measured orientation angles for all four polymer systems were found to be in the range of 130–160°. A summary of an extended study is presented in Fig. 21, which clearly demonstrates that the concerted discrete changes in orientation occurred in a similar way in all the studied polypeptide systems, independent of architecture.

4 Conclusions

OM allows the direct observation in real time of nucleation and growth in thin solution films, here demonstrated for the formation of ordered polypeptide structures. The variation of the nucleation density (number of nuclei per area) with concentration could be determined by combining OM and AFM. Interestingly, the nucleation density was sensitively affected by the humidity of the surrounding gas phase. For example, in dry air up to about 50% of polymer could be homogeneously dissolved in chloroform, whereas only about 20–30% of polymer could be dissolved under ambient air conditions without formation of ordered structures. The influence of humidity can be expressed in terms of the c_{critical} , below which no structures were formed. Increasing the humidity of the surrounding gas phase led to a decrease of the value of the c_{critical} . The functional dependence of the number of ordered objects per unit area on c_p , in combination with theoretical considerations, allowed the determination of a value for the interfacial tension σ between the polymer and the solution. Accordingly, the decrease in c_{critical} with humidity can be linked to

an increase in σ . It is proposed that complexation between water molecules and PBLGlu chains, favored by hydrogen-bonding interactions, is responsible for the decrease of the “solubility” of the polymer in chloroform, leading to ordering at even very low c_p . Furthermore, it could be demonstrated that other protic solvents can also cause a similar decrease in solubility. Consequently, the solubility of complex molecules like polypeptides (which contain sites of different polarity, hydrophilicity, or hydrophobicity) not only depends on the quality of the solvent chosen but can also be varied by the presence of small amounts of a non-solvent, which nonetheless can interact locally with specific sites on the molecule.

At a given concentration, the resulting ellipsoidal structures grew to a certain size and then growth stopped. However, after an abrupt increase of the concentration, additional structures of smaller size but of similar shape formed. This arrest of growth was due to a decrease of the concentration of the surrounding solution below supersaturation, i.e., the reservoir was depleted by molecules integrated into the ordered structures. Consequently, such two-step growth processes led to a bimodal distribution in size of ordered structures in the film.

All structures possessed an anisotropic ellipsoidal shape, which can be attributed to asymmetric growth in lateral directions. The surface of these structures exhibited straight parallel stripes of a width similar to the molecular dimension of the peptide blocks. On the basis of these results, it can be concluded that anisotropic structure formation is due to specific directional interactions acting along the various axes of the molecules. Intermolecular hydrogen bonds act normal to long axis of PBLGlu α -helices. This might explain the existence of parallel straight stripes over large scales and spaced at a molecular distance. The existence of steps in height of molecular dimension, along the axis normal to substrate, suggests a stratified arrangement, i.e., lamellar layering of the molecules.

Large-scale structures formed at a polymer concentration slightly above c_{critical} showed growth morphologies dominated by concerted discrete changes in orientation of a multitude of parallel stripes. The experiments performed in this work proved that the ellipsoidal morphology and the appearance of concerted changes in orientation during the growth of large-scale structures depended on neither the environmental conditions nor the polymer architecture. Thus, the ordering process of polypeptide-based copolymers and the resulting morphology were basically controlled by the solubility of the polymer.

Acknowledgements We are indebted and grateful to Hildegard Kukula for polymer synthesis. We acknowledge financial support provided through the European Community’s “Marie-Curie Actions” under contract MRTNCT- 2003-505027 [POLYAMPHI]. Use of the Center for Nanoscale Materials was supported by the US Department of Energy, Office of Science, Office of Basic Energy Sciences, under Contract No. DE-AC02-06CH11357.

References

1. Stryer L (1988) Biochemistry. W H Freeman, New York
2. Börner HG, Schlaad H (2007) Bioinspired functional block copolymers. *Soft Matter* 3: 394–708

3. Lee M, Cho B-K, Zin W-C (2001) Supramolecular structures from rod-coil block copolymers. *Chem Rev* 101:3869–3892
4. Klok H-A, Lecommandoux S (2006) Solid-state structure, organization and properties of peptide–synthetic hybrid block copolymers. *Adv Polym Sci* 202:75–111
5. Muthukumar M, Ober CK, Thomas EL (1997) Competing interactions and levels of ordering in self-organizing polymeric materials. *Science* 277:1225–1232
6. Chen JT, Thomas EL, Ober CK, Hwang SS (1995) Zigzag morphology of a poly(styrene-*b*-hexyl isocyanate) rod-coil block copolymer. *Macromolecules* 28:1688–1697
7. Chen JT, Thomas EL, Ober CK, Mao G-P (1996) Self-assembled smectic phases in rod-coil block copolymers. *Science* 273:343–346
8. Schlaad H, Krasia T, Antonietti M (2004) Superhelices of poly[2-(acetoacetoxy)ethyl methacrylate]. *J Am Chem Soc* 126:11307–11310
9. Vonau F, Suhr D, Aubel D, Bouteiller L, Reiter G, Simon L (2005) Evolution of multilevel order in supramolecular assemblies. *Phys Rev Lett* 94:066103
10. Zhou Y, Hall CK, Karplus M (1996) First-order disorder-to-order transition in an isolated homopolymer model. *Phys Rev Lett* 77:2822–2825
11. Ludwigs S, Krausch G, Reiter G, Losik M, Antonietti M, Schlaad H (2005) Structure formation of polystyrene-block-poly(γ -benzyl-L-glutamate) in thin films. *Macromolecules* 38:7532–7535
12. Minich EA, Nowak AP, Deming TJ, Pochan DJ (2004) Rod–rod and rod–coil self-assembly and phase behavior of polypeptide diblock copolymers. *Polymer* 45:1951–1957
13. Schlaad H, Antonietti M (2003) Block copolymers with amino acid sequences: molecular chimeras of polypeptides and synthetic polymers. *Eur Phys J E* 10:17–23
14. Botiz I, Grozev N, Schlaad H, Reiter G (2008) The influence of protic non-solvents present in the environment on structure formation of poly(γ -benzyl-L-glutamate) in organic solvents. *Soft Matter* 4:993–1002
15. Losik M, Kubowicz S, Smarsly B, Schlaad H (2004) Solid-state structure of polypeptide-based rod-coil block copolymers: Folding of helices. *Eur Phys J E* 15:407–411
16. Schlaad H, Smarsly B, Below I (2006) Solid-state structure of polystyrene-block-poly(γ -benzyl-L-glutamate): helix folding vs stretching. *Macromolecules* 39:4631–4632
17. Hol WGJ, van Duijnen PT, Berendsen HJC (1979) The α -helix dipole and the properties of proteins. *Nature* 273:443–446
18. Kukula H, Schlaad H, Tauer K (2002) Linear and star-shaped polystyrene-block-poly(sodium glutamate)s as emulsifiers in the heterophase polymerization of styrene. *Macromolecules* 35:2538–2544
19. Sakamoto R (1984) Phase separation of poly(γ -benzyl-L-glutamate) to liquid crystal and isotropic solution in various helicogenic solvents. *Coll Polym Sci* 262:788–792
20. Wee EL, Miller WG (1971) Liquid crystal-isotropic phase equilibria in the system poly(γ -benzyl α -L-glutamate)-methylformamide. *J Phys Chem* 75:1446–1452
21. Flory PJ (1956) Statistical thermodynamics of semi-flexible chain molecules. *Proc R Soc Lond A* 234:60–73
22. Robinson C (1956) Liquid-crystalline structures in solutions of a polypeptide. *Trans Faraday Soc* 52:571–592
23. Watanabe J, Goto M, Nagase T (1987) Thermotropic polypeptides. 3. Investigation of cholesteric mesophase properties of poly(γ -benzyl-L-glutamate-co- γ -dodecyl-L-glutamates) by circular dichroic measurements. *Macromolecules* 20:298–304
24. Russo PS, Miller WG (1983) Coexistence of liquid crystalline phases in poly(γ -benzyl α -L-glutamate)-dimethylformamide. *Macromolecules* 16:1690–1693
25. He S-J, Lee C, Gido SP, Yu SM, Tirrell DA (1998) A twist grain boundary-like twisted smectic phase in monodisperse poly(γ -benzyl α -L-glutamate) produced by recombinant DNA techniques. *Macromolecules* 31:9387–9389
26. Watanabe J, Imai K, Uematsu I (1978) Light scattering studies of poly(γ -benzyl L-glutamate) solutions and films. *Polym Bull* 1:67–72
27. Toriumi H, Minakuchi S, Uematsu Y, Uematsu I (1980) Helical twisting power of poly(γ -benzyl-L-glutamate) liquid crystals in mixed solvents. *Polym J* 12:431–437

28. Uematsu I (1984) Polypeptide liquid crystals. *Adv Polym Sci* 59:37–73
29. Robinson C, Ward JC (1957) Liquid-crystalline structures in polypeptides. *Nature* 180: 1183–1184
30. Robinson C, Ward JC, Beevers RB (1958) Liquid crystalline structure in polypeptide solutions. Part 2. *Discuss Faraday Soc* 25:29–42
31. Hill A, Donald AM (1989) Phase behaviour of poly-(γ -benzyl-L-glutamate) in benzyl alcohol. *Liq Cryst* 6:93–110
32. Block H, Shaw CP (1992) Second-harmonic generation in poly(α -amino acid) and poly(isocyanate) films. *Polymer* 33:2459–2462
33. Oxtoby DW (1992) Homogeneous nucleation: theory and experiment. *J Phys Condens Matter* 4:7627–7650
34. Sear RP (2007) Nucleation: theory and applications to protein solutions and colloidal suspensions. *J Phys Condens Matter* 19:033101
35. Mohanty R, Bhandarkar S, Estrin J (1990) Kinetics of nucleation from aqueous solution. *AIChE J* 36:1536–1544
36. Nielsen AE (1969) Nucleation and growth of crystals at high supersaturation. *Kristall und Technik* 4:17–38
37. Russo PS, Miller WG (1984) On the nature of the poly(γ -benzyl glutamate)-dimethylformamide “complex phase”. *Macromolecules* 17:1324–1331
38. Brandrup J, Immergut EH (1989) *Polymer handbook*, 3rd edn. Wiley, Chichester

Amphiphilic Polymers at Interfaces

**Katarzyna Kita-Tokarczyk, Mathias Junginger, Serena Belegriou,
and Andreas Taubert**

Abstract Self-assembly phenomena in block copolymer systems are attracting considerable interest from the scientific community and industry alike. Particularly interesting is the behavior of amphiphilic copolymers, which can self-organize into nanoscale-sized objects such as micelles, vesicles, or tubes in solution, and which form well-defined assemblies at interfaces such as air–liquid, air–solid, or liquid–solid. Depending on the polymer chemistry and architecture, various types of organization at interfaces can be expected, and further exploited for applications in nanotechnology, electronics, and biomedical sciences.

In this article, we discuss the formation and characterization of Langmuir monolayers from various amphiphilic block copolymers, including chargeable and thus pH-responsive materials. Solid-supported polymer films are reviewed in the context of alteration of surface properties by ultrathin polymer layers and the possibilities for application in tissue engineering, sensors and biomaterials. Finally, we focus on how organic and polymer monolayers influence the growth of inorganic materials. This is a truly biomimetic approach since Nature uses soft interfaces to control the nucleation, growth, and morphology of biominerals such as calcium phosphate, calcium carbonate, and silica.

K. Kita-Tokarczyk (✉)

Department of Chemistry, University of Basel, 4056 Basel, Switzerland
present address: Centre for Molecular Nanoscience, School of Chemistry, University of Leeds,
Leeds LS2 9JT, UK
e-mail: k.kita@leeds.ac.uk

M. Junginger and A. Taubert (✉)

Institute of Chemistry, University of Potsdam, 14476 Golm, Germany
and
Max-Planck-Institute of Colloids and Interfaces, 14476 Golm, Germany
e-mail: junginge@uni-potsdam.de; ataubert@uni-potsdam.de

S. Belegriou

Department of Chemistry, University of Basel, 4056 Basel, Switzerland
e-mail: serena.belegriou@unibas.ch

Keywords Amphiphilic polymers · Langmuir monolayers · Polymers on surfaces · Bio-inspired mineralization

Contents

1	Amphiphilic Polymers at the Air–Water Interface	154
1.1	Soluble and Insoluble Monolayers at the Air–Water Interface	154
1.2	Characterization of Langmuir Monolayers	155
1.3	Polymer Monolayers	159
1.4	Monolayers from Amphiphilic Block Copolymers	160
2	Amphiphilic Block Copolymers on Solid Surfaces	175
2.1	Planar Thin Block Copolymer Films on (Planar) Solid Surfaces	175
2.2	Block Copolymer Aggregates on Planar Solid Surfaces	182
3	Mineralization of Amphiphilic Polymers and Related Compounds	186
3.1	Mineralization at the Air–Water Interface	186
3.2	Mineralization at the Air–Water Interface with Additives in the Subphase	190
3.3	Mineralization at the Solid–Liquid Interface	191
	References	196

Abbreviations

A	Mean area per molecule
AFM	Atomic force microscopy
ATRP	Atom transfer radical polymerization
BAM	Brewster angle microscopy
BF	Breath figure
BSA	Bovine serum albumin
C_s	Compressibility
CA	Contact angle
cac	Critical aggregation concentration
d	Monolayer thickness
DMAP	4-Dimethylamino-pyridine
DOPE	Dioleoyl phosphatidyl ethanolamine
FTIR	Fourier transform infrared (spectroscopy)
G	Gas (monolayer phase)
HOPG	Highly ordered pyrolytic graphite
I	Relative reflectivity
I_0	Incident light intensity
I_r	Reflected light intensity
L–B	Langmuir–Blodgett (film transfer)
LbL	Layer-by-layer
LC	Liquid condensed (monolayer phase)
LCST	Lower critical solution temperature

LE	Liquid expanded (monolayer phase)
LS	Superliquid (monolayer phase)
L-S	Langmuir-Schaefer (film transfer)
MPC	2-Methacryloyloxyethyl phosphorylcholine
m-PDA	10,12-Pentacosadiynoic acid
NTA	Nitrilotriacetic acid
OmpF	Outer membrane protein F
p	Pressure
P2VP	Poly(2-vinyl pyridine)
P4VP	Poly(4-vinyl pyridine)
PAA	Poly(acrylic acid)
PB	Polybutadiene
PBLG	Poly(γ -benzyl-L-glutamate)
PCL	Poly(ϵ -caprolactone)
PDEAM	Poly(2,2-diethylaminoethyl methacrylate)
PDMAEMA	Poly(2,2-dimethylaminoethyl methacrylate)
PDMS	Poly(2-dimethyl siloxane)
PEE	Poly(ethyl ethylene)
PEG	Poly(ethylene glycol)
PEO	Poly(ethylene oxide)
PFMA	Poly(perfluorohexylethyl methacrylate)
PFS	Poly(ferrocenyl silane)
PHEMA	Poly(2-hydroxyethyl methacrylate)
PI	Polyisoprene
PLA	Poly(lactic acid)
PLLys	Poly(L-lysine)
PMAA	Poly(methacrylic acid)
PMBPS	Poly[(+)-2,5-bis(4'-(<i>S</i>)-2-methylbutoxy)phenyl]styrene]
PMOXA	Poly(2-methyl-2-oxazoline)
PNIPAM	Poly(<i>N</i> -isopropylacrylamide)
POPC	Palmitoyl oleoyl phosphatidylcholine
POSS	Polyhedral oligomeric silsesquioxane
PP	Polypropylene
PPO	Poly(propylene oxide)
PPS	Poly(propylene sulfide)
PS	Polystyrene
PSS	Poly(styrene sulfonate)
PtBA	Poly(<i>tert</i> -butyl acrylate)
PTFE	Poly(tetrafluoroethylene)
π	Surface pressure
π_{coll}	Collapse pressure
π_{k}	Surface pressure (from kinetic movements)
π_{r}	Surface pressure (from repulsion of charges)
π_{s}	Surface pressure (from carbon chains repulsion)
RAFT	Reversible addition fragmentation chain transfer (polymerization)

S	Solid (monolayer phase)
SAM	Self-assembled monolayer
SANS	Small angle neutron scattering
SBF	Simulated body fluid
T	Temperature
T_g	Glass transition temperature
TEOS	Tetraethyl orthosilicate
<i>t</i> BA	<i>tert</i> -Butyl acrylate
THF	Tetrahydrofuran
XPS	X-ray photoelectron spectroscopy

1 Amphiphilic Polymers at the Air–Water Interface

1.1 Soluble and Insoluble Monolayers at the Air–Water Interface

The air–water interface is a phase boundary where many physicochemical phenomena take place. Some examples are biofilm formation on the surface of oceans, foaming of soap in a bath tub, and oil lenses on the surface of freshly cooked soup, which are all interface-related phenomena. Each of these examples, however, has a slightly different underlying principle.

The asymmetry of the air–water interface with respect to the dielectric permittivity of the two media, water and air, is responsible for phenomena such as adsorption/desorption from/to solution, and spreading of molecules on the free water surface [1]. When a molecule bearing an electric moment is placed in a phase boundary region between air and water, its orientation will no longer be random. To the contrary, it will strongly depend on the type of intermolecular interactions in the bulk liquid and interactions among the molecules (of the same kind) in the interfacial region. Surfactant molecules in the film will be oriented in such a way that the parts of higher electric field density are directed towards the medium of higher dielectric permittivity. Harkins [1] described the above differently, postulating the rule of the least dramatic change of the force field, which says that molecules adopt such an orientation at the interface so that transferring a molecule from one phase to another is least dramatic.

Adsorption refers to a tendency of water-soluble amphiphilic molecules (surfactants) to preferentially gather at the interface, and thus minimize their free energy by adopting a specific molecular orientation, i.e. hydrophilic parts of the molecule will be anchored in water, while hydrophobic parts will be exposed to air. The number of molecules that adsorb to the interface (and thus the layer lateral density) will depend on the chemical constitution, amphiphilicity, and solubility of the material. It is known that at a specific concentration called the “critical aggregation concentration” (cac), aggregates will start forming in solution and remain in equilibrium with the adsorbed (Gibbs) layer. Therefore, from that point on, no further

adsorption can be expected – instead, various self-assembled morphologies are built in solution. Adsorption in surfactant systems is typically described by the extent of lowering of the surface tension of water. The slope of a Gibbs isotherm (surface tension versus log concentration) defines the interfacial activity of a surfactant and allows calculation of the molecular area in the adsorbed film.

Several classes of amphiphilic compounds, such as lipids and some polymers, are characterized by very low cac values. This means that they are practically insoluble in water, and studies of their adsorption behavior are hardly possible. On the other hand, they dissolve in organic solvents, and from such solvents the compounds can be spread at the air–water interface. This way, after the solvent evaporates, insoluble (Langmuir) films are formed, which also lower surface tension of water. However, due to very poor solubility of the constituting material, the equilibrium between the interfacial film and the molecules in solution is strongly shifted towards film formation. This fact is important for experimental investigations of Langmuir monolayers, where two-dimensional film behavior can be studied assuming that there is no partitioning of the molecules between the film and bulk (subphase).

1.2 Characterization of Langmuir Monolayers

1.2.1 Surface Pressure–Area Isotherms

In practice, Langmuir monolayers are investigated by using a Langmuir trough – a Teflon trough filled with water, aqueous salt solution or buffer, and equipped with one or two moving barriers. The barriers compress the interfacial layer only, therefore the area available for molecules will decrease, and the response of the film can be monitored. Conventionally, surface pressure is measured, which is the difference between the surface tensions of the pure subphase (water or buffer) and the subphase covered by the film. Surface pressure (π) can be thus considered as the two-dimensional analogue of pressure (p).

The most common method for measuring surface pressure is the Wilhelmy method [2, 3]. A thin plate of highly wettable material (platinum, mica or filter paper), is placed in water perpendicularly to the free water surface. By means of a torsion wire, the plate is coupled to a force-measuring device. The force is measured to compensate for the mass increase of the plate due to the contact angle (CA) change when the amphiphilic material makes a film. The CA is, in turn, related to surface tension.

For Langmuir films, surface pressure is plotted against the area per molecule (A), resulting in π – A isotherms. The pattern of such isotherms depends not only on the chemical structure of the film-forming substance, but also on experimental conditions. The increase in surface pressure corresponds to more ordered phases in the film. The π – A isotherm of a monolayer provides basic information on the material's film-forming properties and the area per molecule at different stages of film compression. Additionally, conclusions may be drawn on the presence and

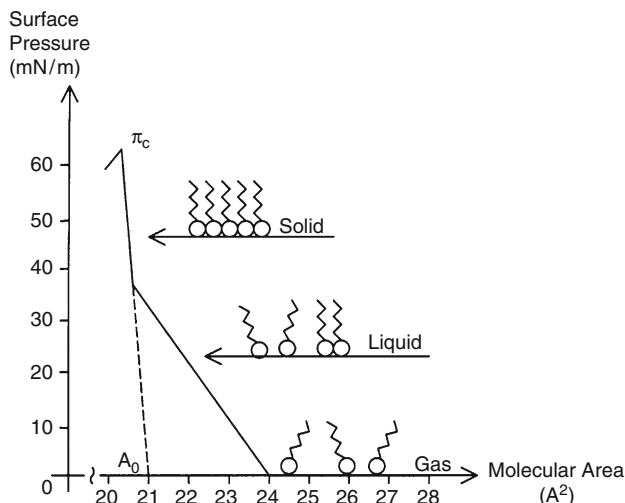


Fig. 1 Surface pressure–area isotherm from stearic acid. π_c is film collapse pressure; A_0 represents the molecular area in the most condensed state of a monolayer. Reprinted from [164] with permission. Copyright 2004 Nima Technology

kind of phase transitions in the film, monolayer stability at given experimental conditions, and the film collapse pressure, π_{coll} . Moreover, compressibility (C_s) of the monolayer phases can be calculated.

In the case of Langmuir films, depending on the number of molecules per unit area (surface density), surface phases are distinguished as the analogues of three-dimensional phases, namely gas (G), condensed liquid (LC) and solid (S), Fig. 1. Additionally, two phases exist: expanded liquid (LE) and superliquid (LS), an intermediate between condensed liquid and solid [1]. The film's physical state is primarily determined by intermolecular interactions between amphiphilic molecules, the range and strength of which change with film compression. Also, changes are observed in the orientation and packing of molecules at the interface.

At very large molecular areas (where the surface pressure is close or equal to zero), a monolayer displays similarity to a two-dimensional gas. Molecules on the surface do not interact and have practically unlimited freedom of translation in two dimensions, analogously to the ideal gas. Because the mean area per molecule is many times larger than the actual molecular size, virtually no limitations are present as to the molecular orientation at the water surface. Monomolecular films in the gas state are not particularly interesting when studying molecular organization in two dimensions; however, when compressing such a gaseous monolayer we can learn at which mean molecular area the molecules actually start interacting and the film formation process starts.

Upon film compression, the area available per molecule in the film decreases and intermolecular interactions become stronger as the molecules approach each other. Additionally, molecular dimensions can no longer be neglected, and interactions

among hydrocarbon chains should be taken into account. Considering ionized monolayers, an increase in surface pressure is observed due to mutual repulsion between charged molecules, which is a deviation from the ideal gas state. Davies and Rideal [4] suggested that the measured surface pressure is the sum of π_s (carbon chain repulsion), π_k (pressure from the kinetic movement of molecules), and π_r (repulsion of the charged fragments).

With continuous film compression, a first-order phase transition from the gaseous phase to a two-dimensional expanded liquid (LE) can be observed [5]. In this region, the π - A dependency is of hyperbolic shape for most compounds, and the monolayer compressibility is considerably lower than in the gas phase, because cohesion forces act between hydrocarbon chains. Harkins and Jura [6] applied the relationship between film compressibility and molecular area as a possible interpretation of the liquid expanded state; compressibility, C_s , was defined as $C_s = -\frac{1}{A} \left(\frac{\partial A}{\partial \pi} \right)_T$.

When the film is compressed further, an increase in surface pressure is observed as compressibility decreases, where the π - A dependency becomes approximately linear. Such a state is called the liquid condensed (LC) phase, and is analogous to a three-dimensional liquid. This phase is characterized by strong intermolecular interactions. Further isothermal compression of a monolayer leads to its conversion from a liquid to solid (S) state, which occurs at low area per molecule. For many alcohols and carboxylic acids, the above transition takes place with the occurrence of an LS phase [7]. The surface pressure at which the above transition appears is strongly dependent on temperature (T), and, for substances whose hydrophobic part is a straight alkyl chain, also on the kind of polar group. In the solid phase, long-range molecular packing is observed. Molecules are oriented perpendicular or almost perpendicular to the free water surface, the π - A isotherm is linear and characterized by a steep slope (typical for low film compressibility) and the presence of strong interactions between the hydrocarbon chains.

The surface phases not only differ with respect to molecular packing, but also regarding ordering within condensed domains [8]. Four parameters describe individual phases [5]: positional ordering, bond direction (crystalline lattice) ordering, ordering with respect to molecular axes inclination, and axis symmetry, which describes the arrangement of double bonds planes. The above parameters allow for differentiation between short-range packing (which decreases exponentially with distance) and quasi long-distance packing.

Further monolayer compression beyond the solid phase is practically impossible, as it would decrease the area per molecule down to values smaller than actual molecular areas. Therefore, the compression of a solid film inevitably leads to multilayer formation and, subsequently, to film collapse. This collapse is observed in the π - A isotherm as a sudden change in the slope of the solid phase line, beyond which surface pressure does not increase anymore.

1.2.2 Brewster Angle Microscopy

The most common microscopy technique for visualizing monolayers at the air–water interface is Brewster angle microscopy (BAM) [9]. The information available from BAM images concern monolayer morphology (domain formation, aggregation and crystallization of molecules at the surface) and the existence of surface phases. The BAM's advantage is that the addition of dyes and markers is not required – images are obtained owing to the difference in light reflectivity by regions of different thickness.

The intensity of light reflected from the phase boundary between two media (air and aqueous solution) whose refractive indices are n_1 and n_2 , respectively, depends on the angle of incidence and polarization of the incident light. In the case of the phase boundary covered with a thin surface film, the intensity of reflected light is minimal at the Brewster angle, but it does not vanish totally and is sufficient to obtain a monolayer image using a sensitive camera (Fig. 2.) The intensity of the reflected light strongly depends on the phase boundary properties, such as monolayer thickness (d), interface roughness [9], and monolayer anisotropy [10].

BAM is an excellent tool for the observation of various changes in monolayers, such as the degree of film ordering at various compression phases, domain formation, phase transitions, monolayer transformation into a multilayer structure, and the influence of ions and other additives contained in the aqueous phase on the properties of surface films [11]. The microscopic observation of monolayer changes with temperature allows the building of phase diagrams of monolayers from amphiphilic substances [5, 12]. In combination with other techniques, BAM may be used for the estimation of the inclination angles of molecules in certain phases of the monolayer [13]. BAM was also applied for the observation of surface structures in adsorption films [14], and in studies on the influence of water-soluble detergents on the behavior of Langmuir monolayers [15, 16].

Rodríguez Patino et al. [17] presented a method for estimating monolayer thickness (d) from relative intensity of light reflected from the interface. The grey level scale of BAM images was correlated to the relative reflectivity (I) – this allows for the estimation of changes in d upon film compression. The above method can only be applied to monolayers displaying no optical anisotropy, i.e. monolayers for which one value of refractive index can be assumed. For the calculation of surface film

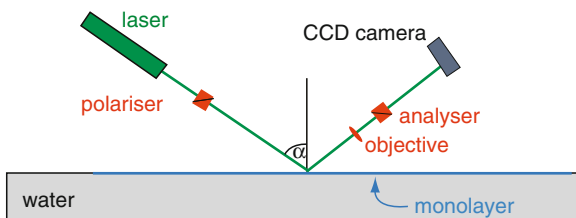


Fig. 2 Scheme of the Brewster angle microscope; α denotes the angle of incidence

thickness, the following formula is used: $I = C \cdot d^2$, where I is relative reflectivity, calculated as the ratio of reflected light intensity, I_r , and incident light intensity I_0 ($I = I_r/I_0$), and C is a constant.

It needs to be mentioned here that many other experimental techniques are available for studying monolayers at the air–water interface. Most frequently, surface potential is measured to evaluate the molecular orientation of amphiphiles at the interface. This method is, however, better suited to the study of small molecules. Polymeric amphiphiles, due to their conformational dynamics, are difficult to analyze and simple dielectric layer models do not apply, or produce large errors. Grazing incidence X-ray diffraction provides information on molecular packing, and spectroscopic methods are used to study molecular interactions and the structural changes of molecules upon compression. Fluorescence microscopy is useful for studying two-dimensional organization of small molecular mass amphiphiles; however, it is not applied to polymer monolayers. For a more comprehensive overview of experimental methods used to study monolayers at the air–water interface, the reader is referred to more specialized articles, e.g. [18].

1.3 Polymer Monolayers

The formation of polymer films at the air–water interface includes slightly different requirements than those known for amphiphiles of small molar mass. In particular, films of homopolymers can be built [19–21], in which cases no amphiphilic balance can be discussed; to the contrary, the balance of interactions between macromolecular chains and between macromolecules and water controls the polymer spreadability. In other words, the bulk (subphase) cohesion has to be overcome by the attraction for the interface for the polymer to build stable monolayers [22]. It is not necessary that the polymer is water-insoluble, but individual monomers must be surface-active, i.e. must be able to adsorb to the interface from bulk solution.

In contrast to small molecules, the two-dimensional behavior of polymers at the air–water interface and the resulting surface pressure isotherms are to a large extent determined by multiple rearrangement possibilities of the polymer chains. In particular, transitions from a pancake to mushroom and brush conformations are observed, uncommon for short-chain amphiphiles (Fig. 3). Additionally, the behavior of water-soluble (hydrophilic) blocks is dramatically different from small polar headgroups (–OH, –COOH, phosphate, etc.). As long as the tendency of hydrophilic blocks to interact with water (buffer) is similar (in particular, that the hydrogen bond formation, electrostatic repulsion, and counter-ion stabilization phenomena are qualitatively the same), the large sizes of hydrophilic blocks in the case of polymers amplify those effects and, therefore, a high sensitivity of some hydrophilic blocks to environmental variables can be observed.

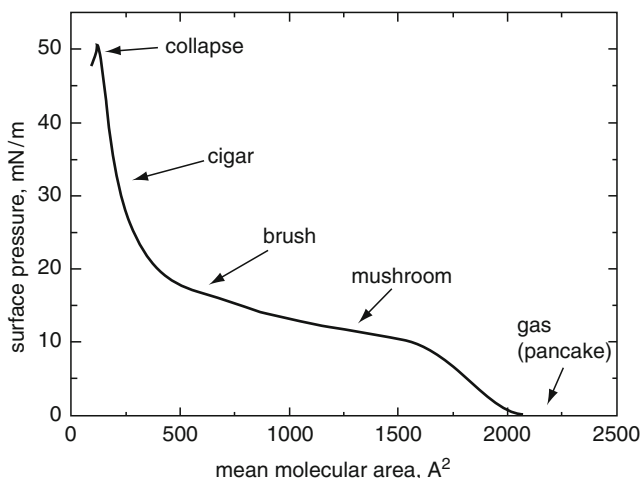


Fig. 3 Surface pressure–mean molecular area isotherm from an amphiphilic triblock copolymer. Nomenclature of polymer phases is shown. Reprinted from [66] with permission. Copyright 2006 American Chemical Society

1.4 Monolayers from Amphiphilic Block Copolymers

A certain class of polymers, block copolymers, is of special interest in the field of surface engineering owing to their unique molecular structure and the vast versatility of the resulting architectures (e.g. di-, tri- and starblock) [23]. Block copolymers are macromolecules composed of covalently linked sequences or blocks of two chemically distinct monomer units. Even monomers that are non-compatible (e.g. in terms of solubility or polarity) can be covalently linked and the resulting material exhibits custom-made novel properties. If the block copolymers are composed of a hydrophilic and a hydrophobic block, an amphiphilic molecule will result, capable of forming self-assembled aggregates in solution, Langmuir monolayers at the free water surface, and various structures on solid supports. In this section, we will review properties of floating (Langmuir) films from such macromolecular amphiphiles. We will then discuss their behavior on solids, and the potential applications of such nanoscale structures for controlling bio-inspired processes such as mineralization.

1.4.1 Poly(ethylene oxide)–Based Block Copolymers

Block copolymers containing poly(ethylene oxide) (PEO) have attracted attention, mainly due to the high hydrophilicity of this polymer and its biocompatible and protein-repellent properties. However, to promote formation of aggregates or monolayers, PEO has to be combined with a hydrophobic block.

The extensive plateau present in π - A isotherms from PEO-containing diblocks corresponds to PEO dehydration, until, at the high surface density regime at ca. 10mNm^{-1} , these hydrophilic blocks assume a brush-like conformation [24] and the mean molecular area is controlled solely by the hydrophobic block. In particular, polystyrene-poly(ethylene oxide), PS-PEO, monolayers were studied [25–27] for block copolymers of different PEO lengths. Experimental data reveal the plateau length scaling to be consistent with theoretical predictions and to show a continuous transition from self-similar layer to quasi-brush arrangement [27]. Additionally, those findings were confirmed by dynamic elasticity experiments [27, 28] on PS-PEO monolayers. More specifically, the methods of surface waves and light scattering were employed to evaluate the film elasticity and, thus, the relative contribution of the individual blocks to the film properties at various stages of compression.

The compressibility of PEO blocks in the subphase clearly depends on the size and properties of the hydrophobic block, and the dimension of the PEO fragment itself. For example, it was shown that PEO can be effectively compressed by a factor of three [29], following the predictions for PEO behavior in a good solvent. As mentioned before, desorption of PEO from the air–water interface and the formation of a brush was also observed in this case, and seems to be a well-established phenomenon.

Additionally, neutron reflectivity experiments for polymers with large PEO fractions show a depletion layer, due to the presence of a densely packed PS layer, with repulsive character towards the PEO blocks [25]. The formation of surface micelles was also suggested, similarly to polystyrene-poly(acrylic acid), PS-PAA, micelles at the air–water interface [30], to explain the film thickness variations at different compression stages. Multiple morphologies were indeed observed after transferring PS-PEO [31, 32] and PEO-PS-PEO [33] block copolymer films from water to solid substrates, including “dots” and spaghetti-like tubes, depending on the polymer structure (Fig. 4). On the other hand, a surface light scattering study on analogous PS-PEO diblock copolymers did not point to aggregation at the air–water interface [34]. To the contrary, significant PEO chain stretching into the aqueous phase was observed.

Apart from spherical and spaghetti-like aggregates, ring and chain morphologies were observed on glass surfaces after monolayer transfer [35], depending on the spreading concentration during film preparation. More specifically, high spreading concentrations lead to spaghetti-like structures, while monolayer compression starting from low surface coverage tends to result in rings and chains. The formation of such structures is attributed to the kinetically trapped mobility of PS chains, which, once entangled, retain this morphology. This observation demonstrates how sample preparation may strongly influence the self-assembly behavior of amphiphilic block copolymers on solid surfaces.

It is interesting to compare monolayers from PS-PEO block copolymers formed by linear and heteroarm star polymers, where the polymer architecture plays a significant role in the morphology of the interfacial film. In particular, star-shaped polymers tend to build well-defined circular domains after transfer to solid

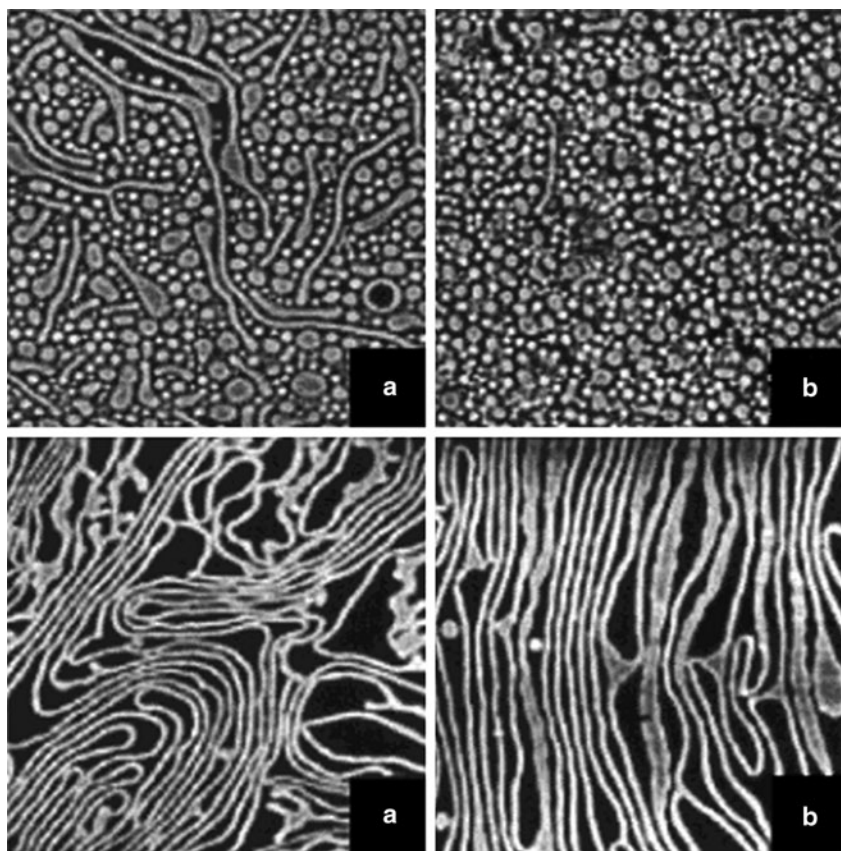


Fig. 4 Atomic force microscopy (AFM) images ($4 \times 4 \mu\text{m}$) of different morphologies observed in L-B films from a diblock copolymer, $\text{PS}_{459}\text{-}b\text{-PEO}_{82}$ (M_w 51,300 g mol^{-1}), transferred to silicon from the air–water interface. These structures are obtained by variation of experimental parameters: *top row (a)*, transfer pressure 1 mN m^{-1} ; *top row (b)*, transfer at 4 mN m^{-1} ; *bottom row (a) and (b)*, transfer at 2 mN m^{-1} . Reprinted from [31] with permission. Copyright 2002 American Chemical Society

substrates, behavior that is uncommon for linear diblock copolymers [36]. For star-shaped polymers, the formation of curved interfaces is favored, even at high surface pressure. In fact, surface pressure–area isotherms resemble isotherms measured for linear block copolymers with small PEO fraction, the difference being a considerable shift towards larger molecular areas. This effect is understandable for star-shaped molecular architectures. The authors suggest a packing model at the air–water interface, including transformation of the interfacial aggregates from lamellar via cylindrical to spherical [37], depending on the content of PEO. This interpretation should be feasible if no rearrangements take place during the film transfer to a solid substrate, which is assumed, but in fact not proven. Therefore, details of the molecular organization of those star copolymers at the air–water interface remain unsolved so far.

In the PS–PEO series, hyperbranched block copolymers were also studied [38], and showed a peculiar spreading behavior that was different from that of their linear and star counterparts. Namely, it is shown that for such hyperbranched polymers there is no clear separation of the monolayer to a hydrophilic and a hydrophobic region. To the contrary, both blocks form a uniform phase on the water surface, and thus the limiting molecular area depends on the total area of the whole polymer, irrespective of the block ratio. On the other hand, liquid and solid phases were observed upon compression, analogous to “classical” unbranched compounds, and the block ratio influenced the film morphology at higher surface pressure, leading to a bilayer formation from compounds of small PS content. The smaller area per molecule for polymers containing larger PS blocks is explained by the fact that such long chains would still have the possibility to orient towards the air phase, instead of spreading flat at the interface. In this way, a certain level of hydrophobic–hydrophilic segregation is observed.

When poly(perfluorohexylethyl methacrylate), PFMA, was used as the hydrophobic block, monolayers from PFMA–PEO–PFMA triblock copolymers [39, 40] essentially resembled the ones reported for PS–PEO diblocks with a low PS content. With longer PFMA blocks, two plateau regions are observed in the compression isotherms: one long region at 10 mNm^{-1} that is typical for PEO-containing monolayers, and one at higher surface pressures, above 30 mNm^{-1} , in the brush regime. This interesting feature is independent of the PEO content in the polymers, indicating a phase transition within the PFMA blocks to a closely packed layer. Good reversibility of the isotherms, however, does not support the possibility of polymer crystallization in that region. Instead, it is interpreted as rearrangement of the hydrophobic blocks from a horizontal to vertical packing at the interface.

In the case of polymers composed of PEO and a dendritic hydrophobic part, the molecular organization on the free water surface strongly depends on the dendrimer generation [41]. More specifically, low generation dendrimers do not exclude PEO from the interface, whereas the dimensions of high generation dendrimers are larger than the PEO hydrodynamic radius and, therefore, the hydrophilic block is forced into the aqueous phase. The hydrophilic–lipophilic balance plays an important role in film stability, again in terms of the dendron generation, i.e. higher generation dendrons are more hydrophobic and considerably increase film stability, making Langmuir–Blodgett (L–B) film transfers possible with a small number of defects.

A combination of PEO with a crosslinkable polybutadiene (PB) segment yields block copolymers that produce monolayers at the air–water interface, which can be further stabilized by crosslinking [42]. For example, Ahmed et al. successfully applied the crosslinking strategy to analysis of intermediate polymeric self-assembled structures formed during the transfer of a monolayer from air–water interface to a solid substrate. It is known that upon transfer, monomolecular films often reorganize due to the contact with a solid substrate – such interactions may lead to very interesting morphologies, however, the aggregates formed on solids most often do not reflect the true monolayer morphology at the free water surface. Therefore, “freezing” the monolayer structure with a crosslinking agent after the transfer, and subsequent immersion in water, prevents rapid reorganization and preserves the monolayer morphology.

Similarly to star-shaped PS-PEO block copolymers, the influence of polymer architecture on monolayer behavior was also studied with PB-PEO diblock copolymers [43]. In this case, four-arm stars were prepared with different volume fractions of the hydrophilic blocks. Analogously to linear and star-shaped PS-PEO copolymers, the PB-PEO stars produce monolayers, the isotherms of which are characterized by three distinct regions. First, at large molecular areas, a “pancake” conformation is assumed, followed by a pseudoplateau at ca. 10 mNm^{-1} , the extent of which depends strongly on the PEO fraction. Third, with further compression, a brush phase is postulated. The isotherm interpretation is essentially similar to that described for other PEO-containing block copolymer monolayers, and in particular the monolayer behavior does not differ much from linear PB-PEO. Films transferred to mica surfaces reveal small domains at low transfer pressure, corresponding to individual stars. Monolayers transferred at high surface pressure have the morphology of entangled wires (stripes), which form at high surface density due to repulsion of PEO blocks and hydrophobic attraction between PB cores.

Detailed modeling of hydrophobic-hydrophilic-hydrophobic (BAB-type) polymers from PEO and a hydrophobic polyester was presented in [44], including the molecular interactions in the monolayers. In particular, it was found that the final polymer conformation, with the hydrophilic block displaced from the interface, is assumed relatively early during the film compression, i.e. at ca. 9 mNm^{-1} . This observation is supported by the fact that there is only a very small contribution to the film surface pressure from chain conformational changes.

Poly(ϵ -caprolactone)-poly(ethylene oxide), PCL-PEO, five-arm star block copolymers, where the hydrophobic blocks are attached as the star peripheral units, show very interesting monolayer properties due to the crystallization of PCL blocks [45]. The investigations of PCL-PEO self-assembly is motivated by the fact that those polymers are biocompatible and could be used for biological and medical applications, especially in drug delivery and tissue engineering. Therefore, understanding their behavior in asymmetric environments, and in particular on various surfaces, is of crucial importance. In the case of PCL-PEO star copolymers, a plateau in the isotherms is also observed, but this time attributed not to PEO dehydration and brush formation, but to the (reversible) formation of the crystalline phase in the hydrophobic film region. Melting of PCL crystals upon film expansion shows a hysteresis effect and happens at surface pressures slightly lower than the plateau region. Additionally, crystallization of the copolymer is observed after film transfer to mica. Because both PCL and PEO tend to form a well-organized solid phase upon the removal of water (drying), the effect is stronger than for any of the homopolymers.

The same group studied linear PCL-PEO at the air-water interface [46], and the authors showed that hair-like crystalline structures form due to crystallization of PCL blocks. At low surface pressure, homogeneous and smooth monolayers were observed after film transfer to mica. A transition was observed at ca. 13 mNm^{-1} that corresponds to the crystallization process. This process was not reversible (on the timescale of the experiment), and the crystal morphology differed markedly from that previously observed for PCL homopolymers, indicating a strong influence of the PEO segments on the crystal structure. PCL-PEO-PCL triblocks of the

BAB type essentially show two regimes when spread and compressed at the air–water interface [47], which is consistent with the behavior of PCL–PEO diblock copolymers discussed above. At a surface pressure below ca. 12 mNm^{-1} (i.e. in the semidilute regime) the films show liquid character, whereas high surface pressure induces the PCL crystallization process, which leads to very small areas per molecule.

PEO–polypeptide block copolymers, another combination potentially interesting for biomedical applications, were also shown to produce stable monolayers with very interesting features relating to the orientation of peptide helices at the interface, additionally influenced by the presence of poly(ethylene glycol), PEG [48]. In particular, PEG seems to adsorb partly at the interface, and thus inhibits the perfect perpendicular arrangement of the polyleucine helices. On the other hand, the helical conformation of peptide segments is unaffected by the monolayer packing state, as shown by CD spectroscopy.

Another PEO–peptide system was investigated by Park et al. [49]. In this case, poly(γ -benzyl-L-glutamate), PBLG, a rod-like helical block, was used as the hydrophobic part. Thermodynamics of the monolayer behavior are governed by two major, competitive effects: (a) entropy loss when PEO blocks form a brush, and (b) decrease in enthalpy when PBLG rods undergo packing. Depending on the prevailing effect, the consequence is either a positive or negative temperature influence on the surface pressure.

Poly(L-lactide) (PLA) blocks were used as hydrophobic moieties [50] to produce cell-growth-supporting polymeric scaffolds. In this context, Langmuir monolayers are a particularly interesting tool as they allow for control of film thickness as long as a brush-like polymer film is formed. Transfer of such a film to a solid support may result in monomolecularly thin and exceptionally well-organized scaffolds. For such applications, it needs to be ensured that the polymer retains its monolayer packing properties after transfer, which may not be the case on every solid surface. In the cited study [50], horizontal deposition (by the Langmuir–Schaefer, L–S method) of PLA–PEO monolayers to a glass slide resulted in an organized brush structure, where PLA blocks, oriented towards the glass, provided good polymer adhesion to the surface; PEO chains, extended towards the aqueous environment, were supposed to control cell adhesion.

Rod-coil diblock copolymers containing poly[(+)-2,5-bis(4'-[(S)-2-methylbutoxy]phenyl)styrene], PMBPS, as the hydrophobic part and hydrophilic PEO blocks form ordered monolayers as a result of coalescence of small, spherical surface aggregates [51]. Such aggregates presumably form during the monolayer deposition and result from the high glass transition temperature (T_g) of PMBPS. Film compression leads to the formation of cylinder-shaped aggregates in which the rod-like PMBPS assumes a flat arrangement, and the subsequent increase in surface pressure leads to the arrangement of the cylinders and the formation of a true, but relatively unstable, monolayer. The monolayer stability strongly depends on the length of the hydrophobic blocks. It is highest for diblock copolymers containing the shortest PMBPS fragments. In comparison to coil–coil diblock copolymers, such as linear PS–PEO, this system is characterized by an additional “control” parameter, i.e. the presence of a rod-like block that controls the monolayer morphology at the air–water interface.

Disturbances of the hydrophilic–hydrophobic balance of the monolayer-forming material could also be a factor to exploit when studying film responsiveness to external stimuli. In combination with the oxidation-responsive poly(propylene sulfide), PPS, PEO forms di- and triblock copolymers whose molecular and supramolecular organization is strongly dependent on the oxidative stress present in the system [52]. Monolayers from PPS–PEO on an aqueous subphase remain stable due to PPS hydrophobicity. However, in the presence of hydrogen peroxide in the subphase, oxidation of the PPS blocks occurs and the hydrophilic-to-lipophilic balance is disturbed, producing hydrophilic species. Obviously, an increased hydrophilicity favors dissolution of the material in the subphase and, consequently, a decrease of the mean molecular area. In this study [52], the monolayer model was used to explain physical details of vesicle degradation under the oxidative stress.

Partly soluble triblock copolymers are also sometimes used for monolayer studies. Such investigations could provide data on desorption kinetics, and allow for comparison of the film structure, whether spread or adsorbed. However, attention should be paid to data interpretation in such cases because intricate equilibria take place in such systems. A somewhat confusing study has been presented concerning the monolayer miscibility between PLA and PEO–PPO–PEO (also known as Pluronic) in monolayers [53]. The authors attempted to discuss interactions between the triblock copolymer and a homopolymer (PLA) on the basis of Langmuir monolayer experiments; however, the results show unrealistic values for molecular areas, and therefore conclusions from those measurements cannot be quantitative. In particular, surface pressure–area isotherms for pure polymers and their mixtures reveal, in the compressed state, areas per monomer unit of the order of 3 \AA^2 and below. Such low values cannot be real and most probably result either from material dissolution in the subphase or poor spreading at the air–water interface. Indeed, the isotherms do not appear smooth, which suggests low film stability and difficulties in forming a true monolayer.

The same system was used to study the interactions between the polymer monolayer and a water-soluble protein, bovine serum albumin (BSA) [54]. As could be expected, an increasing amount of PLA in monolayers considerably hindered BSA adsorption, as did the increase of PEO length in the block copolymers. However, many points of this study remain unclear, for example the details of polymer–protein molecular interactions and the protein concentration dependence. No proof was presented that the protein was actually integrated into the monolayer, rather than the interaction being unspecific adsorption (despite PEO–protein repellence), and there was no discussion on the diffusion limit of protein integration.

The same group showed that pure Pluronics produced reasonably stable Langmuir monolayers, which seemed, however, to be far from thermodynamic equilibrium due to the fact that high compression rates were applied [55]. The monolayers were of liquid expanded character, and a short pseudo-plateau at 12 mNm^{-1} was only observed for the polymers with short PEO blocks. This result does not seem consistent with the interpretation of the monolayer morphology, where the plateau is described as the result of PEO desorption from the air–water

interface. For many other PEO-containing polymers studied (see examples above), the extent of the plateau transition is longer for longer PEO blocks, yet in this case the overcompression effect and a kinetic trapping of the chains out of equilibrium are likely to produce the artifact.

Pluronic monolayers were subject to surface rheology investigations at the air–water interface, both after adsorption from solution and after film spreading [56]. The difficulty in studying spread monolayers from this class of polymers obviously results from their high solubility, but nevertheless some clues on the elastic film behavior could be demonstrated. In particular, up to surface pressure values of ca. 10 mN m^{-1} , the viscoelastic behavior of spread and adsorbed monolayers appears identical. At higher pressure, the film behavior strongly depends on the block ratio, where rearrangements within the interfacial layer and possibly desorption of the polymer molecules take place.

On the other hand, Pluronic-based pentablocks (ABCBA), where A is poly(2,2-diethylaminoethyl methacrylate), PDEAM, build stable and reversibly temperature-responsive monolayers [57]. This behavior, however, was only observed in a narrow pH range, consistent with the pH responsiveness of the terminal blocks (see Sects. 1.4.3 and 1.4.4). Both pH and temperature enhance the hydrophobicity of PDEAM blocks, leading to multiple possibilities for triggering polymer conformations at the air–water interface. At constant temperature, very high and very low pH subphase values tend to influence the system most, while at physiological pH of ca. 7.4 the temperature effect is most pronounced. Crossing the lower critical solution temperature (LCST) changes the hydrophilic–hydrophobic balance in this material, leading to the formation of more hydrophobic surface aggregates.

1.4.2 Silicon-Containing Block Polymers

Silicon-based polymers have interesting properties for the development of new materials. They are characterized by high hydrophobicity and low glass transition temperatures, thus yielding soft materials. Polydimethylsiloxanes, for example, are known for their oxygen permeability, which leads to their application in biomedical sciences. Therefore, a number of studies have concentrated on the amphiphilic self-assembly of block copolymers based on silicon-containing blocks.

For example, siloxane phosphonate ester macromolecules were studied in the context of molecular rearrangements during film compression at the air–water interface [58]. The authors analyzed thermodynamic contributions to the film stability, mainly resulting from formation and breaking of the hydrogen bonds between the phosphate groups and subphase water. Due to the irregular shapes of those macromolecular amphiphiles, including multiple side chains and large three-dimensional hydrophobic parts, their organization at the air–water interface is hindered and a simple model for molecular packing could not be suggested.

Block copolymers containing a silabutane hydrophobic part were investigated by surface pressure–area isotherms and X-ray reflectivity [59–61]. Stable monolayers were obtained, with a typical smooth transition from a pancake to brush-like

conformation. X-ray experiments clearly show two layers: the melt of silabutane exposed to the air, and a hydrated layer of poly(2-hydroxyethyl methacrylate), PHEMA, (containing 29% of water) extending towards water. As expected, the film thickness increases with increasing surface pressure.

Mixed films of polystyrene-*b*-poly(ferrocenyl silane) (PS-PFS) and polystyrene-*b*-poly(2-vinyl pyridine) (PS-P2VP) were prepared at the air–water interface [62] and studied in the context of new superstructure formation resulting from the system complexity. PS-PFS is, in fact, a hydrophobic copolymer and as such does not spread on the water surface; however, a certain proportion of this polymer can be embedded in the monolayer from PS-P2VP. The morphology of monolayers transferred to silicon wafers was studied by scanning tunneling microscopy, and revealed a hexagonal lattice of spherical micelles from PS-P2VP (Fig. 5). Similar structures were observed when polystyrene–poly(4-vinyl pyridine), PS-P4VP, was co-spread with liquid crystalline 4'-pentyl-4-cyanobiphenyl [63], from PS-P2VP of different P2VP lengths spread from various solvents [64], and from mixed films of PS-P2VP with the addition of PS homopolymer [65]. The addition of PS-PFS leads to increased micelle density and the formation of tubular structures, which first coexist with the micelles and become a prevailing morphology with increasing content of PS-FS. Interestingly, higher surface pressure favors the formation of tubes and, finally, of thin wires of very monodisperse dimensions, which can be compacted into a mesh by application of electric field. Again, such structures on solid surfaces may or may not be directly correlated with the morphology of a floating monolayer, and the assumption that they form at the air–water interface remains to be confirmed experimentally. In any case, this study demonstrates that a film transfer could lead to multiple nanoscale morphologies that can be additionally trigged by external stimuli.

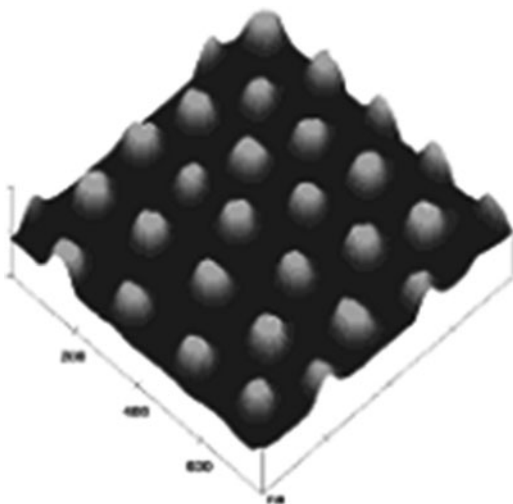


Fig. 5 Morphology of an L–B film of a PS-*b*-P2VP blend transferred to silicon at 10 mN m^{-1} ; scan size $1 \times 1\text{ }\mu\text{m}$. Reprinted from [62] with permission. Copyright 2004 American Chemical Society

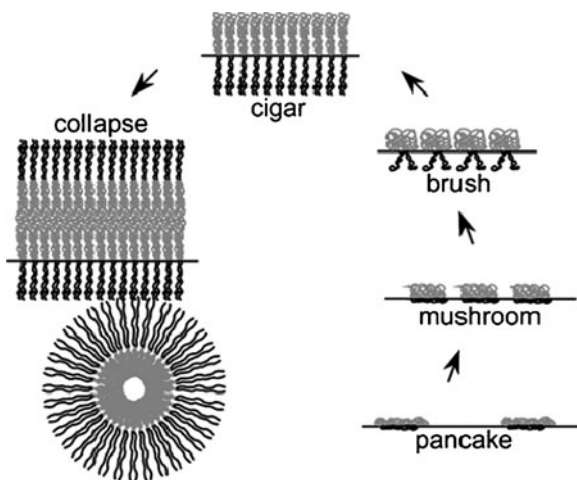


Fig. 6 Representation of different film organization during PMOXA–PDMS–PMOXA monolayer compression at the air–water interface. Hydrophobic and hydrophilic blocks are depicted in gray and black, respectively. Reprinted from [66] with permission. Copyright 2006 American Chemical Society

The structure of poly(2-methyl-2-oxazoline)–poly(dimethylsiloxane)–poly(2-methyl-2-oxazoline) (PMOXA–PDMS–PMOXA) triblock copolymer monolayers was investigated in the context of hosting an amphiphilic peptide, alamethicin [66]. Compression isotherms, BAM, and lateral film compressibility studies show that the triblock copolymers at the water surface assume the pancake conformation at low surface pressure, and that compression causes the PDMS coils to transform to loops during the extensive plateau region at ca. $15\text{--}20\text{ mN m}^{-1}$ (Fig. 6). The steep rise of surface pressure following the plateau corresponds to stretching of the loops and, finally, of the whole polymer molecules, to yield a thick polymer layer, as shown by relative light reflectivity measurements. PMOXA–PDMS–PMOXA block copolymers successfully mimic lipid bilayers in terms of hosting transmembrane peptides and proteins. Alamethicin, a channel peptide, was found to adopt a similar aggregation pattern in those polymer monolayers, and the influence of the polymer matrix prevented the peptide aggregates from early collapse [66]. Additionally, the excess mixing energy in the polymer–peptide monolayers was lower than in analogous lipid–peptide films, showing that soft and flexible polymers can be a proper matrix for biomolecules. Indeed, the insertion of outer membrane protein F (OmpF), a channel protein, into polymer films depends strongly on the polymer size, yet seems to be more hindered than insertion into palmitoyl oleoyl phosphatidylcholine (POPC) lipid monolayers [67].

Interesting PEO-containing block copolymers were synthesized by Lee et al. [68]. These authors attached oligomeric silsesquioxane (POSS) cages to the termini of a middle PEO block to produce BAB-type block copolymers. The resulting polymers form stable monolayers, the properties of which depend on the block

ratio. Brewster angle imaging shows no particular features in the film morphology. However, compared to other PEO-containing amphiphiles, block copolymers studied here are of more liquid-condensed character and do not reveal the typical plateaus associated with PEO desorption/dehydration. The films remain stable up to surface pressures above 30 mN m^{-1} , where multilayer structures supposedly form, indicated by heterogeneous features in BAM images. A large PEO fraction, on the other hand, leads to unstable monolayers as the material desorbs to the subphase due to increased hydrophilicity. The most interesting feature of POSS-PEO-POSS films is the arrangement of POSS cages into a bilayer structure at high surface pressure, as evidenced by X-ray reflectivity studies. This packing, however, contributes to film instability, despite anchoring in water by PEO blocks.

1.4.3 Charged and pH-Responsive Polymers

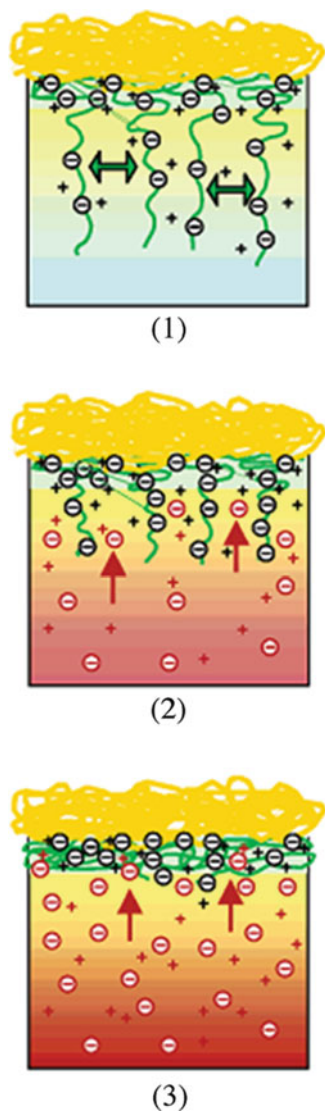
Several examples of pH-responsive block copolymer monolayers have been described, primarily formed by polymers containing at least one chargeable block. For charged amphiphiles, a significant contribution to surface pressure from the electrostatic term needs to be considered, independently from van der Waals interactions [4]. For example, the strong pH-responsiveness of P2VP-PS-P2VP [69] is due to the higher water solubility of P2VP blocks at low pH. π -A isotherms are shifted to larger areas at basic pH (where the chains are at the interface and thus occupy larger areas). Interestingly, the formation of “nano-donuts” is observed after the films are transferred to solid substrates at high pH. The formation of such structures is supposed to result from kinetic trapping of aggregates during the monolayer spreading, where PS blocks would form the aggregate core and P2VP chains, floating at the interface, would build a corona. On the other hand, it remains unclear whether such nano-donuts indeed form at the air–water interface or during the L–B transfer due to polymer interactions with the substrate.

A very interesting pH-dependent behavior was observed for monolayers from polymers carrying oppositely charged moieties: phenylboronic acid and tertiary amino groups [70]. In this case, condensed films form on pure water, which considerably expand at low pH due to the electrostatic repulsion between protonated ammonium cations. This electrostatic effect weakens with pH increase and is also demonstrated by decreased molecular areas.

Polymer brushes at the air–water interface were formed from poly(ethyl ethylene)–poly(styrene sulfonate), PEE–PSS, diblock copolymers [71]. In this system, PEE is the hydrophobic part with liquid properties at room temperature, whereas PSS is the water-soluble polyelectrolyte. Experiments at different salt concentrations show a transition from the osmotically swollen to the salted brush, in which about 90% of the counter-ions remain immobile.

The carpet-brush monolayer structure was also found in poly(isoprene)-*b*-poly(styrene sulfonate), (PI–PSS), monolayers, depending on the compression state and salt concentration in the subphase [72]. The brush formation is controlled primarily by electrostatic interactions, and not so much by steric hindrance,

Fig. 7 PSS (hydrophilic) layer structure change by salt concentration: (1) The brush is not influenced by salt addition in the bulk at low concentration. (2) Added salt ions enter the brush layer and a screening effect results in shrinking of the brush chains. (3) Structural transition from the carpet + brush to carpet-only PSS layer by further addition of salt. Reprinted from [72] with permission. Copyright 2007 American Chemical Society



with density increasing beyond a threshold salt concentration. It is shown that a transition from carpet-brush to a carpet-only morphology occurs with increasing salt concentration (Fig. 7) as the hydrophilic portion of the film changes from the osmotic regime via the salted brush region. Furthermore, film compression leads to expulsion of ions from the hydrophilic film section, leading to chain extension and therefore an increase in brush thickness.

The morphology of poly(*tert*-butyl styrene)-*b*-poly(styrene sulfonate) monolayers at the air–water interface was studied in situ by microscopy and X-ray scattering [73]. Although the surface–pressure area isotherms did not reveal any particular features (plateaus, kinks etc.), microscopy shows reversible interfacial modulation in the direction perpendicular to the compression direction, above 10mNm^{-1} . This phenomenon is not due to density modulations in the film, but rather results from film buckling. Because the hydrophilic blocks are charged, it could be expected that film buckling reduces the electrostatic energy by separating charges. On the other hand, considering film rigidity, the wrinkling mechanism for an elastic rigid layer seems more plausible.

Apart from synthetic polymers, peptidic polymers with pH-responsive blocks were investigated in the context of Langmuir monolayers. In this case, apart from hydrophobicity differences between different blocks, the monolayer properties depend on the secondary structure of the individual blocks at different pH. Hydrophobic interactions between blocks with different secondary structures may be different, as shown in [74], leading to different molecular packing in the film.

1.4.4 Acrylate-Based Polymers

Block copolymers containing acrylates as hydrophilic blocks are interesting not only for their surface micellization properties [30, 75], but also because their aggregation and film-forming characteristics can be regulated by subphase pH and the concentration of counter-ions [76]. The responsiveness of PAA to pH leads to the expansion of those blocks in the aqueous phase (thus increasing the molecular area) at high pH, and contraction to a more globular form at low subphase pH [77].

In monolayers of poly(1,1-diethylsilacyclobutane)–poly(methacrylic acid) a very interesting phenomenon was observed concerning the behavior of the water-soluble blocks. Namely, Mouri et al. [78] found by X-ray reflectivity that the hydrophilic layer is divided into two parts of very distinct behavior. Its first part, positioned closer to the hydrophobic part of the film (and thus closer to the air–water interface), behaves like a dense carpet-like layer, while the second part, immersed deeper in the aqueous phase, has the character of a less dense polyelectrolyte brush layer. Additionally, the “roughness” of this diffuse brush layer is considerably larger than that of the densely packed, upper poly(methacrylic acid), PMAA, layer. This behavior is governed by the size of the hydrophilic block: for small PMAA blocks, a limiting size is observed, below which only a dense, carpet-like layer forms. Additionally, it is shown that the thickness of the dense layer is independent of the surface pressure, while the presence of a brush layer can only be detected at surface pressure higher than 20mNm^{-1} . This could be either due to low X-ray reflectivity contrast of the diffuse layer, or simply due to the fact that at low surface pressure no brush-like layer is formed because the hydrophilic chains are fully hydrated in the subphase. At higher surface pressure, however, the brush layer thickness increases

with monolayer compression. With the addition of the hydrophobic homopolymer, only the carpet layer is formed to reduce the interfacial energy of the film [79].

The same group investigated the pH-dependent behavior of the above polymers [80], and in particular the presence and characteristics of the dense and diffuse parts of the hydrophilic layer. Interestingly, the monolayer nanostructure was similar at acidic and neutral conditions; however, at basic pH, long PMAA blocks did not reveal the carpet or brush structures anymore, due to strong dissociation of weakly acidic hydrophilic blocks and sodium condensation.

Niwa et al. [77] reported that the mean molecular area occupied by PAA–PS diblock copolymers is primarily controlled by the size of the hydrophobic block: with very large PS chains, coiled conformation is assumed, whereas systematic decrease in length of PS leads to a brush-like morphology of the film. This result is consistent with other studies on acrylate-based diblock copolymers [81], showing that the hydrophobic block controls the molecular dimensions at the interface, independent of its chemistry. Interestingly, when monolayers of PEO–PS are prepared and PAA homopolymer is added to the subphase, a significant influence is only observed at acidic pH [82]. This suggests strong interactions between PEO and unionized PAA, explained by reversible interpolymer complexation and formation of hydrogen bonds.

A similar effect on PAA hydrophilic blocks takes place when PVP is present in the subphase at low pH [83]. This particular pH-dependent behavior was further applied to obtain solid films with pH-controlled permeability to small molecules [84]. Membranes were prepared from ABA-type polyelectrolytes containing PAA middle blocks and PSS side blocks with the addition of small cationic amphiphiles. The membranes possessed pH-switchable properties towards hydrophilic molecules, whereas transport of hydrophobic species was pH-independent. This result is explained by pH-dependent disturbance of cationic amphiphile monolayers by the polyon (formation of “pores”), the conformation of which is strongly pH-dependent.

PS–PAA monolayers turned out to be an excellent “template” for polyelectrolyte layer-by-layer (LbL) deposition [85]. In contrast to a lipid monolayer, the block copolymer film enabled monolayer viscosity measurements after adsorption of each added layer. In addition, it seems that the viscoelastic properties of the polyelectrolyte multilayer are dominated by the properties of the underlying block copolymer monolayer.

Dendronized polystyrene–poly(*tert*-butyl acrylate), PS–PtBA, polymers produce stable monolayers, in contrast to dendronized PS–PAA [86]. Interestingly, PS–PtBA seems to aggregate at the air–water interface into monodisperse spherical structures, up to a plateau region at 24 mN m^{-1} . At higher surface pressures, the film becomes unstable and large aggregates form. This behavior is due to the fact that both blocks are relatively hydrophobic, and the amphiphilic balance to allow for spontaneous film spreading is not present in this material. On the other hand, the hydrophobicity difference is still sufficient to maintain the monolayer at the free water surface, without any evidence of large-scale aggregation or collapse. The appearance of

surface aggregates with a very low aggregation number is explained by the molecular architecture of dendronized polymers, and the authors suggested that a different ratio of the two polymer blocks within a dendritic molecule should lead to homogeneous monolayers composed entirely of surface micelles.

Poly(2,2-dimethylaminoethyl methacrylate)–poly(methacrylic acid), PDMA-EMA–PMAA, block copolymer monolayers were transferred to solid substrates to produce interlayers for pH-controlled solid supports to host biological species [87]. In this particular case, the pH dependence of the floating monolayers was investigated by in situ titration. At high pH, the slightly hydrophilic PDMAEMA blocks (in their uncharged state) occupy a larger area at the air–water interface, whereas a pH decrease leads to protonation and extension of those blocks into water. This way, the molecular area decreases (at constant pressure), and the blocks segregate to produce distinct hydrophilic and hydrophobic regions of the monolayer. The resulting increase of film thickness was confirmed by ellipsometry after film transfer to solid substrates.

Poly(*N*-isopropylacrylamide), PNIPAM, is a well-known temperature-responsive polymer and has also been used as a hydrophilic block. When coupled to PS, this material produced monolayers at the air–water interface that also show a temperature-dependent change in the film packing [88]. The film packing is discussed as a “train” conformation (PNIPAM adsorbed on the interface at low surface pressure) and as “loops and tails”, which are present at higher surface pressure (above 24 mNm^{-1}), and is characterized by a certain level of immersion of the hydrophilic blocks in the subphase. It is found that the train conformation is temperature-independent, whereas the more condensed phase exhibits higher compressibility with increasing temperature. This shows that the temperature-dependent behavior of this polymer is strongly related to the hydration state of the PNIPAM blocks.

In summary, Langmuir monolayers are an excellent model for investigating the principles of amphiphilic organization in systems containing water-insoluble block copolymers. In particular, details on monolayer morphology can be obtained, and valuable information is available on the block responsiveness to either environmental stimuli or to the increase in film packing during monolayer compression. Importantly, the behavior of hydrophilic blocks in water (including dehydration processes, hydrogen bond formation, carpet/brush organization) can be analyzed in detail and correlated to the formation of amphiphilic self-assemblies in solution. Moreover, the monolayer approach is excellent for producing LbL films and mono- or multilayers on solid substrates. Such thin and organized films on solid supports are more applicable and thus exceptionally interesting, in particular in the context of responsiveness to an electric field, controlled permeability, and scaffold production for tissue engineering.

2 Amphiphilic Block Copolymers on Solid Surfaces

Surface characteristics of materials are decisive for their performance. The ever-increasing number of publications on block copolymer-modified surfaces shows that such modifications impart novel properties to surfaces, which are essential for the design of tailor-made materials and their specific applications.

The inherent ability of block copolymers to self-assemble into various well-ordered supramolecular structures makes them attractive for numerous technological applications. For instance, thin films self-assembled from block copolymers have been used as building blocks in nanotechnology and materials science [89–91]. Block copolymers have been employed directly without further manipulation as nanomaterials [92], or used as self-organized templates for the creation of nanostructured materials [92, 93]. Block copolymer blends demonstrated their applicability as patterning templates for the fabrication of well-ordered arrays [94], as well as for nanoscale manufacturing of more complex patterns [95]. The use of amphiphilic block copolymers for templating applications has been reviewed by Förster [96].

This section provides an overview of the recent scientific literature on amphiphilic block copolymer-modified solid surfaces, including some application examples. The reader's attention should be particularly drawn to amphiphilic block copolymer films and aggregates on planar solid supports. Interesting examples of other substrates such as nanoparticles [97–99] or carbon nanotubes [100–102] have been reported as well; however, such contributions will not be the subjects of this section.

2.1 *Planar Thin Block Copolymer Films on (Planar) Solid Surfaces*

Surface modification with thin planar films from amphiphilic block copolymers yields versatile materials with many potential applications. For instance, the wetting or lubrication behavior can be tuned in a desired way. Additionally, systems for biomaterials science can be designed. Moreover, such modifications are also effective in fields like nanoparticle synthesis or membrane mimics. These and more examples of planar surfaces functionalized with amphiphilic block copolymers will be presented. Since the possibilities for the preparation of such materials are as diverse as their potential use, a short section introducing the main preparation techniques will precede this discussion. Generally speaking, either a polymer film or a film of polymer aggregates can be deposited. In Sect. 2.1, we will discuss the preparation, structure, and applications of polymer films. The formation, structure, and application of surface aggregates follows in Sect. 2.2.

2.1.1 Film Preparation

A widely employed and easy technique for the production of reproducible, well-controlled, and structurally uniform thin films is spin-coating. This method was extensively discussed by Norrman [103]. Another deposition method transfers well-ordered, compressed monomolecular amphiphilic polymer films (i.e. Langmuir films) from the air–water interface to solid substrates [104]. The Langmuir monolayer transfer can be accomplished either as vertical L–B transfer [105] or horizontal L–S transfer [106]. The resulting films possess a high degree of molecular ordering. Furthermore, thickness and architecture control is achievable via Langmuir monolayer transfer methods. On the other hand, L–B and L–S transfers may not preserve the Langmuir monolayer structure and, depending on the polymer–substrate interactions, lead to considerable rearrangements. Examples are known of micelle formation during film transfer [75] and thin film dewetting [107]. Therefore, the solid substrate must be chosen carefully to minimize undesired and amplify desired interaction effects.

Physisorption, i.e. physical adsorption, from a selective solvent to a selective surface is a common and simple way to prepare thin polymer films on solid surfaces [108, 109]. This method is usually employed for reversible immobilization of polymer chains to surfaces. However, due to the rather weak interactions between the substrate and block copolymers (mostly van der Waals forces or hydrogen bonding), the polymer brushes are likely to desorb. Desorption can occur upon exposure to good solvents or the polymer chains can be displaced by other, more strongly bound adsorbates. Under certain conditions, the films might also be thermally unstable.

Irreversible attachment of block copolymers to solid substrates can be achieved by grafting techniques involving a chemical bond between polymer and support. The covalent bond provides the polymer-modified surface with a certain chemical resistance and robustness. Covalent immobilization can be accomplished either by grafting-to or grafting-from methods [108]. Grafting-to refers to the attachment of preformed, end-functionalized polymers to substrates exhibiting adequate reactivity. This method offers the advantage of precise control and thorough characterization of the preformed polymers. Prior to immobilization, the chemical structure, molecular weight, and polydispersity can be adjusted. However, high grafting densities and, thus, high thicknesses are hardly achievable because diffusion of the preformed macromolecules through the already immobilized polymer chains to the active sites on the surface becomes more difficult with growing polymer film thickness [109].

This obstacle can be overcome by using the grafting-from approach, yielding high grafting densities and high film thicknesses [110]. Polymerization strategies for grafting-from were reviewed by Edmondson et al. [111]. As the surface-initiated growth of (block co)polymers brushes emerged more than one decade ago, the interested reader is referred to a review and references therein [112]. Other well-established techniques for surface modification, such as drop- or zone-casting, immersion, vapor deposition, lithography, printing, or stamping, have been described [113–116] and can also be applied for surface functionalization with block copolymers.

2.1.2 Planar Solid-Supported Amphiphilic Block Copolymer Membranes

Rakhmatullina et al. reported the synthesis of amphiphilic triblock copolymers grafted on gold surfaces [117]. The polymer brushes were composed of two terminal hydrophilic poly(2-hydroxyethyl methacrylate) blocks and a hydrophobic poly(*n*-butyl methacrylate) core. As the triblock copolymers were synthesized by surface-initiated atom transfer radical polymerization (ATRP), a good control over the brush thickness through the molecular weights was achievable. Molecular weight, and thus block length, could be easily controlled by varying the polymerization times. Gel permeation chromatography and nuclear magnetic resonance spectroscopy revealed the molecular weight and composition of the block copolymers. Grafted on the substrate, the polymers were investigated by ellipsometry, CA measurements, and atomic force microscopy (AFM). These analytical techniques provided information about layer thickness and surface topography. Additionally, the orientation of methacrylate ester groups directly connected to the polymer backbone could be preliminarily estimated from the results of polarization modulation infrared reflection absorption spectroscopy. These measurements revealed an increase of the chain tilt towards the gold surface during growth of the individual blocks. Rakhmatullina et al. suggested that the brush orientation is influenced by the chain length, as well as by interchain interactions. Due to the structural analogy of this triblock copolymer system to naturally occurring lipid membranes [118–120], the authors suggested that they could serve as mimics of complex biological membranes or a robust platform for sensing applications. Most recently, it was demonstrated that solid-supported bilayers from diblock amphiphilic copolymers can be also achieved by a combination of covalent and hydrophobic interactions. Such largely defect-free bilayers can be produced after consecutive L-B and L-S transfers [196].

For the preparation of smart responsive materials, Rowe et al. applied a combination of ATRP and reversible addition fragmentation chain transfer (RAFT) polymerization techniques to produce, among others, PS–PNIPAM and PMAA–PDMEAMA block copolymer brushes grafted from flat silicon surfaces [121]. The brushes were subjected to different solvents to monitor their rearrangement properties, which were investigated by CA measurements. The brushes exhibited rearrangement capabilities in response to different solvents, which is particularly interesting with regard to the possibility of using microphase separation to impart novel properties to the material for a wider field of applications.

Amphiphilic triblock copolymer membranes have also been prepared by vesicle fusion through interfacial adsorption of polyelectrolyte vesicles on different model substrates [122]. In contrast to the system reported before, PDMAEMA was used as the hydrophilic block. The resulting amphiphilic polymer self-assembled in aqueous solution into vesicles of 40–50 nm [123]. Under the experimental conditions chosen, the hydrophilic PDMAEMA blocks were positively charged. Through electrostatic interactions, these vesicles could be adsorbed on negatively charged surfaces. A reorganization of block copolymer vesicles into a thin polymeric layer on neutral,

highly ordered pyrolytic graphite (HOPG) surfaces could be observed. However, these films were not stable and started disrupting and dewetting upon drying. In contrast, negatively charged SiO₂ and mica substrates induced fusion of adsorbed vesicles, resulting in the formation of planar supported block copolymer films.

2.1.3 Alteration of Surface Properties Through Modifications with Block Copolymers

Altering surface properties such as wettability or lubrication through surface modification with block copolymers is very interesting for industrial applications. For example, Pluronic triblock copolymers were found to adsorb on hydrophobic model surfaces such as PS [124] or PDMS [125]. Lee et al. investigated the adsorption of a series of PEO–PPO–PEO triblock copolymers on a PDMS model surface and the resulting lubrication properties [125]. The lubrication behavior was strongly correlated to the adsorption properties of the triblock copolymers on the PDMS surface. An increase in PPO block molecular weight led to an increase of adsorbed copolymer amount. Increasing the PEO molecular weight, while keeping the PPO block size constant, resulted in increased adsorption of the PEO blocks. Thus, both blocks play an important role for the adsorption and lubrication properties. The lubrication capabilities of PEO–PPO–PEO copolymers in aqueous media were attributed to the reduction of hydrophobic interactions between PDMS surfaces by coating the surfaces with the copolymer and facilitating the formation of an aqueous lubricating film at the sliding interface. Such systems might find applications as aqueous lubricants, which are, compared to conventional oil-based lubricants, environmentally compatible.

Block copolymer coatings for tuning the interfacial properties of PDMS surfaces also play an important role in biomaterials science because PDMS surfaces are often employed in biomedical devices [126]. Iwasaki et al. reported the functionalization of pretreated PDMS films with well-defined triblock copolymers by spin coating [127]. The polymers were prepared using RAFT polymerization. Hydrophobic PDMS-based polymers were copolymerized with 2-methacryloyloxyethyl phosphorylcholine (MPC). The polymeric coating material was spin-coated on thin PDMS films and chemically immobilized via hydrosilylation. The block copolymers were very effective in reducing the surface friction coefficient and improving wettability.

As mentioned above, such materials are promising coatings in biomaterials science. Therefore, Sect. 2.1.4 will be dedicated to the use of amphiphilic block copolymers for biomedical and biotechnological applications.

2.1.4 Application in Biomaterials Science and Nanotechnology

Thin block copolymer films on surfaces are interesting materials for biomedical and/or biotechnological applications, e.g. tissue engineering. Their chemical versatility allows for the adjustment of desired properties, such as protein repellence or adhesion, and biocompatibility. Mostly, biodegradable PLA- or PCL-based block

copolymers are used as biomaterials. Chemical modifications offer the possibility of introducing functional (bioactive) groups, which could affect cell adhesion and proliferation. One possibility is the surface modification of PLA-based supports by introducing amphiphilic block copolymer derivatives. Therefore, Kubies et al. employed the L–S monolayer transfer technique to prepare well-organized stable brush structures of amphiphilic block copolymers containing PLA blocks for surface functionalization of PLA-based biomaterials [50]. Di- and triblock copolymers were prepared with PLA as hydrophobic block and with varying hydrophilic blocks, such as PEO or poly(L-aspartic acid). The densely packed block copolymer monolayers were horizontally transferred to PLA-covered, silanized glass slides. Dynamic CA measurements were used to study the stability and changes occurring at the modified PLA support upon exposure to water. These investigations aim to reveal the system's feasibility for potential applications in tissue engineering. In a further step, the hydrophilic blocks could be functionalized with special moieties (binding ligands or charges) protruding into the aqueous medium. This enables cell adhesion and proliferation upon contact with the extracellular matrix to be influenced.

Even though PLA-based polymers are already widely used biomedical materials, there are still difficulties concerning controlled degradation, material defects caused by unstable melt viscosity, and high crystallinity causing poor compatibility with soft tissue. One way to overcome these issues is by altering the polymer architecture into branched systems. Recently, the synthesis and characterization of a PLA-derived linear-dendritic copolymer was reported [128]. Specifically, a triblock copolymer was prepared by polycondensation of multihydroxyl-terminated PEG polymers with lactic and glycolic acids. The resulting barbell-like block copolymers are biocompatible and biodegradable. Floating monolayers at the air–water interface were transferred by the L–B method to pretreated silicon wafers and investigated by AFM and CA measurements. Non-homogeneous films resulted, with the hydrophobic blocks pointing away from the solid substrate. The degradation properties could be tuned by the degree of branching. Hydrolytic degradation experiments showed that the degradation rate increased with increasing number of arms and with decreasing arm length. These results could create new possibilities for the use of such novel polymers as biomaterials.

Another PLA-based amphiphilic polymer exhibiting favorable degradation properties was presented by Mert et al. [129]. Diblock copolymers with hydrophobic PLA and hydrophilic methoxy-PEG moieties were prepared. Polymer solutions were dip-coated from chloroform and toluene solutions onto glass slides. In this work, a systematic CA (static and dynamic) and surface free energy characterization of the polymer films was performed. Interestingly, the solvent used for the dip-casting deposition of the block copolymer films had an influence on the equilibrium water CA values. If toluene was used instead of chloroform, the CAs decreased. This effect became even more pronounced with increasing PEG content. This comprehensive study revealed more insight into structure-properties relations on the surface and might improve the understanding of bio- and physico-chemical events occurring at surfaces of biomaterials.

Apart from PLA-based polymers, amphiphilic polymers containing fluorinated blocks are also favorable materials for biomedical applications. Due to their anti-fouling properties, fluorinated polymers are feasible materials for coatings in biomaterials science. However, their inert nature hampers chemical modification for the development of novel materials. In order to alter the properties of fluorinated polymers, rather harsh conditions have to be employed.

Controlled radical polymerization techniques, such as ATRP or RAFT, offer synthetic pathways for the design of tailor-made fluoropolymers. In a recent contribution, three different fluorine-containing monomers were polymerized and copolymerized with *tert*-butyl acrylate (*t*BA) via RAFT [130]. Hydrolysis of the *tert*-butyl groups yielded well-defined fluorinated block copolymers with water-soluble PAA blocks. The copolymers irreversibly adsorbed to non-functional poly(tetrafluoroethylene) (PTFE) surfaces from a series of organic solvents. X-ray photoelectron spectroscopy (XPS) revealed that poly(2,3,4,5,6-pentafluorostyrene)-*block*-*t*BA, and its hydrolyzed derivative showed the highest adsorption degree to the PTFE substrate. Receding CA values indicated fast deprotonation of PAA during the wetting process. Consequently, modification of PTFE with amphiphilic block copolymers led to a surface with switchable wetting properties: hydrophobic in air and hydrophilic in aqueous environment.

Martinelli et al. used ATRP to prepare amphiphilic diblock copolymers from styrene and modified styrene monomers [131]. In order to impart amphiphilicity and low surface energy to the material, styrene monomers were modified with PEGylated-fluoroalkyl side chains. By introducing the fluorinated moieties, it was supposed that surface and interface segregation will enhance the organization in the surface region. In order to investigate microphase separation, thin polymer films were produced by spin-coating from chloroform or tetrahydrofuran (THF) solutions onto glass slides or silicon wafers. Films on glass were investigated by CA and XPS measurements; films on silicon wafers by AFM, X-ray absorption, and X-ray scattering techniques. Figure 8 shows a tapping mode AFM phase image of a block copolymer bearing 51 styrene units and 17 styrene units with PEGylated-fluoroalkyl functionalization. AFM, as well as X-ray scattering measurements, suggest a lying-cylinder morphology of the thin polymeric film with a nearest neighbor spacing of 20 nm. This approach offers a suitable preparation pathway for the creation of complex, dynamic surfaces, which are potentially applicable as biofouling-resistant coatings.

In a related study, these polymeric coatings were used in bioassays to explore their ability to resist the settlement and reduce the adhesion strength of two different marine algae [132]. The films consisted of PS and functionalized PS carrying amphiphilic fluorinated side chains. The test organisms (macroalga *Ulva linza* and unicellular diatom *Navicula perminuta*) differ in their settlement characteristics and in their adhesion biology. Consequently, the two species showed different adhesion behavior on the amphiphilic films. *Ulva* sporelings (i.e. young plants) exhibited a much weaker adhesion on the films with a higher content of amphiphilic PS derivative, whereas *Navicula* cells adhered weaker to coatings with a lower percentage of amphiphilic side chains.

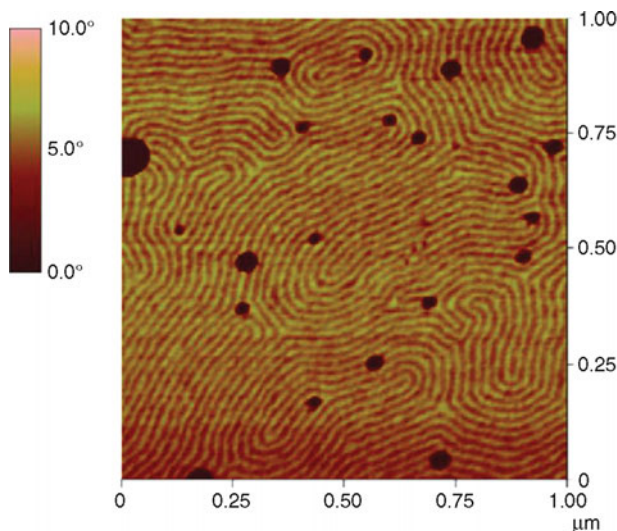


Fig. 8 Tapping mode AFM phase image of styrene-PEGylated-fluoroalkyl styrene polymer film. Reprinted from [131], with permission from Wiley-VCH 2008

It is known that surface morphology and topography strongly influence the adhesion strength of biomaterials on polymer coatings. In this case, rearrangements of the surface structure and changes in roughness after immersion of the films in water were observed by AFM, which might be the reason for the reported differences in the biological performance of the polymeric coatings. However, the results provided by AFM might rather be a hint than a proof for the suggested explanations. As long as deep insights into the chemical processes related to the adhesion mechanisms are missing, the explanation will remain speculative.

The inherent ability of (amphiphilic) block copolymers to spontaneously self-assemble into well-defined and adjustable nanodomains can also be used for a variety of nanotechnological applications, such as nanolithography or nanopatterning [133–135]. Nanostructured templates from block copolymers are an effective tool for the synthesis of nanoparticles [96] and a few interesting examples are presented below.

One recent study describes the synthesis of nanoparticles with an unconventional donut-like shape [136]. In this example, thin films from PS–P2VP–PEO triblock copolymers, spin-coated under high humidity conditions, serve as a template for nanoparticle preparation. Since both the PEO and P2VP blocks can be swollen with water, the authors suggest that kinetically frozen holes form during this process. Thus, cavity formation is assumed to take place, which could result in the observed donut-like structures in the polymer films. The nanoparticle precursors, inorganic salts, were selectively coordinated to the periphery of the holes and, by applying an oxygen plasma, donut-like oxide nanoparticles were synthesized under preservation of the nanostructure. This procedure is schematically depicted in Fig. 9.

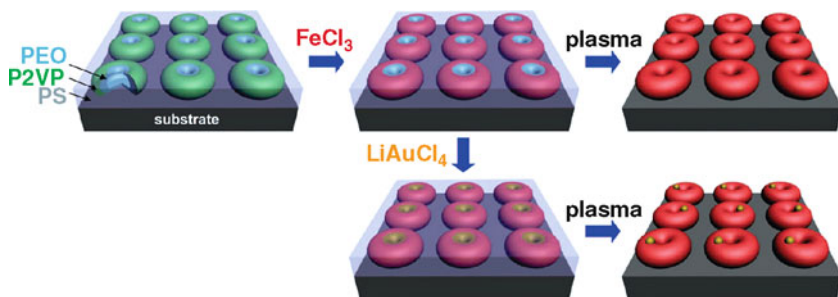


Fig. 9 Nanostructure in a thin film of PS–P2VP–PEO and the fabrication of atypical nanoparticles from the nanostructure. Reprinted from [136] with permission. Copyright 2008 American Chemical Society

Additionally, spherical nanoparticles could be attached to the donut-like structures by incorporating other types of inorganic salts to the center of the holes. This example demonstrates the application of block copolymer templates beyond the synthesis of typical spherical nanoparticles and proves the potential of such templates to control the shape and complexity of the synthesized nanoparticles.

Comparable polymer film features were observed by Bolognesi et al. [137]. Thin films were formed from amphiphilic block copolymers with hydrophobic PS and hydrophilic polyfluorene derivatives by the breath figure (BF) technique. Similar to the example before, a polymer solution evaporates in the presence of wet air. The films are prepared by casting a small amount of polymer solution in carbon disulfide on a glass microscopy slide under a flow of moist nitrogen. The thickness of such films is approximately 10 μm . The presence of humidity in the atmosphere is crucial: as the solvent starts evaporating, water droplets condense on the cooled surface of the solution, and holes are formed in the film. After evaporation is completed, a thin film remains and the temperature increases rapidly; thus, evaporating water droplets produce cavities within the film, and holes on the film surface [138]. In this case, the BF technique allowed the preparation of thin polymeric films with a controlled morphology, exhibited by regularly arranged holes on the film surface. Due to their photoluminescence, such polyfluorene-based films like those shown in Fig. 10 have been suggested for potential applications in electronic and electrochromic devices.

2.2 Block Copolymer Aggregates on Planar Solid Surfaces

In solution, amphiphilic block copolymers self-assemble into various morphologies, such as micelles, rods, vesicles, or larger aggregates. A number of factors, including the structure of the amphiphile (chemical constitution and relative block lengths of the individual blocks) and properties of the solution (concentration, pH, temperature, and solvent) affect the size and shape of such aggregates [139].

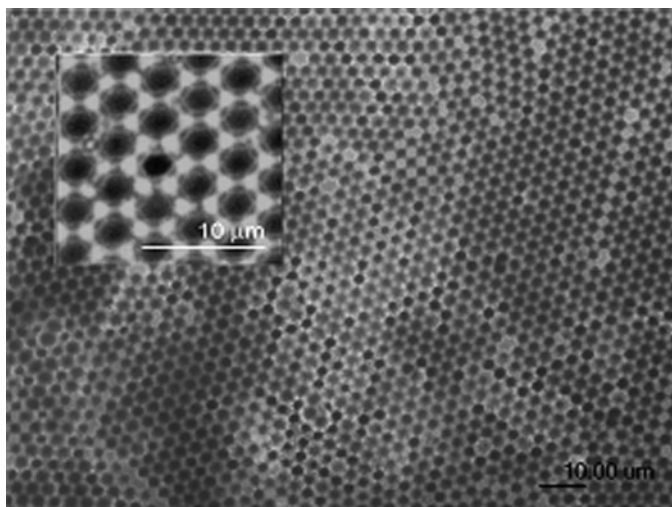


Fig. 10 Fluorescence optical and confocal (*inset*) microscopy image showing a honeycomb-structured porous film. The average hole diameter is 2.2 μm. Reprinted from [137] with permission. Copyright 2009 American Chemical Society

This section is mainly dedicated to micellar and vesicular structures on solid surfaces. In particular, current examples of interesting features concerning the morphology and architecture of such aggregates on surfaces will be presented and discussed.

Some techniques suitable for the deposition of planar thin block copolymer films, such as spin-coating or drop-casting, are also feasible for the preparation of surface-immobilized aggregates from amphiphilic block copolymers. They have been described previously (Sect. 2.1.1); however, one method frequently used for the preparation of polymer aggregate films, the LbL assembly, will be briefly described here. LbL involves consecutive adsorption steps of polyanions and polycations from solution to solid substrates. It is applicable to substrates varying in size and topography. The adsorbates can be selected from a pool of small organic molecules, polymers, proteins, or particles. In particular, the use of polyelectrolytes rather than small molecules is advantageous because good adhesion of a layer to the underlying substrate requires a certain number of ionic bonds [140].

In aqueous media, micelle formation is driven by the minimization of the interactions between the surrounding medium and the hydrophobic chains, leading to a core-shell structure with the non-soluble segments situated in the core and the hydrophilic blocks building the corona. Such nanometer-sized aggregates are successfully used in different industrial and technological fields like drug delivery, cosmetics, or as colloidal stabilizers. A system potentially interesting for biological engineering was reported by Bougard et al. [141]. The amphiphilic block copolymers were composed of PDMAEMA and PCL. The hydrophilic PDMAEMA provided pH and temperature responsiveness, whilst hydrophobic PCL is biocompatible and biodegradable. Micelles were prepared by adding water

to a polymer solution in THF. The resulting aggregates were deposited onto freshly cleaved mica sheets and studied by AFM. Several deposition methods were applied: the micellar films on mica were either dried under ambient conditions or freeze-dried before surface investigations. By employing the latter method, micelle aggregation during solvent evaporation and deformation by interaction with the substrate can be avoided. Indeed, individual spherical micelles on mica could be visualized by AFM, proving that the applied freeze-drying procedure effectively preserved the original morphology of the micelles.

One contribution that made use of the LbL self-assembly of polymeric micelles also reported the persistence of the micellar structure by AFM investigations [142]. Micellar multilayer films were produced from two different polymers. Anionic micelles were produced from poly(2,2-diethylaminoethyl methacrylate)-*block*-poly(methacrylic acid) (PDEAM-*b*-PMAA) block copolymers. Here, the PMAA block is negatively charged at pH 9. Cationic micelles were produced by replacing PMAA block with a PDMAEMA block that was positively charged due to quaternization, which imparted a permanent cationic charge to the corona-forming PDMAEMA blocks [143]. Micellar multilayer films were produced on planar silica by alternate LbL self-assembly from those polymers. By soft-contact AFM investigations at each step of this procedure, micelle-like surface aggregates were clearly observed, suggesting that the micellar morphology could be retained throughout the whole multilayer structure.

Electrostatic LbL self-assembly was also applied to the preparation of photoactive nanostructured micellar films on quartz or silicon plates from amphiphilic poly(sodium styrenesulfonate-*stat*-2-vinylnaphthalene) and the cationic polyelectrolytes poly(diallyldimethylammonium chloride) or poly(allylamine hydrochloride) [144]. Similar to the examples described before, AFM studies evidenced the preservation of the micellar structure in the films. Such materials might be interesting for (bio)sensing applications, light emitting and photochromic devices, or energy conversion systems.

In contrast to these three examples of preserved micellar film morphologies on solid surfaces, the time-dependent evolution of the shape and height of the deposited structures on mica has also been reported [145]. Directly after the deposition of amphiphilic PI-PEO diblock copolymers on freshly cleaved mica, ultrathin and flat islands showing asymmetric and/or irregular features were observed by AFM. Due to the physicochemical properties of the particular PI-PEO polymer, it was assumed that micelle dissociation took place. However, during exposure to ambient conditions, the mica surface became less hydrophilic and the amount of adsorbed water decreased. The surface structures observed initially gradually changed from asymmetric/irregular to circular.

Additionally, a current publication demonstrates that external stimuli, for instance pH, can trigger the surface patterns of the deposited aggregates [146]. Mixed aggregates of PS-*block*-poly(L-lysine) (PS-PLLYs) polymers were dispersed in water with the aid of a nonionic surfactant, and deposited on HOPG substrates. Since PLLys is a pH-responsive peptide, it is able to undergo conformational transitions depending on the pH. Resulting changes in the wetting behavior of the surfaces

were studied by AFM. At pH 8, the mixed aggregates on graphite exhibit a spherical geometry and are well separated, whereas at pH 11 the interaction of the aggregates with the surface changes and a tendency to fuse is noticeable.

Polymersomes, i.e. polymer vesicles, are hollow spherical structures with dimensions ranging from nanometers to hundreds of micrometers. Due to their morphology, they can be applied to the encapsulation of various agents or as nanoreactors for controlled processes taking place in the aqueous core [139].

In a recent work, Rosenkranz et al. immobilized biotin-functionalized PMOXA–PDMS–PMOXA polymersomes on pretreated glass slides via streptavidin–biotin binding [147]. The authors showed that these particular polymersomes are ideal tools for protein folding studies on a single-molecule level. Therefore, fluorescently labeled phosphoglycerate kinase was encapsulated during vesicle formation. Alternating unfolding and refolding transitions were monitored via photoinduced electron transfer between the fluorescent dye and the tryptophan residues.

Scientific interest in surface-immobilized polymersomes is not limited to their encapsulation capabilities, as they are fascinating objects to study in their own right. Lately, a study has been performed in which commercially available, nonionic Pluronic block copolymers were utilized as vesicle-forming building blocks [148]. The vesicles used in this work are not very stable and tend to aggregate and change their size within a few hours. In order to overcome these problems, the vesicles were stabilized with a permanent interpenetrating polymer network from pentaerythritol tetraacrylate. These stabilized vesicles were further immobilized on glass or mica surfaces by Mg^{2+} -mediated electrostatic interactions. Interestingly, the immobilization was reversible and detachment of the vesicles from the surfaces occurred with increasing temperature. At 35°C, almost all immobilized vesicles were released; however, up to now, there are merely speculative explanations for this effect. Responsiveness to external stimuli of the immobilized vesicles was probed by introducing a second, more hydrophilic Pluronic, to the system. Using confocal laser scanning microscopy, the shape transformation from spherical to cylindrical upon addition of the more hydrophilic polymer could be visualized, as shown in Fig. 11.

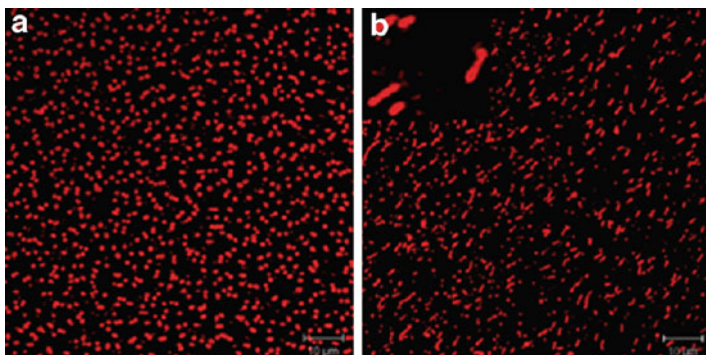


Fig. 11 Confocal laser scanning microscopy images: (a) immobilized vesicles containing a membrane-encapsulated dye, and (b) after Pluronic addition to the immobilized vesicles. Reprinted from [148] with permission. Copyright 2008 American Chemical Society

In summary, this section gives an overview of the recent fundamental, technological, and industrial interest in amphiphilic block copolymer-modified planar solid surfaces. Apart from the wide range of possible applications, such systems are particularly interesting for their accessibility to numerous surface-sensitive analytical techniques, in contrast to systems in solution, for instance. This advantage of amphiphilic block copolymers on planar solid supports allows for deeper investigations and insight into the fascinating world of self-assembling processes, resulting morphologies, and the underlying mechanisms. As a consequence, the alteration, development, and improvement of surface properties can be accomplished in a targeted and controlled way. Thinking of contact lenses or medical implants, polymer-modified materials already play an important role in our everyday lives.

3 Mineralization of Amphiphilic Polymers and Related Compounds

The previous paragraphs have discussed the structure and dynamics of amphiphilic polymers at the air–water interface and at solid surfaces. In this section, we will discuss the use and impact of these functional soft interfaces for studying biomimetic and bio-inspired crystal growth. Interfaces have been recognized as a key element, which controls nucleation, growth, growth kinetics, chemistry of the deposited mineral, crystal shape, crystal organization, crystal phase, and crystal size. However, the exact pathway by which the surface or interface controls the mineralization is still under investigation.

Initially, surfactant monolayers and similar systems were employed for investigating mineralization processes, a development that was spearheaded by Addadi, Mann and others [149–151]. These developments were also reviewed several times [152–156]. Although it has been recognized that biological templates are mostly polymeric, there have been surprisingly few studies on how polymeric surfaces and interfaces regulate crystallization [81, 157]. These and related studies will be discussed in the remainder of the text.

3.1 Mineralization at the Air–Water Interface

Although the study of mineralization of polymeric monolayers at the air–water interface is so far not well-developed, there are related studies showing that the chemical nature of the interface is a key factor in the nucleation and growth of an inorganic solid beneath organic monolayers [153–155]. DiMasi and colleagues performed a series of studies on the mineralization of calcium carbonate beneath various fatty acid monolayers. Using synchrotron X-ray techniques, the authors show that, unlike earlier hypotheses, there is no indication of an epitaxial or quasi-epitaxial interaction of the calcium ions and the crystals with the monolayer [158]. Rather, they found

that crystals nucleated on the stearic and arachidic acid monolayers are not oriented specifically with respect to the monolayer. Moreover, X-ray reflectivity measurements show that four to eight fatty acid molecules bind to one Ca^{2+} , which supports the notion that there is no epitaxial growth of the mineral beneath the monolayer. Finally, the authors show that the escape of CO_2 is the dominant factor for polymorph selectivity. This latter statement will have to be reconsidered in light of a recent study by Gebauer et al., who showed that the calcium carbonate crystal phases are already selected at the nucleation stage [159].

Zhang et al. used Langmuir monolayers to study the initial stage of nucleation and crystallization of calcium phosphate [160]. The monolayers used in their study consisted of dipalmitoylphosphatidylcholine, arachidic acid, and octadecylamine. The experiments show that the adsorption of calcium ions to the respective monolayer is a prerequisite for subsequent nucleation. The authors also demonstrate that calcium phosphate forms through a multistage assembly process, in which first an amorphous calcium phosphate dihydrate layer forms, which then recrystallizes to form a crystalline hydroxyapatite layer (Fig. 12). This transformation of an amorphous phase to a crystalline phase provides direct evidence of a multistep crystallization process, which the authors claim is similar to the processes occurring in biomineralization.

Besides calcium carbonate and phosphate, only a few minerals have been studied with bio-inspired monolayers. Letellier et al. investigated the formation of calcium oxalate monohydrate at phospholipid monolayers [161]. The authors claim that lattice matching and hydrogen bonding cannot be a dominant factor in the control of crystal orientation. Rather, non-specific electrostatic interactions, similar to those reported for calcium carbonate [162], seem to control the crystallization of calcium oxalate monohydrate.

In support of this, Sommerdijk and colleagues recently reported that an epitaxial interaction between organic template and the inorganic phase is not required for nucleation and growth control [163]. Rather, charge and polarization matching, or mutual templating effects, play key roles in nucleation and growth. Mutual templating means that residual mobility of the monolayer enables a more flexible

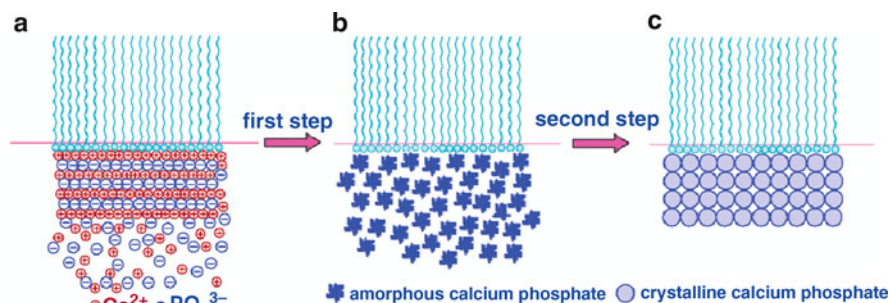


Fig. 12 Schematic of multistep crystal assembly process: (a) increase of the precursor concentration; (b) formation of amorphous calcium phosphate; (c) phase transformation from amorphous to crystalline calcium phosphate. Reprinted from [160] with permission. Copyright 2004 American Chemical Society

interaction between the organic and the inorganic. This results in an optimized surface energy configuration of both the nucleus and the monolayer. Charge and polarization matching are related to charge distributions in a given system. Besides Coulomb, polarization and van der Waals forces also need to be considered, but a quantification of these different contributions is difficult at the moment.

In short, the experiments above suggest that the older hypothesis of epitaxial interaction [156] is probably not the key interaction governing (bio)mineralization processes. Indeed, Fricke et al. show that self-assembled monolayers (SAMs) of highly charged amphiphilic dendron-calix [164] arenes template different calcium carbonate crystal phases. At high charge densities of 6.7–7.2 COO^-/nm^2 , vaterite forms. At lower charge densities of 4.65–5.00 COO^-/nm^2 , aragonite crystals form beneath the monolayer. The same authors and other groups [162, 165, 166] also showed that the formation of calcite with a highly polar [01.2] face oriented towards the monolayer is favored at relatively low charge densities of 2.0–2.4 COO^-/nm^2 .

Similarly, Pichon et al. used Langmuir monolayers to investigate the role and importance of nondirectional electrostatic interactions in mineralization [165]. Instead of calixarenes, they varied the charge density at the monolayers via supramolecular interactions of bis-urea-based surfactants. By mixing three different surfactants in different ratios, domains with different distributions of ammonium groups could be generated. The charge densities did not change at a macroscopic level but were found to differ at a nanoscopic level. The data by Pichon et al. [165] and by Fricke et al. [162] thus support the concept of a more complex interaction between the organic interface and the growing inorganic phase.

Besides the type(s) of interaction (charge density vs. epitaxial vs. others) another effect to consider is internal rearrangement of the template during mineralization. Ahn et al. investigated the mineralization of calcium carbonate at the air–water interface via reflection-absorption Fourier transform infrared (FTIR) spectroscopy on monolayers of stearic acid, octadecylsulfate sodium salt, and 10,12-pentacosadiynoic acid (m-PDA) polymerized by UV irradiation [167]. With stearic acid, calcite nucleates at its (010) face. During mineralization, however, the stearic acid molecules tilt away from the surface normal to accommodate the geometry of the (010) of calcite plane. For the octadecyl sulfate monolayers, calcite nucleates at its (001) face. The hydrocarbon chains become more disordered during mineralization to better fit the carbonate spacing in the calcite (001) plane. With the acidic polydiacetylene m-PDA, calcite nucleates at its (012) face. FTIR measurements show that the alkyl side chains of the polymer reorganize to optimize the interaction with the (012) calcite surface. These data thus suggest that symmetry reduction along with stereochemical and lattice matching are important in inducing the unique co-alignment of the crystalline phase.

One of the major issues associated with the translation of monolayer data into true biological processes is that many monolayers, such as stearic acid monolayers, are only loosely related to natural nucleation sites. For example, synthetic monolayers such as the ones discussed above often crystallize, which leads to a rather stiff template. Presumably, this is one reason why epitaxial interactions keep coming up in discussions. Moreover, the density of functional groups in a crystalline monolayer is much higher than in a natural protein or carbohydrate. Finally, the

chemistry in biological environments is more complex than that of carboxylic acids alone. In summary, there are three requirements that need to be fulfilled for near-biological model surfaces in order to better understand the nucleation and growth of biominerals: (a) the surfaces must be “softer” than simple fatty acid monolayers, (b) their chemistry must be more closely related to natural compounds associated with crystal growth, and (c) the distance between the nucleation sites must be more closely related to natural systems.

A few attempts towards such templates have been reported, but the situation is still far from clear. Buijinsters et al. investigated the influence of the chemistry of organic SAMs by using amide-containing phospholipids [168]. Calcium ions and amide-containing phospholipids self-assemble into well-defined two-dimensional domains at the air–water interface, which are templates for the crystallization of calcium carbonate. Under these monolayers, calcium carbonate crystallized in the unexpected [10.0] orientation. It is assumed that this preference is related to the high degree of organization of the SAM and the restricted conformational freedom of the headgroups in these molecules.

Volkmer et al. used amphiphilic cyclic peptides based on asparagines and phenylalanine. These peptides favor the formation of calcite crystals. Furthermore, in addition to the “normal” [10.4] faces, a new set of diamond-shaped [01.2] crystal faces formed, depending on the concentration of the amphiphilic peptides. These additional crystal faces also form in the presence of proteins isolated from sea urchin spicules or sponge spicules [169]. There, similar calcite crystals were formed with [01.*l*] (*l* = 1–5) faces [166].

In a related study, Cavalli et al. investigated octapeptides consisting of four leucine and four glutamic acid units with (a) a free amino N-terminus, (b) terminated with dioleoyl phosphatidyl ethanolamine (DOPE), or (c) *N*-acetyl residues [170]. All peptides formed stable monolayers, with $189 \text{ \AA}^2 \text{ molecule}^{-1}$ for (b) and $61 \text{ \AA}^2 \text{ molecule}^{-1}$ for (c). With monolayers of (b), calcium carbonate crystallized as calcite with two different habits. Apart from a small amount of pyramidal [01.*l*]-oriented crystals (*l* = 1, 2), a new type of indented crystals nucleated from a [10.0] face. With monolayers of (c), similar crystals formed, but less efficiently.

The above studies show that although there has been some work on calcium carbonate mineralization at the air–water interface, we are far from a quantitative and robust model of how interfaces control (bio)mineral formation. The situation is even more difficult for other minerals. Calcium phosphate is an equally important biomineral, and a number of studies have been done on the synthesis, structure, and properties of bio-inspired polymer/calcium phosphate materials [154]. However, there are even less data on the effect of surfaces and interfaces on calcium phosphate nucleation and growth than for calcium carbonate.

Unlike with calcium carbonate, there are a few computational studies on the interaction of organic molecules with calcium phosphate. Leeuw and Rabone investigated the adsorption of citric acid to the (01 $\bar{1}$ 0) and (0001) faces of hydroxyapatite [171]. Their molecular dynamics simulations show that, in vacuo, citric acid adsorbs very strongly to the hydroxyapatite surfaces. In solution, citric acid competes with water molecules at the surfaces. As a consequence, only those surfaces whose

geometry closely matches with the structure of citric acid are viable adsorption sites. Indeed the adsorption energy of citric acid on the (01 $\bar{1}$ 0) surface is much larger than on the (0001) surface. The differences in these energies are 225.1 kJ mol⁻¹ and 308.8 kJ mol⁻¹ for vacuum and in solution. These studies show that citric acid can be an efficient growth inhibitor for the (01 $\bar{1}$ 0) surface. As a result, the crystal shape of hydroxyapatite grown in the presence of citric acid would become elongated along the *c*-direction.

So far, the only study on mineralization of polymer monolayers was reported by Casse et al. [81]. They used PAA-*block*-poly(*n*-butylacrylate) block copolymers, which form stable monolayers even at high ionic strength and relatively high and low pH values of the subphase. With lower concentrations of calcium and phosphate, uniform polymer-calcium phosphate hybrid films composed of ca. 40 nm spherical calcium phosphate particles are formed. At higher precursor concentration, the films are less ordered with large blocks of material beneath the polymer monolayer. The key result of this study is that a rather flexible polymer film at the air-water interface is well suited for the templating of uniform particles with identical sizes and a high degree of two-dimensional organization. Furthermore, it shows that low supersaturation of calcium phosphate and a well-defined, non-crystalline interface are crucial for controlling calcium phosphate mineralization.

3.2 Mineralization at the Air-Water Interface with Additives in the Subphase

In an extension of the pure monolayer experiments discussed above, admixtures in the subphase have also been shown to dramatically influence crystallization at the interface. DiMasi and colleagues showed that PAA present in the subphase affects the induction time and growth rate of calcium carbonate films from supersaturated calcium carbonate subphase [172]. The PAA additive was used as a simple model for the acidic proteins believed to play a role in many biomineralization processes. The addition of PAA led to a density reduction in the region of the hydrocarbon tails of the monolayer. The density dropped from $\rho_{C20}/\rho_W \approx 0.98$ to $\rho_{C20}/\rho_W \approx 0.7$. These findings indicate interruptions of the molecular packing at the interface, caused by small amounts of PAA coming to the surface. In contrast to the PAA, the presence of calcium ions led to an increase in the surface ordering of fatty acid films.

In a further study, DiMasi and colleagues investigated the kinetics of amorphous CaCO₃ formation at a fatty acid monolayer interface using synchrotron X-ray reflectivity measurements [173]. In-situ experiments found three different parameters that control CaCO₃ mineralization in the presence of arachidic acid monolayers, PAA, and Mg²⁺ ions. Firstly, the crystal growth rate depends on the concentration of counterions and not on the polymer concentration in solution. Secondly, the soluble polymer only affects the lifetime of the amorphous calcium carbonate. And finally, the sole effect of Mg²⁺ is to delay the mineral film formation. These data thus suggest that competitive adsorption (e.g. Mg²⁺ vs. Ca²⁺) is another parameter to consider in controlled mineralization processes.

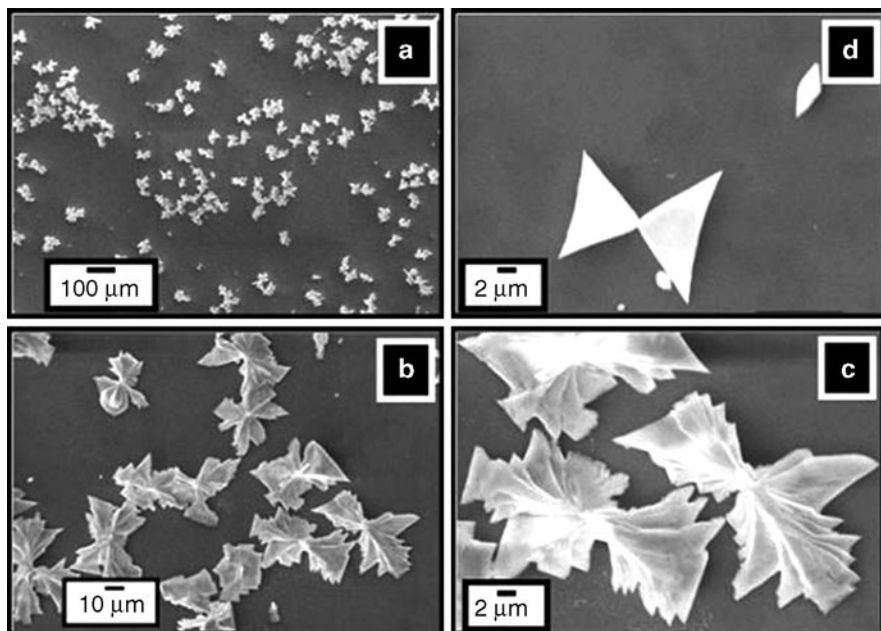


Fig. 13 (a–d) SEM micrographs at different magnifications recorded from BaSO₄ crystals grown at the air–water interface with a monolayer of stearic acid in the presence of ethanol. Reprinted from [174]. Reproduced by permission of The Royal Society of Chemistry

Rautaray et al. showed that BaSO₄ crystallization beneath stearic acid monolayers is strongly affected by traces of alcohol (Fig. 13) [174]. The reason for this effect is not understood so far. It is believed that the adsorption of ethanol at the air–water interface affects the organization of stearic acid molecules, which in turn affects the interaction of the monolayer with the growing inorganic phase. It has also been suggested that the dielectric constant changes as ethanol accumulates at the monolayer. This could lead to enhanced barium binding at the monolayer and lead to different levels of supersaturation and different crystallization rates.

3.3 Mineralization at the Solid–Liquid Interface

Besides the air–water interface, a number of studies have been performed at solid surfaces, mostly on SAMs. Similarly to the work discussed above, most studies on the mineralization of solid surfaces were performed with calcium phosphate and calcium carbonate. There are few studies directly focusing on amphiphilic polymers, but there are a number of reports that include amphiphilic molecules or polymers in conjunction with other compounds.

In a rather technical approach, Sciaratta et al. deposited acrylic acid on poly(propylene) (PP) via a plasma approach [175]. Although the number of -COOH groups increased with the duration of the plasma treatment, the nucleation of CaCO_3 on the modified PP decreased significantly. The authors suggest that the CaCO_3 nucleation efficiency is reduced because the specific interactions of the inorganic material with the carboxylic groups were overcompensated by the influence of the disordered gelatinous film structure generated by the plasma technique. The porous gel-like film of PAA showed a non-regular arrangement on PP. The authors claim that this arrangement could not support LbL deposition of cations and anions. These data are consistent with other data showing that higher supersaturations are required for nucleation on gel-like films [176].

A completely different approach for the modification of solid surfaces, which involves SAMs, has attracted quite some attention [163] and some reports on the mineralization of SAMs have also appeared [177, 178]. Pokroy and Aizenberg studied the growth of calcium carbonate on a wide variety of SAMs terminated with different functional groups [179]. Their SAMs were responsible for two effects. Firstly, they controlled crystal orientation and, secondly, they modulated the crystal shape. The authors explain the change of the crystal shape by way of the anisotropy of lattice mismatch strains between the SAM and the nucleated crystal plane. This means that the change in crystal shape occurs by adjusting the lattice misfits between the SAM and the nucleating crystal. Calculations of the mismatched strains and reconstruction of the crystal shape based on the strain-induced differences in the growth rates supported the hypothesis.

Aizenberg studied the crystallization of calcium carbonate with the aid of organized organic surfaces patterned with specific initiation domains on a submicrometer scale to control patterned crystal growth. She used specifically tailored SAMs of ω -terminated alkenethiols micropatterned on metal surfaces by soft lithography. These SAMs enabled the investigation of various aspects of the crystallization process, including crystal size, crystallographic orientation, and morphology selection [180].

Onuma et al. deposited regular calcium phosphate nanodot arrays on SAMs of carboxylic acid-terminated thiols. The arrangement of the initial calcium phosphate nanodots reflects the structure of the thiol surface. After some time, the calcium phosphate particles become more disordered than in the initial stage. These experiments show that the growth rate and the morphology differ from the initial stage to the late stage of nucleation [181].

Besides calcium minerals, the growth of a few other inorganic salts on solid surfaces has also been studied. Silica is another important biomineral [81, 182], yet it has not been studied extensively in the context of surface mineralization. Tahir et al. synthesized a new nitrilotriacetic acid (NTA)-terminated alkenethiol, which can self-assemble on gold surfaces. Using the well-known coordination of Ni^{2+} and NTA, the enzyme silicatein could be immobilized on the surface of gold nanoparticles. Exposure of these functional particles and control experiments in the absence of silicatein showed that silica precipitates only on silicatein-modified

surfaces. Furthermore, the formation of interconnected silica spheres in the vicinity of surface-bound silicatein indicates that its active site is oriented towards the solution [183].

Although many research groups have studied the effects of acidic moieties on the mineralization of various inorganics, there have only been a few studies on the effect of basic polymers [184–186]. In the context of surface mineralization, Schwahn et al. investigated calcium carbonate mineralization on gold nanoparticles modified with 4-dimethylamino-pyridine (DMAP). Small-angle neutron scattering (SANS) experiments showed that at least three different template structures were formed. The larger aggregates mainly consist of DMAP and the smaller ones consist of colloidal gold attached to DMAP. After 15 h of mineralization, SANS detects an increased number of larger particles. In contrast, the amount of smaller particles decreased with further mineralization [187].

Rautaray et al. grew hydroxyapatite on the surface of gold nanoparticles [188]. The gold particles were capped with aspartic acid such that calcium ions could bind to the carboxylate residues. The authors suggested that upon Ca^{2+} addition, the surface-modified gold nanoparticles form aggregates that serve as templates for the growth of hydroxyapatite. Although this hypothesis was not proven, the data suggest that the morphology of calcium phosphate crystals strongly depends on the nanogold surface modifier [188] (Fig. 14).

DiMasi et al. used two examples of SAMs with variable structural adaptability. The monolayers were constructed from bisureido-heptylene surfactants carrying

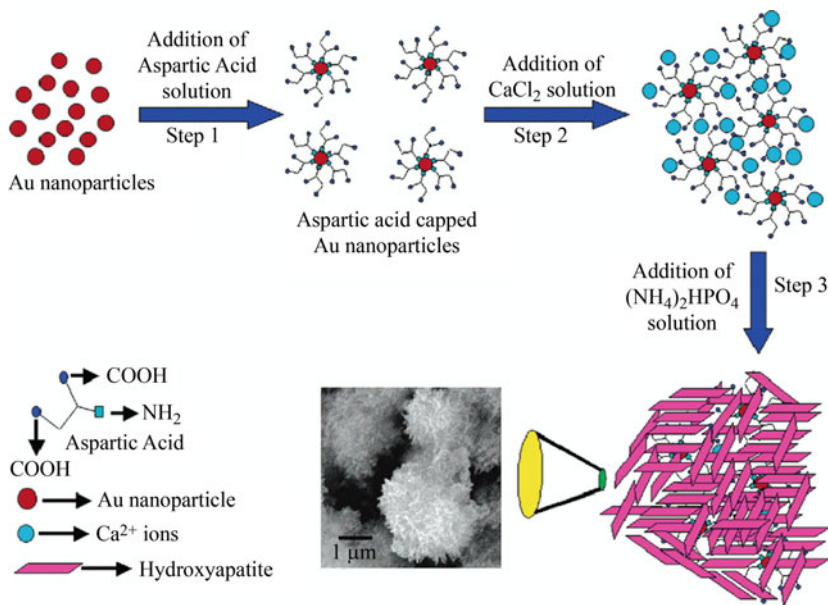


Fig. 14 Different steps involved in the growth of calcium phosphate crystals on aspartic-acid-capped gold nanoparticles. Reprinted from [188] with permission. Copyright 2005 American Chemical Society

dodecyl chains and valine- and glycine-based headgroups [157]. This study showed that the valine headgroups make the monolayer sufficiently flexible that it rearranges upon calcium ion addition. The mineralization studies showed that with valine headgroups, calcite nucleates in rhombohedral tablets with modified faces. SAMs of the glycine-based surfactant undergo no structural change in the presence of calcium ions, which is why calcite nucleates as polycrystalline particles surrounding a spherulitic core. DiMasi et al. speculate that the one-dimensional order and hydrogen-bond-controlled spacing in the valine film has similarities to protein-based organic matrices in living organisms, which direct biomineralization.

Buijnsters et al. show that a high degree of organization is responsible for the efficient nucleation growth of [10.0]-oriented calcite, irrespective of the surface concentration of the lipid [168]. They assign this preference to the high order in the SAM, which leads to a correspondingly high order of the functional groups on the surface. This is caused by the formation of intramolecular hydrogen bonds between the phosphate group and the phenoxy moiety of the SAM.

Ball et al. used poly-L-lysine (PLLys), poly-L-glutamic acid (PLGlu), and poly-L-aspartic acid (PLAsp) polyelectrolyte multilayers for the investigation of calcium phosphate nucleation. The content of PLGlu in the multilayers (0–100%) dramatically affects the lag time preceding crystal growth. Polyelectrolyte multilayers containing 0% PLGlu induce crystal growth after 475 ± 55 min, whereas with 100% PLGlu crystal growth occurred in a shorter time of 275 ± 60 min. Furthermore, by mixing PLAsp and PLGlu in the multilayers, β -sheet formation occurred within the polyanion layer. The β -sheet content increased with a higher amount of PLGlu until it reached a plateau at a ratio of PLGlu of 40%. Coincidentally, the lag time is longest at ca. 1100 min at PLGlu fractions between 30 and 40% PLGlu, and decreases again at larger fractions of PLGlu. The reason for this behavior is not fully understood, but it is suggested that this effect could be caused by variations of the surface potential of the polyelectrolyte multilayer or by phase segregation between regions rich in PLAsp and PLGlu [184].

Leonor et al. synthesized a bioactive polyethylene (PE) by incorporating sulfonic acid functional groups and by soaking in a calcium hydroxide solution [189]. One type of PE was soaked in simulated body fluid (SBF) right after sulfonation, while the other type of PE was treated with calcium hydroxide before soaking in SBF. Samples treated only by sulfonation did not induce apatite nucleation. When the PE sample was further treated with calcium hydroxide after sulfonation, apatite formed after 48 h of immersion in SBF. On the basis of the ζ -potential and XPS data, the authors proposed a reason for the differences in the mineralization effectivity (Fig. 15). The first step is the formation of $-\text{SO}_3\text{H}$ groups with negative charges by releasing Ca^{2+} from the PE. Next is the formation of amorphous calcium sulfate with a positive charge by combining $-\text{SO}_3\text{H}$ with Ca^{2+} ions from the SBF. With the positively charged calcium sulfate at the surface, negatively charged phosphate ions from the SBF can combine to form an amorphous layer of calcium phosphate. The last step is the transformation of amorphous calcium phosphate into crystalline apatite.

Finally, the controlled deposition of other minerals on polymer surfaces with at least partly amphiphilic character has also been studied. Dutschke et al. investigated

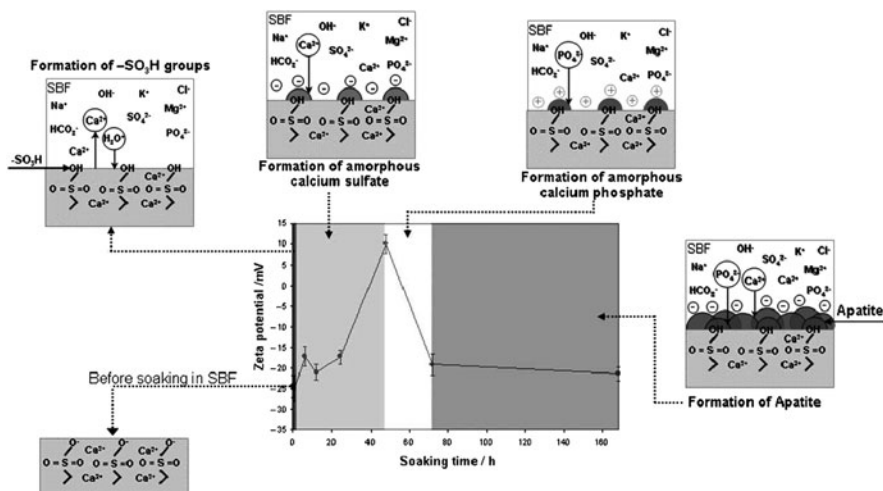


Fig. 15 Relationship between the changes in the surface structure and the potential of the incorporation of $-\text{SO}_3\text{H}$ groups into PE in the apatite formation process on its surface in SBF. Reprinted from [189]. Reproduced by permission of The Royal Society of Chemistry

TiO_2 formation on PS surfaces [190]. The study shows that only hydroxylated PS surfaces induced mineralization. In contrast, PS surfaces treated with H_2SO_4 or SO_3 do not lead to mineralization except for a few TiO_2 spots. Subsequently, Strohm et al. observed TiO_2 mineralization on PS spheres modified with poly(dialkyldimethylammonium chloride) [191]. These studies show that (at least for TiO_2) nucleation and growth on hydrophobic surfaces is not favored. It is necessary to induce hydrophilic sites where nucleation and growth can occur. Moreover, the chemistry of the hydrophilic surface is a key parameter that governs the details of the mineralization, similarly to other examples discussed above.

Filmon et al. initiated calcium phosphate mineralization by immobilizing alkaline phosphatases (AlkP) on PHEMA [192]. The authors also modified the neutral surface of PHEMA by carboxymethylation and further investigated the mineralization process in an in vitro assay that compared the effect of additional carboxylic acid groups and the effect of AlkP/PHEMA hybrid. In both systems, the formation of globular calcospherites could be observed. These findings confirm the assumption that molecules containing carboxylic residues act as mineralization nucleators [193].

Although not specifically related to surface mineralization, two theoretical studies are also of interest. Schepers et al. investigated the very early steps of calcite/collagen biomineral formation via molecular dynamics simulation of teleopeptides mimicking the tail of a collagen fiber protein [194]. Based on the simulated energy profiles obtained for several putative adsorption sites, quantitative analysis of protein-ion bonds could be provided. In a nutshell, the data suggest that proteins have the ability to trap and pre-organize specific ions from the aqueous solution, and hence promote local aggregate formation.

Yang and coworkers performed a series of simulations on α -D-galactose, α -D-mannose, α -D-xylose, and α -L-rhamnose, which represent the active side

chain of coccolith-associated polysaccharides [195]. These polysaccharides control calcite growth of *Emiliania huxleyi*. The simulations showed that crystal formation depends on two main parameters. Firstly, the strength of the binding and the shape of the resulting crystal are important. The majority of the saccharides bind more strongly to acute stepped surfaces than to planar surfaces, and most bind more weakly to obtuse-shaped surfaces. Moreover, crystal formation depends on the termination of the crystal surface (CO_3^{2-} vs. Ca^{2+}), which directly affects the binding of the polysaccharide to the mineral. The second influencing factor depends on the stereochemistry between the polysaccharide and crystal surface. The polysaccharides can influence hydrogen bond formation between solution and surface. In some cases, the interactions between polysaccharide and surface can block the water and disrupt its ordering.

In summary, this chapter shows that the interaction between (polymer) surfaces and inorganic minerals is far from understood, although some interaction principles can be formulated. It clearly shows that the mineralization is a multistep process. Furthermore, polarization matching, mutual templating, molecular rearrangements etc. appear to be key factors for mineralization, not epitaxial interaction between organic template and nucleating inorganic phase. First studies also suggest that amphiphilic polymers could be a robust and flexible tool for the study of interface-controlled mineralization processes.

Acknowledgement We thank Prof. W. Meier (University of Basel) and Prof. M. Antonietti (MPI of Colloids and Interfaces) for their support and the Swiss National Science Foundation, the German Research Foundation, the University of Basel, the University of Potsdam, the MPI of Colloids and Interfaces (Colloid Chemistry Department), and the Holcim Foundation for supporting our research.

References

1. Harkins WD (1952) Physical chemistry of surface films. Rheinhold, New York
2. Heertjes PM, De Smet EC, Witvoet WC (1971) Chem Eng Sci 26:1479–1480
3. Harkins WD, Anderson TF (1937) J Am Chem Soc 59:2189–2197
4. Davies JT, Rideal EK (1963) Interfacial phenomena, 2nd edn. Academic, New York
5. Ramos S, Castillo R (1999) J Chem Phys 110:7021–7030
6. Jura G, Harkins WD (1944) J Chem Phys 12:113–114
7. Shih MC, Bohanon TM, Mikrut JM, Zschack P, Dutta P (1992) Phys Rev A 45:5734–5737
8. Knobler CM (1997) Physica A 236:11–18
9. Henon S, Meunier J (1991) Rev Sci Instrum 62:936–939
10. Bercegol H, Gallet F, Langevin D, Meunier J (1989) J Phys 50:2277–2289
11. Mobius D (1996) Curr Opin Colloid Interface Sci 1:250–256
12. Teer E, Knobler CM, Lautz C, Wurlitzer S, Kildae J, Fischer TM (1997) J Chem Phys 106:1913–1920
13. Melzer V, Weidemann G, Vollhardt D, Brezesinski G, Wagner R, Struth B, Moehwald H (1997) J Phys Chem B 101:4752–4758
14. Vollhardt D, Melzer V (1997) J Phys Chem B 101:3370–3375
15. Prieto I, Martin Romero MT, Camacho L, Moebius D (1998) Langmuir 14:4175–4179
16. Lipp MM, Lee KYC, Waring A, Zasadzinski JA (1997) Biophys J 72:2783–2804

17. Rodriguez Patino JM, Carrera Sanchez C, Rodriguez Nino MR (1999) *Langmuir* 15: 2484–2492
18. Dynarowicz-Latka P, Dhanabalan A, Oliveira ON (2001) *Adv Colloid Interface Sci* 91: 221–293
19. Crisp DJ (1946) *J Colloid Sci* 1:49–70
20. Crisp DJ (1946) *J Colloid Sci* 1:161–184
21. Gaines GL, Jr. (1991) *Langmuir* 7:834–839
22. Breton M (1981) *J Macromol Sci Rev Macromol Chem* C21:61–87
23. Bates FS, Fredrickson GH (1990) *Annu Rev Phys Chem* 41:525–557
24. Rother G, Findenegg GH (1998) *Colloid Polym Sci* 276:496–502
25. Faure MC, Bassereau P, Lee LT, Menelle A, Lheveder C (1999) *Macromolecules* 32: 8538–8550
26. Baker SM, Leach KA, Devereaux CE, Gragson DE (2000) *Macromolecules* 33:5432–5436
27. Rivillon S, Munoz MG, Monroy F, Ortega F, Rubio RG (2003) *Macromolecules* 36: 4068–4077
28. Akentiev AV, Miller R, Noskov BA (2002) *Colloid J* 64:653–660
29. Wesemann A, Ahrens H, Steitz R, Foerster S, Helm CA (2003) *Langmuir* 19:709–716
30. Li S, Clarke CJ, Eisenberg A, Lennox RB (1999) *Thin Solid Films* 354:136–141
31. Devereaux CA, Baker SM (2002) *Macromolecules* 35:1921–1927
32. Francis R, Skolnik AM, Carino SR, Logan JL, Underhill RS, Angot S, Taton D, Gnanou Y, Duran RS (2002) *Macromolecules* 35:6483–6485
33. Deschenes L, Bousmina M, Ritcey AM (2008) *Langmuir* 24:3699–3708
34. Sauer BB, Yu H, Tien CF, Hager DF (1987) *Macromolecules* 20:393–400
35. Cheyne RB, Moffitt MG (2005) *Langmuir* 21:5453–5460
36. Peleshanko S, Jeong J, Gunawidjaja R, Tsukruk VV (2004) *Macromolecules* 37:6511–6522
37. Gunawidjaja R, Peleshanko S, Genson KL, Tsitsilianis C, Tsukruk VV (2006) *Langmuir* 22:6168–6176
38. Peleshanko S, Gunawidjaja R, Petrash S, Tsukruk VV (2006) *Macromolecules* 39:4756–4766
39. Peetla C, Graf K, Kressler J (2006) *Colloid Polym Sci* 285:27–37
40. Busse K, Peetla C, Kressler J (2007) *Langmuir* 23:6975–6982
41. Iyer J, Hammond PT (1999) *Langmuir* 15:1299–1306
42. Ahmed F, Hategan A, Discher DE, Discher BM (2003) *Langmuir* 19:6505–6511
43. Matmour R, Francis R, Duran RS, Gnanou Y (2005) *Macromolecules* 38:7754–7767
44. Myrvold R, Hansen FK, Balinour B (1996) *Colloids Surf A* 117:27–36
45. Joncheray TJ, Denoncourt KM, Mathieu C, Meier MAR, Schubert US, Duran RS (2006) *Langmuir* 22:9264–9271
46. Joncheray TJ, Denoncourt KM, Meier MAR, Schubert US, Duran RS (2007) *Langmuir* 23:2423–2429
47. Leiva A, Farias A, Gargallo L, Radic D (2008) *Eur Polym J* 44:2589–2598
48. Doi T, Kinoshita T, Tsujita Y, Yoshimizu H (2000) *Sen'i Gakkaishi* 56:221–226
49. Park Y, Choi Y-W, Park S, Cho CS, Fasolka MJ, Sohn D (2005) *J Colloid Interface Sci* 283:322–328
50. Kubies D, Machova L, Brynda E, Lukas J, Rypacek F (2003) *J Mater Sci Mater Med* 14: 143–149
51. Zhang J, Cao H, Wan X, Zhou Q (2006) *Langmuir* 22:6587–6592
52. Napoli A, Bermudez H, Hubbell JA (2005) *Langmuir* 21:9149–9153
53. Kiss E, Vargha A, Vargha-Butler EI (2004) *Phys Chem Chem Phys* 6:1575–1579
54. Kiss E, Dravetzky K, Hill K, Kutnyanszky E, Varga A (2008) *J Colloid Interface Sci* 325: 337–345
55. Kiss E, Keszthelyi T, Kormany G, Hakkel O (2006) *Macromolecules* 39:9375–9384
56. Blomqvist BR, Waernheim T, Claesson PM (2005) *Langmuir* 21:6373–6384
57. Peleshanko S, Anderson KD, Goodman M, Determan MD, Mallapragada SK, Tsukruk VV (2007) *Langmuir* 23:25–30
58. Cabasso I, Stesikova E (2008) *J Phys Chem B* 112:14379–14389

59. Nakano M, Deguchi M, Endo H, Matsumoto K, Matsuoka H, Yamaoka H (1999) *Macromolecules* 32:6088–6092
60. Matsumoto K, Mizuno U, Matsuoka H, Yamaoka H (2002) *Macromolecules* 35:555–565
61. Mouri E, Wahnes C, Matsumoto K, Matsuoka H, Yamaoka H (2002) *Langmuir* 18:3865–3874
62. Seo Y-S, Kim KS, Galambos A, Lammertink RGH, Vancso GJ, Sokolov J, Rafailovich M (2004) *Nano Lett* 4:483–486
63. Nagano S, Matsushita Y, Ohnuma Y, Shinma S, Seki T (2006) *Langmuir* 22:5233–5236
64. Wen G, Chung B, Chang T (2006) *Polymer* 47:8575–8582
65. Wen G, Chung B, Chang T (2008) *Macromol Rapid Commun* 29:1248–1253
66. Haefele T, Kita-Tokarczyk K, Meier W (2006) *Langmuir* 22:1164–1172
67. Ho D, Chang S, Montemagno CD (2006) *Nanomedicine* 2:103–112
68. Lee W, Ni S, Deng J, Kim B-S, Satija SK, Mather PT, Esker AR (2007) *Macromolecules* 40:682–688
69. Park JY, Liu M, Mays J, Dadmun M, Advincula R (2009) *Soft Matter* 5:747–749
70. Niwa M, Sawada T, Higashi N (1998) *Langmuir* 14:3916–3920
71. Ahrens H, Forster S, Helm CA (1998) *Phys Rev Lett* 81:4172–4175
72. Kaewsaiha P, Matsumoto K, Matsuoka H (2007) *Langmuir* 23:7065–7071
73. Dubreuil F, Fontaine P, Alba M, Daillant J, Mays JW, Zalczer G, Guenoun P (2005) *Europhys Lett* 70:176–182
74. Higashi N, Koga T, Niwa M (2000) *Langmuir* 16:3482–3486
75. Meszaros M, Eisenberg A, Lennox RB (1995) *Faraday Discuss* 98:283–294
76. Iemura T, Hotta H, Otsuka S (1954) *Bull Chem Soc Jpn* 27:93–97
77. Niwa M, Katsurada N, Higashi N (1988) *Macromolecules* 21:1878–1880
78. Mouri E, Matsumoto K, Matsuoka H (2003) *J Polym Sci B Polym Phys* 41:1921–1928
79. Matsuoka H, Furuya Y, Kaewsaiha P, Mouri E, Matsumoto K (2005) *Langmuir* 21:6842–6845
80. Mouri E, Matsumoto K, Matsuoka H (2003) *J Appl Crystallogr* 36:722–726
81. Casse O, Colombani O, Kita-Tokarczyk K, Muller AHE, Meier W, Taubert A (2008) *Faraday Discuss* 139:179–197
82. Niwa M, Higashi N (1989) *Macromolecules* 22:1000–1002
83. Niwa M, Hayashi T, Higashi N (1990) *Langmuir* 6:263–268
84. Niwa M, Mukai A, Higashi N (1991) *Macromolecules* 24:3314–3318
85. Safouane M, Miller R, Moehwald H (2005) *J Colloid Interface Sci* 292:86–92
86. Joncheray TJ, Bernard SA, Matmour R, Lepoittevin B, El-Khoury RJ, Taton D, Gnanou Y, Duran RS (2007) *Langmuir* 23:2531–2538
87. Rehfeldt F, Steitz R, Armes SP, Von Klitzing R, Gast AP, Tanaka M (2006) *J Phys Chem B* 110:9171–9176
88. Liu G, Yang S, Zhang G (2007) *J Phys Chem B* 111:3633–3639
89. Fasolka MJ, Mayes AM (2001) *Annu Rev Mater Res* 31:323–355
90. Krausch G, Magerle R (2002) *Adv Mater* 14:1579–1583
91. Park M, Harrison C, Chaikin PM, Register RA, Adamson DH (1997) *Science* 276:1401–1404
92. Lazzari M, Lopez-Quintela MA (2003) *Adv Mater* 15:1583–1594
93. Cheng JY, Ross CA, Chan VZH, Thomas EL, Lammertink RGH, Vancso GJ (2001) *Adv Mater* 13:1174–1178
94. Thurn-Albrecht T, Schotter J, Kastle GA, Emley N, Shibauchi T, Krusin-Elbaum L, Guarini K, Black CT, Tuominen MT, Russell TP (2000) *Science* 290:2126–2129
95. Stoykovich MP, Mueller M, Kim SO, Solak HH, Edwards EW, de Pablo JJ, Nealey PF (2005) *Science* 308:1442–1446
96. Foerster S (2003) *Top Curr Chem* 226:1–28
97. Wang X, Kawanami H, Islam NM, Chattergee M, Yokoyama T, Ikushima Y (2008) *Chem Commun* 37:4442–4444
98. Chen S, Li Y, Guo C, Wang J, Ma J, Liang X, Yang L-R, Liu H-Z (2007) *Langmuir* 23:12669–12676
99. Chen X, An Y, Zhao D, He Z, Zhang Y, Cheng J, Shi L (2008) *Langmuir* 24:8198–8204
100. Zhang Y, He H, Gao C (2008) *Macromolecules* 41:9581–9594
101. Shen J, Hu Y, Qin C, Li C, Ye M (2008) *Compos Part A* 39A:1679–1683

102. Xu G, Wu W-T, Wang Y, Pang W, Zhu Q, Wang P (2007) *Nanotechnology* 18:145606/145601–145606/145607
103. Norrman K, Ghanbari-Siahkali A, Larsen NB (2005) *Ann Rep Prog Chem Sect C: Phys Chem* 101:174–201
104. Schwartz DK (1997) *Surf Sci Rep* 27:241–334
105. Blodgett KB (1935) *J Am Chem Soc* 57:1007–1022
106. Langmuir I, Schaefer VJ (1938) *J Am Chem Soc* 60:2803–2810
107. Reiter G (1992) *Mater Res Soc Symp Proc* 248:393–398
108. Brittain WJ, Minko S (2007) *J Polym Sci A Polym Chem* 45:3505–3512
109. Zhao B, Brittain WJ (2000) *Prog Polym Sci* 25:677–710
110. Prucker O, Ruehe J (1998) *Langmuir* 14:6893–6898
111. Edmondson S, Osborne VL, Huck WTS (2004) *Chem Soc Rev* 33:14–22
112. Matyjaszewski K, Xia J (2001) *Chem Rev* 101:2921–2990
113. Davis F, Higson SPJ (2005) *Biosens Bioelectron* 21:1–20
114. Gomar-Nadal E, Puigmarti-Luis J, Amabilino DB (2008) *Chem Soc Rev* 37:490–504
115. Senaratne W, Andruzzi L, Ober CK (2005) *Biomacromolecules* 6:2427–2448
116. Hamley IW (2003) *Nanotechnology* 14:R39–R54
117. Rakhmatullina E, Manton A, Burgi T, Malinova V, Meier W (2008) *J Polym Sci A Polym Chem* 47:1–13
118. Kita-Tokarczyk K, Meier W (2008) *Chimia* 62:820–825
119. Mecke A, Dittrich C, Meier W (2006) *Soft Matter* 2:751–759
120. Taubert A, Napoli A, Meier W (2004) *Curr Opin Chem Biol* 8:598–603
121. Rowe MD, Hammer BAG, Boyes SG (2008) *Macromolecules* 41:4147–4157
122. Rakhmatullina E, Meier W (2008) *Langmuir* 24:6254–6261
123. Rakhmatullina E, Braun T, Chami M, Malinova V, Meier W (2007) *Langmuir* 23:12371–12379
124. Green RJ, Tasker S, Davies J, Davies MC, Roberts CJ, Tendler SJB (1997) *Langmuir* 13:6510–6515
125. Lee S, Iten R, Mueller M, Spencer ND (2004) *Macromolecules* 37:8349–8356
126. Colas A, Curtis J (2004) *Silicone biomaterials: history and chemistry*. In: Rutner BD, Hoffman AS, Schoen FJ, Lemons JE (eds). *Biomaterials science*, 2nd edn. Elsevier, Boston, pp. 80–86
127. Iwasaki Y, Takamiya M, Iwata R, Yusa S-I, Akiyoshi K (2007) *Colloids Surf B* 57:226–236
128. Lu DD, Yuan JC, Li H, Lei Z-Q (2008) *J Polym Sci A Polym Chem* 46:3802–3812
129. Mert O, Doganci E, Erbil HY, Demir AS (2008) *Langmuir* 24:749–757
130. Suzuki S, Whittaker MR, Wentrup-Byrne E, Monteiro MJ, Grondahl L (2008) *Langmuir* 24:13075–13083
131. Martinelli E, Menghetti S, Galli G, Glisenti A, Krishnan S, Paik MY, Ober CK, Smilgies D-M, Fischer DA (2008) *J Polym Sci A Polym Chem* 47:267–284
132. Martinelli E, Agostini S, Galli G, Chiellini E, Glisenti A, Pettitt ME, Callow ME, Callow JA, Graf K, Bartels FW (2008) *Langmuir* 24:13138–13147
133. Bosworth JK, Paik MY, Ruiz R, Schwartz EL, Huang JQ, Ko AW, Smilgies D-M, Black CT, Ober CK (2008) *ACS Nano* 2:1396–1402
134. Feng CL, Embrechts A, Vancso GJ, Schoenherr H (2006) *Eur Polym J* 42:1954–1965
135. Watanabe R, Kamata K, Iyoda T (2008) *J Mater Chem* 18:5482–5491
136. Jeon S-M, Jang K-Y, Lee SH, Park H-W, Sohn B-H (2008) *Langmuir* 24:11137–11140
137. Bolognesi A, Galeotti F, Giovannella U, Bertini F, Yunus S (2009) *Langmuir* 25:5333–5338
138. Bolognesi A, Mercogliano C, Yunus S, Civardi M, Comoretto D, Turturro A (2005) *Langmuir* 21:3480–3485
139. Kita-Tokarczyk K, Grumelard J, Haeefe T, Meier W (2005) *Polymer* 46:3540–3563
140. Decher G (1997) *Science* 277:1232–1237
141. Bougard F, Giacomelli C, Mespouille L, Borsali R, Dubois P, Lazzaroni R (2008) *Langmuir* 24:8272–8279
142. Sakai K, Webber GB, Vo C-D, Wanless EJ, Vamvakaki M, Buetuen V, Armes SP, Biggs S (2008) *Langmuir* 24:116–123

143. Webber GB, Wanless EJ, Armes SP, Biggs S (2004) *Faraday Discuss* 128:193–209
144. Zapotoczny S, Golonka M, Nowakowska M (2008) *Langmuir* 24:5868–5876
145. Glynos E, Pispas S, Koutsos V (2008) *Macromolecules* 41:4313–4320
146. Gil GO, Losik M, Schlaad H, Drechsler M, Hellweg T (2008) *Langmuir* 24:12823–12828
147. Rosenkranz T, Katranidis A, Atta D, Gregor I, Enderlein J, Grzelakowski M, Rigler P, Meier W, Fitter J (2009) *Chem Bio Chem* 10:702–709
148. Li F, Ketelaar T, Cohen Stuart MA, Sudhoelter EJR, Leermakers FAM, Marcelis ATM (2008) *Langmuir* 24:76–82
149. Mann S (1988) *Nature* 332:119–124
150. Addadi L, Moradian J, Shay E, Maroudas NG, Weiner S (1987) *Proc Natl Acad Sci USA* 84:2732–2736
151. Addadi L, Weiner S (1985) *Proc Natl Acad Sci USA* 82:4110–4114
152. Calvert P, Mann S (1988) *J Mater Sci* 23:3801–3815
153. Calvert P, Rieke P (1996) *Chem Mater* 8:1715–1727
154. Schweizer S, Taubert A (2007) *Macromol Biosci* 7:1085–1099
155. Coelfen H, Page MG, Dubois M, Zemb T (2007) *Colloids Surf A* 303:46–54
156. Mann S, Heywood BR, Rajam S, Birchall JD (1988) *Nature* 334:692–695
157. DiMasi E, Kwak S-Y, Pichon BP, Sommerdijk NAJM (2007) *CrystEngComm* 9:1192–1204
158. DiMasi E, Olszta MJ, Patel VM, Gower LB (2003) *CrystEngComm* 5:346–350
159. Gebauer D, Voelkel A, Coelfen H (2008) *Science* 322:1819–1822
160. Zhang L-J, Liu H-G, Feng X-S, Zhang R-J, Zhang L, Mu Y-D, Hao J-C, Qian D-J, Lou Y-F (2004) *Langmuir* 20:2243–2249
161. Letellier SR, Lochhead MJ, Campbell AA, Vogel V (1998) *Biochim Biophys Acta Gen Subj* 1380:31–45
162. Fricke M, Volkmer D, Krill CE, III, Kellermann M, Hirsch A (2006) *Cryst Growth Des* 6:1120–1123
163. Sommerdijk NAJM, de With G (2008) *Chem Rev* 108:4499–4550
164. Martin P, Szablewski M (2004) *Langmuir–Blodgett troughs operating manual*, 6th edn. <http://www.nima.co.uk/manuals-2.aspx>. Accessed 06 January 2010
165. Pichon BP, Cantin S, Smulders MMJ, Vos MRJ, Chebotareva N, Popescu DC, Van Asselen O, Perrot F, Sijbesma R, Sommerdijk NAJM (2007) *Langmuir* 23:12655–12662
166. Volkmer D, Fricke M, Huber T, Sewald N (2004) *Chem Commun* 16:1872–1873
167. Ahn DJ, Berman A, Charych D (1996) *J Phys Chem* 100:12455–12461
168. Buijnsters PJJA, Donners JJJM, Hill SJ, Heywood BR, Nolte RJM, Zwanenburg B, Sommerdijk NAJM (2001) *Langmuir* 17:3623–3628
169. Aizenberg J, Hanson J, Koetzle TF, Weiner S, Addadi L (1997) *J Am Chem Soc* 119:881–886
170. Cavalli S, Popescu DC, Tellers EE, Vos MRJ, Pichon BP, Overhand M, Rapaport H, Sommerdijk NAJM, Kros A (2006) *Angew Chem Int Ed* 45:739–744
171. de Leeuw NH, Rabone JAL (2007) *CrystEngComm* 9:1178–1186
172. DiMasi E, Patel VM, Sivakumar M, Olszta MJ, Yang YP, Gower LB (2002) *Langmuir* 18:8902–8909
173. DiMasi E, Kwak S-Y, Amos FF, Olszta MJ, Lush D, Gower LB (2006) *Phys Rev Lett* 97:045503/045501–045503/045504
174. Rautaray D, Sainkar SR, Pavaskar NR, Sastry M (2002) *CrystEngComm* 4:626–630
175. Sciaratta V, Oehr C, Diegelmann C, Loebmann P (2004) *Plasma Process Polym* 1:51–56
176. Henisch HK (1988) *Crystals in gels and liesegang rings*. Cambridge University Press, Cambridge, UK
177. Kewalramani S, Kim K, Stripe B, Evmenenko G, Dommert GHB, Dutta P (2008) *Langmuir* 24:10579–10582
178. Balz M, Barriau E, Istratov V, Frey H, Tremel W (2005) *Langmuir* 21:3987–3991
179. Pokroy B, Aizenberg J (2007) *CrystEngComm* 9:1219–1225
180. Aizenberg J (2004) *Adv Mater* 16:1295–1302
181. Onuma K, Oyane A, Kokubo T, Treboux G, Kanzaki N, Ito A (2000) *J Phys Chem B* 104:11950–11956

182. Kooistra WHCF (2007) The evolution of the diatoms. In: Baeuerlein E (ed) Handbook of biomineralization: biological aspects and structure formation. Wiley, Weinheim
183. Tahir MN, Theato P, Mueller WEG, Schroeder HC, Janshoff A, Zhang J, Huth J, Tremel W (2004) Chem Commun 24:2848–2849
184. Ball V, Michel M, Boulmedais F, Hemmerle J, Haikel Y, Schaaf P, Voegel JC (2006) Cryst Growth Des 6:327–334
185. Ngankam PA, Lavalle P, Voegel JC, Szyk L, Decher G, Schaaf P, Cuisinier FJG (2000) J Am Chem Soc 122:8998–9005
186. Shkilnyy A, Graef R, Hiebl B, Neffe AT, Friedrich A, Hartmann J, Taubert A (2009) Macromol Biosci 9:179–186
187. Schwahn D, Balz M, Bartz M, Fomenko A, Tremel W (2003) J Appl Crystallogr 36:583–586
188. Rautaray D, Mandal S, Sastry M (2005) Langmuir 21:5185–5191
189. Leonor IB, Kim H-M, Balas F, Kawashita M, Reis RL, Kokubo T, Nakamura T (2007) J Mater Chem 17:4057–4063
190. Dutschke A, Diegelmann C, Loebmann P (2003) Chem Mater 15:3501–3506
191. Strohm H, Loebmann P (2004) J Mater Chem 14:138–140
192. Filmon R, Basle MF, Barbier A, Chappard D (2000) J Biomater Sci Polym Ed 11:849–868
193. Filmon R, Grizon F, Basle MF, Chappard D (2002) Biomaterials 23:3053–3059
194. Schepers T, Brickmann J, Hochrein O, Zahn D (2007) Z Anorg Allg Chem 633:411–414
195. Yang M, Stipp SLS, Harding J (2008) Cryst Growth Des 8:4066–4074
196. Belegriou S, Dorn J, Kreiter M, Kita-Tokarczyk K, Sinner EK, Meier W (2010) Soft Matter 6:179–186

Index

A

Acrylate-based polymers 172
Air–water interface, monolayer 154
Alamethicin 169
Alkylglycidylethers 61
Amphiphilic block copolymers (BCPs) 1
 efficiency-boosting effect 20
Amphiphilic polymers 29
 air–water interface 154
Anisotropy 16, 139, 140, 158
 lattice mismatch strains 192
 monolayer 158
 ordered structures 117
 transport 140

B

Bis(2,6-dicarboxypyridin-4-yloxy)-3,6,9-trioxaundecans 95
2,6-Bis(benzimidazolyl)-pyridine (BIP) 95
Bisligands 92, 108
Bisphenanthroline ligands 95
Block copolymers, amphiphilic 1
 α -helical 117
Block polymers, silicon-containing 167
Breath figure (BF) technique 182
Brewster angle microscopy (BAM) 158
1,4-Butanediol diglycidyl ether 66

C

Calcium phosphate, mineralization 195
 nanodot arrays 192
Cetyl pyridinium chloride (CPC) 12
Colloidal stability 47
Co-micellization 2, 17
Complex coacervate 91
Complex coacervate core micelles (C3Ms) 105

Coordination polymers 91
 nanostructures 102
 reversible 93
Critical aggregation concentration (CAC) 48, 154
Critical micellar concentration (CMC) 7, 17, 48, 107
Critical micellization temperature 6

D

Degenerative chain transfer polymerization (DTP) 33
Dendrimers 67
Diblock copolymers 11
Dihexadecyl phosphate (DHP) 104
4-Dimethylamino-pyridine (DMAP) 193
Dioleoyl phosphatidyl ethanolamine (DOPE) 189
DLVO theory 47
Dodecyl trimethyl ammonium bromide (DTAB) 4, 6
Dynamic light scattering (DLS) 107

E

Elastin-like polymers (ELPs) 29, 46, 57
Emiliana huxleyi, calcite growth 196
2-Ethyl-2-oxazoline 74
Ethylene oxide (EO) 10, 11, 20, 65, 95
 spacers 95

F

Fe(II)-MEPEs 104
Fish diagram 20

H

Hexadecyltrimethylammonium bromide (HDTAB) 6
Hexadecyltrimethylammonium chloride (CTAC) 4

Highly ordered pyrolytic graphite (HOPG) 178
 Homopolymers, thermoresponsive 51
 Humidity 117
 Hydrogen bonding 31, 41, 44, 75, 117, 119,
 124, 130, 167, 174, 187, 194
 Hyper-netted chain model (HNC) 7
 Hysteresis 71

I

Inverse solubility temperature (ITT) 46
 2-Isopropyl-2-oxazoline 74

L

Langmuir monolayers 151, 155
 Langmuir–Blodgett (L–B) layers 104, 163
 Layer-by-layer 91
 films 102
 LCST 12, 29, 32, 75, 167

M

MEPEs 101, 102
 MesoDyn approach 5
 Mesoglobules, homopolymers 50
 Metallosupramolecules 92
 Micelles 1, 49, 91, 105ff
 mixed 2
 wormlike 109
 Microemulsions 109
 Mineralization, air–water interface 186, 190
 amphiphilic polymers 186
 bioinspired 151
 solid–liquid interface 191
 Monolayers 159
 MPEG-*b*-PNIPAM 14

N

Nanoribbons 110
Navicula perminuta 180
 Nitrilotriacetic acid (NTA)-terminated
 alkenethiol 192
 Nitroxide-mediated polymerization (NMP) 33
 Nucleation 117

O

Oligo ethylene glycol mono-*n*-alkyl ethers 10
 (Oligooxa)-alkanediyl- α , ω -
 bis(dimethyldodecylammonium
 bromide)/(12-EO_{*x*}-12) 7

P

P2VP–PS–P2VP 170
 PAA-*b*-poly(*n*-butylacrylate) 190
 Packing parameter 1
 Palmitoyl oleoyl phosphatidylcholine (POPC)
 lipid monolayers 169
 PB–PEO 12
 Penta(oxyethylene) oleyl ether 11
 Penta(oxyethylene) dodecyl ether 11
 PEO-*b*-poly(butylene oxide) (PEO-*b*-PBO)
 14
 PEO-*b*-poly(*N*-isopropylacrylamide)
 (PEO-*b*-PNIPAM) 12
 PEO-*b*-poly(methacrylate) (PEO-*b*-PMA) 12,
 15
 PEO–PPO–PEO 3, 177
 PEO–protein 166
 PEO–PS–PEO 161
 PEP–PEO 20
 PFMA–PEO–PFMA 163
 Phenanthroline 94
 Pluronic-based pentablocks 167
 Plurionics 5
 PMOXA–PDMS–PMOXA 169
 polymersomes 185
 Poloxamers 2
 Poly-L-aspartic acid (PLAsp) 194
 Poly-L-glutamic acid (PLGlu) 194
 Poly(L-lactide) (PLA) 165
 Poly-L-lysine (PLLys) 194
 Poly(L-proline) (PPro) 57
 Poly(acrylamide)s, *N*-substituted 52
 Poly(*N*-acryloyl-4-*trans*-hydroxy-L-proline
 methyl ester) (PAHProMEs) 57
 Poly(*N*-acryloylmorpholine) pAOM 63
 Poly(*N*-acryloylpiperidine) (PAOPip) 56
 Poly(*N*-acryloylpyrrolidine) 55
 Poly(*N*-alkyl(meth)acrylamide)s 63
 Poly[6-(acryloyloxymethyl)uracil] 68
 Poly(*N*-acryloyl-L-proline methyl ester)
 (PAProMEs) 57
 Poly(*N*-acrylylglycinamide) 69
 Poly(amidoamine), isobutyramide-terminated
 67
 Poly(amidohydroxyurethane) (PAmHU) 66
 Poly(γ -benzyl-L-glutamate) 117, 165
 Poly[(+)-2,5-bis(4-[(*S*)-2-
 methylbutoxy]phenyl)styrene],
 PMBPS 165
 Poly(butadiene)-*b*-PEO 3
 Poly(*N*-*tert*-butylacrylamide) 63
 Poly(*tert*-butyl styrene)-*b*-poly(styrene
 sulfonate), monolayers 171

- Poly(ϵ -caprolactone)–poly(ethylene oxide)
 (PCL–PEO) 164
 Poly(*N*-cyclopropylacrylamide) (PcPAAm) 55
 Poly(dialkyldimethylammonium chloride) 195
 Poly(*N,N'*-diethylacrylamide) (PDEAAm) 53
 Poly(2,2-diethylaminoethyl methacrylate)
 (PDEAM) 167
 Poly(2,2-diethylaminoethyl methacrylate)-
b-poly(methacrylic acid)
 (PDEAM-*b*-PMAA) 184
 Poly(*N,N'*-dimethylacrylamide) (PDMAAm)
 62
 Poly(2,2-dimethylaminoethyl methacrylate)–
 poly(methylacrylic acid)
 (PDMAEMA–PMAA) 174
 Poly(1,1-diethylsilacyclobutane)–
 poly(methacrylic acid) 172
 Poly(ether)s 29, 59
 Poly[2-(2-ethoxyethoxy)ethylacrylate]
 (PEEO2A) 65
 Poly(2-(2-ethoxy)ethoxyethylvinylether) 61
 Poly(2-ethoxyethylvinylether) (PEOVEth) 61
 Poly(ethoxyethyl glycidyl ether) 61
 Poly(2-ethoxy-2-oxo-1,3,2-dioxaphospholane)
 62
 Poly(ethyl ethylene phosphate) 62
 Poly(ethyl ethylene)–poly(styrene sulfonate)
 (PEE–PSS) 170
 Poly(ethyl glycidyl ether) 61
 Poly(*N*-ethylacrylamide) (PEAAm) 42
 Poly(ethylene glycol) (PEG) 59
 Poly(ethylene oxide) (PEO) 2, 44, 160
 Poly(ethylene propylene)-*b*-PEO 20
 Poly(ethyleneoxide) (PEO) 59, 64, 68
 Poly(*N*-ethylmethacrylamide) (PEMAAm) 52
 Poly(2-ethyl-2-oxazolines) (PEOz) 58, 72, 74
 Poly(4-hydroxybutylvinylether) 61
 Poly(2-hydroxyethyl methacrylate) blocks 177
 Poly(2-hydroxyethylmethacrylate) (PHEMA)
 66
 Poly(*N*-(L)-(1-
 hydroxymethyl)propylmethacrylamide)
 55
 Poly(2-hydroxypropylacrylate) (PHPA) 65
 Poly(isoprene)-*b*-PEO (PI–PEO) 20
 Poly(isoprene)-*b*-poly(styrene sulfonate)
 (PI–PSS) 170
 Poly(2-isopropoxy-2-oxo-1,3,2-
 dioxaphospholane) 62
 Poly(isopropyl ethylene phosphate) 62
 Poly(*N*-isopropylacrylamide)
 (PiPAAm/PNIPAM) 31, 32, 53,
 174
 structural isomers 70
 Poly(*N*-isopropylmethacrylamide)
 (PiPMAAm) 54
 Poly(2-isopropyl-2-oxazolines) (PiPOz) 32,
 59, 74
 Poly(methacrylamide)s, *N*-substituted 29, 52,
 72
 Poly(methacrylic acid) (PMAA) 172
 Poly(*N*-methacrylylglycinamide) 69
 Poly[2-(2-methoxyethoxy)ethylmethacrylate]]
 (PMEO2MA) 65
 Poly(2-[2-(2-methoxyethoxy)
 ethoxy]ethylmethacrylate)
 (PMEO3MA) 65
 Poly(2-methoxyethylvinylether) (PMOVEth)
 61
 Poly(2-methoxy-2-oxo-1,3,2-
 dioxaphospholane) 62
 Poly(methyl 2-alkylamidoacrylate)s 58
 Poly(methyl ethylene phosphate) 62
 Poly(methyl glycidyl ether) 61
 Poly(methyl 2-isobutyrylacrylate) 58
 Poly(*N*-methylacrylamide) (PMAAm) 62, 68
 Poly(2-methyl-2-oxazoline) (PMOXA/PMOz)
 58, 74
 poly(dimethylsiloxane)–PMOXA 169
 Poly(methyl 2-propionamidoacrylate) 58
 Poly(methylvinylether) (PMVEth) 43, 50, 60,
 68
 Poly[oligo(ethyleneglycol)methacrylate]
 (POEGMA) 65
 Poly(organophosphazene)s 67
 Poly(oxazoline)s 29, 39
 Poly(oxide)s 59
 Poly(oxyalkylene) 6
 Poly(*p*-phenylenes) (PPP) 3, 22
 Poly(perfluorohexylethyl methacrylate)
 (PFMA) 163
 Poly(phosphoester)s 62, 72
 Poly(propylene glycol) 60
 Poly(propylene oxide) (PPO) 2, 60, 64
 Poly(*N*-*n*-propylacrylamide) (PnPAAm) 53
 Poly(*N*-*n*-propylmethacrylamide)
 (PnPMAAm) 53
 Poly(2-*n*-propyl-2-oxazoline) (PnPOz) 59
 Poly(styrene oxide)–PEO 13
 Poly(2-substituted-2-oxazoline)s 58, 63
 Poly(tetrafluoroethylene) (PTFE) 180
 Poly(vinyl acetate) (PVAc) 69
 Poly(*N*-vinyl isobutyramide) (PViBAAm) 56
 Poly(*N*-vinyl propylacetamide) 56
 Poly(vinylalcohol) (PVAL) 64, 69
 Poly(*N*-vinylamide)s 29
 Poly(*N*-vinylcaprolactam) (PVCL) 43, 56
 Poly(vinylether)s 72

Poly(*N*-vinyl-5-methyl-2-oxazolidone) 56
 Poly(vinylpyrrolidone) 63
 Poly(VPGVG) 46, 57
 Polydimethylsiloxanes 167
 Polyelectrolytes 91
 amphiphile complex 104
 Polyethylene (PE), bioactive 194
 Polyion coacervate (PIC) micelles 105
 Polyisoleucine 69
 Poly lactides, oligo(ethylene oxide)-grafted 67
 Polyleucine 32, 70
 Polymers, acrylate-based 172
 amphiphilic 151
 cyclic 73
 monolayers 159
 solution 29
 surfaces 151
 Polymethacrylates, dendronized 67
 Polyoxazolines 72
 Polystyrene (PS) 12, 40, 41, 72, 116, 119, 161, 168, 173
 Polystyrene–poly(γ -benzyl-L-glutamate) 117
 Polystyrene–poly(*tert*-butyl acrylate) (PS–PrBA) 173
 Polystyrene-*b*-poly(ferrocenyl silane) (PS–PFS) 168
 Polystyrene-*b*-poly(2-vinyl pyridine) (PS–P2VP) 168
 POSS–PEO–POSS 170
 PPO–PEO 11
 Propylene oxide 11
 Protein-like polymers/copolymers 29, 50
 PS 12, 40, 41, 72, 116, 119, 161, 168, 173
 PS-*b*-PEO 12
 PS-*b*-poly(acrylic acid) 17
 PS-*b*-poly(L-lysine) (PS–PLLys) 184
 PS–P2VP–PEO 181, 182
 PS–PAA 161
 monolayers 173
 Pyrazolopyridine 94
 Pyridine-2,6-dicarboxylic acid 94

R

Rod–coil block copolymers 118

S

Scattering methods 1
 Schiff base 94
 Self-assembled monolayers (SAMs) 188
 Self-assembly 31, 91, 117
 Self-association, hydrophobic 48
 Self-organization 47
 Sensitivity 39
 Siloxane phosphonate ester 167
 Simulated body fluid (SBF) 194
 Sodium dodecyl sulfate (SDS) 4
 Solvent effects 117
 Steric stabilization 47
 Supersaturation 117
 Supramolecular polymers 91
 Surfactants 1
 gemini 7
 ionic 4, 12
 nonionic 10, 17

T

Terpyridine 94
 Tetradecyltrimethylammonium bromide (TTAB) 6
 Thermoresponsiveness 29, 39
 Transition metal ions 93
 Triblock copolymers 3
 Trimethylolethane 66
 Trimethylolpropane 66

U

Ulva linza 180

V

N-Vinylamides 37
N-Vinyl lactams 37
N-Vinylpyrrolidone 37

W

Water, free energy of mixing 31
 nucleation, ellipsoidal ordered structures 134
 Water-soluble thermoresponsive polymer 32
 Water–air interface 154